universität wien

DISSERTATION / DOCTORAL THESIS

Titel der Dissertation /Title of the Doctoral Thesis

Ustilago bromivora – Brachypodium: A biotrophic fungal pathosystem showing multifactorial virulence

verfasst von / submitted by

Jason Bosch

angestrebter akademischer Grad / in partial fulfilment of the requirements for the degree of

Doctor of Philosophy (PhD)

Wien 2019 / Vienna 2019

Studienkennzahl lt. Studienblatt / degree programme code as it appears on the student record sheet:	A 794 685 490
Dissertationsgebiet lt. Studienblatt / field of study as it appears on the student record sheet:	Molekulare Biologie
Betreut von / Supervisor:	Dipl.-Biol. Dr. Armin Djamei, Privatdoz.

Table of Contents

Acknowledgements

This thesis is the end result of a journey which has taken many years and had its fair share of ups and downs. It is my journey but it is not one that I did, or could have done, alone. There were many people who played a role in helping, guiding, pushing and supporting me through the years and I would like to take a moment to acknowledge them.

I would first like to thank Armin for taking me into his lab and giving me a project to work on. None of this would be possible without him and I am very grateful for having had this opportunity. Along with him, I must also thank Florian and Ulrich who served on my thesis advisory committee and provided their input throughtout the project. I would also like to extend further thanks to Ulrich and his colleagues for hosting me in Munich after I had just moved to Europe. I am also very grateful to Ines and Christopher who organised and ran the PhD programme.

My lab work was made immeasurably easier thanks to the help of everyone at the Vienna BioCenter. I especially want to thank the other members of the Djamei lab, all of whom offered help or advice at one point or another, the support staff at the GMI, the members of the Molecular Biology Services and the VBCF, particularly the NGS facility and Plant Sciences. I would also like to thank any of my co-authors and collaborators who may not have fallen in the previous groups as well as Patrick Reilly, for helping me set up the analysis tools which I needed to complete my project.

This research was only possible thanks to the generous funding provided by the European Research Council (ERC), the Austrian Science Fund (FWF) and the Deutsche Forschungsgemeinschaft (DFG).

Life is not all about work. It is necessary to have time to recharge and expand in other areas. To this end I want to thank my family and friends, both online and off, for giving me someone to talk to and many great memories and experiences. I had a lot of fun with the other organisers of the VBC PhD Symposium and I think we organised an amazing event. I want to thank my PhD selection for their support and friendship on campus. I also want to thank Angelika who was a great source of support during my PhD and with whom I had so many interesting conversations. Lastly, I want to thank my family; who haven't seen me much over the past few years. I wouldn't have been here without your support and its great to know you're there for me and that I can always go back to relax and recharge.

I sincerely apologise if I have missed anyone. So many have contributed in so many different ways that it is quite likely that I have forgotten someone. Please don't take it personally, I appreciate all of you for your efforts! Thank you!

> “After sleeping through a hundred million centuries we have finally opened our eyes on a sumptuous planet, sparkling with colour, bountiful with life. Within decades we must close our eyes again. Isn’t it a noble, and enlightened way of spending our brief time in the sun, to work at understanding the universe and how we have come to wake up in it?”
>
> ~Richard Dawkins~

Publications

A list of all publications that were produced during my PhD.

- Rabe, F.[†], **Bosch, J.**[†], Stirnberg, A., Guse, T., Bauer, L., Seitner, D., … Djamei, A. (2016). A complete toolset for the study of *Ustilago bromivora* and *Brachypodium* sp. as a fungal-temperate grass pathosystem. ELife, 5, 1–35. https://doi.org/10.7554/eLife.20522
- **Bosch, J.**, & Djamei, A. (2017). Isolation of *Ustilago bromivora* Strains from Infected Spikelets through Spore Recovery and Germination. BIO-PROTOCOL, 7(14). https://doi.org/10.21769/BioProtoc.2392
- **Bosch, J.** (2018). Four proposals for a more reliable scientific literature. South African Journal of Science, 114(3/4), 3–4. https://doi.org/10.17159/sajs.2018/a0257
- **Bosch, J.**, Czedik-Eysenberg, A., Hastreiter, M., Khan, M., Güldener, U., Djamei, A. (2019) Two is better than one: Studying host plant/fungal compatibility by using a hybrid pathogen. (*Submitted to Mpmi*)
- Alcântara, A.[†], **Bosch, J.**[†], Nazari, F., Hoffmann, G., Gallei, M., Uhse, S., Darino, M., Olukayode, T., Reumann, D., Baggaley, L., Djamei, A. (2019) Teaming up for infection – effector complexes in a biotrophic interaction. (*Submitted to Frontiers in Plant Science*)

[†]Shared first authorship

Abstract

Plants and fungi interact widely in nature. Approximately 90% of plant species form mutualistic interactions with mycorrhizal fungi and all plants are known to be infected by at least one pathogenic fungus. Due to their large, negative effect on agriculture special focus in research is put on understanding plant pathogenic fungi. In order to study biotrophic interactions, where the pathogen requires a living host, one suitable model system is *Ustilago maydis* infecting maize. However genetic manipulation and growth of maize is both difficult and requires extensive space.

In this thesis, the alternative pathosystem of *Ustilago bromivora* infecting the model grass *Brachypodium distachyon* is described. I analyse and compare the *U. bromivora* genome with five other smut fungi, including prediction of orthologous genes, the construction of a high-confidence phylogeny, prediction of secreted proteins and detection of signals of positive selection.

I further extend the possibilities of the *U. bromivora – B. distachyon* pathosystem through the use of a hybrid fungus obtained by mating *U. bromivora* and *U. hordei*. This hybrid system is used to investigate the factors underlying host specificity of *U. bromivora* and reveals that virulence on *Brachypodium* is a quantitative trait with three loci contributing the greatest effect. In addition, no genomic locus is identified as essential for infection, suggesting that multiple different combinations of virulence factors can overcome host defence and contribute to establishment of biotrophy.

In summary, the new *U. bromivora – B. distachyon* pathosystem is described and provides new opportunities for research on biotrophic pathogens with an easily-manipulated host. The comparison with other smut fungi allows rapid transfer of existing knowledge to the new system and the possibility of a hybrid fungus creates a tool which can be used to answer questions in a different way to traditional approaches.

Zusammenfassung

Pflanzen und Pilze interagieren in der Natur sehr stark. Etwa 90% der Pflanzenarten bilden mutualistische Wechselwirkungen mit Mykorrhizapilzen und alle Pflanzen sind bekanntlich mit mindestens einem pathogenen Pilz infiziert. Aufgrund ihrer großen, negativen Auswirkungen auf die Landwirtschaft liegt ein besonderer Fokus in der Forschung auf dem Verständnis pflanzenpathogener Pilze. Um biotrophe Wechselwirkungen zu untersuchen, bei denen der Erreger einen lebenden Wirt benötigt, ist ein geeignetes Modellsystem *Ustilago maydis* infizierender Mais. Genmanipulation und Maiswachstum sind jedoch schwierig und erfordern viel Platz.

In dieser Arbeit wird das alternative Pathosystem von *Ustilago bromivora* beschrieben, das das Modell Gras *Brachypodium* distachyon infiziert. Ich analysiere und vergleiche das *U. bromivora*-Genom mit fünf anderen Smut-Pilzen, darunter die Vorhersage orthologer Gene, der Aufbau einer hochvertrauenswürdigen Phylogenie, die Vorhersage sekretierter Proteine und der Nachweis von Signalen positiver Selektion.

Ich erweitere die Möglichkeiten des *U. bromivora – B. distachyon* Pathosystems durch die Verwendung eines Hybridpilzes, der durch die Paarung von *U. bromivora* und *U. hordei* gewonnen wird. Dieses Hybridsystem wird verwendet, um die Faktoren zu untersuchen, die der Wirtsspezifität von *U. bromivora* zugrunde liegen, und zeigt, dass die Virulenz auf *Brachypodium* ein quantitatives Merkmal ist, wobei drei Loci den größten Effekt haben. Darüber hinaus wird kein genomischer Locus als wesentlich für eine Infektion identifiziert, was darauf hindeutet, dass mehrere verschiedene Kombinationen von Virulenzfaktoren die Wirtsabwehr überwinden und zur Etablierung der Biotrophie beitragen können.

Zusammenfassend wird das neue *U. bromivora – B. distachyon* Pathosystem beschrieben und bietet neue Möglichkeiten für die Erforschung biotroper Krankheitserreger mit einem leicht zu handhabenden Wirt. Der Vergleich mit anderen Schmutzpilzen ermöglicht eine schnelle Übertragung des vorhandenen Wissens auf das neue System und die Möglichkeit eines Hybridpilzes schafft ein Werkzeug, mit dem Fragen anders beantwortet werden können als mit herkömmlichen Ansätzen.

Übersetzt mit www.DeepL.com/Translator

Preamble

Biologists all have their favourite organisms to work with but everyone would agree that no species exists in isolation. All life is connected to other life forms in one way or another. The nature of these relationships can vary widely; some species merely share the same environment, others are predator and prey, we see co-operation, competition and parasitism and have discovered scores of microorganisms which live out their entire existence inside of other species. Understanding these lifeforms and how they interact with each other is the overarching goal of biology. In this thesis, I hope to shed some light on the way that plants and fungi interact.

Plant-fungal interactions

Plant-fungal interactions are extremely common, with nearly all plant species known to associate with a group of fungi known as mycorrhiza[1]. These symbiotic interactions, which may be intracellular in the form of arbuscular mycorrhiza or extracellular in the form of ectomycorrhiza, involve a close association between fungal species and plant roots in order to exchange nutrients for the benefit of both parties. Primarily, this involves the fungus providing nitrogen and phosphorus to the plant in exchange for sugars. Ectomycorrhiza have also been shown to facilitate carbon exchange in forest ecosystems[2] and different ectomycorrhizal genotypes can influence how plants respond to drought stress[3].

For plants which do not form mycorrhizal symbioses, some of the functions of those interactions can be taken over by endophytic fungi. Neither mycorrhizal nor endophytic relationships are constant and change according to the nutritional status of the plant. An example of this is the relationship between *Arabidopsis thaliana* and the endophyte *Colletotrichum tofieldiae*. In low phosphate conditions, *A. thaliana* suppresses its defence systems to allow colonisation by *C. tofieldiae* in order to enable phosphate exchange with the fungus[4]. In conditions where is sufficient phosphate, or in low phosphate conditions when exposed to the related-but-pathogenic *Colletotrichum incanum*, *A. thaliana* activates its defences. This shows that the lack of a defence response is not merely due to nutrient limitations. Similarly, a strain of endophytic *Helotiales* has been shown to transport phosphorous to *Arabis alpina* in low-phosphorous environments[5].

A more harmful form of plant-fungal interactions is the infection of a plant host by a pathogenic fungus. This is always detrimental to the plant, though the exact consequences depend on the type of pathogen. The two main types are necrotrophic pathogens which feed on dead plant tissue and biotrophic pathogens which require a living host plant. There are also hemi-biotrophic pathogens

which switch from a biotrophic to a necrotrophic lifestyle according to specific cues. Plants exhibit different defence responses when dealing with a necrotrophic versus a biotrophic pathogen[6].

All plants are known to be infected by at least one type of fungus and fungi are considered the main plant pathogen[7,8]. Monoculture farming can contribute to the emergence of plant pathogens[9] whose effects differ according to the specific crop but which can be devastating[10,11]. Wheat blast outbreaks, caused by *Magnaporthe oryzae*, result in the loss of 10-30% of the global rice harvest every year[12]. Such outbreaks can originate from all over the globe due to international trade. The 2016 wheat blast outbreak in Bangladesh, the first in Asia, was determined to, most-likely, have come from strains native to Brazil[13]. One study estimates that at a 10% production loss across India, Bangladesh and Pakistan, due to wheat blast would lead to the loss of 1.77 million tonnes of harvest and US$ 264 million[14]. The 2016 outbreak led to crop losses between 5-51% over the region where it occurred which suggests that these numbers could be an underestimate of the potential consequences.

Given the reality of climate change, it is not sufficient to consider only the impact of fungi on the world today but also what could happen in the future. Changes in climate could result in the spread of dangerous fungal species to regions which are currently inhospitable to them. For example, there is speculation that the poisonous, ectomycorrhizal death cap mushroom, *Amanita phylloides*, which has been responsible for human fatalities, could spread to Eastern Canada due to climate change[15]. There is also the possibility that new fungal diseases may emerge. If fungi expand into new areas, they may encounter species which could serve as potential hosts or provide opportunities for gene exchange through hybridisation or horizontal gene transfer.

It is even hypothesised that a warming climate, which reduces the difference between ambient and mammalian body temperatures, could result in many environmental fungi gaining the ability to become pathogenic on humans or other animals[16]. While this is unlikely to be a major factor in plant-fungal interactions, there are fears that a changing climate could thaw out microorganisms that have been frozen in arctic permafrost and potentially reintroduce extinct diseases[17,18]. This is speculation but, given the impact that fungi have on the world today, it should not be taken lightly[19].

How to study biotrophic interactions

My focus is on biotrophic pathogens. One widely-used system for studying biotrophic interactions is that of *Ustilago maydis* which infects *Zea mays* (maize)[20,21]. Its importance for studying the mechanisms of pathogenesis earned it a spot in a list of the top 10 fungal pathogens in molecular

plant pathology[11]. It is also used in homeopathic remedies, eaten in Mexico as *huitlacoche*[22] and has been proposed as a platform for vaccine delivery[23].

There are many features of *U. maydis* which make it a great model for plant-pathogen interactions and it has been continuously studied for many decades[24]. It is a facultative biotroph which needs to infect maize to complete its sexual life cycle but which can be grown saprophytically. This is in contrast to some other biotrophic models, such as rust fungi, which cannot be cultured independently of the host, preventing the use of many standard techniques[25]. Its life cycle consists of a free-living haploid stage and a pathogenic dikaryotic stage formed when individuals of different mating types combine. Although it usually requires mating in order to infect maize, haploid, solopathogenic strains have been developed[26] which allow for easy genetic manipulation. Infection symptoms on maize can be seen within one week of infection which allows for rapid testing of mutant strains. In addition to this, many tools have been developed for *U. maydis* as well as many data sets including the full genome sequence[27], tissue specific gene expression[28,29] and detailed time courses of gene expression[30].

However, the *U. maydis*-maize system suffers from a big drawbacks. Maize requires large amounts of space, has a relatively slow life-cycle and is not easily amenable to genetic manipulation as it has a large, polyploid genome[31]. Maize varieties have been developed to address some of these problems, such as Fast-Flowering Mini-Maize[32], but not all of them. We wanted to establish another system which could work as a model for biotrophic plant pathogens with a host that is easier to manipulate.

We chose to work with was *Ustilago bromivora.* It is related to *U. maydis* and displays many similar biological traits which make it a good system, such as the ability to grow saprophytically. Although originally described as infecting brome grasses[33], a chance infection showed that *U. bromivora* was also capable of infecting *Brachypodium distachyon*[34].

B. distachyon is a model grass which does not need large amounts of space, has a small, sequenced genome[35,36], various tools available, including T-DNA insertion lines[37], as well as protocols for microscopy[38] and transformation[35]. In addition, *B. distachyon* has been used as a model for understanding non-host resistance of fungal pathogens[34,37,38] which would provide an interesting comparison with a native, biotrophic, fungal pathogen.

Effectors as the key to plant-pathogen interactions

In order to understand the interaction between plants and their pathogens, it is necessary to understand effectors. Effectors are small molecules which are secreted by pathogens in order to manipulate the host's defences to ensure a successful infection. They are as common as they are

diverse and can be found in bacteria[39,40], oomycetes[41,42], fungi[42–45] and nematodes[46]. While any molecule can potentially function as an effector, e.g. RNA[47], I will only be considering effector proteins due to the ease of protein predictions and the many molecular techniques available for them.

As all effectors need to be secreted, this is usually where prediction efforts begin. In the most simple approaches, one merely uses a tool like SignalP to detect a signal peptide which will mark the protein for export from the cell[48]. As this will likely lead to many false positives, it is overlaid with other predictive tools which provide localisation predictions or the number of transmembrane domains. Different combinations of tools result in differing numbers of predicted secreted proteins, even when working on the same fungus[27,49,50]. There are also attempts to use machine learning over various protein data sets to directly predict effector proteins, such as EffectorP[51,52].

Once secreted, effectors can either act in the apoplastic space or be translocated and act inside the plant cell. Bacteria and nematodes can inject effector proteins directly into the host cell through either the type III secretion system[53] or the stylet[46] respectively. In oomycetes and fungi, effectors are first secreted into the apoplast before translocation into the host cell. While many translocated oomycete effectors share an RxLxR domain, whose exact mechanism is still unclear[41,54], fungal effectors do not have any domains in common. Cytoplasmic and apoplastic effectors of *M. oryzae* are known to be secreted via different processes but the details of how those effectors are translocated is still unclear[55]. This uncertainty is representative for the vast majority of fungal effectors, although several different theories exist[56,57].

However, predictions should always be confirmed experimentally through experimentation and this is especially important in the case of effectors which are defined by their function and not by any particular sequence or structural property. It is necessary to determine whether deletion of a putative effector has an effect on virulence. Although there are methods for rapidly screening effector deletions, at least in *U. maydis*[58], this can still be complicated by redundant effector functions or cultivar-specific effects. For example, deletion of the *U. maydis* effector ApB73 shows severe loss of symptom formation in maize cultivar B73 but only partial loss of symptoms in EGB[59]. As a result of these difficulties, despite at least 409 predicted secreted proteins in *U. maydis*[27,49,50], we understand the molecular function of fewer than 10 of them.

Due to the importance of overcoming host defences for the pathogen and of protecting themselves for the host, evolution in host-pathogen interactions tends to be very rapid[60,61]. Some pathogens have what has been termed a two speed genome[62], where there are gene dense, repeat poor regions with low mutation rates and gene poor, repeat rich regions with elevated mutation rates.

Effector genes have often been observed to occur within these repeat rich regions and this rapid evolution complicates effector prediction.

The advantage in this evolutionary arms race tends to move and back and forth and can be understood by a simple model. When a pathogen first infects a plant, pathogen associated molecular patterns, from molecules such as chitin, are detected by the plant and trigger a generic defence response. Pathogens then evolve effectors to overcome this. The plant, in turn, evolves the ability to sense the effector or its action on a host target[63] and restores the defence response. Again, pathogens evolve new ways to counter this development and the balance continues to shift back and forth. This model was termed the zigzag model by Jonathon Jones and Jeffrey Dangl[64].

What is needed for host specificity?

In Publication 1[49] and Publication 2[65], we described the *U. bromivora-Brachypodium* pathosystem as well as the genome sequence, predicted secreted proteins and a comparison with other smut fungi but we did not have any functional information on what genes were important for the interaction. However, we had learned that *U. bromivora* was able to mate with the closely-related *Ustilago hordei* and still infect *Brachypodium*. This opened up a new way of understanding virulence and host specificity of *U. bromivora* by studying hybrid fungi.

For a pathogen to exhibit virulence on a host, several things need to happen. (1) It is necessary for the pathogen to be able to resist the basic host defences and begin an infection. This is the step where most pathogens fail. The air is full of millions of viruses and bacteria per cubic metre[66]. Fungal spores can also be found in the air and includes pathogens of both humans and plants[67]. Despite this, most potential hosts remain free of disease. (2) Once the primary plant defences are breached, a pathogen needs to overcome more specific defences. Plants have nucleotide-binding, leucine-rich repeat receptors (NLRs) which are capable of recognising fungal effectors and triggering a hypersensitive response resulting in cell death. The structure of the network of detector and helper NLRs allows for a small number of NLRs to target many effectors and increases the robustness of the defence response[68]. (3) If all the plant defences have been overcome, then it is necessary for a pathogen to obtain the required nutrients in order to grow. In the case of biotrophic pathogens such as *U. bromivora*, there is another step (4) where a pathogen needs to adapt itself to grow alongside the host for a prolonged period of time.

Pathogens with different lifestyles can approach the question of host specificity in different ways. For necrotrophic pathogens, which feed on dead plant tissue, being able to grow with the host is a non-issue. This can allow necrotrophic pathogens which only need to kill host tissue, such as *Botrytis cinerea* and *Sclerotinia sclerotiorum*, to have a wide range of host plants[11,69–71]. On the

other hand, biotrophic pathogens not only need to overcome plant defences but also need to grow in close contact with, obtain nutrients from and not kill the host plant. This can result in more restrictive host ranges and, at the extreme end, obligate biotrophs, such as the rust fungi, which are only able to survive on their host[72].

Virulence on a specific host is not a binary trait. In most cases it is true that a pathogen either can or can not infect a specific host but, when an infection fails, it can fail at many different stages. *U. maydis Stp1* deletion strains exhibit a failure of plant cell penetration[73]. This demonstrates a complete inability to infect. In contrast, the stripe rust *Puccinnia striiformis,* which usually infects wheat and barley, is able to colonise the leaves of the non-host *B. distachyon,* although, except in rare cases, it is unable to form pustules to complete its life cycle[74]. Despite a similar final outcome, the failure of *P. striiformis* and the failure of *U. maydis Stp1* deletion mutants clearly occur at different stages of the infection process. Furthermore, host specificity can be more fine-grained than the species level. In our own work on *U. bromivora* we found that it was only able to infect two out of 29 *B. distachyon* cultivars[49].

Hybrids and host jumps

Following the definition of Olson and Stenlid, hybrids are individuals produced from either the successful mating or vegetative fusion of individuals from two populations that are distinguishable on the basis of one or more heritable characters[75]. In animals, hybrids are rare but can occur in the wild between closely related species[76]. For plants, which can grow vegetatively, hybridisation is a major driver of speciation[77]. Similarly, hybridisation is possible for many microbes. In the *Ustilagenaceae*, including *U. maydis, U. bromivora* and *U. hordei*, widespread interspecific mating has been observed[78,79].

A fungal hybrid is of great interest for research and agriculture as the combination of two separate effectomes can lead to the formation of new host symptoms or pathogenicity on a new host, termed a host jump. In at least one case, pathogenicity of the hybrid was correlated with mitochondrial origin[80]. Several examples of pathogenesis by hybrid fungi have been described and been the subject of much discussion[75,81,82].

A good example of a host jump due to hybridisation concerns powdery mildew. *Blumeria graminis*, the causal agent of powdery mildew, has several *formae speciales*. *B. graminis secalis* infects Rye and *B. graminis tritici* infects Bread wheat. In the 1960's, triticale, an artificial hybrid crop created by crossing rye and bread wheat was introduced[83]. Triticale seemed to be immune to powdery mildew until infection was reported in 2001. The strain of powdery mildew which infects triticale, *B. graminis triticale,* was determined to be a hybrid of *B. graminis secalis* and *B. graminis*

tritici[84]. The combination of the two previously-uninfecting pathogens allowed the hybrid to overcome the plant's defences.

With Publication 3(Bosch et al., 2019 (submitted to Mpmi)) we extend our previously described pathosystem by using a hybrid of *U. bromivora* and *U. hordei* which is still able to infect *B. distachyon* in order to investigate host specificity in *U. bromivora*.

Aims of the thesis

Establish *Ustilago bromivora-Brachypodium distachyon* as a model system for studying biotrophic interactions

This first aim of this thesis, covered by Publication 1 and Publication 2, is to establish the *U. bromivora-B. Distachyon* interaction as a model system for studying biotrophic plant pathogen interactions. Specifically, my focus is on the bioinformatic analysis of the *U. bromivora* genome including the prediction of effector proteins and the comparison of the genome with that of other smuts.

Dissect the molecular basis for *Ustilago bromivora* host specificity on *Brachypodium distachyon*

In Publication 3, I intend to gain a greater understanding of the important aspects of *U. bromivora* that allow it to infect *B. distachyon.* This is accomplished through the use of a hybrid fungal pathogen created through the artificial mating of *U. bromivora* with its close relative, *U. hordei.*

Publication 1: A complete toolset for the study of Ustilago bromivora and Brachypodium sp. as a fungal-temperate grass pathosystem

Contribution to the paper:

Drafted the paper, analysed and interpreted the data.

eLIFE elifesciences.org

RESEARCH ARTICLE

A complete toolset for the study of *Ustilago bromivora* and *Brachypodium* sp. as a fungal-temperate grass pathosystem

Franziska Rabe[1,2†], Jason Bosch[1†], Alexandra Stirnberg[1], Tilo Guse[1], Lisa Bauer[1‡], Denise Seitner[1], Fernando A Rabanal[1], Angelika Czedik-Eysenberg[1], Simon Uhse[1], Janos Bindics[1], Bianca Genenncher[1§], Fernando Navarrete[1], Ronny Kellner[3], Heinz Ekker[4], Jochen Kumlehn[5], John P Vogel[6], Sean P Gordon[6], Thierry C Marcel[7], Martin Münsterkötter[8], Mathias C Walter[9¶], Christian MK Sieber[8], Gertrud Mannhaupt[2,8], Ulrich Güldener[8,9], Regine Kahmann[2], Armin Djamei[1,2*]**

[1]Gregor Mendel Institute, Austrian Academy of Sciences, Vienna Biocenter, Vienna, Austria; [2]Max Planck Institute for Terrestrial Microbiology, Marburg, Germany; [3]Max Planck Institute for Plant Breeding Research, Cologne, Germany; [4]Vienna Biocenter Core Facilities GmbH, Vienna, Austria; [5]Leibniz-Institut für Pflanzengenetik und Kulturpflanzenforschung, Gatersleben, Germany; [6]DOE Joint Genome Institute, California, United States; [7]INRA UMR BIOGER, AgroParisTech, Université Paris-Saclay, Thiverval-Grignon, France; [8]Institute of Bioinformatics and Systems Biology, Helmholtz Zentrum München, German Research Center for Environmental Health, Neuherberg, Germany; [9]Department of Genome-oriented Bioinformatics, Wissenschaftszentrum Weihenstephan, Technische Universität München, Freising, Germany

***For correspondence:** armin.djamei@gmi.oeaw.ac.at

[†]These authors contributed equally to this work

Present address: [‡]Department of Infectious Diseases and Immunology, Virology Division, Faculty of Veterinary Medicine, University of Utrecht, Utrecht, Netherlands; [§]Max F Perutz Laboratories, Vienna Biocenter, Vienna, Austria; [¶]Bundeswehr Institute of Microbiology, Munich, Germany; [**]Department of Energy, Joint Genome Institute, University of California, Berkeley, United States

Competing interests: The authors declare that no competing interests exist.

Funding: See page 28

Received: 10 August 2016
Accepted: 12 October 2016
Published: 11 November 2016

Reviewing editor: Daniel J Kliebenstein, University of California, Davis, United States

Abstract Due to their economic relevance, the study of plant pathogen interactions is of importance. However, elucidating these interactions and their underlying molecular mechanisms remains challenging since both host and pathogen need to be fully genetically accessible organisms. Here we present milestones in the establishment of a new biotrophic model pathosystem: *Ustilago bromivora* and *Brachypodium* sp. We provide a complete toolset, including an annotated fungal genome and methods for genetic manipulation of the fungus and its host plant. This toolset will enable researchers to easily study biotrophic interactions at the molecular level on both the pathogen and the host side. Moreover, our research on the fungal life cycle revealed a mating type bias phenomenon. *U. bromivora* harbors a haplo-lethal allele that is linked to one mating type region. As a result, the identified mating type bias strongly promotes inbreeding, which we consider to be a potential speciation driver.
DOI: 10.7554/eLife.20522.001

Introduction

Knowledge of basic molecular principles in biology has mainly been gained through intensive studies of relatively few but technically well accessible model systems ranging from prokaryotes to eukaryotes, including the bacterium *Escherichia coli*, the fungus *Saccharomyces cerevisiae*, the insect *Drosophila melanogaster*, the mammal *Mus musculus*, as well as the dicot plant *Arabidopsis thaliana*. However, findings in these model organisms cannot always be generalized to more distantly related species (***Mohammadi et al., 2015***; ***Rine, 2014***). This has led to the development of new model

eLife digest Fungi cause many diseases in plants, and reduce the yield of important crops like wheat, corn and rice – all of which belong to the family of grasses. Much research into how disease-causing fungi infect plants will look at a given fungus that infects a specific plant in order to understand plant diseases in general. Over the years, scientists have generated suites of research tools to study these pairs of fungi and plants. However, many of these organism pairs (often called "model pathosystems") have drawbacks when it comes to research in the laboratory, either on the side of the fungus or the side of plant.

Brachypodium is a small grass that grows quickly and, unlike crop plants, it grows well in the laboratory. These characteristics make *Brachypodium* a promising model organism for studying many aspects of plant biology. Recently, a fungus called *Ustilago bromivora* – which is related to a fungus that infects corn – was reported to infect *Brachypodium*. This raised the question: could this fungus and this small grass become a new model pathosystem?

Rabe, Bosch et al. set out to answer this question and now provide a toolkit that will help to establish *U. bromivora* and *Brachypodium* as a new model pathosystem. In all of *U. bromivora*'s close relatives, two compatible strains must meet and mate before the fungus can infect the plant; first Rabe, Bosch et al. confirmed that this is also the case for *U. bromivora*. Studying the life cycle of the *U. bromivora* fungus also unexpectedly revealed that while both mating partners are needed to infect the plant, only one of the strains survives outside of the plant after the infection. This phenomenon, referred to as a "mating type bias", has been described for a few other related fungi.

Next, Rabe, Bosch et al. conducted a genetic screen and identified two compatible strains that can grow without the plant as yeast-like cells. This means that these cells can be manipulated genetically, and indeed protocols to grow and genetically engineer the fungus and plant to address different research questions are included in the toolkit as well.

Other new tools include the complete genetic sequence of the fungus with all its genes annotated, and a dataset of which genes are active in *U. bromivora* growing yeast-like in liquid culture versus those active when the fungus grows as a pathogen inside the plant.

Together these new tools and datasets will provide a foundation to study different aspects of the interactions between grasses and disease-causing fungi. This in turn may lead to new methods to reduce fungal growth and reduce yield losses caused by fungal diseases in crop plants. Finally, the discovery that *U. bromivora* shows a mating type bias could provide a starting point for future studies into sexual reproduction in fungi and how new species arise.

DOI: 10.7554/eLife.20522.002

systems, closer to species of economic relevance for humans. For temperate poaceous crops like wheat and barley, the small, fast growing grass *Brachypodium distachyon* has become a promising model organism (**Mur et al., 2011**; **Brkljacic et al., 2011**; **Vogel and Hill, 2008**; **Huo et al., 2008**; **Yordem et al., 2011**; **Garvin, 2008**; **Draper et al., 2001**). The intrinsic properties of *B. distachyon*, including self-fertility, its short life cycle, a small sequenced diploid genome, and its genetic accessibility, make it highly suitable as a laboratory model plant. Symbiotic and biotrophic interactions of plants with fungi or other microbes can have major impacts on plant development and crop yield (**Oerke, 2006**). Therefore, the study of these interactions is important for research-driven pest control. Biotrophic plant pathogens rely on a living host to proliferate and complete their life cycles. To successfully colonize their host plants, these pathogens employ small secreted molecules, termed effectors. By means of these molecules, biotrophic pathogens are able to avoid host recognition, suppress plant defense responses, and redirect the host metabolism for their needs (**Djamei et al., 2011**; **Doehlemann and Hemetsberger, 2013**; **Djamei and Kahmann, 2012**; **Deslandes and Rivas, 2012**; **Bozkurt et al., 2012**). Since most effectors target processes on the host side, the understanding of biotrophy and the molecular study of effectors profits strongly from both, a fully genetically accessible host plant as well as a pathogen that is amenable to genetic manipulation.

Among the facultative biotrophic pathogens, the smut fungus *Ustilago maydis* is a valuable model to study biotrophic interactions (**Djamei et al., 2011**; **Brefort et al., 2014**; **Kämper et al., 2006**; **Horst et al., 2010**; **Brefort et al., 2009**; **Doehlemann et al., 2009**). Although *U. maydis* is

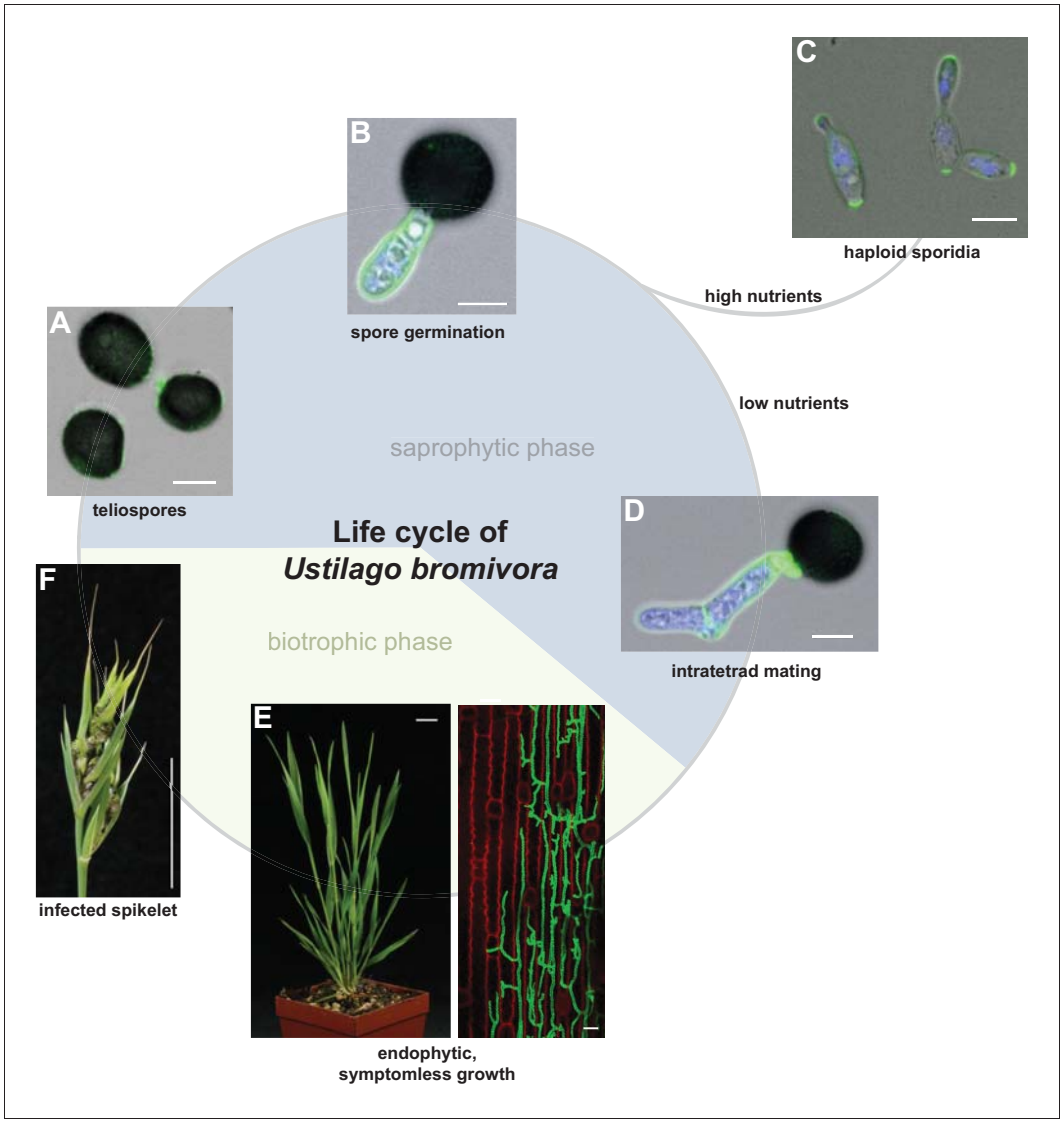

Figure 1. The life cycle of *Ustilago bromivora*. *U. bromivora* spores germinate (**A**) and form a promycelium (**B**). Under high nutrient conditions, haploid yeast-like progeny (sporidia) are released and proliferate via budding (**C**). Under low nutrient conditions intratetrad mating occurs between two adjacent cells of a promycelium by formation of a loop-like mating structure that connects both cells (**D**). After plant penetration, fungal filaments grow mainly along the stem without triggering macroscopic symptoms (**E**) until flower development occurs. Upon flowering, macroscopic symptoms are detectable as black, smutted spikelets filled with fungal spores (**F**). Fungal cell walls and nuclei were stained with WGA-Alexa Fluor 488 and DAPI, respectively (**A–D**). Plant membranes were stained with FM4-64, fungal hyphae with WGA-Alexa Fluor 488 (**E**). Scale bars: 5 µm (**A–D**), 10 µm (**E**, right panel), or 1 cm (**E**, left panel) and (**F**).

DOI: 10.7554/eLife.20522.003

The following figure supplement is available for figure 1:

Figure supplement 1. The morphology of *U. bromivora* sporidia is similar to *U. hordei*, but not to *U. maydis*.

DOI: 10.7554/eLife.20522.004

genetically fully accessible with a small, completely sequenced genome of 20.5 Mb and many molecular tools available, its host plant *Zea mays* is not as suitable as laboratory model organism due to its large size, demanding growth requirements, cross-pollinating nature, elaborate transformation requirements, and complex genome (***Kämper et al., 2006***; ***Que et al., 2014***; ***Schnable et al., 2009***). Accordingly, a more suitable model system where both, plant and pathogen are more

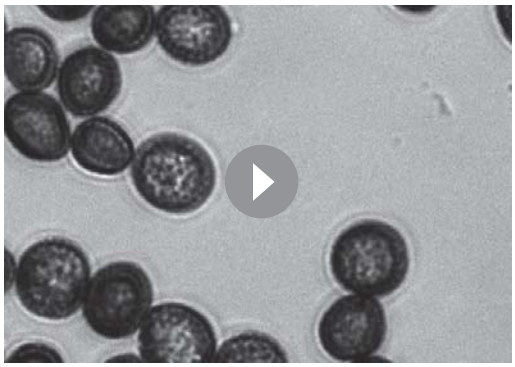

Video 1. Spore germination under high nutrient conditions (PD agar).
DOI: 10.7554/eLife.20522.005

accessible is highly desirable. The recent rediscovery that the *U. maydis*-relative *U. bromivora* can infect *Brachypodium* sp. provided the impetus to explore the suitability of the *U. bromivora-Brachypodium* system as a novel plant-pathogen model to study biotrophic interactions (***Barbieri et al., 2011***).

Here we describe the characterization of this valuable model pathosystem. This encompasses (i) the detailed understanding of the life cycle *of U. bromivora*, (ii) the identification of a sequenced compatible host, (iii) the establishment of transformation systems for both the pathogen and the plant, and (iv) the sequencing and analysis of the fungal genome. Moreover, the observation of a mating type bias present in *U. bromivora* provided first insights into the biology of this pathogen.

Results and Discussion

The life cycle of *U. bromivora* and its mating type bias

Descriptive studies on the life cycle and mating behavior of smut fungi have been performed for more than 100 years (***Bauch, 1922***; ***Brefeld, 1883***). In all grass smuts (family Ustilaginaceae) studied so far, sexual and pathogenic development are coupled (***Begerow et al., 2014***). Infection mostly occurs at the early seedling stage of the respective host plant. After penetrating the plant, the dikaryotic pathogen grows biotrophically inter- and intracellularly in its host and macroscopic symptoms are usually exclusively limited to the inflorescences (***Brefort et al., 2009***). In these plant organs, fungal proliferation finally occurs after systemic growth and eponymous black teliospores are

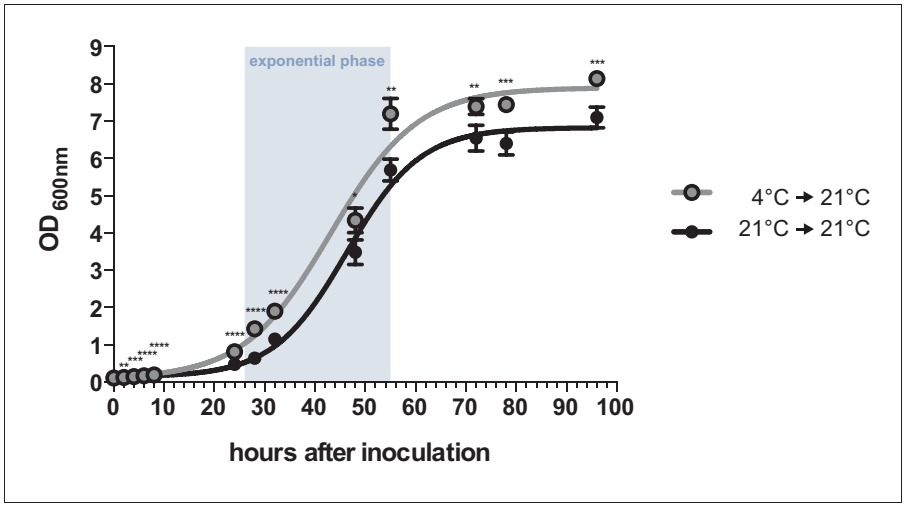

Figure 2. Axenic growth of *U. bromivora*. Growth of *U. bromivora* UB1 was assessed by monitoring cell density spectrophotometrically at λ = 600 nm in liquid PD medium at 21˚C in a time course of 96 hr. Growth was compared between axenic cultures inoculated from plate with cold-treated fungal cell material (24 hr at 4˚C) or cell material that was kept at 21˚C. Experiments were performed in 3 biological replicates. Significance between cell densities of cold-treated and non-treated cells at each time point was calculated by unpaired *t* test. **p<0.01, ***p<0.001, ****p<0.0001. The doubling time was calculated by taking the slope of a linear regression during exponential phase.
DOI: 10.7554/eLife.20522.006

formed. *U. maydis* is a prominent exception as it induces spore filled galls on all aerial parts of its host (**Brefort et al., 2009**). As described in the early 20th century by Robert Bauch (**Bauch, 1925**), *U. bromivora* grows in its host plant after infection at the seedling stage, and only exhibits macroscopic symptoms during inflorescence development by replacing flowers with black teliospore-filled sori (**Figure 1**). Teliospores are the diploid resting stage of these fungi and are able to survive harsh environmental conditions. In a humid, favorable environment, spores germinate, undergo meiosis and form a promycelium from which haploid cells are released. The haploid yeast-like cells are non-pathogenic and grow saprophytically (**Brefort et al., 2009**). To elucidate this part of the life cycle of *U. bromivora*, we followed germination of fungal spores by widefield and confocal laser scanning microscopy. Under nutrient-rich conditions, *U. bromivora* spores germinated, formed a promycelium and yeast-like cells were released (**Figure 1A–C**, **Video 1**). The egg-shaped cells of *U. bromivora*, which are released after germination, show high morphological similarity to the sporidia of the barley-infecting covered smut *Ustilago hordei*, and their morphology differ from the cigar-like shaped haploid cells of *U. maydis* (**Figure 1—figure supplement 1**). The high morphological similarity between *U. bromivora* and *U. hordei* is in line with phylogenetic analysis based on internal transcribed spacer (ITS) and large subunit (LSU) rDNA sequence comparison, which suggested that *U. bromivora* is more closely related to *U. hordei* than to *U. maydis* (**Stoll et al., 2005**).

During saprophytic growth, daughter cells bud off from the mother cell at the side of the oval tip. For a better visualization of the fungal cells, we employed the chitin stain Wheat Germ Agglutinin (WGA) that is conjugated to Alexa Fluor 488 (**Figure 1C**). The WGA-Alexa Fluor 488 conjugate distinctively stained the tip of the sporidia indicating cell wall composition differences at the sporidial

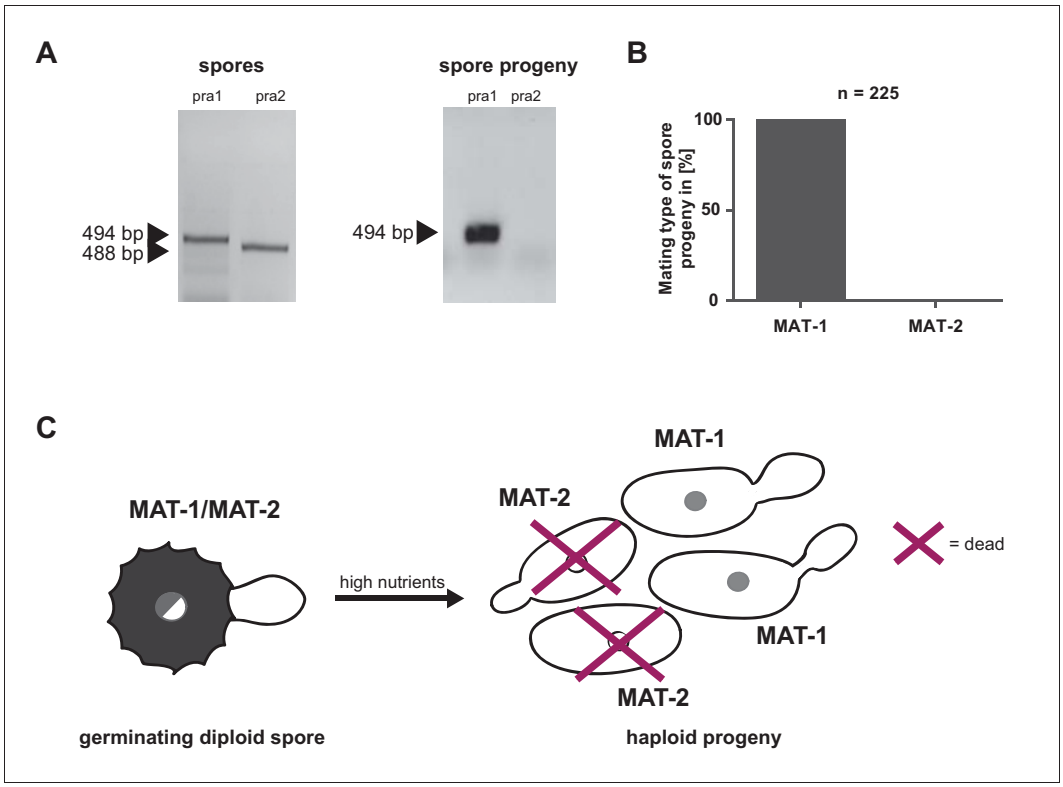

Figure 3. Mating type bias of *U. bromivora*. (**A**) Diagnostic PCR on genomic DNA derived from spores and spore progeny to test for mating type 1 (MAT-1) or mating type 2 (MAT-2). To this end, primers targeting a conserved region of pheromone receptor alleles 1 (*pra1*) and 2 (*pra2*), adapted from **Kellner et al. (2011)**, were used. Sizes of PCR products are indicated with arrow heads. Representative PCR results are shown. (**B**) Quantification of mating type alleles of 225 progeny derived from 21 spores by PCR as described in (**A**). (**C**) Schematic model illustrating the observed mating type bias phenomenon.

DOI: 10.7554/eLife.20522.007

poles. This could be due to either an uneven chitin distribution or an uneven accessibility of chitin for the stain along the sporidial cell wall (***Figure 1C***).

By performing growth analyses we determined the doubling time of *U. bromivora* sporidia. In comparison to *U. maydis* sporidia that exhibit a doubling time of about 2 hr (***Steinberg, 2007***), *U. bromivora* sporidia grow much slower (doubling time in exponential phase at 21°C: 5 1/3 hr; ***Figure 2***). Interestingly, we observed that the lag-phase of the *U. bromivora* culture could be significantly shortened when *U. bromivora* was kept for 24 hr at 4°C prior to inoculation (***Figure 2***). The underlying mechanism for this phenomenon is unclear and awaits further research.

Video 2. Spore germination under low nutrient conditions (water agar).
DOI: 10.7554/eLife.20522.008

Prior to pathogenic growth, in case of the well-studied smut fungus *U. maydis,* two haploid cells of compatible mating type recognize each other via a pheromone-receptor system on the plant surface, grow towards each other, fuse, and form a dikaryotic filament. This dikaryotic filament represents the pathogenic form of the fungus. It penetrates the leaf cuticle and grows intra- and intercellularly inside the maize plant. After proliferation in the aerial parts of the host, the filaments fragment and, after karyogamy, form diploid spores (***Brefort et al., 2009***; ***Martinez-Espinoza et al., 2002***). The molecular regulation of the dimorphic switch is based on the bi-allelic *a* locus encoding the pheromone receptor system and the multiallelic *b* locus coding for a heterodimeric homeodomain transcription factor that controls pathogenic development (***Schulz et al., 1990***; ***Bölker et al., 1992***). While *U. maydis* has a tetrapolar mating type system with *a* and *b* loci that segregate during meiosis, these two loci are genetically and physically linked in *U. hordei*, leading to a bipolar mating system with only two mating types, mating type 1 (MAT-1) and mating type 2 (MAT-2) (***Bakkeren and Kronstad, 1994***; ***Lee et al., 1999***). To test for the presence of the mating system described for related smuts we assessed whether *U. bromivora* spores, that are considered to contain the genetic information of both mating partners, harbor known pheromone-receptor alleles. To this end, we employed a diagnostic PCR approach described by ***Kellner et al. (2011)*** using primers that target conserved regions of either the pheromone receptor allele *pra1* or *pra2* -. The PCR analysis revealed amplicons for *pra1* and *pra2* indicating the presence of both mating type alleles (***Figure 3A***). To subsequently identify haploid *U. bromivora* cells of compatible mating type after spore germination, 225 randomly chosen progeny of 21 spores were tested. Surprisingly, by testing these progeny, we identified only cells of mating type 1 (MAT-1; ***Figure 3A,B***). These findings indicate a mating type bias after spore germination (***Figure 3C***). This phenomenon of biased strains was previously described in other related fungi where recessive alleles linked to the mating type-locus were found to be causative for the observed biases (***Nielsen, 1968***; ***Hood and Antonovics, 2000***).

Due to the putative haplo-lethal allele, we assumed that haploid MAT-2 cells have only a very short period of time to be rescued by finding and mating with a compatible partner, allowing the subsequent formation of a dikaryotic filament. To observe mating events, spores were germinated on water agar and monitored by light microscopy (***Video 2***, ***Figure 1D***). After spore germination, the cytoplasmic connection to the spore content becomes separated and, in the majority of germination events, only two cells are visible outside the spores. These cells frequently form a cytoplasmic bridge-like mating structure and fuse (***Video 2***, ***Figure 1D***). The mating of progeny derived from the same spore is also known as an intratetrad mating event (***Antonovics and Abrams, 2004***). Using DAPI staining at this stage, we most commonly observed a diffuse distribution of signal across the two mating cells and, more rarely, a distinct nuclei-like area (***Figure 1D***). In contrast to these mating cells, distinct nuclei-like structures could be visualized with this stain in saprophytically growing cells (***Figure 1C***). The destiny of the other two meiotic products, which, in the majority of observed cases, seemed to stay inside the spore shell, is unclear and awaits further research. The formation of conjugation hyphae that loop directly to neighboring, conjoined cells of the same tetrad could be a

Table 1. Tested *Brachypodium* accessions for *U. bromivora* susceptibility/resistance.

Name	Species	Sequenced	Susceptible to *U. bromivora*	Accession number	Source	Country of origin
ABR3	*B. distachyon*	Y	N (2x)*	ABY-Bs 5088	Brachyomics collections (C. Stace and P. Catalán), Aberystwyth, UK	Spain
ABR4	*B. distachyon*	Y	Y (many)	ABY-Bs 5089	Brachyomics collections (C. Stace and P. Catalán), Aberystwyth, UK	Spain
ABR6	*B. distachyon*	Y	N (2x)*	ABY-Bs 5091	Brachyomics collections (C. Stace and P. Catalán), Aberystwyth, UK	Spain
ABR7	*B. distachyon*	Y	N (2x)*	ABY-Bs 5092	Brachyomics collections (C. Stace and P. Catalán), Aberystwyth, UK	Spain
ABR9	*B. distachyon*	Y	N	-	unknown	Croatia
Adi-10	*B. distachyon*	Y	N	W6 39243	USDA-ARS-WRPIS; ***Vogel et al. (2009)***	Turkey
Adi-12	*B. distachyon*	Y	N	W6 39245	USDA-ARS-WRPIS; ***Vogel et al. (2009)***	Turkey
Adi-2	*B. distachyon*	Y	N	W6 39235	USDA-ARS-WRPIS; ***Vogel et al. (2009)***	Turkey
Bd1-1	*B. distachyon*	Y	Y	PI 170218 / W6 46201	GRIN Germplasm; ***Vogel et al. (2006)***	Turkey
Bd18-1	*B. distachyon*	Y	N	PI 245730 / W6 46204	USDA-ARS-WRPIS; ***Vogel et al. (2006)***	Turkey
Bd21	*B. distachyon*	Y	N	PI 254867 / W6 36678	GRIN Germplasm; ***Vogel et al. (2006)***	Iraq
Bd21-3	*B. distachyon*	Y	N	W6 39233	GRIN Germplasm; ***Vogel and Hill (2008)***	Iraq
Bd2-3	*B. distachyon*	Y	N	PI 185133 / W6 46202	***Vogel et al. (2006)***	Iraq
Bd3-1	*B. distachyon*	Y	N (2x)*	PI 185134 / W6 46203	USDA-ARS-WRPIS; ***Vogel et al. (2006)***	Iraq
BdTR10C	*B. distachyon*	Y	N	W6 39406	USDA-ARS-WRPIS	Turkey
BdTR11I	*B. distachyon*	Y	N	W6 39426	USDA-ARS-WRPIS; ***Filiz et al. (2009)***	Turkey
BdTR13a	*B. distachyon*	Y	N	W6 39430	USDA-ARS-WRPIS; ***Filiz et al. (2009)***	Turkey
BdTR13C	*B. distachyon*	Y	N	W6 39432	USDA-ARS-WRPIS; ***Filiz et al. (2009)***	Turkey
BdTR1I	*B. distachyon*	Y	N	W6 39308	USDA-ARS-WRPIS; ***Filiz et al. (2009)***	Turkey
BdTR2B	*B. distachyon*	Y	N	W6 39314	USDA-ARS-WRPIS; ***Filiz et al. (2009)***	Turkey
BdTR2G	*B. distachyon*	Y	N	W6 39319	USDA-ARS-WRPIS; ***Filiz et al. (2009)***	Turkey
BdTR3C	*B. distachyon*	Y	N	W6 39332	USDA-ARS-WRPIS; ***Filiz et al. (2009)***	Turkey
BdTR5I	*B. distachyon*	Y	N	W6 39366	USDA-ARS-WRPIS; ***Filiz et al. (2009)***	Turkey
Foz1	*B. distachyon*	Y	N	-	***Mur et al. (2011)***	Spain
Gaz8	*B. distachyon*	Y	N	W6 39269	USDA-ARS-WRPIS; ***Vogel et al. (2009)***	Turkey
Kah1	*B. distachyon*	Y	N	W6 39278	USDA-ARS-WRPIS; ***Vogel et al. (2009)***	Turkey

Table 1 continued on next page

Table 1 continued

Name	Species	Sequenced	Susceptible to *U. bromivora*	Accession number	Source	Country of origin
Koz1	*B. distachyon*	Y	N	W6 39284	USDA-ARS-WRPIS; ***Vogel et al. (2009)***	Turkey
Mur1	*B. distachyon*	Y	N	-	***Mur et al. (2011)***	Spain
S8iiC	*B. distachyon*	Y	N	-	Ana Caicedo Lab, University of Massachusetts	Spain
ABR114	*B. stacei*	Y	Y (2x)*	-	unknown	Spain
ABR113	*B. hybridum*	Y	N	-	unknown	Portugal
ABR117, Bd117, Bd6	*B. hybridum*	N	Y (2x)*	PI - 219965	GRIN Germplasm	Afghanistan
Bal-P7	*B. hybridum*	N	Y (2x)*	W6 - 39259	GRIN Germplasm	Turkey
Bd23	*B. hybridum*	N	Y (2x)*	PI - 287783	GRIN Germplasm	Spain
Bd26	*B. hybridum*	N	Y (2x)*	PI - 372187	GRIN Germplasm	Uruguay
Bd28	*B. hybridum*	N	Y (many)*	PI - 533015	GRIN Germplasm	Australia
Bd4	*B. hybridum*	N	Y (2x)*	PI - 208216	GRIN Germplasm	South Africa
Bd8	*B. hybridum*	N	Y (2x)*	PI - 219971	GRIN Germplasm	Afghanistan
Isk-P4	*B. hybridum*	N	Y (2x)*	W6 - 39273	GRIN Germplasm	Turkey

Y = yes, N = no; * = times tested

DOI: 10.7554/eLife.20522.010

necessary result of the mating type bias and ensures an efficient re-entry into the pathogenic stage of the life cycle. At the same time, the haplo-lethal allele that is likely linked to the MAT-2 locus promotes an inbreeding mode of *U. bromivora* with direct consequences on speciation, genome size, and selection on recessive alleles as it has been observed in other organisms (***Wright et al., 2008***; ***Ellegren and Galtier, 2016***; ***Joly, 2011***).

Isolation of a haplo-viable *U. bromivora* MAT-2 strain

Although the observed mating type bias is an interesting biological phenomenon, it is an undermining factor for the use of *U. bromivora* as genetically accessible model system to study biotrophic interactions. It creates a situation where one mating partner can only be maintained in the pathogenic, dikaryotic stage together with its compatible mating type and, as a consequence, it can neither be cultured axenically nor transformed under laboratory conditions. Depending on the physical distance of the MAT-2 locus to the haplo-lethal allele that causes the mating type bias, homologous recombination can lead to an uncoupling and the formation of a haplo-viable MAT-2 strain. Therefore, we screened for such viable haploid MAT-2 recombinants by using a pooled infection assay where a pool of spore-derived progeny was grown saprophytically and used for re-infection of *Brachypodium* sp. (for details see Material and Methods). By pursuing this approach, we identified one MAT-2 strain that we named UB2. This strain, which is not derived from the same spore as UB1, retained the capability to mate with the *U. bromivora* MAT-1 strain UB1, which we isolated in a classical spore germination assay. Moreover, upon inoculation of *Brachypodium* sp., UB2 along with UB1 formed viable spores demonstrating a successful completion of their life cycle. Infection symptoms of UB1xUB2-inoculated plants were indistinguishable from infected spikelets of spore-inoculated plants (data not shown).

Figure 4. ABR4, ABR114, and Bd1-1 are susceptible to *U. bromivora*. Representative pictures of infected ABR4, ABR114, and Bd1–1 spikelets. Sequenced *B. distachyon* accessions ABR4 and Bd1-1 as well as the sequenced *B. stacei* accession ABR114 were inoculated with *U. bromivora* spore material and screened for infection symptoms. Upon flowering macroscopic infection symptoms could be observed as spore-filled spikelets. This figure relates to ***Table 1***. Scale bars: 1 cm.

DOI: 10.7554/eLife.20522.009

Identification of a sequenced compatible host of *U. bromivora*

Phylogenetic analysis recently led to a taxonomy split within the *Brachypodium* lineages, separating *B. distachyon* with cytotype 2n = 10 from *Brachypodium stacei* (2n = 20) and the allotetraploid *Brachypodium hybridum* (2n = 30) (***Catalan et al., 2012***). The spontaneous infection event by *U. bromivora* reported by ***Barbieri et al. (2011)*** occurred in the *B. hybridum* accession Bd28. The *B. hybridum* accession Bd28 undergoes self-fertilization, grows fast, and is easy to handle (***Barbieri et al., 2011***). One slightly complicating fact is its allotetraploid genetic background but its genome is currently being sequenced and will be available to the community in near future (J. Vogel, unpublished). In order to identify additional *Brachypodium* sp. accessions susceptible to *U. bromivora*, in total, 39 accessions were infected with spores and analyzed for macroscopic infection symptoms in the spikelets. Whereas *B. distachyon* Bd21, along with 27 other tested accessions, did not show infection symptoms, we found eleven accessions to be fully susceptible to *U. bromivora* (***Table 1***). The finding that susceptible host plant accessions originate from Europe, Asia, Africa, Australia as well as South America (***Table 1***) underlines that *U. bromivora* is considered as a cosmopolite (***Bauch, 1925***). The natural host range of *U. bromivora* comprises various species of the genera *Agropyron, Austrofestuca, Brachypodium including B. distachyon, Bromus, Critesion, Elymus, Festuca, Hordeum, Lolium, Sitanion and Trachynia* (***Bauch, 1925***; ***Fisher and Holton, 1957***; ***Vanky, 2011***) and our experiments can confirm at least three host species, *B. distachyon*, *B. hybridum* and *B. stacei*. Among the susceptible accessions are the *B. distachyon* accessions ABR4, originally collected from Southern Spain, and Bd1-1, an inbred line, as well as the *B. stacei* accession ABR114 (***Figure 4***). The genomes of all three susceptible diploid accessions have been sequenced (J. Vogel, unpublished), providing the foundation for valuable tools and studies of our novel plant pathosystem. While, to our knowledge, ABR4 has not been tested for susceptibility to other important fungal pathogens, Bd1-1 shows resistance to the wheat pathogen *Zymoseptoria tritici* as well as to *Puccinia graminis* (***Figueroa et al., 2013***; ***O'Driscoll et al., 2015***). Therefore, Bd1-1 represents a suitable model accession to study compatible interactions with *U. bromivora* as well as incompatible interactions with *P. graminis* and *Z. tritici*. Moreover, the comparison of susceptible *B. distachyon* accessions such as Bd1-1 and ABR4, with the resistant accession Bd21 allows the study of

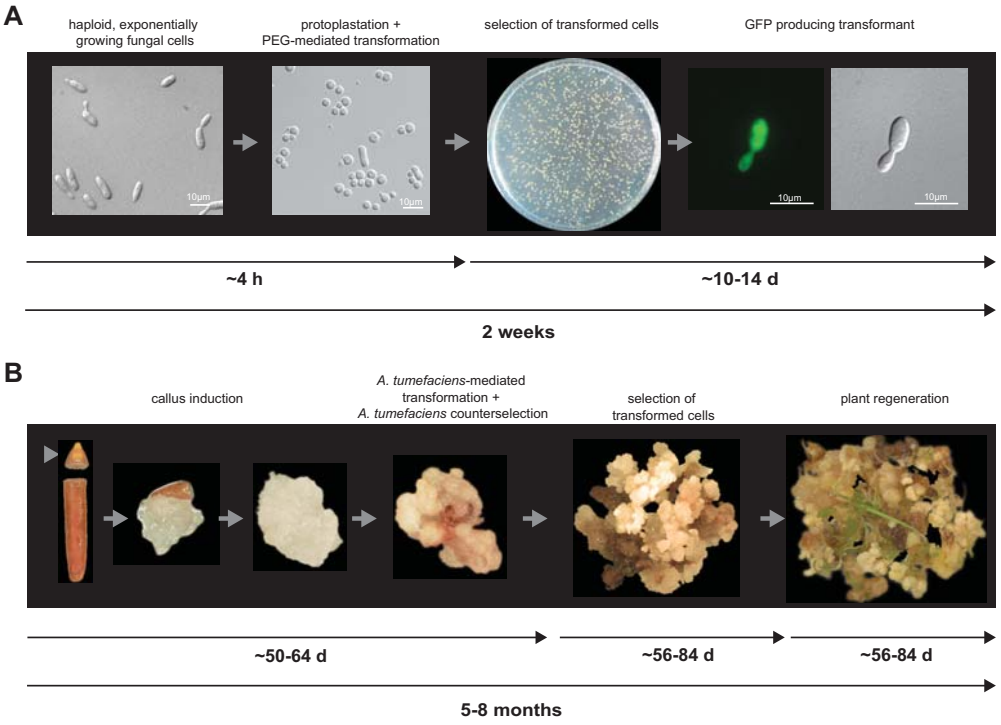

Figure 5. Establishment of transformation for the fungal pathogen *U. bromivora* and its host plant *B. hybridum* Bd28. (**A**) Schematic representation and timeline of protoplastation and transformation of *U. bromivora* UB1 with the autonomously replicating pNEBuC-GFP plasmid conferring Carboxin resistance and encoding GFP. (**B**) Schematic representation and timeline of *A. tumefaciens*-mediated transformation of *B. hybridum* Bd28. Illustrations are not to scale.

DOI: 10.7554/eLife.20522.011

The following figure supplements are available for figure 5:

Figure supplement 1. Several resistance markers can be employed for selection of *U. bromivora* transformants.

DOI: 10.7554/eLife.20522.012

Figure supplement 2. UB2 can mate with UB1-GFP, form filaments, and produce viable spores.

DOI: 10.7554/eLife.20522.013

Figure supplement 3. Microscopy of transgenic Bd28 eCFP-SKL marker line.

DOI: 10.7554/eLife.20522.014

compatible and incompatible interactions with *U. bromivora* without switching pathosystems. The discovery of several *Brachypodium* accessions resistant to *U. bromivora*, comprising accessions of *B. distachyon*, *B. stacei*, and *B. hybridum*, suggests that resistance likely evolved in a common ancestor of *B. distachyon* and *B. stacei*. As there is evidence that *B. hybridum* is the product of an interspecies cross between these two diploid taxa (***Petersen et al., 2011***), this scenario would suggest that smut resistance was independently lost several times in each taxon. Alternatively, resistance based on single or even multiple factors could have evolved independently several times in the different closely related species. Within the limits of a relatively small sample size we observe a trend of *B. hybridum* accessions to be susceptible to *U. bromivora*. This could be due to suppression of resistance in polyploid genomes, a previously described phenomenon found in tetra- and hexaploid wheat (***Knott, 2000***; ***Kerber, 1991***).

Since Bd28 is an excellent host for *U. bromivora* and needs only very short vernalization to induce flowering and to show infection symptoms, we used this accession for the establishment of a model host. To this end, we developed an efficient growth and infection method providing high germination rate, reliable floral induction, and high infection rate by *U. bromivora* (for details see Material and Methods). These protocols could be also applied for the diploid and sequenced accession

ABR4. However, in contrast to Bd28, ABR4 requires a minimum of four weeks vernalization to induce flowering and needs six weeks of vernalization to induce fast bulk flowering. 95 days after the initiation of vernalization, flowering of ABR4 is completed and we observed infection rates of almost 100%. Due to its shorter vernalization requirement, Bd28 can complete its life cycle in approximately 70 days. Interestingly, different time points of spore inoculation as well as the spore load seem to lead to varying infection efficiency. We regularly observed infected plants showing a few healthy spikelets beside spore-filled ones (data not shown). The presence of healthy spikelets might be the evolutionary result of a sustainable virulence strategy of this host-specific, biotrophic pathogen to avoid complete sterilization of its host and therefore its local extinction.

Transformation establishment for *U. bromivora* and its host *B. hybridum* Bd28

The establishment of transformation protocols for both the pathogen and its host plant is an important requirement to employ *U. bromivora and Brachypodium* sp. as a genetically accessible biotrophic model system.

For initial transformation tests of *U. bromivora*, we used the self-replicating pNEBuC-GFP and pNEBuC-mCherry-HA vectors, which were developed for *U. maydis* (**Brachmann, 2001**). These plasmids contain a gene conferring Carboxin resistance and a gene encoding either the green fluorescent protein (GFP-HA) or mCherry-HA protein. *GFP-HA* or *mCherry-HA* are under control of the artificial *otef* promoter, which is constitutively active in axenic culture (**Spellig et al., 1996**). Expression of these genes allows a fast readout of the transformation efficiency. Although different transformation protocols were tested, PEG-mediated protoplast transformation turned out to be most efficient (average transformation efficiency: 314 colonies per µg plasmid DNA; **Figure 5A**). Since appropriate selection markers are essential for high-efficiency transformations, we concomitantly tested three different antibiotics and selection markers. While wild type cells could not be propagated, transformants harboring self-replicating plasmids conferring Carboxin, Geneticin G418, or Hygromycin resistance were able to grow on respective selection media (**Figure 5—figure supplement 1**). We also tested integrative constructs for various loci such as the mating type region or the predicted *pep1* gene locus, encoding an effector ortholog that has been shown to contribute to virulence in *U. maydis* (**Doehlemann et al., 2009**). However, our results suggest, that in contrast to *U. maydis,* DNA uptake or other steps during transformation seem to be less efficient in *U. bromivora* preventing high transformation rates and strongly reduced the number of stable integration events. Therefore, we conducted a restriction enzyme mediated integration (REMI) approach which should promote genomic integrations (**Bölker et al., 1995**). By employing this technique, we obtained a UB1 derivative with a stable integration of *GFP* driven by the *otef* promoter (UB1-GFP). To ensure that after REMI mutagenesis, UB1-GFP has retained its capability to infect, we inoculated germinating Bd28 caryopses with a mixture of UB1-GFP and UB2. Spore-filled spikelets and GFP producing progeny derived from these spores demonstrated a successful infection and completion of the fungal life cycle (**Figure 5—figure supplement 2**).

To establish transformation for the *B. hybridum* accession Bd28, we adapted a Bd21 transformation protocol (**Vain et al., 2008**) for its specific needs (**Figure 5B**). As a proof of principle, we generated transgenic lines harboring a fluorescently tagged peroxisome-targeting construct (eCFP-SKL). On the one hand, this construct provides a fast visual read out of a successful transformation; on the other hand, respective transgenic lines might be a valuable tool for studying cell biological questions in *Brachypodium* sp. (**Figure 5—figure supplement 3**).

The genome of *U. bromivora*

By comparative rDNA analysis, *U. hordei* has been shown to be the most closely related smut to *U. bromivora* that has been sequenced to date (**Stoll et al., 2005**). The presence of extensive repetitive elements and transposable elements (TE) in the *U. hordei* genome complicated its genome assembly (**Laurie et al., 2012**). To circumvent possible assembly problems with the related *U. bromivora* genome, we performed Single Molecule Real-Time (Pacific Biosciences, Menlo Park, CA) sequencing of UB1, the isolated MAT-1 strain. PacBio sequencing has been shown to deliver long reads, facilitating fast and accurate genome assembly. After subread filtering, 376,645 reads (3.1 Gb total) with 84.5% accuracy and a mean length of 8,186 bp (approximately 154x coverage of the ~20.7 Mb

Table 2. Genome comparison of sequenced smut fungi.

	U. bromivora	*U. maydis*[1]	*S. reilianum*[2]	*S. scitamineum*[3]	*U. hordei*[4]	*M. pennsylvanicum*[5]
Assembly statistics						
Total contig length (Mb)		19.7	18.2	19.5	20.6	19.2
Total scaffold length (Mb)	20.5	19.8	18.4	19.6	21.15	19.2
Average base coverage	154x	10x	20x	30x	25x	339x
N_{50} contig (kb)		127.4	50.3	37.6	48.7	43.4
N_{50} scaffold (kb)	877	817.8	738.5	759.2	307.7	121.7
Chromosomes	23	23	23		23	
GC-content (%)	52.4	54	59.7	54.4	52	50.9
coding (%)	54.4	56.3	62.6	57.8	54.3	54
non-coding (%)	49.4	50.5	54.3	51.1	43.4	46.9
Coding sequence						
Percent coding (%)	59.8	61.1	65.9	62	57.5	56.6
Average gene size (bp)	1699	1836	1858	1819	1705	1734
Average gene density (gene/kb)	0.35	0.34	0.36	0.34	0.33	0.33
Protein-coding genes	7233	6786	6648	6693	7113	6279
Exons	11154	9783	9776	10214	10907	9278
Average exon size	1101	1230	1221	1191	1107	
Exons/gene	1.5	1.44	1.47	1.5	1.53	1.48
tRNA genes	133	111	96	116	110	126
Secretome						
Predicted secreted proteins	409	485	461	466	405	300
Non-coding sequence						
Introns	3921	2997	3103	3521	3161	2999
Introns/gene	0.54	0.44	0.46	0.53	0.44	0.48
Average intron length (base)	163	142	144	130.1	141	191.4
Average intergenic distance (bp)	1054	1127	929	1114	1186	1328
Repeat sequences						
DNA Transposon	1.89%	0.29%	0.13%	0.25%	0.89%	0.29%
LINE	4.38%	0.35%	0.04%	0.27%	4.62%	0.40%
SINE	0.18%	0.05%	0.03%	0.05%	0.27%	0.10%
LTR Retrotransposon	5.83%	1.15%	0.13%	0.69%	4.82%	1.17%
Unclassified non LTR-Retrotransposon	0.06%	0.02%	0.01%	0.01%	0.10%	0.032
Unclassified Retrotransposon	2.03%	0.21%	0.12%	0.29%	1.47%	0.39%
Unclassfied	0.06%	0.08%	0.02%	0.08%	0.38%	0.04%
Total TE class	14.33%	2.11%	0.45%	1.60%	11.84%	2.32%
Simple sequence repeats	1.31%	1.75%	2.00%	1.59%	1.59%	1.54%
Total excl. Tandem repeats	15.72%	3.90%	2.49%	3.23%	13.56%	3.95%
Tandem repeats	5.14%	4.22%	6.97%	4.54%	5.20%	5.16%
Total repeat coverage	18.51%	6.70%	8.26%	6.68%	16.45%	6.72%

[1]***Kämper et al., 2006***; [2]***Schirawski et al., 2010***; [3]***Dutheil et al., 2016***; [4]***Laurie et al., 2012***; [5]***Sharma et al., 2014***

DOI: 10.7554/eLife.20522.015

genome) were obtained. Assembly and polishing resulted in 25 contigs of which 23 showed good synteny with the optically mapped synthetic chromosomes of *U. hordei* (***Laurie et al., 2012***). Based on this, *U. bromivora* has 23 chromosomes (20.5 Mb), the mitochondrial genome and an unassigned

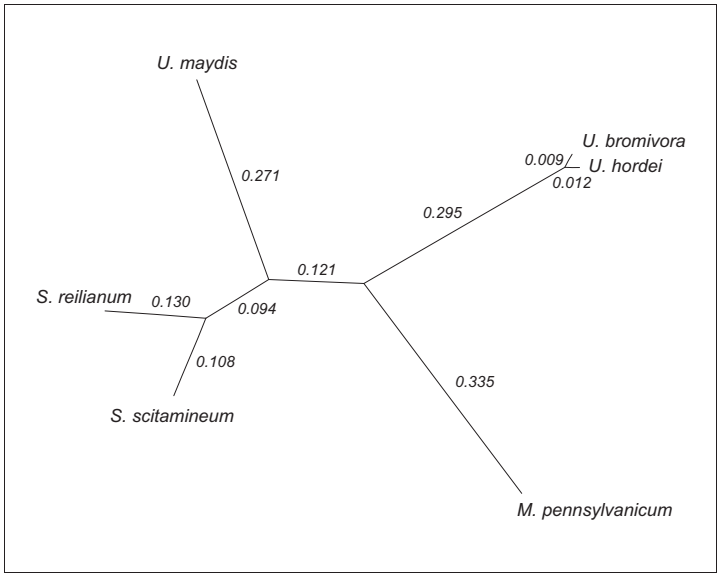

Figure 6. Phylogeny of *U. bromivora* and related smuts. Unrooted phylogeny created from 4,947 one-to-one orthologs. Branch lengths represent the mean number of substitutions per DNA site. Terminal branch lengths for *U. bromivora* and *U. hordei* are not to scale.
DOI: 10.7554/eLife.20522.016

smaller contig. Gene model prediction led to the identification of 7,233 protein coding genes (***Table 2***). All gene models were manually curated by extensive comparative analysis to the existing Ustilaginaceae annotations and 82.3% of all gene models were confirmed by assembled transcripts obtained from Illumina-based RNA-seq of axenically grown UB1. With 7,233 protein coding genes, *U. bromivora* harbors 120 more genes than the close relative *U. hordei* that has an assembled genome 0.65 Mb larger than *U. bromivora* (***Laurie et al., 2012***). The compactness of the *U. bromivora* genome is underscored by the fact that 67.9% of the genes are intron-less, 19.3% have one intron, whereas only 12.8% are predicted to contain multiple introns.

To assess the completeness of the *U. bromivora* genome, a BLAST search was performed with highly conserved core genes present in higher eukaryotes (***Aguileta et al., 2008***; ***Parra et al., 2009***). From the expected 248 single-copy orthologs extracted from 21 genomes (***Parra et al., 2009***), 247 are present in the *U. bromivora* genome (missing KOG1468, translation initiation factor eIF-2B), indicating that >99% of the gene space is covered by the assembly.

To assess the difference of UB1 and its compatible mating partner UB2 on a genomic level, we performed Illumina 125 paired-end sequencing of UB2 and single nucleotide polymorphism (SNP) calling. By using stringent parameters, we identified 1,323 SNPs between the two strains (***Figure 7—source data 1***). 783 of them are found in coding sequences and 429 lead to non-synonymous mutations. Since UB1 and UB2 were independently isolated from different spores, SNPs might be a result of the prevalent inbreeding due to intratetrad mating which over time leads to significant differences between progenies of different spore tetrads.

We constructed a phylogenetic tree using one-to-one orthologous genes as identified by OrthoMCL (***Figure 6***). The resulting phylogeny shows *Sporisorium reilianum* and *Sporisorium scitamineum* forming one cluster and *U. bromivora* and *U. hordei* forming a second cluster. *U. maydis* shows a closer relationship to the tested species of the *Sporisorium* genus than to the ones of the *Ustilago* genus that are more closely related to *Melanopsichium pennsylvanicum*. This is in agreement with the relationships found by ***Stoll et al. (2005)*** and ***Sharma et al. (2014)*** . The phylogeny also illustrates the close relationship between *U. hordei* and *U. bromivora*, which share orthologs for a large number of genes and between which protein sequence conservation is much higher than between other fungi (data not shown).

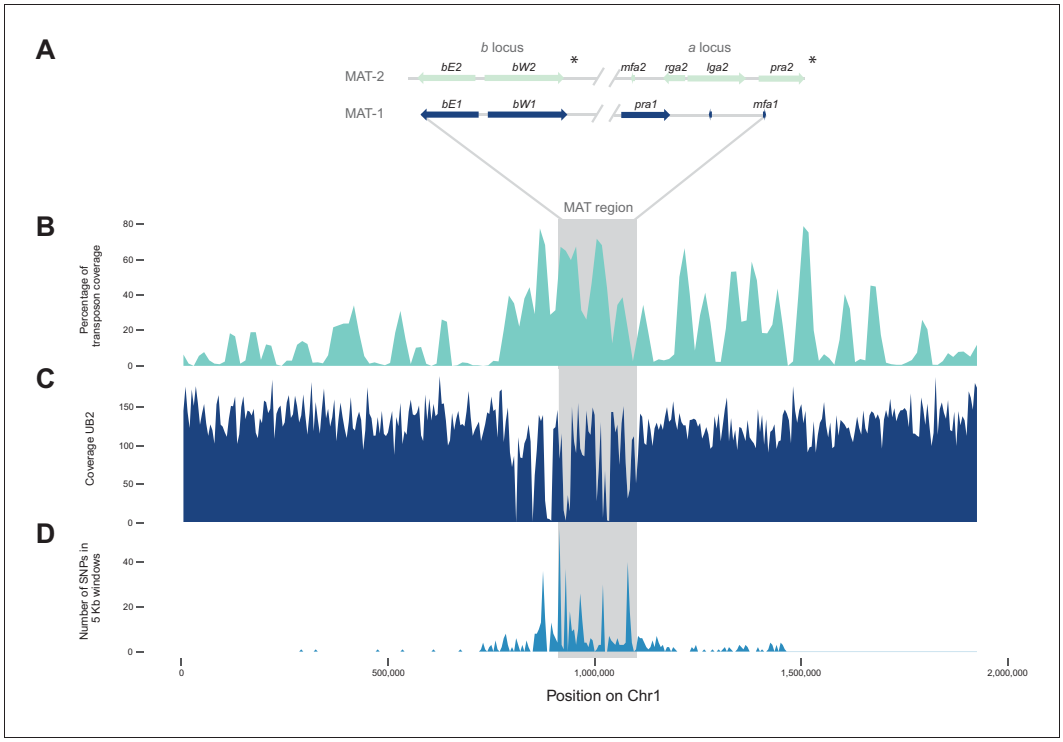

Figure 7. The mating type chromosome (chromosome 1) of *U. bromivora* UB1 (MAT-1) and UB2 (MAT-2). (**A**) Schematic representation of the *a* locus (encoding the predicted pheromone receptor system) and the *b* locus (encoding the putative heterodimeric transcription factor for pathogenic development) of UB1 (MAT-1 strain) and UB2 (MAT-2 strain) according to de novo assembly of both strains. Potential *rga2* and *lga2* orthologs, encoding proteins for uniparental mitochondrial inheritance (***Fedler et al., 2009***), are located in the *a2* region between *mfa2* and *pra2*. *Due to rearrangements in the mating type region of UB2, the orientation of *a2* and *b2* locus could not be exactly determined. However, data suggest an inversion of the *a2* locus. (**B**) The mating type region of UB1 is enriched for transposable elements. Graph depicts percentage of transposon coverage in 25 kb windows occurring every 12.5 kb along the chromosome. (**C**) Mapping of UB2 to the UB1 reference genome shows large non-mapped stretches in the MAT-1 locus indicating sequence differences in this region between MAT-1 and MAT-2. (**D**) Enrichment of single nucleotide polymorphisms (SNPs) in and around the mating type region between the genomes of UB1 and UB2. Number of SNPs is shown in 5 kb windows.

DOI: 10.7554/eLife.20522.017

The following source data and figure supplements are available for figure 7:

Source data 1. List of Single Nucleotide Polymorphisms (SNPs) identified in UB2.

DOI: 10.7554/eLife.20522.018

Figure supplement 1. Transposon content along *U. bromivora* chromosomes.

DOI: 10.7554/eLife.20522.019

Figure supplement 2. Genes of the mating type regions are up to 98% identical between *U. bromivora* and *U. hordei*.

DOI: 10.7554/eLife.20522.020

The mating type chromosome

The mating type locus of *U. bromivora* UB1 is located on chromosome 1. We identified genes encoding a putative pheromone receptor (UBRO_03901) and pheromone (UBRO_03899) as well as bEast (UBRO_00885) and bWest (UBRO_00887) orthologs encoding a putative homeodomain-transcription factor (***Figure 7A***). The pheromone/receptor genes (*a* locus) are separated from the *bEast* and *bWest* genes (*b* locus) by a 183 kb long region highly enriched in transposable elements (TE; 39.85% compared to an average of 17.18% over the length of the chromosome and to an overall genome average of 14.33%; ***Figure 7B***, ***Figure 7—figure supplement 1***). This bipolar mating system resembles the structural organization found in the close relative *U. hordei* although the region

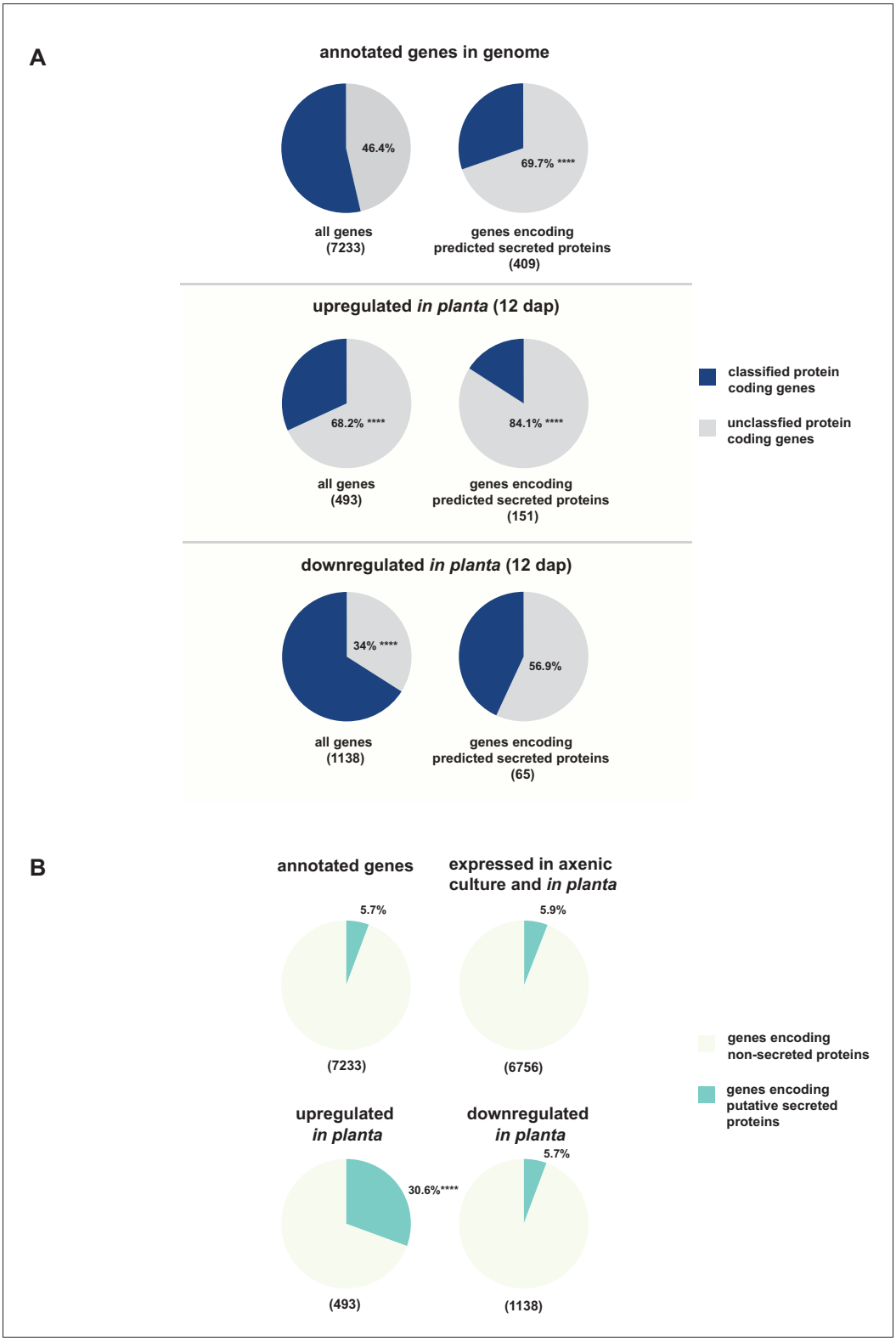

Figure 8. Enrichment of classes of interest among predicted secreted proteins and *in planta* differentially expressed transcripts. (**A**) Proportions of genes encoding unclassified proteins based on FunCat classification within all annotated *U. bromivora* genes, within genes encoding secreted proteins, within all genes up- and downregulated *in planta* twelve days after planting (dap) as well as within the genes that are differentially regulated and encode secreted proteins. (**B**) Proportions of genes encoding predicted secreted proteins within all annotated *U. bromivora* genes, within all genes

Figure 8 continued on next page

Figure 8 continued

found to be expressed in axenic culture and *in planta*, and within genes significantly up- or downregulated *in planta*. Fisher exact test was used to test whether the proportion of selected genes within a given class differs significantly from the proportion within all annotated genes; ****p-value < 0.0001, ***p-value < 0.001. The total number of genes is shown in brackets below each chart.

DOI: 10.7554/eLife.20522.021

The following figure supplement is available for figure 8:

Figure supplement 1. Functional categorization of putatively secreted proteins and all proteins encoded in the genome.

DOI: 10.7554/eLife.20522.022

between the *a* and *b* locus in *U. hordei* is, at ~500 kb, larger (***Figure 7—figure supplement 2***) (***Bakkeren and Kronstad, 1994***).

Mapping of Illumina reads from UB2 to the UB1 reference genome and subsequent SNP calling showed that the mating type region flanked by the *a* and *b* loci is highly diverse between the two compatible strains, as evidenced by segments depleted of reads, rearrangements and a high number of SNPs in the regions covered (***Figure 7C,D***; ***Figure 7—source data 1***). We calculated for the mating type region a SNP frequency of 1.8E-03 SNPs bp^{-1} compared to a frequency of 6.5E-05 SNPs bp^{-1} for the entire genome. This sequence divergence is likely a result of recombination suppression in the mating type region leading to a bipolar mating system at the cost of losing a recombination-based repair in this region.

Analysis of genes encoding putatively secreted proteins

One class of proteins which is of special interest for biotrophic interactions is secreted proteins. In addition to functions such as cell wall remodeling and hydrolytic enzymes for substrate degradation, this class includes effector proteins, which might directly impact the outcome of the biotrophic interaction with the host and often target the host defense system or its metabolism (***Asai and Shirasu, 2015***). Several criteria had to be fulfilled for a predicted *U. bromivora* protein to be considered a

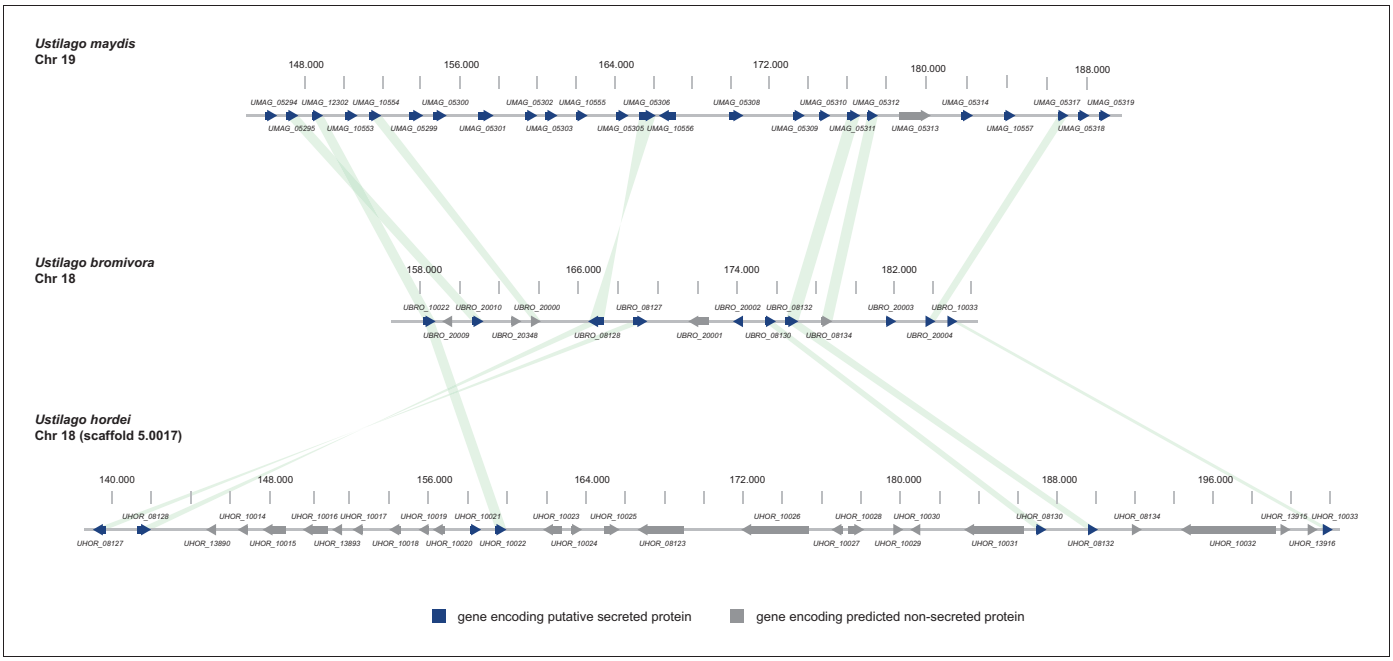

Figure 9. Gene by gene comparison between the largest secreted virulence cluster of *U. maydis* (cluster 19) with the corresponding region in the *U. bromivora* and *U. hordei* genome on chromosome 18. The scheme depicts *U. maydis* cluster 19 on chromosome 19, the predicted *U. bromivora* cluster 18 on chromosome 18 and the corresponding region on chromosome 18 (scaffold 5.0017) of *U. hordei*. Syntenic orthologs between *U. maydis* and *U. bromivora* as well as between *U. bromivora* and *U. hordei* are connected with a green bar. Genes encoding predicted non-secreted proteins are displayed in grey, genes encoding putative secreted proteins in blue.

DOI: 10.7554/eLife.20522.023

secreted protein: it had to contain a signal peptide, fewer than two transmembrane helices, no endoplasmatic reticulum (ER) retention signal, and it had to be predicted not to target mitochondria. These strict criteria led to the prediction of 409 secreted proteins encoded in the *U. bromivora* genome.

The majority of putatively secreted proteins are of unknown function and their transcripts are overrepresented *in planta*

While for 46.3% of all *U. bromivora* proteins we could not assign a potential function based on BLAST sequence similarity ('unclassified proteins'), this fraction increases to 69.7% for the proteins that are predicted to be secreted. This makes proteins of unknown function the most significantly enriched functional category of *U. bromivora* secreted proteins (***Figure 8A***, ***Figure 8—figure supplement 1***).

To provide insights into expression patterns of the genes encoding putatively secreted proteins in *U. bromivora* during saprophytic growth and *in planta*, we conducted RNA-seq analyses. To this end, we isolated RNA from axenic UB1 culture and from stems of twelve day old *B. hybridum* Bd28 plants that were spore-inoculated with *U. bromivora*. Among the 6,756 transcripts found to be expressed in our dataset, 493 were significantly upregulated *in planta* compared to axenic culture (logFC > 2, adjusted p-value < 0.1), while 1,138 transcripts were significantly downregulated. Notably, transcripts predicted to encode secreted proteins are significantly enriched among the upregulated transcripts compared to all annotated genes (30.8% compared to 5.7%; Fisher exact test, p-value $\leq$ 2.2E-16; ***Figure 8B***). Moreover, we could show by functional protein classification that among the putatively secreted proteins that are induced *in planta*, unclassified proteins are significantly overrepresented (84.1% compared to 46.4% within all annotated genes; p-value = 2.2E-16; ***Figure 8A***). In contrast, in the subset of down-regulated genes, a functional overrepresentation of genes encoding secreted, unclassified proteins could not be observed. Our findings are in line with the observation that the vast majority of effector proteins are so far functionally not characterized. At the sequence level these proteins are only poorly conserved between distant fungal pathogens making the prediction of protein function difficult.

The majority of putative *U. bromivora* effectors are not clustered

In the case of *U. maydis,* many of the small secreted protein encoding genes are organized in pathogenicity clusters and a large number of them were shown to play a role in virulence (***Kämper et al., 2006***). To assess the presence of potential pathogenicity clusters in the *U. bromivora* genome, we defined clusters as containing at least three adjacent genes encoding predicted secreted proteins or three genes encoding secreted proteins interrupted by maximal one single non-secreted protein-coding gene. These in comparison to the analysis of ***Kämper et al. (2006)*** relatively relaxed criteria led to the identification of only eleven secretion clusters comprising a total of 10.51% of all putative secreted proteins of *U. bromivora*. Although some of the putative effector clusters identified in *U. maydis* also show a syntenic organization in the *U. bromivora* genome, many others do not and the vast majority of the predicted secreted proteins of *U. bromivora* are not clustered. Among all clusters, the largest is cluster 18, related to *U. maydis* cluster 19. Whereas cluster 19 (as located on chromosome 19) in *U. maydis* comprises 24 putative effector genes (***Brefort et al., 2014***), the syntenic cluster in *U. bromivora* comprises less than half the number of putative secreted protein encoding genes and is located on chromosome 18 (***Figure 9***). In the close relative *U. hordei* the clustering of genes encoding predicted secreted proteins in this region is even less compact and disrupted to a greater extent than in *U. bromivora* (***Figure 9***) (***Laurie et al., 2012***). Our analysis of the *U. bromivora* clusters further showed that the syntenic genes missing from cluster 18 have not moved to other parts of the genome but are simply absent from *U. bromivora* and occur only in *U. maydis* or are shared between *U. maydis*, *S. reilianum*, and *S. scitamineum* (data not shown).

Orthologous and orphan genes

One indication of how suitable a specific model system is for generalizing knowledge to other related species is the presence of orthologous genes. Excluding mitochondrial genes, among the 7,193 genes present in the *U. bromivora* genome, 5,121 one-to-one orthologs were predicted with *U. maydis*, *U. hordei*, *S. scitamineum*, *S. reilianum*, *and M. pennsylvanicum*. These one-to-one

A

U. maydis		*U. bromivora*	Identity (%)	Similarity (%)
UMAG_02239	(See1)	UBRO_03678	32.77	41.11
UMAG_01375	(Pit2)	UBRO_02064	32.25	41.93
UMAG_02475	**(Stp1)**	**UBRO_12209**	**41.93**	**47.78**
UMAG_02011	(ApB73)	UBRO_02986	38.88	50.42
UMAG_05731	(Cmu1)	UBRO_07433	46.10	56.69
UMAG_03223	(Mig1)	UBRO_20685	51.02	62.24
UMAG_01987	**(Pep1)**	**UBRO_02965**	**61.41**	**70.10**

B

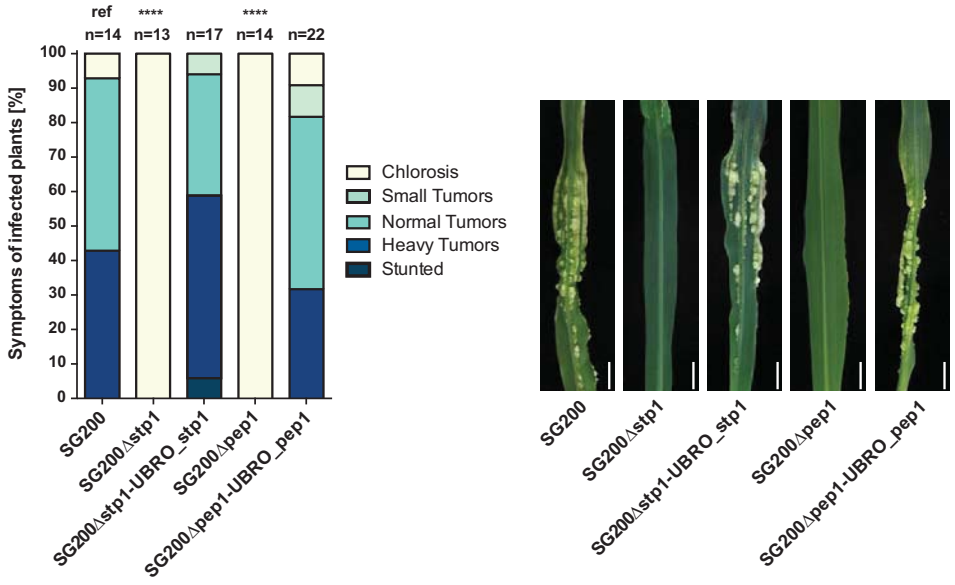

Figure 10. Testing orthologs of core effectors for functional interchangeability between *U. bromivora* and *U. maydis*. (**A**) List of known effector orthologs in *U. bromivora* and *U. maydis* and their amino acid identity and similarity. Identity shows the percentage of identical positions in the alignment, taking gaps into account. Percentage identity = 100 (identical positions / length of alignment). Similarity gives a measure of how similar two protein sequences are to one another based on the physical and chemical properties of their amino acids. Sequences were aligned using T-Coffee and identity and similarity scores were given by SIAS (Sequence Identity and Similarity; http://imed.med.ucm.es/Tools/sias.html). (**B**) Core-effector mutants of *U. maydis* (SG200Δstp1 and SG200Δpep1) can be complemented with the respective *U. bromivora* ortholog. Disease symptoms of infected plants were scored at twelve days post inoculation (dpi) according to ***Kämper et al., 2006***. The darker the color, the more severe the symptoms. Numbers of infected plants are indicated above each column. p-values are calculated by Fisher exact test, MTC by Benjamini-Hochberg algorithm, ****p<0.0001. Leaves of representative plants twelve days after inoculation with indicated strains are shown next to the stacked bar plot. Scale bars: 1 cm.
DOI: 10.7554/eLife.20522.024

orthologs are genes which have one ortholog in each of the other species and no paralogs. *M. pennsylvanicum* and *U. bromivora* share 5,470 orthologs. In contrast, *U. bromivora* shares 5,841 orthologs with *U. maydis* and 6,180 orthologs with *U. hordei*. The lower number of orthologs in *M. pennsylvanicum* is in line with the observation that this smut genome has lost genes that might be associated with a switch from a monocot to a dicot host plant (***Sharma et al., 2014***).

Among the 409 *U. bromivora* predicted secreted proteins, we found 216 of them among the 5,121 one-to-one orthologs. All of the *U. maydis* effectors functionally characterized or described in the literature, including Tin2, See1, Cmu1, Pep1, Pit2 and Mig1 (***Djamei et al., 2011***; ***Redkar et al., 2015a***, ***2015b***; ***Hemetsbergeret al., 2012***; ***Doehlemann et al., 2009***; ***Mueller et al., 2013***;

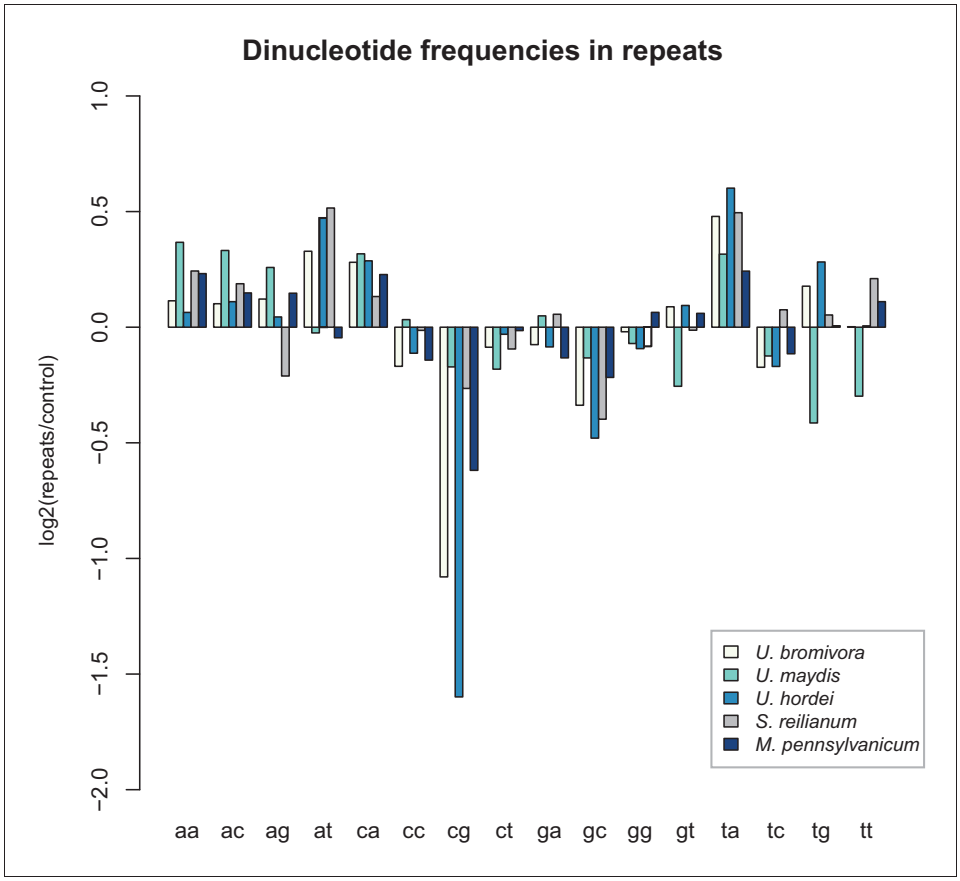

Figure 11. *U. bromivora* shows a decrease in the occurrence of CpG dinucleotides. Dinucleotide frequencies in repeat regions were determined using RIPCAL and were compared to those of control regions. A noticeable decrease in the occurrence of CpG dinucleotides was detectable for both *U. hordei* and *U. bromivora* as well as, to a lesser extent, *M. pennsylvanicum*.

DOI: 10.7554/eLife.20522.025

Basse et al., 2000; ***Tanaka et al., 2014***), share orthologs with *U. bromivora* (***Figure 10A***). The amino acid similarity between each *U. maydis* effector and its corresponding *U. bromivora* ortholog ranges from 41% for the organ specific effector See1 to 70% for the widely conserved peroxidase inhibitor effector Pep1 (***Figure 10A***). To experimentally test if *U. bromivora* effectors can functionally complement their respective orthologs in the *U. maydis* / *Zea mays* pathosystem, we chose two conserved effectors for that assay, Stp1 and Pep1 (***Doehlemann et al., 2009***; ***Schipper, 2009***). These effectors were recently shown to play an essential role for virulence of *U. maydis*. The avirulent phenotype of both *U. maydis* deletion mutants could be complemented by introducing the corresponding *U. bromivora* ortholog (***Figure 10B***). This demonstrates that the *U. bromivora* / *Brachypodium* system could be indeed suitable to study the functional role and host targets of conserved effectors from related species.

Besides the described orthologs, we found 427 orphan *U. bromivora* genes that lack orthologs in the five other fungi they were compared with. Of these, 21 are predicted to encode secreted proteins. None of the orphan genes had a predicted function according to either FunCat or Blast2GO.

Transposable elements and genome defense machinery

Comparing the currently available smut genomes both, *U. hordei* and, to an even greater extent, *U. bromivora* contain a high number of transposable elements and other repetitive sequences, encompassing up to 14.33% of the genome (***Table 2***). Similar to the other smuts sequenced to date, the *U. bromivora* genome has a low frequency of small interspersed nuclear elements (SINEs) (0.18% of the genome), a class of retrotransposons that lost the coding region for their own reverse transcriptase.

Table 3. Positive selection among sequenced smut fungi

	U. bromivora	*U. maydis*	*U. hordei*	*S. scitamineum*	*S. reilianum*	*M. pennsylvanicum*
Genes analysed						
Total	4947	4947	4947	4947	4947	4947
Under selection (q = 0.05)	140	345	188	170	256	2390
Under selection (q = 0.01)	96	116	135	90	91	1434
Non-PSEPs						
Total	4738	4735	4733	4748	4743	4753
Under selection (q = 0.05)	128	318	168	153	240	2287
Under selection (q = 0.01)	86	105	122	81	84	1377
PSEPs						
Total	209	212	214	199	204	194
Under selection (q = 0.05)	12	27	20	17	16	103
Under selection (q = 0.01)	10	11	13	9	7	57

*Number of genes under positive selection in each of the six fungi used in this study. The number of genes predicted to be under positive selection is given for both a FDR of 0.05 and 0.01 and are grouped in three categories: total genes analyzed, the subset of genes that are not predicted to be secreted and the subset of genes that are predicted to be secreted. This analysis is limited to the 4,947 one-to-one orthologs that were used for the construction of the phylogeny.

DOI: 10.7554/eLife.20522.026

However, it contains a high percentage of long terminal repeat (LTR) retrotransposons (5.83%), which are independent from other mobile genomic elements and encode all proteins necessary for transposition. Similar ratios of long interspersed elements (LINE) have spread in the *U. hordei* and the *U. bromivora* genome (4.62% and 4.38%, respectively; ***Table 2***). With few exceptions, such as the mating type chromosome (Chr1), transposable elements are evenly distributed over the *U. bromivora* chromosomes (***Figure 7—figure supplement 1***). These results are in line with those made in *U. hordei*, where except for the mating type region, repetitive sequences are also evenly distributed across the genome (***Laurie et al., 2012***; ***Bakkeren et al., 2006***).

While transposable elements have clearly shaped the genome of *U. bromivora*, their action might be counter-balanced by the presence of a functional core machinery of the RNA interference pathway. Homology searches identified *UBRO_08937* that likely encodes the PAZ-domain (Piwi/Argonaute/Zwille-domain) containing endoribonuclease DICER. *UBRO_20628*, *UBRO_01631*, and *UBRO_08874* encode three RNA-dependent RNA Polymerases (RdRP) which are necessary for the formation of the complementary strands of target RNA, and therefore represent a prerequisite for RNA-directed silencing. *UBRO_06256* is predicted to encode the argonaute protein, the catalytic subunit of the RISC-complex. We also identified the small RNA methyltransferase Hen1 (UBRO_08578). Moreover, the chromodomain (CD) protein CHP1 and CHP2 important for heterochromatic gene silencing are with UBRO_05116 and UBRO_07750 as well present. Analysis of dinucleotide frequencies in repetitive regions of the genome shows a lack of CpG dinucleotides similar to that observed in *U. hordei* (***Laurie et al., 2012***) (***Figure 11***). This may indicate the presence of repeat induced point-mutations (RIP) which can serve as an additional genomic defense mechanism against transposable elements (***Selker, 2002***).

Genes under positive selection in *U. bromivora*

Genes under positive selection are indicative of an ongoing adaptation process often found either upon a host jump, neofunctionalization of a protein, or during the arms race between the host and the pathogen. We analysed the proteins of our six fungal genomes for signs of positive selection. Our analysis of the one-to-one orthologs between the six smut fungi we compared (***Table 3***) confirmed the previously reported finding of high levels of positive selection in *M. pennsylvanicum* (***Sharma et al., 2014***). It also showed that *U. bromivora* has the lowest levels of selection when measured at a false discovery rate (FDR) of 0.05 but is between *U.maydis* and *S. reillianum* when using an FDR of 0.01. Among the genes being under positive selection, only twelve encode predicted

secreted proteins. In contrast to the twelve genes found in *U. bromivora*, *M. pennsylvanicum*, which adapts to its dicot host, harbors 103 genes encoding predicted secreted proteins that were shown to be under positive selection. The evolutionary pressures driving the observed incidents of selection in *U. bromivora* remain unclear.

Conclusion

Smut fungi, especially *U. maydis*, have become models for studying recombination (**Holliday, 1964**), cell biology (**Steinberg et al., 2008**; **Haag et al., 2015**), and, due to their nature, biotrophic interactions (**Brefort et al., 2009**). This has resulted in *U. maydis* being considered as an important model pathogen in the scientific community (**Dean et al., 2012**). In recent years, the importance of small secreted molecules termed effectors, which shape the biotrophic interaction between the pathogen and its host, has become increasingly evident. One major challenge for effector research is that most effector proteins have no sequence similarity to any known protein and are therefore difficult to functionally characterize. Although these important molecules are produced by the pathogen, in many cases they target host processes and therefore require a completely accessible host system for complementary functional studies in both the host and pathogen. In our search to identify a biotrophic model pair for a smut and a temperate host grass that due to their genetic accessibility will enable these complementary functional studies, we chose the smut fungus *U. bromivora* and its compatible host grass *Brachypodium* sp.

Although *U. bromivora* is closely related to other sequenced model smuts, it displays interesting peculiarities in its lifestyle, especially in connection with its mating system. Most strikingly is one major feature: the mating type bias. Upon spore germination and meiosis, the *a* and *b* loci located on chromosome 1 co-segregate, and progeny with two different mating types arise from one spore, MAT-1 and MAT-2. Interestingly, the locus that causes the mating type bias co-segregates with the MAT-2 mating type region leading to the inability to survive under saprotrophic conditions. Independent of its cause, it has important implications for the biology of *U. bromivora*. The bipolar mating system and the intratetrad mating entail a strong tendency for inbreeding which could be an advantageous driving speciation of this highly specialized plant pathogen (**Hoekstra, 2005**). This holds especially true as the pheromone receptor based cell-cell recognition system is rather promiscuous between different smut species and might not be sufficient as a speciation barrier (**Kellner et al., 2011**). Besides the removal of detrimental DNA, like transposable elements and deleterious mutations, sexual reproduction is a way to efficiently reshuffle alleles over generations to provide an opportunity for natural selection to produce efficient allele combinations (**Goddard et al., 2005**; **Lee et al., 2010**). The relative abundance of transposable elements in *U. bromivora* could potentially serve as a source of variation to counterbalance the assumed loss of heterozygosity due to inbreeding between progeny from the same spore. This could enable the population to adapt to evolving challenges such as host defense mechanisms. As a consequence, it might be essential to keep the functional machinery for RNA silencing intact to limit the uncontrolled spreading of transposable elements with potentially deleterious effects. In contrast to *U. bromivora*, *U. maydis* has evolved a very efficient recombination system enabling the removal of most of its invasive transposable elements. This was likely a prerequisite to allow the loss of the silencing machinery in *U. maydis*, which subsequently led to the gain of a competitive advantage through symbiosis with double-stranded RNA totiviruses, which encode for killer toxins that target non-killer containing competitive microbes (**Drinnenberg et al., 2011**; **Koltin and Day, 1976**).

The deleterious allele which leads to the mating type bias in *U. bromivora* is still unidentified. In the related smut *Microbotryum violaceum* (formerly described as *Ustilago violacea*), intratetrad mating was observed as a result of a recessive haplo-lethal allele (**Hood and Antonovics, 2000**). In *Ustilago nuda*, a recessive proline biosynthesis allele linked to the mating type locus led to a similar result in the haploid stage of the dimorphic life cycle (**Nielsen, 1968**). Alternatively, a dominant mechanism via meiotic drive elements as described for *Neurospora crassa* (**Turner and Perkins, 1979**) and other ascomycetes such as *Gibberella fujikuroi* (*Fusarium verticillioides*) (**Kathariou and Spieth, 1982**) and *Podospora anserina* (**Bernet, 1967**) could be causative for the observed mating type bias in *U. bromivora*. While, in this scenario, the 'killer'-allele and 'resistance'-allele would form a locus and would be linked to the recombination-suppressed MAT-1 region, the corresponding 'Non-killer/susceptibility' alleles would co-segregate with the MAT-2 region. The alleles of the MAT-

2 strain would therefore lead to its haplo-lethality. Future research will clarify the cause of the mating type bias in *U. bromivora*.

In summary, the newly established model system *U. bromivora* and *Brachypodium* sp. has tremendous potential for the study of biotrophy related questions on both the pathogen and host side as well as evolutionary questions such as sex and speciation. The high quality, manually curated fungal genome, available RNA-seq data, and growth as well as transformation protocols for both the host and the pathogen, provide a solid basis for scientists to gain new insights into biotrophic plant pathogen interactions.

Materials and methods

Strains, plasmids, and fungal culture conditions

DNA manipulation and plasmid generation were performed according to standard molecular cloning procedures (**Chong, 2001**; **Ausubel et al., 1987**). All DNA manipulations were performed with *E. coli* MACH1 (Thermo Fisher Scientific, Waltham, MA). Primers and plasmids are compiled in **Supplementary file 1**. All sequences of plasmids created in this study are provided as gb/gbk files in **Supplementary file 2**. Strains used in this study are listed in **Supplementary file 1**. The *Ustilago bromivora* spore material used in this study was obtained from Thierry Marcel and originated from spontaneous repetitive infections which occurred in a greenhouse at INRA UMR BIOGER, Avenue Lucien Brétignières BP01, 78850 Thiverval-Grignon, France (**Barbieri et al., 2012**). *U. bromivora* UB1 (formerly named UB2112) and UB2 were cultivated in Potato dextrose (PD) liquid medium (2.4% PD dissolved in H_2O; Becton, Dickinson and Company, Franklin Lakes, New Jersey) at 21°C, shaking at 200 rpm in baffled flasks. *U. maydis* and *U. hordei* were cultivated according to **Kämper et al. (2006)** and **Laurie et al. (2012)**. *U. maydis* strains were generated by gene replacement via homologous recombination as described by **Kämper (2004)** or by insertion of p123 derivatives into the *ip* locus (**Loubradou et al., 2001**).

U. maydis virulence assays

U. maydis virulence assays were performed as described by **Kämper et al. (2006)**. In brief, the solopathogenic strain SG200 and its derivatives were cultivated in $Yeps_{Light}$ (0.4% yeast extract, 0.4% peptone, 2% sucrose) at 28°C, under continuous shaking (200 rpm), until they reached an $OD_{600\ nm}$ of 0.8. After centrifugation at 2400 g for 5 min, cultures were adjusted in H_2O_{dd} to an $OD_{600\ nm}$ = 1. The suspensions were subsequently used for syringe-inoculation of seven day old maize seedlings (variety Early Golden Bantam). Infection symptoms were scored twelve days post infection employing the scoring system described by **Kämper et al. (2006)**.

Genomic DNA extraction for Single Molecule Real-Time (PacBio) and Illumina sequencing

Genomic DNA (gDNA) extraction was performed as previously described for *U. maydis* (**Kämper et al., 2006**). *U. bromivora* cultures were grown to an exponential phase and subjected to Phenol-Chloroform extraction. For Single Molecule Real-Time (PacBio) sequencing of UB1, Phenol-Chloroform extraction was followed by an additional purification step via the Power Clean DNA Kit (MO BIO Laboratories, Carlsbad, CA). For Illumina sequencing of UB2, Phenol-Chloroform extracted gDNA was purified using the MasterPure Complete DNA and RNA Purification Kit (Epicentre, Madison, WI).

Library preparation and Single Molecule Real-Time (PacBio) sequencing

The SMRT bell was produced using the DNA Template Prep Kit 1.0 (Pacific Biosciences, Menlo Park, CA). The input genomic DNA concentration was measured using a Qubit Fluorometer dsDNA Broad Range assay (Thermo Fisher Scientific, Waltham, MA). 10 µg of gDNA was mechanically sheared to an average size distribution of 15 kb, using a Covaris gTube (Kbiosciences, Hoddesdon, UK). A Bioanalyzer 2100 12K DNA Chip assay (Agilent, Santa Clara, CA) was used to assess the fragment size distribution. 5 µg of sheared gDNA was DNA damage repaired and end-repaired using polishing enzymes. A blunt end ligation reaction followed by exonuclease treatment was performed to create the SMRT bell template. A Blue Pippin device (Sage Science, Beverly, MA) was used to size select

the SMRT bell template and enrich for large fragments > 10 kb. The size selected library was quality inspected and quantified on an Agilent Bioanalyzer 12 kb DNA Chip and on a Qubit Fluorimeter (Thermo Fisher Scientific, Waltham, MA), respectively.

A ready to sequence SMRT bell-Polymerase Complex was created using the P6 DNA/Polymerase binding kit 2.0 (Pacific Biosciences, Menlo Park, CA) according to the manufacturer's instructions.

The Pacific Biosciences RS2 instrument was programmed to load and sequence the sample on 5 SMRT cells (v3.0; Pacific Biosciences, Menlo Park, CA), taking 1 movie of 240 min each per SMRT cell. A MagBead loading (Pacific Bioscience, Menlo Park, CA) method was chosen in order to improve the enrichment of longer fragments.

After the run, a sequencing report was generated for every cell via the SMRT portal, in order to assess the adapter dimer contamination, the sample loading efficiency, the obtained average read-length, and the number of filtered sub-reads.

UB1 de novo genome assembly

The genome was assembled with Pacific Bioscience's SMRTanalysis software version 2.2.0 and the hierarchical genome-assembly process (HGAP) v3 protocol (**Chin et al., 2013**) including polishing with Quiver. Default settings were used, except for selecting only reads with a minimum length of 10,000 bp and read quality above 0.8. Assembly and polishing resulted in 25 contigs with an overall length of 20.7 Mb.

Transcriptome assembly

U. bromivora UB1 was grown in axenic culture (21˚C, 200 rpm, PD medium) in three independent biological replicates to an exponential phase ($OD_{600\ nm}$ = 0.8). RNA was extracted using the TRIzol method (**Chomczynski and Sacchi, 2006**) according to the manufacturer's protocol (Thermo Fisher Scientific, Waltham, MA). Residual DNA was removed with the DNA-*free* Kit (Thermo Fisher Scientific, Waltham, MA). The extracted and purified RNA was used for library generation with the NEB Next Ultra RNA Library Prep Kit according to the manufacturer's protocol (cutout size 200–800 bp; New England Biolabs, Ipswich, MA) and was sequenced with an Illumina HiSeq2000 instrument in paired-end 100 mode. The resulting data was pooled to yield 68M read pairs. The overall quality metrics were verified with fastqc (http://www.bioinformatics.babraham.ac.uk/projects/fastqc). The pooled reads were then assembled using Trinity (vr20140413p1) using the built-in trimmomatic quality trimming, in-silico read normalization and jaccard clipping procedures (**Grabherr et al., 2011**). The resulting transcriptome assembly consisted of 11,918 contigs with an N50 of 3,027 bp.

Prediction of open reading frames and proteome analysis

Primary structural annotation was achieved by mapping the protein sequences of *U. hordei* on the scaffolds using exonerate (v2.2.0) unless the protein sequences could not be mapped (**Slater and Birney, 2005**). As a de novo gene predictor, GeneMark-ES version 2 was applied (**Ter-Hovhannisyan et al., 2008**). In addition, the orthologous protein sequences of *U. maydis*, *S. reilianum* and *U. hordei* were inspected by multi T-Coffee (v8.69) alignments to further validate the gene structure in *U. bromivora* (**Notredame et al., 2000**). As transcriptional evidences, RNA-seq reads were mapped on the genome using tophat2 (v2.0.8). The interval for allowed intron lengths was set to a minimum of 20 nt and a maximum of 1 kb (**Langmead et al., 2009**; **Trapnell et al., 2012**). The Trinity assembled RNA reads were mapped as transcripts (**Grabherr et al., 2011**). The different gene structures and supporting evidence were displayed in GBrowse (**Donlin, 2009**), allowing manual validation and correction of all coding sequences. The final call set comprises 7,233 protein coding genes. In addition, 133 tRNA-encoding genes are predicted using tRNAscan-SE (**Lowe and Eddy, 1997**). The protein coding genes were analyzed and functionally annotated using the PEDANT system (**Walter et al., 2009**), accessible at http://pedant.helmholtz-muenchen.de/genomes.jsp?category=fungal. The genome and annotation were submitted to the European Nucleotide Archive (http://www.ebi.ac.uk/ena) under the study number PRJEB7751.

The predicted protein set was searched for highly conserved single (low) copy genes to assess the completeness of the sequence dataset. Orthologous genes to all 246 single copy genes were identified by BLASTP comparisons (eValue: 10^{-3}) against the single-copy families from all 21 species available from the FunyBASE (**Aguileta et al., 2008**). Additionally, 247 of 248 core-genes commonly

present in higher eukaryotes (CEGs) could be identified by BLASTP comparisons (eValue: 10^{-3}) (**Parra et al., 2009**).

Differential expression and overrepresentation analyses in the transcriptomic dataset

For differential expression analysis, RNA from axenic culture of UB1 (see 'Transcriptome assembly') and from seedlings, 12 days after planting of germinating caryopses that were incubated with spore material for 1 week at 4°C, was isolated using the TRIzol method and DNA was removed with the DNA-*free* Kit (Thermo Fisher Scientific, Waltham, MA). After library preparation (cutout size: 200–800 bp; NEB Next Ultra RNA Library Prep Kit; New England Biolabs, Ipswich, MA) three independent biological replicates were sequenced with an Illumina HiSeq2000 instrument, paired-end 100 bp.

RNA-Seq was quantified against the combined transcriptome extracted from *Brachypodium distachyon* Bd21 (Bdistachyon_283_v2.1) and *Ustilago bromivora* UB1 annotations with kallisto using default parameters (**Bray et al., 2016**). In our dataset we identified 20 cases, where more than one splicing variant encoded by the same gene was present. In all subsequent analyses, splicing variants were treated and counted as individual genes. Differential expression statistics between axenic and *in planta* samples were computed using the DeSeq2 R package under the assumption that the overall expression level is similar between the two samples (**Love et al., 2014**). Transcripts were considered significantly up- or downregulated *in planta*, if the log2fold-change compared to axenic culture was $\geq 2/\leq -2$ and the Benjamini-Hochberg (**Hochberg and Benjamini, 1990**) corrected p-value was ≤ 0.1. Over-/underrepresentation of individual functional classes of interest (e.g. predicted secreted proteins) among the *in planta* up- and downregulated transcripts was tested by Fisher exact test in the R statistical environment (**Core Team, R, 2011**). Systematic over-/underrepresentation analysis for all functional classes present in the FunCat annotation of the given dataset was conducted with the FunCat workflow (**Ruepp et al., 2004**). Expression data were submitted to GeneExpressionOmnibus (http://www.ncbi.nlm.nih.gov/geo/) under the accession number GSE87751.

Bioinformatics analysis: Secreted protein prediction, orthologs, and transposons

To predict putative secreted proteins, protein sequences were retrieved from the PEDANT 3 Genome Database and analysed for specific features that are associated with secreted proteins. We used SignalP (v4.0) (**Petersen et al., 2011**) to predict the existence of a signal peptide, TMHMM (v2.0c) (**Sonnhammer et al., 1998**; **Krogh et al., 2001**) to predict the existence of transmembrane domains, Phobius (v1.01) (**Kall et al., 2004**) to detect both signal peptides and transmembrane domains, TargetP (v1.1b) (**Emanuelsson et al., 2000**) to predict the final location of a protein, and ScanProsite (**Gattiker et al., 2002**) to detect the presence of the ER retention motif [KRHQSA]-[DENQ]-E-L. A list of putative secreted proteins was generated that met the criteria of (1) signal peptide predicted by both SignalP and Phobius, (2) fewer than two transmembrane domains predicted by both TMHMM and Phobius, (3) no ER retention motif and (4) not predicted to target the mitochondrion.

Orthologs were detected using OrthoMCL (v2.0.9) using default settings (**Fischer, 2011**). OrthoMCL takes a list of proteins as an input and was provided with the full proteomes of *U. maydis*, *U. bromivora*, *U. hordei*, *S. scitamineum*, *S. reilianum*, and *M. pennsylvanicum*. Orthologous proteins from the different genomes are then sorted into groups. OrthoMCL makes use of the MCL algorithm (**Enright et al., 2002**). Only nuclear genes were used for the prediction of orthologous relationships.

Protein alignments were performed in T-Coffee (v11.00.8cbe486) using the default settings. BLAST searches were performed with the stand-alone BLAST+ suite (**Camacho et al., 2009**) where possible. However, some programs required the older C legacy toolkit. We used RepeatScout (**Price et al., 2005**) for the de novo identification of repeat families in combination with the RepBase database (**Jurka et al., 2005**) to detect previously published transposable elements, pseudogenes, and retroviruses. The combined library of de novo and RepBase repeats were used to identify individual repeat elements on the genome using RepeatMasker (**Smit et al., 1996-2010**). All determined repeat elements were classified using TEclass (**Abrusan et al., 2009**) and analyzed for fingerprints of

repeat-induced point mutations (RIP) regarding overrepresented dinucleotide frequencies using RIP-CAL (**Hane and Oliver, 2008**).

Fungal phylogeny and prediction of positive selection

5,121 genes were predicted as one-to-one orthologs, that means that there was an ortholog detected in each of the six fungal species and there was only a single copy in each genome. After removal of genes that were unsuitable for the positive selection analysis like genes without one-to-one orthologs or which had more than one predicted transcript in one or more species, 4,947 sequences remained. The ORF sequences were converted to amino acid sequences with T-Coffee (v11.00.8cbe486), aligned and then converted back into nucleotide sequences. These nucleotide alignments were concatenated to form a single alignment which was used as the input for RAxML (v8.1.16) (**Stamatakis, 2014**). The tree was generated using the rapid bootstrapping and best-scoring maximum likelihood tree algorithm, GTRGAMMA nucleotide model and 1000 bootstraps.

The individual alignments and the unrooted species tree were used as inputs for the codeml program from PAML 4.8A. (**Yang, 1997**). Two control files were used, both, allowing two or more dN/dS ratios for branches, checking for positive selection and having an initial omega value of 1. One allowed the omega value to vary while the second kept it constant. The likelihood ratios under the two models were compared for each gene with the formula $\Delta LRT = 2 \times (lnL1 - lnL0)$. The resulting value could be assessed using the chi-squared distribution with 1 degree of freedom to determine if the gene was under positive selection or not. Raw p-values were adjusted to take into account the false discovery rate using the qvalue R package (http://qvalue.princeton.edu/, http://github.com/jdstorey/qvalue) (**Storey, 2015**).

Illumina sequencing of UB2, mapping to UB1, and SNP calling

Genomic DNA of UB2 was used for library generation (insert size 600–900 bp; NEBNext Ultra DNA Library Prep Kit for Illumina; New England Biolabs, Ipswich, MA) and sequenced with an Illumina HiSeq2500 instrument in 125 bp paired-end mode. Reads were mapped to the genome of UB1 using CLC Genomics Workbench (v.7.0.3; Qiagen, Hilden, Germany) with the following parameters: mismatch cost = 2, insertion cost = 3, deletion cost = 3, length fraction = 0.5, similarity fraction = 0.8, no global alignment. SNP calling was performed via the quality-based variant detection mode with the following parameters: neighbourhood radius = 4, maximum gap and mismatch count = 2, minimum central quality = 10, non-specific matches, broken pairs and variants in non-specific regions were ignored, minimum coverage = 90, minimum variant frequency = 95%, maximum expected alleles = 2, maximum coverage = 203, sufficient variant count = 85, required variant count = 85. For calling SNPs the presence in both forward and reverse reads was a requirement. Heterozygous SNPs as well as small insertions and deletions were not considered. Moreover, the mitochondrial genome was not included in the analysis.

UB2 de novo genome assembly from Illumina paired-end reads

De novo assembly of the MAT-2 strain UB2 was performed with SOAPdenovo2 (**Luo et al., 2012**) (127mer version 1.4.10) with kmer lengths ranging from 43 to 115 in steps of 6 with the following parameters: max_rd_len = 120, avg_ins = 470, asm_flags = 3, rd_len_cutoff = 120, rank = 1, pair_num_cutoff = 3, map_len = 32. While assemblies with kmer lengths 73–91 performed good at diverse metrics, kmer 91, at 4,712 bp and 8,160 bp, had the best mean size for both contigs and scaffolds, respectively, and the highest number of contigs larger than 100 kb. The resulting assembly (kmer 91) had a contig and scaffold N50 of 23,058 bp and 113,827 bp. Scaffolds obtained after de novo assembly as well as the raw sequencing reads were submitted to the European Nucleotide Archive (http://www.ebi.ac.uk/ena) under the study number PRJEB7751.

Spore recovery and sterilisation

Infected spikelets were dehusked and ground with a pistil in a 1.5 ml microcentrifuge tube. After the addition of 250 µl water, grinding continued until a black spore suspension was visible. The spore suspension was subjected to $CuSO_4$ treatment to kill vegetative fungal cells and bacteria. $CuSO_4$ was added to the suspension at a final concentration of 1.5%, solution and spores were incubated for 15 min, and washed 3 times with water to remove all traces of $CuSO_4$. $CuSO_4$-treated spore

material was resuspended either in 500 µl of water supplemented with 100 µg ml^{-1} ampicillin, 50 µg ml^{-1} tetracycline, and 25 µg ml^{-1} chloramphenicol and plated on PD agarose plates (2.4% PD supplemented with 2% agarose) in serial dilutions for the isolation of haploid progeny or resuspendend in 1 ml of the above-mentioned antibiotic solution and spotted on objective slides for microscopy.

WGA, FM4-64, and DAPI staining

Cell walls of fungal hyphae were stained with the chitin specific Wheat Germ Agglutinin - Alexa Fluor 488 conjugate dye (WGA-AF 488; Thermo Fisher Scientific, Waltham, MA). Plant membranes were stained with FM4-64 (Thermo Fisher Scientific, Waltham, MA). Staining and confocal laser scanning microscopy was performed as previously described by ***Doehlemann et al. (2008)***. For DAPI and WGA staining of germinating spores and sporidia, germinating spores/sporidia were pelleted and fixed by incubating them with acetone for 15 min. Fixation was followed by 10 min incubation with WGA-AF 488 to visualize fungal cell walls and 15 min incubation with 1 µg ml^{-1} DAPI solution (Sigma-Aldrich, Taufkirchen, Germany) to stain nucleic acid. Cell/spore pellets were resuspended in PBS and subjected to confocal laser scanning microscopy. Images were acquired with a LSM780 Axio Observer confocal laser scanning microscope (Zeiss, Jena, Germany). WGA-AF excitation was at 488 nm and detection at 517–552 nm, DAPI excitation at 405 nm and detection at 421–508 nm.

Monitoring of germination by microscopy

$CuSO_4$-treated spore suspensions were spotted on objective slides (µm dish 35 mm; IBIDI, Planegg, Germany). After freezing them for 20 min on a metal block to avoid spreading of the liquid, they were covered with a thin (<2 mm) layer of PD agar or 1.5% water agar, respectively. After a 15–17 hr incubation at 21°C, the picture acquisition was performed with an inverted microscope (Zeiss Axiovert 200 M with 40×/1.3 Plan-Neofluar Oil objective). Picture acquisition occurred every 20 min. Image processing was done with Fiji Imaging software.

Transformation of *U. bromivora*

The transformation protocol was adapted from ***Schulz et al. (1990)*** and ***Gillissen et al. (1992)***. *U. bromivora* cells were grown to an $OD_{600\ nm}$ of 0.3–0.6. Cells were harvested at 2400 g (10 min, RT), and washed once with Mg^{2+}-MES buffer (20 mM MES buffer, pH 5.8, 1 M $MgSO_4$). The Pellet was resuspended in 1 ml Mg^{2+}-MES buffer containing 10 mg ml^{-1} Glucanex (Sigma-Aldrich, Taufkirchen, Germany) and 5 mg ml^{-1} Yatalase (Takara Bio, Saint-Germain-en-Laye, France) and kept on ice. Protoplastation was monitored and stopped by addition of 10 ml ice-cold Mg^{2+}-MES buffer when 30–40% of the cells appeared round due to the loss of the cell wall. Cells were washed 3 times (2400 g, 10 min, 4°C) in Mg^{2+}-MES and once in STC buffer (STC: 100 mM $CaCl_2$, 10 mM Tris-HCL pH 7.5, 0.9 M sorbitol). Protoplastation was followed by PEG-mediated transformation. To this end, 5 µg plasmid DNA and 1 µl 100 mg ml^{-1} Heparin were added to 100 µl protoplasts and incubated for 30 min on ice. 500 µl STC-PEG (40% PEG4000 in STC buffer) were added and mixed by pipetting gently up and down. After 15 min incubation on ice, the mixture was plated on PD regeneration agar plates composed of an lower layer of PD regeneration agar with twice the concentration of antibiotic (2.4% PD, 0.9 M sorbitol, 1.5% agar supplemented with either 4 µg ml^{-1} Carboxin, 200 µg ml^{-1} Geneticin G418, or 200 µg ml^{-1} Hygromycin B) overlaid by an antibiotic-free layer of PD regeneration agar. Colonies were visible after 10 to 14 days. For stable genomic integrations, restriction enzyme mediated transformation was performed according to ***Bölker et al. (1995)***. In brief, 25 U of the restriction enzyme XbaI and XbaI-linearized p123UB-GFP were added to protoplasts and the aforementioned transformation protocol was followed immediately after addition of enzyme and plasmid.

Plant growth conditions and sexual propagation

Caryopses of *B. distachyon* accession Bd21 were kindly provided by Phillipe Vain (***Vain et al., 2008***), caryopses of accession ABR4 by John Vogel. For production of donor material, caryopses of each accession were gas-sterilized and transferred to Ø = 10 cm pots with a 4:1 mixture of standard potting soil (Einheitserde Werkverband e.V., Sinntal-Altengronau, Germany) and perlite (Granuflor, Vechta, Germany). Germination and early plant growth took place in a phyto chamber (Johnson Controls, Milwaukee, WI) under the following conditions: 20 hr light (150 µE), 24°C; 4 hr dark, 18°C; 60% humidity. After 10 days, pots were transferred to a cold room to vernalize plants for 6 weeks at

4˚C, 40 µE, 13 hr light period. Pots were then moved back to the phyto chamber to allow plants to flower. Four weeks after anthesis, plants were transferred to the greenhouse for caryopses maturation and drying. Harvested caryopses were stored at 4˚C in the dark.

Surface-sterilization of *B. distachyon* caryopses, vernalization, and infection with *U. bromivora* spores and planting

Caryopses within husks were gas sterilized (***Clough and Bent, 1998***). After sterilization, caryopses were moistened with a few ml of sterile water without submerging the caryopses and incubated in the dark at 4˚C for 1 week to germinate. The seedlings were then moistened with a spore/water suspension for infection for one additional week at 4˚C in the dark. Subsequently the seedlings were potted in a mixture of 3:1:1:1 standard potting soil (Einheitserde Werkverband e.V., Sinntal-Altengronau, Germany): perlite (Granuflor, Vechta, Germany): silica sand (min2C GmbH, Melk, Austria): germination soil (Neuhaus 'Huminsubstrat', Klasmann-Deilmann GmbH, Geeste, Germany), at a depth of ~1 cm, so that the emerged shoot remained exposed to the air and light. After 10 days in the growth chamber (20 hr light (150 µE), 24˚C; 4 hr dark, 18˚C; 60% humidity) the pots were transferred to 4˚C, 40 µE, 13 hr light period for 3 weeks (Bd28) or 6 weeks (ABR4), for vernalization and subsequently returned to the growth chamber. 4–5 weeks later, the infected, spore filled spikelets were visible.

Screen to isolate a compatible mating partner

U. bromivora spore material was surface sterilized and germinated on PD plates (see spore recovery and sterilization). After spore germination, all derived colonies were pooled and used as an inoculum for further proliferation in liquid PD medium for 24 hr to ensure that only strains, which are viable in axenic culture, would grow. These mixtures were used as an infection inoculum of 300 vernalized *B. hybridum* caryopses (Bd28). After six weeks the infected spikelets were harvested, derived spores were surface sterilized and plated on solid PD medium. Colonies derived from single spores were singled out and tested by diagnostic PCR for the presence of *pra2*.

Infection of *B. hybridum* with *U. bromivora* liquid culture

To infect *B. hybridum* Bd28 with a pair of compatible mating partners, both strains were grown until they reach the exponential phase ($OD_{600\ nm}$ = 0.8) and set to an $OD_{600\ nm}$ = 2 with H_2O_{dd}. Both strains were mixed in equal amounts. One or two days before inoculation, vernalized *B. hybridum* caryopses were placed to RT to promote germination. Upon inoculation with the fungal mixture, the onset of coleoptiles should be visible. Seedlings were moistened with the fungal mixture and incubated in an appropriate tube, e.g. 2 ml microcentrifuge tube, at 21˚C in the dark. After 24 hr incubation, seedlings were potted.

Callus culture generation of Bd28

Mature embryos from dormant caryopses were used for callus culture, plant regeneration, and transformation. In brief, dry dormant caryopses were surface-sterilized for 45 min with 6% NaClO including 0.03% Tween20. After surface-sterilization, caryopses were rinsed five times with sterile tap water. Embryo preparation was carried out in two steps. First, the embryo was cut away from the endosperm. Second, the embryo was cut in a longitudinal direction into two pieces. Forty bisected embryos were transferred to a Ø = 10 cm petri dish with longitudinal wound in direct contact with the callus induction medium (CIM). Callus induction of *B. hybridum* Bd28 took place on CIM (4.3 g l^{-1} MS No.4 (Murashige and Skoog medium modification No. 4; Duchefa Biochemie, Haarlem, The Netherlands), 30 g l^{-1} maltose, 11.1 µM 2,4-D, 2 mM NH_4NO_3, 1.9 mM MES-monohydrate, 1x B5 vitamin mixture (Duchefa Biochemie, Haarlem, The Netherlands), 3.5 g l^{-1}phytagel (Sigma-Aldrich, Taufkirchen, Germany), pH 5.8. Before transformation, bisected embryos were pre-cultured for 6–8 weeks at 24˚C without light. Every 14 days, calli were transferred to fresh CIM. Developing roots and shoots were cut away.

A. tumefaciens-mediated transformation of *B. hybridum* Bd28

Agrobacterium tumefaciens strain AGL1 was used for transformation (***Lazo et al., 1991***). The plant transformation vector p6U contains a hygromycin phosphotransferase gene driven by the *Zea mays*

ubiquitin promoter to confer hygromycin resistance to transformed plant cells. For *B. hybridum* Bd28 transformation, AGL1 harboring the respective p6U derivative was cultivated at 28˚C and 210 rpm in Erlenmeyer flasks containing 10 ml MG/L medium (***Jones et al., 2005***) supplemented with 100 µg ml^{-1} Carbenicillin, 50 µg ml^{-1} Rifampicin, and 100 µg ml^{-1} Spectinomycin. After 22 hr, 500 µM Acetosyringone (Sigma-Aldrich, Taufkirchen, Germany) was added and the p6U-containing AGL1 strain was cultivated for additional 2 hr. For inoculation of pre-cultured *B. hybridum* calli, the *A. tumefaciens* culture was diluted with infection solution (4 g l^{-1} Chu (N6) minerals (Duchefa Biochemie, Haarlem, The Netherlands), 6.75 µM 2,4-D, 36 g l^{-1} glucose, 68.4 g l^{-1} sucrose, 0.7 g l^{-1}, 6 mM L-proline, 1x Chu (N6) vitamin mixture (Duchefa Biochemie, Haarlem, The Netherlands), 500 µM Acetosyringone (Sigma-Aldrich, Taufkirchen, Germany), pH 5.2) to $OD_{550\ nm}$ = 0.8.

6–8 weeks after callus induction, forty calli were transferred into 15 ml tubes and inoculated with *A. tumefaciens* suspension. After 30 min, the *A. tumefaciens* suspension was discarded, calli were transferred to sterile filter paper and dried for 30 min. Calli were then transferred to *Co-culture-medium* (2 g l^{-1} Chu (N6) minerals, 34.2 g l^{-1} sucrose, 2 mM $CaCl_2$, 20 µM Dicamba, 25 mM L-proline, 2.3 mM MES-monohydrate, 3.3 mM L-cysteine, 1x B5 vitamin mixture (Duchefa Biochemie, Haarlem, The Netherlands), 500 µM Acetosyringone (Sigma-Aldrich, Taufkirchen, Germany), 3.5 g l^{-1} phytagel, pH 5.8) and co-cultivated for 3 days, at 21˚C without light. After co-cultivation, calli were transferred to CIM supplemented with 300 mg l^{-1} Timentin (Duchefa Biochemie, Haarlem, The Netherlands) for a 5 days resting phase (counterselection of agrobacteria) at 24˚C without light. After the resting phase, calli were transferred to CIM supplemented with 300 mg l^{-1} Timentin and 50 mg l^{-1} Hygromycin B (Sigma-Aldrich, Taufkirchen, Germany) for an 8–12 week selection phase at 24˚C without light. During that time, calli were transferred to fresh selection medium every two weeks. After these 8–12 weeks of selection, surviving calli were transferred to regeneration medium (K4N) (***Kumlehn et al., 2006***) including 150 mg l^{-1} Timentin and 25 mg l^{-1} Hygromycin B and cultivated for 8–12 weeks at 25˚C with a 16/8 hr (light/dark) photoperiod. Regenerating plantlets from independent calli were transferred to pots with a substrate mixture of 3:1:1:1 Einheitserde:perlite: sand and grown as described previously (see 'Plant growth conditions and sexual propagation). Cyan fluorescent protein peroxisome (eCFP-SKL) Bd28-marker lines were tested by PCR and confocal laser scanning microscopy.

Acknowledgements

We would like to thank the GMI / IMBA / IMP service facilities as well as the Campus Scientific Facilities for excellent technical support. We would like to thank Julia Riefler, Marina Pérez and Meritxell Amigo for excellent technical support, Andrea Patrignani and the Functional Genomics Center Zürich for outstanding PacBio sequencing, Eva Stukenbrock for alerting us about the existence of *U. bromivora* as well as James Matthew Watson and Nick Fulcher for valuable input on the manuscript. We thank the Max Planck Society for their generous financial support. The research leading to these results has received funding from the European Research Council under the European Union's Seventh Framework Programme (FP7/2007–2013) / ERC grant agreement n˚ [EUP0012 „Effectomics"], the Austrian Science Fund (FWF): [P27429-B22, P27818-B22], and the Austrian Academy of Science (OEAW). The work conducted by the US DOE Joint Genome Institute is supported by the Office of Science of the US Department of Energy under Contract no. DE-AC02-05CH11231. FR received a scholarship of the International Max Planck Research School for Environmental, Molecular and Cellular Microbiology in Marburg.

Additional information

Funding

Funder	Grant reference number	Author
European Research Council	EUP0012 Effectomics	Franziska Rabe Alexandra Stirnberg Denise Seitner Simon Uhse Janos Bindics

Austrian Science Fund	P27429-B22	Franziska Rabe Angelika Czedik-Eysenberg
Austrian Academy of Sciences		Franziska Rabe Jason Bosch Alexandra Stirnberg Tilo Guse Lisa Bauer Denise Seitner Fernando A Rabanal Angelika Czedik-Eysenberg Simon Uhse Janos Bindics Bianca Genenncher Fernando Navarrete Armin Djamei
Max-Planck-Gesellschaft		Franziska Rabe Gertrud Mannhaupt Regine Kahmann Armin Djamei
Austrian Science Fund	P27818-B22	Franziska Rabe Angelika Czedik-Eysenberg
U.S. Department of Energy	DE-AC02-05CH11231	John P Vogel Sean P Gordon

The funders had no role in study design, data collection and interpretation, or the decision to submit the work for publication.

Author contributions

FR, Drafting the article, Acquisition of data, Analysis and interpretation of data; JBo, AC-E, Drafting the article, Analysis and interpretation of data; AS, DS, SU, JBi, BG, FN, Revising the article, Acquisition of data; TG, LB, Acquisition of data; FAR, MM, MCW, CMKS, UG, Revising the article, Analysis and interpretation of data; RKe, JK, JPV, SPG, Revising the article, Contributed unpublished essential data or reagents; HE, Analysis and interpretation of data; TCM, Contributed unpublished essential data or reagents; GM, Revising the manuscript, Analysis and interpretation of data; RKa, Discussion of data, Revising the article; AD, Conception and design, Acquisition of data, Analysis and interpretation of data, Drafting and revising the article

Author ORCIDs

Ronny Kellner, http://orcid.org/0000-0002-4618-0110
Mathias C Walter, http://orcid.org/0000-0003-3012-2626
Ulrich Güldener, http://orcid.org/0000-0001-5052-8610
Armin Djamei, http://orcid.org/0000-0002-8087-9566

Additional files

Supplementary files

• Supplementary file 1. Primers, plasmids and strains used in this study.
DOI: 10.7554/eLife.20522.027

• Supplementary file 2. Maps of plasmids used in this study. Plasmid maps are provided as gb/gbk files.
DOI: 10.7554/eLife.20522.028

Major datasets

The following datasets were generated:

Author(s)	Year	Dataset title	Dataset URL	Database, license, and accessibility information
Güldener U	2016	UB1 and UB2 genome	http://www.ebi.ac.uk/ena/data/view/PRJEB7751	Publicly available at European Nucleotide Archive (accession no: PRJEB7751)
Czedik-Eysenberg A	2016	Global transcriptional profiling of Ustilago bromivora during axenic growth and pathogenic development	https://www.ncbi.nlm.nih.gov/geo/query/acc.cgi?acc=GSE87751	Publicly available at NCBI Gene Expression Omnibus (accession no: GSE87751)

References

Abrusán G, Grundmann N, DeMester L, Makalowski W. 2009. TEclass–a tool for automated classification of unknown eukaryotic transposable elements. *Bioinformatics* **25**:1329–1330. doi: 10.1093/bioinformatics/btp084, PMID: 19349283

Aguileta G, Marthey S, Chiapello H, Lebrun MH, Rodolphe F, Fournier E, Gendrault-Jacquemard A, Giraud T. 2008. phylogenies. *Systematic Biology* **57**:613–627. doi: 10.1080/10635150802306527, PMID: 18709599

Antonovics J, Abrams JY. 2004. Intratetrad mating and the evolution of linkage relationships. *Evolution* **58**:702–709 . doi: 10.1111/j.0014-3820.2004.tb00403.x

Asai S, Shirasu K. 2015. Plant cells under siege: plant immune system versus pathogen effectors. *Current Opinion in Plant Biology* **28**:1–8. doi: 10.1016/j.pbi.2015.08.008, PMID: 26343014

Ausubel FM, Brenz R, Kongston RE, Moore DD, Seidmann JG, Smith JA, Strukl K. 1987. *Current Protocols in Molecular Microbiology*. John Wiley & Sons Inc.

Bakkeren G, Jiang G, Warren RL, Butterfield Y, Shin H, Chiu R, Linning R, Schein J, Lee N, Hu G, Kupfer DM, Tang Y, Roe BA, Jones S, Marra M, Kronstad JW. 2006. Mating factor linkage and genome evolution in basidiomycetous pathogens of cereals. *Fungal Genetics and Biology* **43**:655–666. doi: 10.1016/j.fgb.2006.04.002, PMID: 16793293

Bakkeren G, Kronstad JW. 1994. Linkage of mating-type loci distinguishes bipolar from tetrapolar mating in basidiomycetous smut fungi. *PNAS* **91**:7085–7089. doi: 10.1073/pnas.91.15.7085, PMID: 7913746

Barbieri M, Marcel TC, Niks RE, Francia E, Pasquariello M, Mazzamurro V, Garvin DF, Pecchioni N. 2012. QTLs for resistance to the false brome rust Puccinia brachypodii in the model grass Brachypodium distachyon L. *Genome* **55**:152–163. doi: 10.1139/g2012-001, PMID: 22321152

Barbieri M, Marcel TC, Niks RE. 2011. Host status of false brome grass to the leaf rust fungus puccinia brachypodii and the stripe rust fungus P. striiformis. *Plant Disease* **95**:1339–1345. doi: 10.1094/PDIS-11-10-0825

Basse CW, Stumpferl S, Kahmann R. 2000. Characterization of a Ustilago maydis gene specifically induced during the biotrophic phase: evidence for negative as well as positive regulation. *Molecular and Cellular Biology* **20**:329–339. doi: 10.1128/MCB.20.1.329-339.2000, PMID: 10594035

Bauch R. 1922. Kopulationsbedingungen und sekundäre Geschlechtsmerkmale bei Ustilago violacea. *Biologischen Zentralblatt* **42**:33.

Bauch R. 1925. Untersuchungen über die Entwicklungsgeschichte und Sexualphysiologie der Ustilago bromivora und Ustilago grandis. *Zeitschrift Für Botanik* **17**:129–177.

Begerow D, Schäfer AM, Kellner R, Yurkov A, Kemler M, Oberwinkler F, Bauer R. 2014. Ustilaginomycotina. In: McLaughlin D. J, Spatafora J. W (Eds). *The Mycota VII, Part A, Systematics and Evolution*, 2nd ed. Springer.

Bernet J. 1967. [Systems of incompatibility in Podospora anserina]. *Comptes Rendus Hebdomadaires Des Seances De l'Academie Des Sciences Serie D* **265**:1330–1333. PMID: 4967243

Bozkurt TO, Schornack S, Banfield MJ, Kamoun S. 2012. Oomycetes, effectors, and all that jazz. *Current Opinion in Plant Biology* **15**:483–492. doi: 10.1016/j.pbi.2012.03.008, PMID: 22483402

Brachmann A. 2001. Die frühe Infektionsphase von U. maydis: Genregulation durch das bW/bEHeterodimer. LMU München: Faculty of Biology.

Bray NL, Pimentel H, Melsted P, Pachter L. 2016. Near-optimal probabilistic RNA-seq quantification. *Nature Biotechnology* **34**:525–527. doi: 10.1038/nbt.3519, PMID: 27043002

Brefeld O. 1883. *Untersuchungen Auf Dem Gesamtgebiet Der Mycologie*. Heft 5.(Brandpilze I.).

Brefort T, Doehlemann G, Mendoza-Mendoza A, Reissmann S, Djamei A, Kahmann R. 2009. Ustilago maydis as a Pathogen. *Annual Review of Phytopathology* **47**:423–445. doi: 10.1146/annurev-phyto-080508-081923, PMID: 19400641

Brefort T, Tanaka S, Neidig N, Doehlemann G, Vincon V, Kahmann R. 2014. Characterization of the largest effector gene cluster of Ustilago maydis. *PLoS Pathogens* **10**:e1003866. doi: 10.1371/journal.ppat.1003866, PMID: 24992561

Brkljacic J, Grotewold E, Scholl R, Mockler T, Garvin DF, Vain P, Brutnell T, Sibout R, Bevan M, Budak H, Caicedo AL, Gao C, Gu Y, Hazen SP, Holt BF, Hong SY, Jordan M, Manzaneda AJ, Mitchell-Olds T, Mochida K, et al. 2011. Brachypodium as a model for the grasses: today and the future. *Plant Physiology* **157**:3–13. doi: 10.1104/pp.111.179531, PMID: 21771916

Bölker M, Böhnert HU, Braun KH, Görl J, Kahmann R. 1995. Tagging pathogenicity genes in Ustilago maydis by restriction enzyme-mediated integration (REMI). *Molecular & General Genetics* **248**:547–552. doi: 10.1007/BF02423450, PMID: 7476854

Bölker M, Urban M, Kahmann R. 1992. The a mating type locus of U. maydis specifies cell signaling components. *Cell* **68**:441–450. doi: 10.1016/0092-8674(92)90182-C, PMID: 1310895

Camacho C, Coulouris G, Avagyan V, Ma N, Papadopoulos J, Bealer K, Madden TL. 2009. BLAST+: architecture and applications. *BMC Bioinformatics* **10**:421. doi: 10.1186/1471-2105-10-421, PMID: 20003500

Catalán P, Müller J, Hasterok R, Jenkins G, Mur LA, Langdon T, Betekhtin A, Siwinska D, Pimentel M, López-Alvarez D. 2012. Evolution and taxonomic split of the model grass Brachypodium distachyon. *Annals of Botany* **109**:385–405. doi: 10.1093/aob/mcr294, PMID: 22213013

Chin CS, Alexander DH, Marks P, Klammer AA, Drake J, Heiner C, Clum A, Copeland A, Huddleston J, Eichler EE, Turner SW, Korlach J. 2013. Nonhybrid, finished microbial genome assemblies from long-read SMRT sequencing data. *Nature Methods* **10**:563–569. doi: 10.1038/nmeth.2474, PMID: 23644548

Chomczynski P, Sacchi N. 2006. The single-step method of RNA isolation by acid guanidinium thiocyanate-phenol-chloroform extraction: twenty-something years on. *Nature Protocols* **1**:581–585. doi: 10.1038/nprot.2006.83, PMID: 17406285

Chong L. 2001. Molecular cloning - A laboratory manual, 3rd edition. *Science* **292**:446 . doi: 10.1126/science.1060677

Clough SJ, Bent AF. 1998. Floral dip: a simplified method for Agrobacterium-mediated transformation of Arabidopsis thaliana. *The Plant Journal* **16**:735–743. doi: 10.1046/j.1365-313x.1998.00343.x, PMID: 10069079

Core Team R. 2011. A language and environment for statistical computing. Austria: Vienna: R Foundation for Statistical Computing.

Dean R, Van Kan JA, Pretorius ZA, Hammond-Kosack KE, Di Pietro A, Spanu PD, Rudd JJ, Dickman M, Kahmann R, Ellis J, Foster GD. 2012. The Top 10 fungal pathogens in molecular plant pathology. *Molecular Plant Pathology* **13**:414–430. doi: 10.1111/j.1364-3703.2011.00783.x, PMID: 22471698

Deslandes L, Rivas S. 2012. Catch me if you can: bacterial effectors and plant targets. *Trends in Plant Science* **17**:644–655. doi: 10.1016/j.tplants.2012.06.011, PMID: 22796464

Djamei A, Kahmann R. 2012. Ustilago maydis: dissecting the molecular interface between pathogen and plant. *PLoS Pathogens* **8**:e1002955. doi: 10.1371/journal.ppat.1002955, PMID: 23133380

Djamei A, Schipper K, Rabe F, Ghosh A, Vincon V, Kahnt J, Osorio S, Tohge T, Fernie AR, Feussner I, Feussner K, Meinicke P, Stierhof YD, Schwarz H, Macek B, Mann M, Kahmann R. 2011. Metabolic priming by a secreted fungal effector. *Nature* **478**:395–398. doi: 10.1038/nature10454, PMID: 21976020

Doehlemann G, Hemetsberger C. 2013. Apoplastic immunity and its suppression by filamentous plant pathogens. *The New Phytologist* **198**:1001–1016. doi: 10.1111/nph.12277, PMID: 23594392

Doehlemann G, van der Linde K, Assmann D, Schwammbach D, Hof A, Mohanty A, Jackson D, Kahmann R. 2009. Pep1, a secreted effector protein of Ustilago maydis, is required for successful invasion of plant cells. *PLoS Pathogens* **5**:e1000290. doi: 10.1371/journal.ppat.1000290, PMID: 19197359

Doehlemann G, Wahl R, Vranes M, de Vries RP, Kämper J, Kahmann R. 2008. Establishment of compatibility in the Ustilago maydis/maize pathosystem. *Journal of Plant Physiology* **165**:29–40. doi: 10.1016/j.jplph.2007.05.016, PMID: 17905472

Donlin MJ. 2009. Using the generic genome browser (GBrowse). *Current Protocols in Bioinformatics*. John Wiley and Sons, Inc. **Unit 9.9** 9.9.1–9.9.9 . doi: 10.1002/0471250953.bi0909s28

Draper J, Mur LA, Jenkins G, Ghosh-Biswas GC, Bablak P, Hasterok R, Routledge AP. 2001. Brachypodium distachyon. A new model system for functional genomics in grasses. *Plant Physiology* **127**:1539–1555. doi: 10.1104/pp.010196, PMID: 11743099

Drinnenberg IA, Fink GR, Bartel DP. 2011. Compatibility with killer explains the rise of RNAi-deficient fungi. *Science* **333**:1592. doi: 10.1126/science.1209575, PMID: 21921191

Dutheil JY, Mannhaupt G, Schweizer G, M K Sieber C, Münsterkötter M, Güldener U, Schirawski J, Kahmann R. 2016. A Tale of genome compartmentalization: the evolution of virulence clusters in smut fungi. *Genome Biology and Evolution* **8**:681–704. doi: 10.1093/gbe/evw026, PMID: 26872771

Ellegren H, Galtier N. 2016. Self fertilization and population variability in the higher plants (vol 91, pg 41, 1957). *Nature Reviews Genetics* **17**:422–433. doi: 10.1038/nrg.2016.58

Emanuelsson O, Nielsen H, Brunak S, von Heijne G. 2000. Predicting subcellular localization of proteins based on their N-terminal amino acid sequence. *Journal of Molecular Biology* **300**:1005–1016. doi: 10.1006/jmbi.2000.3903, PMID: 10891285

Enright AJ, Van Dongen S, Ouzounis CA. 2002. An efficient algorithm for large-scale detection of protein families. *Nucleic Acids Research* **30**:1575–1584. doi: 10.1093/nar/30.7.1575, PMID: 11917018

Fedler M, Luh KS, Stelter K, Nieto-Jacobo F, Basse CW. 2009. The a2 mating-type locus genes lga2 and rga2 direct uniparental mitochondrial DNA (mtDNA) inheritance and constrain mtDNA recombination during sexual development of Ustilago maydis. *Genetics* **181**:847–860. doi: 10.1534/genetics.108.096859, PMID: 19104076

Figueroa M, Alderman S, Garvin DF, Pfender WF. 2013. Infection of brachypodium distachyon by formae speciales of puccinia graminis: early infection events and host-pathogen incompatibility. *PLoS One* **8**:e56857. doi: 10.1371/journal.pone.0056857

Filiz E, Ozdemir BS, Budak F, Vogel JP, Tuna M, Budak H. 2009. Molecular, morphological, and cytological analysis of diverse Brachypodium distachyon inbred lines. *Genome* **52**:876–890. doi: 10.1139/g09-062, PMID: 19935911

Fischer S. 2011. Using OrthoMCL to assign proteins to OrthoMCL-DB groups or to cluster proteomes into new ortholog groups. *Current Protocal Bioinformatics* **6**:1–19 . doi: 10.1002/0471250953.bi0612s35
Fisher GW, Holton CS. 1957. *Biology and Control of the Smut Fungi*. New York: The Ronald Press Company.
Garvin DF. 2008. Development of genetic and genomic research resources for Brachypodium distachyon, a new model system for grass crop research. *Crop Science* **48**:S69–S84 . doi: 10.2135/cropsci2007.06.0332tpg
Gattiker A, Gasteiger E, Bairoch A. 2002. ScanProsite: a reference implementation of a PROSITE scanning tool. *Applied Bioinformatics* **1**:107–108. PMID: 15130850
Gillissen B. 1992. A 2-component regulatory system for self non-self recognition in ustilago-maydis. *Cell* **68**:647–657. doi: 10.1016/0962-8924(92)90097-7
Goddard MR, Godfray HC, Burt A. 2005. Sex increases the efficacy of natural selection in experimental yeast populations. *Nature* **434**:636–640. doi: 10.1038/nature03405, PMID: 15800622
Grabherr MG, Haas BJ, Yassour M, Levin JZ, Thompson DA, Amit I, Adiconis X, Fan L, Raychowdhury R, Zeng Q, Chen Z, Mauceli E, Hacohen N, Gnirke A, Rhind N, di Palma F, Birren BW, Nusbaum C, Lindblad-Toh K, Friedman N, et al. 2011. Full-length transcriptome assembly from RNA-Seq data without a reference genome. *Nature Biotechnology* **29**:644–U130. doi: 10.1038/nbt.1883, PMID: 21572440
Haag C, Steuten B, Feldbrügge M. 2015. Membrane-Coupled mRNA trafficking in fungi. *Annual Review of Microbiology* **69**:265–281. doi: 10.1146/annurev-micro-091014-104242, PMID: 26274025
Hane JK, Oliver RP. 2008. RIPCAL: a tool for alignment-based analysis of repeat-induced point mutations in fungal genomic sequences. *BMC Bioinformatics* **9**:478. doi: 10.1186/1471-2105-9-478
Hemetsberger C, Herrberger C, Zechmann B, Hillmer M, Doehlemann G. 2012. The Ustilago maydis effector Pep1 suppresses plant immunity by inhibition of host peroxidase activity. *PLoS Pathogens* **8**:5. doi: 10.1371/journal.ppat.1002684, PMID: 22589719
Hochberg Y, Benjamini Y. 1990. More powerful procedures for multiple significance testing. *Statistics in Medicine* **9**:811–818. doi: 10.1002/sim.4780090710, PMID: 2218183
Hoekstra RF. 2005. Evolutionary biology: why sex is good. *Nature* **434**:571–573. doi: 10.1038/434571a, PMID: 15800605
Holliday R. 1964. A mechanism for gene conversion in fungi. *Genetical Research* **5**:282–290. doi: 10.1017/S0016672300001233
Hood ME, Antonovics J. 2000. Intratetrade mating, heterozygosity, and the maintenance of deleterious alleles in Microbotryum violaceum. *Heredity* **85**:231–241. doi: 10.1046/j.1365-2540.2000.00748.x
Horst RJ, Doehlemann G, Wahl R, Hofmann J, Schmiedl A, Kahmann R, Kämper J, Sonnewald U, Voll LM. 2010. Ustilago maydis infection strongly alters organic nitrogen allocation in maize and stimulates productivity of systemic source leaves. *Plant Physiology* **152**:293–308. doi: 10.1104/pp.109.147702, PMID: 19923237
Huo N, Lazo GR, Vogel JP, You FM, Ma Y, Hayden DM, Coleman-Derr D, Hill TA, Dvorak J, Anderson OD, Luo MC, Gu YQ. 2008. The nuclear genome of Brachypodium distachyon: analysis of BAC end sequences. *Functional & Integrative Genomics* **8**:135–147. doi: 10.1007/s10142-007-0062-7, PMID: 17985162
Joly E. 2011. The existence of species rests on a metastable equilibrium between inbreeding and outbreeding. An essay on the close relationship between speciation, inbreeding and recessive mutations. *Biology Direct* **6**:62. doi: 10.1186/1745-6150-6-62, PMID: 22152499
Jones HD, Doherty A, Wu H. 2005. Review of methodologies and a protocol for the Agrobacterium-mediated transformation of wheat. *Plant Methods* **1**:5. doi: 10.1186/1746-4811-1-5, PMID: 16270934
Jurka J, Kapitonov VV, Pavlicek A, Klonowski P, Kohany O, Walichiewicz J. 2005. Repbase Update, a database of eukaryotic repetitive elements. *Cytogenetic and Genome Research* **110**:462–467. doi: 10.1159/000084979, PMID: 16093699
Kathariou S, Spieth PT. 1982. Spore killer polymorphism in FUSARIUM MONILIFORME. *Genetics* **102**:19–24. PMID: 17246093
Kellner R, Vollmeister E, Feldbrügge M, Begerow D. 2011. Interspecific sex in grass smuts and the genetic diversity of their pheromone-receptor system. *PLoS Genetics* **7**:e1002436. doi: 10.1371/journal.pgen.1002436, PMID: 22242007
Kerber ER. 1991. Stem-rust resistance in 'Canthatch' hexaploid wheat induced by a nonsuppressor mutation on chromosome 7DL. *Genome* **34**:935–939. doi: 10.1139/g91-144
Knott DR. 2000. Inheritance of resistance to stem rust in medea durum wheat and the role of suppressors. *Crop Science* **40**:98–102. doi: 10.2135/cropsci2000.40198x
Koltin Y, Day PR. 1976. Inheritance of killer phenotypes and double-stranded RNA in Ustilago maydis. *PNAS* **73**:594–598. doi: 10.1073/pnas.73.2.594, PMID: 1061159
Krogh A, Larsson B, von Heijne G, Sonnhammer EL. 2001. Predicting transmembrane protein topology with a hidden Markov model: application to complete genomes. *Journal of Molecular Biology* **305**:567–580. doi: 10.1006/jmbi.2000.4315, PMID: 11152613
Kumlehn J, Serazetdinova L, Hensel G, Becker D, Loerz H. 2006. Genetic transformation of barley (Hordeum vulgare L.) via infection of androgenetic pollen cultures with Agrobacterium tumefaciens. *Plant Biotechnology Journal* **4**:251–261. doi: 10.1111/j.1467-7652.2005.00178.x, PMID: 17177801
Käll L, Krogh A, Sonnhammer EL. 2004. A combined transmembrane topology and signal peptide prediction method. *Journal of Molecular Biology* **338**:1027–1036. doi: 10.1016/j.jmb.2004.03.016, PMID: 15111065
Kämper J, Kahmann R, Bölker M, Ma LJ, Brefort T, Saville BJ, Banuett F, Kronstad JW, Gold SE, Müller O, Perlin MH, Wösten HA, de Vries R, Ruiz-Herrera J, Reynaga-Peña CG, Snetselaar K, McCann M, Pérez-Martín J, Feldbrügge M, Basse CW, et al. 2006. Insights from the genome of the biotrophic fungal plant pathogen Ustilago maydis. *Nature* **444**:97–101. doi: 10.1038/nature05248, PMID: 17080091

Kämper J. 2004. A PCR-based system for highly efficient generation of gene replacement mutants in Ustilago maydis. *Molecular Genetics and Genomics* **271**:103–110. doi: 10.1007/s00438-003-0962-8, PMID: 14673645

Langmead B, Trapnell C, Pop M, Salzberg SL. 2009. Ultrafast and memory-efficient alignment of short DNA sequences to the human genome. *Genome Biology* **10**:R25. doi: 10.1186/gb-2009-10-3-r25, PMID: 19261174

Laurie JD, Ali S, Linning R, Mannhaupt G, Wong P, Güldener U, Münsterkötter M, Moore R, Kahmann R, Bakkeren G, Schirawski J. 2012. Genome comparison of barley and maize smut fungi reveals targeted loss of RNA silencing components and species-specific presence of transposable elements. *The Plant Cell* **24**:1733–1745. doi: 10.1105/tpc.112.097261, PMID: 22623492

Lazo GR, Stein PA, Ludwig RA. 1991. A DNA transformation–competent Arabidopsis genomic library in Agrobacterium. *Bio/technology* **9**:963–967. doi: 10.1038/nbt1091-963

Lee N, Bakkeren G, Wong K, Sherwood JE, Kronstad JW. 1999. The mating-type and pathogenicity locus of the fungus Ustilago hordei spans a 500-kb region. *PNAS* **96**:15026–15031. doi: 10.1073/pnas.96.26.15026, PMID: 10611332

Lee SC, Ni M, Li W, Shertz C, Heitman J. 2010. The evolution of sex: a perspective from the fungal kingdom. *Microbiology and Molecular Biology Reviews* **74**:298–340. doi: 10.1128/MMBR.00005-10, PMID: 20508251

Lohse M, Nagel A, Herter T, May P, Schroda M, Zrenner R, Tohge T, Fernie AR, Stitt M, Usadel B. 2014. Mercator: a fast and simple web server for genome scale functional annotation of plant sequence data. *Plant, Cell & Environment* **37**:1250–1258. doi: 10.1111/pce.12231, PMID: 24237261

Loubradou G, Brachmann A, Feldbrügge M, Kahmann R. 2001. A homologue of the transcriptional repressor Ssn6p antagonizes cAMP signalling in Ustilago maydis. *Molecular Microbiology* **40**:719–730. doi: 10.1046/j.1365-2958.2001.02424.x, PMID: 11359577

Love MI, Huber W, Anders S. 2014. Moderated estimation of fold change and dispersion for RNA-seq data with DESeq2. *Genome Biology* **15**:550. doi: 10.1186/s13059-014-0550-8, PMID: 25516281

Lowe TM, Eddy SR. 1997. tRNAscan-SE: a program for improved detection of transfer RNA genes in genomic sequence. *Nucleic Acids Research* **25**:955–964. doi: 10.1093/nar/25.5.0955, PMID: 9023104

Luo R, Liu B, Xie Y, Li Z, Huang W, Yuan J, He G, Chen Y, Pan Q, Liu Y, Tang J, Wu G, Zhang H, Shi Y, Liu Y, Yu C, Wang B, Lu Y, Han C, Cheung DW, et al. 2012. SOAPdenovo2: an empirically improved memory-efficient short-read de novo assembler. *GigaScience* **1**:18. doi: 10.1186/2047-217X-1-18, PMID: 23587118

Martínez-Espinoza AD, García-Pedrajas MD, Gold SE. 2002. The Ustilaginales as plant pests and model systems. *Fungal Genetics and Biology* **35**:1–20. doi: 10.1006/fgbi.2001.1301, PMID: 11860261

Mohammadi S, Saberidokht B, Subramaniam S, Grama A. 2015. Scope and limitations of yeast as a model organism for studying human tissue-specific pathways. *BMC Systems Biology* **9**:96. doi: 10.1186/s12918-015-0253-0, PMID: 26714768

Mueller AN, Ziemann S, Treitschke S, Aßmann D, Doehlemann G. 2013. Compatibility in the Ustilago maydis-maize interaction requires inhibition of host cysteine proteases by the fungal effector Pit2. *PLoS Pathogens* **9**:e1003177. doi: 10.1371/journal.ppat.1003177, PMID: 23459172

Mur LA, Allainguillaume J, Catalán P, Hasterok R, Jenkins G, Lesniewska K, Thomas I, Vogel J. 2011. Exploiting the Brachypodium Tool Box in cereal and grass research. *The New Phytologist* **191**:334–347. doi: 10.1111/j.1469-8137.2011.03748.x, PMID: 21623796

Nielsen J. 1968. Isolation and culture of monokaryotic haplonts of Ustilago nuda, the role of proline in their metabolism, and the inoculation of barley with resynthesized dikaryons. *Canadian Journal of Botany* **46**:1193–1200. doi: 10.1139/b68-159

Notredame C, Higgins DG, Heringa J. 2000. T-Coffee: a novel method for fast and accurate multiple sequence alignment. *Journal of Molecular Biology* **302**:205–217. doi: 10.1006/jmbi.2000.4042, PMID: 10964570

O'Driscoll A, Doohan F, Mullins E. 2015. Exploring the utility of Brachypodium distachyon as a model pathosystem for the wheat pathogen Zymoseptoria tritici. *BMC Research Notes* **8**:132. doi: 10.1186/s13104-015-1097-9, PMID: 25888730

Oerke E-C. 2006. Crop losses to pests. *Journal of Agricultural Science* **144**:31–43. doi: 10.1017/S0021859605005708

Parra G, Bradnam K, Ning Z, Keane T, Korf I. 2009. Assessing the gene space in draft genomes. *Nucleic Acids Research* **37**:289–297. doi: 10.1093/nar/gkn916, PMID: 19042974

Petersen TN, Brunak S, von Heijne G, Nielsen H. 2011. SignalP 4.0: discriminating signal peptides from transmembrane regions. *Nature Methods* **8**:785–786. doi: 10.1038/nmeth.1701, PMID: 21959131

Price AL, Jones NC, Pevzner PA. 2005. De novo identification of repeat families in large genomes. *Bioinformatics* **21**:i351–358. doi: 10.1093/bioinformatics/bti1018, PMID: 15961478

Que Q, Elumalai S, Li X, Zhong H, Nalapalli S, Schweiner M, Fei X, Nuccio M, Kelliher T, Gu W, Chen Z, Chilton MD. 2014. Maize transformation technology development for commercial event generation. *Frontiers in Plant Science* **5**:379. doi: 10.3389/fpls.2014.00379, PMID: 25140170

Redkar A, Hoser R, Schilling L, Zechmann B, Krzymowska M, Walbot V, Doehlemann G. 2015a. A secreted effector protein of Ustilago maydis guides maize leaf cells to form tumors. *The Plant Cell* **27**:1332–1351. doi: 10.1105/tpc.114.131086, PMID: 25888589

Redkar A, Villajuana-Bonequi M, Doehlemann G. 2015b. Conservation of the Ustilago maydis effector See1 in related smuts. *Plant Signaling & Behavior* **10**:e1086855. doi: 10.1080/15592324.2015.1086855, PMID: 26357869

Rine J. 2014. A future of the model organism model. *Molecular Biology of the Cell* **25**:549–553. doi: 10.1091/mbc.E12-10-0768, PMID: 24577733

Ruepp A, Zollner A, Maier D, Albermann K, Hani J, Mokrejs M, Tetko I, Güldener U, Mannhaupt G, Münsterkötter M, Mewes HW. 2004. The FunCat, a functional annotation scheme for systematic classification of proteins from whole genomes. *Nucleic Acids Research* **32**:5539–5545. doi: 10.1093/nar/gkh894, PMID: 15486203

Schipper K. 2009. *Charakterisierung eines Ustilago maydis Genclusters, das für drei neuartige sekretierte Effektoren kodiert*. Philipps-Universität Marburg.

Schirawski J, Mannhaupt G, Münch K, Brefort T, Schipper K, Doehlemann G, Di Stasio M, Rössel N, Mendoza-Mendoza A, Pester D, Müller O, Winterberg B, Meyer E, Ghareeb H, Wollenberg T, Münsterkötter M, Wong P, Walter M, Stukenbrock E, Güldener U, et al. 2010. Pathogenicity determinants in smut fungi revealed by genome comparison. *Science* **330**:1546–1548. doi: 10.1126/science.1195330, PMID: 21148393

Schnable PS, Ware D, Fulton RS, Stein JC, Wei F, Pasternak S, Liang C, Zhang J, Fulton L, Graves TA, Minx P, Reily AD, Courtney L, Kruchowski SS, Tomlinson C, Strong C, Delehaunty K, Fronick C, Courtney B, Rock SM, et al. 2009. The B73 maize genome: complexity, diversity, and dynamics. *Science* **326**:1112–1115. doi: 10.1126/science.1178534, PMID: 19965430

Schulz B, Banuett F, Dahl M, Schlesinger R, Schäfer W, Martin T, Herskowitz I, Kahmann R. 1990. The b alleles of U. maydis, whose combinations program pathogenic development, code for polypeptides containing a homeodomain-related motif. *Cell* **60**:295–306. doi: 10.1016/0092-8674(90)90744-Y, PMID: 1967554

Selker EU. 2002. Repeat-induced gene silencing in fungi. *Homology Effects* **46**:439–450. doi: 10.1016/s0065-2660(02)46016-6

Sharma R, Mishra B, Runge F, Thines M. 2014. Gene loss rather than gene gain is associated with a host jump from monocots to dicots in the Smut Fungus Melanopsichium pennsylvanicum. *Genome Biology and Evolution* **6**:2034–2049. doi: 10.1093/gbe/evu148, PMID: 25062916

Slater GS, Birney E. 2005. Automated generation of heuristics for biological sequence comparison. *BMC Bioinformatics* **6**:31. doi: 10.1186/1471-2105-6-31, PMID: 15713233

Smit A, Hubley R, Green P. 1996-2010. *RepeatMasker. Open - 3.0.*

Sonnhammer EL, von Heijne G, Krogh A. 1998. A hidden Markov model for predicting transmembrane helices in protein sequences. *Proceedings. International Conference on Intelligent Systems for Molecular Biology* **6**:175–182. PMID: 9783223

Spellig T, Bottin A, Kahmann R. 1996. Green fluorescent protein (GFP) as a new vital marker in the phytopathogenic fungus Ustilago maydis. *Molecular & General Genetics* **252**:503–509. doi: 10.1007/BF02172396, PMID: 8914511

Stamatakis A. 2014. RAxML version 8: a tool for phylogenetic analysis and post-analysis of large phylogenies. *Bioinformatics* **30**:1312–1313. doi: 10.1093/bioinformatics/btu033, PMID: 24451623

Steinberg G, Perez-Martin J. 2008. Ustilago maydis, a new fungal model system for cell biology. *Trends in Cell Biology* **18**:61–67. doi: 10.1016/j.tcb.2007.11.008, PMID: 18243705

Steinberg G. 2007. Tracks for traffic: microtubules in the plant pathogen Ustilago maydis. *The New Phytologist* **174**:721–733. doi: 10.1111/j.1469-8137.2007.02072.x, PMID: 17504456

Stoll M, Begerow D, Oberwinkler F. 2005. Molecular phylogeny of Ustilago, Sporisorium, and related taxa based on combined analyses of rDNA sequences. *Mycological Research* **109**:342–356. doi: 10.1017/S0953756204002229, PMID: 15912952

Storey J. 2015. *Qvalue: Q-Value Estimation for False Discovery Rate Control*. R package version 2.0.0.

Tanaka S, Brefort T, Neidig N, Djamei A, Kahnt J, Vermerris W, Koenig S, Feussner K, Feussner I, Kahmann R. 2014. A secreted Ustilago maydis effector promotes virulence by targeting anthocyanin biosynthesis in maize. *eLife* **3**:e01355. doi: 10.7554/eLife.01355, PMID: 24473076

Ter-Hovhannisyan V, Lomsadze A, Chernoff YO, Borodovsky M. 2008. Gene prediction in novel fungal genomes using an ab initio algorithm with unsupervised training. *Genome Research* **18**:1979–1990. doi: 10.1101/gr.081612.108, PMID: 18757608

Trapnell C, Roberts A, Goff L, Pertea G, Kim D, Kelley DR, Pimentel H, Salzberg SL, Rinn JL, Pachter L. 2012. Differential gene and transcript expression analysis of RNA-seq experiments with TopHat and Cufflinks. *Nature Protocols* **7**:562–578. doi: 10.1038/nprot.2012.016, PMID: 22383036

Turner BC, Perkins DD. 1979. Spore killer, a chromosomal factor in neurospora that kills meiotic products not containing it. *Genetics* **93**:587–606. PMID: 17248973

Usadel B, Nagel A, Steinhauser D, Gibon Y, Bläsing OE, Redestig H, Sreenivasulu N, Krall L, Hannah MA, Poree F, Fernie AR, Stitt M. 2006. PageMan: an interactive ontology tool to generate, display, and annotate overview graphs for profiling experiments. *BMC Bioinformatics* **7**:535. doi: 10.1186/1471-2105-7-535, PMID: 17176458

Vain P, Worland B, Thole V, McKenzie N, Alves SC, Opanowicz M, Fish LJ, Bevan MW, Snape JW. 2008. Agrobacterium-mediated transformation of the temperate grass Brachypodium distachyon (genotype Bd21) for T-DNA insertional mutagenesis. *Plant Biotechnology Journal* **6**:236–245. doi: 10.1111/j.1467-7652.2007.00308.x, PMID: 18004984

Vanky K. 2011. *Smut Fungi of the World*. APS Press, Minnesota.

Vogel J, Hill T. 2008. High-efficiency Agrobacterium-mediated transformation of Brachypodium distachyon inbred line Bd21-3. *Plant Cell Reports* **27**:471–478. doi: 10.1007/s00299-007-0472-y, PMID: 17999063

Vogel JP, Garvin DF, Leong OM, Hayden DM. 2006. Agrobacterium-mediated transformation and inbred line development in the model grass Brachypodium distachyon. *Plant Cell, Tissue and Organ Culture* **84**:199–211. doi: 10.1007/s11240-005-9023-9

Vogel JP, Tuna M, Budak H, Huo N, Gu YQ, Steinwand MA. 2009. Development of SSR markers and analysis of diversity in Turkish populations of Brachypodium distachyon. *BMC Plant Biology* **9**:88. doi: 10.1186/1471-2229-9-88, PMID: 19594938

Walter MC, Rattei T, Arnold R, Güldener U, Münsterkötter M, Nenova K, Kastenmüller G, Tischler P, Wölling A, Volz A, Pongratz N, Jost R, Mewes HW, Frishman D. 2009. PEDANT covers all complete RefSeq genomes. *Nucleic Acids Research* **37**:D408–D411. doi: 10.1093/nar/gkn749, PMID: 18940859

Wright SI, Ness RW, Foxe JP, Barrett SCH. 2008. Genomic consequences of outcrossing and selfing in plants. *International Journal of Plant Sciences* **169**:105–118. doi: 10.1086/523366

Yang Z. 1997. PAML: a program package for phylogenetic analysis by maximum likelihood. *Computer Applications in the Biosciences : CABIOS* **13**:555–556. doi: 10.1093/bioinformatics/13.5.555, PMID: 9367129

Yordem BK, Conte SS, Ma JF, Yokosho K, Vasques KA, Gopalsamy SN, Walker EL. 2011. Brachypodium distachyon as a new model system for understanding iron homeostasis in grasses: phylogenetic and expression analysis of Yellow Stripe-Like (YSL) transporters. *Annals of Botany* **108**:821–833. doi: 10.1093/aob/mcr200, PMID: 21831857

Publication 2: Isolation of Ustilago bromivora Strains from Infected Spikelets through Spore Recovery and Germination

Contribution to the paper:

Wrote the paper.

bio-protocol www.bio-protocol.org/e2392 Vol 7, Iss 14, Jul 20, 2017
DOI:10.21769/BioProtoc.2392

Isolation of *Ustilago bromivora* Strains from Infected Spikelets through Spore Recovery and Germination

Jason Bosch and Armin Djamei*

Gregor Mendel Institute (GMI), Austrian Academy of Sciences, Vienna Biocenter (VBC), Dr. Bohr-Gasse 3, 1030 Vienna, Austria
*For correspondence: armin.djamei@gmi.oeaw.ac.at

[Abstract] *Ustilago bromivora* is a biotrophic smut fungus infecting *Brachypodium* sp. It is closely related to the barley-infecting smut *Ustilago hordei,* and related to the well-studied, gall-inducing model pathogen *Ustilago maydis.* Upon flowering, the spikelets of *U. bromivora*-infected plants are filled with black fungal spores. While it is possible to directly use this spore material to infect *Brachypodium* seeds, in many cases it is more useful to isolate individual strains of *U. bromivora* for a genetically homogenous population. This protocol describes how to collect and germinate the spores of *U. bromivora* on plate in order to obtain strains derived from a single cell.
Keywords: *Brachypodium distachyon*, *Ustilago bromivora*, Biotrophic interaction, Plant pathogen, Filamentous fungus, Head smut

[Background] *Ustilago maydis* infecting maize (*Zea mays*) has long been established as a model system for studying biotrophic pathogens (Brefort *et al.*, 2009). This has led to many discoveries concerning the nature of biotrophic interactions but has limitations due to the practical difficulties of working with maize in the laboratory. The same is true for the model fungus *Ustilago hordei* infecting barley (*Hordeum vulgare*) (Laurie *et al.,* 2012). In contrast to these crop plants, the model grass *Brachypodium distachyon* has a small genome, undemanding growth conditions and is amenable to genetic manipulation (Draper *et al.,* 2001). *B. distachyon* has also been used to study non-host resistance to *Puccinia striiformis* f. sp. *tritici* due to the genetic complexity of its usual host, wheat (An *et al.,* 2016). Recently, we have described *Ustilago bromivora*, a smut fungus related to *U. maydis,* which is able to infect *Brachypodium* sp. and proposed this as a new model system for studying biotrophic interactions (Rabe *et al*., 2016).

During infection of *Brachypodium* sp. by *U. bromivora,* no visible symptoms can be detected for most of the infection. The only visible symptom of infection occurs during flowering when the plant produces spikelets that are filled with black, fungal spores. These spores can be used to directly infect new seeds but contain genetically disparate fungal strains. For most purposes a pure culture from a single cell is preferable as it can be cultured axenically, characterized and genetically manipulated before being used to infect further seeds. This protocol describes the process of germinating the *U. bromivora* spores *in vitro*. It bears similarities to spore germination protocols of other smut fungi, for example *U. maydis* (Heinze, 2009; Nadal *et al*., 2016), but has been modified to account for differences in the host species and infected organs. Please be aware that *U. bromivora* shows a mating type bias leading to the survival

Vol 7, Iss 14, Jul 20, 2017
DOI:10.21769/BioProtoc.2392

of only one mating type (mat a) on plate after spore germination (Rabe *et al*., 2016). This means that it will require additional effort to generate the second mating type or the use of the strain which we have previously isolated.

Materials and Reagents

1. Paper bag (HERA, catalog number: 716P50)
2. 1.5 ml microcentrifuge tubes (SARSTEDT, catalog number: 72.690.001)
3. Petri dish (SARSTEDT, catalog number: 82.1473.001)
4. Micro-homogenizer (Carl Roth, catalog number: K994.1)
5. Pipetman Diamond tips, D200 (Gilson, catalog number: F161931)
6. Pipetman Diamond tips, D1000 (Gilson, catalog number: F161671)
7. Glass beads (Sigma-Aldrich, catalog number: 18406)
8. Copper sulfate ($CuSO_4$) (AppliChem, catalog number: 131270)
9. Ampicillin (Carl Roth, catalog number: K029.2)
10. Tetracycline (Duchefa Biochemie, catalog number: T0150)
11. Chloramphenicol (AppliChem, catalog number: A1806)
12. Potato dextrose broth (BD, catalog number: 254920)
13. Agar (BD, catalog number: 214040)
14. $PD_{Amp, Tet, ChlA}$ plates (see Recipes)

Equipment

1. Scissors
2. Cooled incubator (ST) ST 1 (Pol-Eko Aparatura, catalog number: ST 1)
3. Pipetman P1000 (Gilson, catalog number: F123602)
4. Pipetman P200 (Gilson, catalog number: F123601)
5. Vortex
6. Heraeus™ Pico™ 17 Microcentrifuge (Thermo Fisher Scientific, Thermo Scientific™, model: Heraeus™ Pico™ 17, catalog number: 75002410)

Procedure

1. Harvest the infected spikelets from the plant by cutting them off using a pair of scissors. Figure 1 shows the appearance of the infected spikelets. Spikelets should be stored in a paper bag for ~10 days at 28 °C to dry out. They can then be stored at room temperature until use.

Vol 7, Iss 14, Jul 20, 2017
DOI:10.21769/BioProtoc.2392

Figure 1. Spikelets of *B. distachyon* infected by *U. bromivora*. The black masses of fungal spores are clearly visible in both the hydrated (right) and dehydrated (left) spikelet. The scale bar represents approximately 1 cm. The image background of the spikelets was digitally removed.

2. Carefully grind the spikelets filled with spore material with a micro-homogenizer in 1.5 ml microcentrifuge tubes to break up the spikelet. The spores are very robust to survive harsh environments and will not be damaged by the grinding.
3. Add 500 µl ddH_2O and continue to grind softly. It is best to use a rotating motion to grind the spikelet as pushing into the microcentrifuge tube will cause the liquid to splash out. The liquid will turn black as it is ground, indicating that the spores have been released and are properly suspended.
4. Incubate the ground spores in ddH_2O for 1 h at room temperature to allow faster-germinating, contaminating, fungal spores to germinate. This will leave them more susceptible to the sterilisation treatment and reduce overall contamination levels.
5. Add 500 µl 3% $CuSO_4$ and mix the solution either by pipetting up and down or by using a vortex. This will kill most, if not all, of the contaminating spores that have germinated but not the *U. bromivora* spores which can take up to 17 h to germinate.
   Note: $CuSO_4$ is a heavy metal and should be handled and discarded according to its MSDS.
6. Incubate the spore/$CuSO_4$ mixture for 15 min at room temperature.
7. Centrifuge the spore mixture at 1,200 *x g* for 5 min. This will cause the spores to pellet. Carefully pour out the liquid and re-suspend the spores in 1 ml ddH_2O.
8. Repeat step 7 three times but, on the third time, instead of re-suspending the spores in ddH_2O, proceed to step 9.
9. Re-suspend the spores in 300 µl ddH_2O with antibiotics (ampicillin, tetracycline and chloramphenicol). These will kill any non-fungal cells that might have survived the $CuSO_4$ treatment.

Vol 7, Iss 14, Jul 20, 2017
DOI:10.21769/BioProtoc.2392

10. Make a dilution series of the fungal spore suspension (10^0-10^{-4}) in ddH_2O with the three antibiotics.
11. Plate 100 µl of each dilution on a $PD_{Amp, Tet, ChlA}$ plate (see Recipes), spread using glass beads and incubate at 21 °C for several days to obtain colonies.
12. As *U. bromivora* spores contain tetrads, the original colonies should be singled out on PD plates (with or without antibiotics) to obtain colonies derived from a single cell.

Notes

While we have provided information on the specific equipment and reagents used, we have no reason to believe that it is essential to use them exactly. The equivalent equipment or reagents from other manufacturers should be just as suitable.

Antibiotic	**Final concentration** (µg/ml)
Ampicillin	100
Tetracycline	25
Chloramphenicol	25

Recipes

1. $PD_{Amp, Tet, ChlA}$ plates
   2.4% (weight/volume) potato dextrose broth
   2.0% (weight/volume) agar
   Note: Measure out the appropriate amount of potato dextrose broth and agar for the intended volume. Dissolve them in ddH_2O then autoclave the mixture at 121 °C for 15 min. Once it has cooled to approximately 50 °C, add ampicillin, tetracycline and chloramphenicol to their final concentrations. Pour the mixture into Petri dishes (20 ml per 9 cm Petri dish) and wait ~20 min for it to set.

Acknowledgments

This protocol was developed in the Djamei laboratory and has had aspects contributed and/or changed by multiple members of the Djamei group. Due to this, the people listed as authors are not the only ones who have been involved in developing the protocol (for this see Rabe *et al*., 2016) but are merely the ones who have prepared it for publication. The research leading to these results has received funding from the European Research Council under the European Union's Seventh Framework Programme (FP7/2007-2013)/ERC grant agreement No. [EUP0012 'Effectomics'], the Austrian Science Fund (FWF): [P27429-B22, P27818-B22, I 3033-B22], and the Austrian Academy of Science (OEAW).

Vol 7, Iss 14, Jul 20, 2017
DOI:10.21769/BioProtoc.2392

References

1. An, T., Cai, Y., Zhao, S., Zhou, J., Song, B., Bux, H. and Qi, X. (2016). *Brachypodium distachyon* T-DNA insertion lines: a model pathosystem to study nonhost resistance to wheat stripe rust. *Sci Rep* 6: 25510.
2. Brefort, T., Doehlemann, G., Mendoza-Mendoza, A., Reissmann, S., Djamei, A. and Kahmann, R. (2009). *Ustilago maydis* as a pathogen. *Annu Rev Phytopathol* 47: 423-445.
3. Draper, J., Mur, L. A., Jenkins, G., Ghosh-Biswas, G. C., Bablak, P., Hasterok, R. and Routledge, A. P. (2001). *Brachypodium distachyon*. A new model system for functional genomics in grasses. *Plant Physiol* 127(4): 1539-1555.
4. Heinze, B. (2009). Comparative analysis of the maize smut fungi *Ustilago maydis* and *Sporisorium reilianum*. *Philipps-Universitat Marburg*.
5. Laurie, J. D., Ali, S., Linning, R., Mannhaupt, G., Wong, P., Guldener, U., Munsterkotter, M., Moore, R., Kahmann, R., Bakkeren, G. and Schirawski, J. (2012). Genome comparison of barley and maize smut fungi reveals targeted loss of RNA silencing components and species-specific presence of transposable elements. *Plant Cell* 24(5): 1733-1745.
6. Nadal, M., Takach, J., Andrews, D., and Gold, S. (2016). Mating and progeny isolation in the corn smut fungus *Ustilago maydis*. *Bio Protoc*: e1793.
7. Rabe, F., Bosch, J., Stirnberg, A., Guse, T., Bauer, L., Seitner, D., Rabanal, F. A., Czedik-Eysenberg, A., Uhse, S., Bindics, J., Genenncher, B., Navarrete, F., Kellner, R., Ekker, H., Kumlehn, J., Vogel, J. P., Gordon, S. P., Marcel, T. C., Munsterkotter, M., Walter, M. C., Sieber, C. M., Mannhaupt, G., Guldener, U., Kahmann, R. and Djamei, A. (2016). A complete toolset for the study of *Ustilago bromivora* and *Brachypodium* sp. as a fungal-temperate grass pathosystem. *Elife* 5.

Publication 3: Two is better than one: Studying host plant/fungal compatibility by using a hybrid pathogen

Contribution to the paper:

Wrote the paper, performed the experiments and analysed the data.

Molecular Plant-Microbe Interactions® MPMI

Two is better than one: Studying host plant/ fungal compatibility by using a hybrid pathogen

Journal:	*Molecular Plant-Microbe Interactions*
Manuscript ID	MPMI-05-19-0148-R
Manuscript Type:	Research
Date Submitted by the Author:	31-May-2019
Complete List of Authors:	Bosch, Jason; Gregor Mendel Institute of Molecular Plant Biology GmbH Czedik-Eysenberg, Angelika; Gregor Mendel Institute of Molecular Plant Biology GmbH Hastreiter, Maximilian; Technische Universitat Munchen Fakultat Wissenschaftszentrum Weihenstephan fur Ernahrung Landnutzung und Umwelt Khan, Mamoona; Gregor Mendel Institute of Molecular Plant Biology GmbH; Leibniz-Institut fur Pflanzengenetik und Kulturpflanzenforschung Gatersleben Gueldener, Ulrich; Technische Universitat Munchen Fakultat Wissenschaftszentrum Weihenstephan fur Ernahrung Landnutzung und Umwelt Djamei, Armin; Leibniz-Institut fur Pflanzengenetik und Kulturpflanzenforschung Gatersleben, Plant Breeding ; Gregor Mendel Institute of Molecular Plant Biology GmbH
Area That Best Describes Your Manuscript:	Fungus–plant interactions, genomics, proteomics, metabolomics < Fungus–plant interactions, Genomics

Two is better than one: Studying host plant/fungal compatibility by using a hybrid pathogen

Jason Bosch(https://orcid.org/0000-0003-1027-1210)[1], Angelika Czedik-Eysenberg(https://orcid.org/0000-0002-7027-802X)[1], Maximilian Hastreiter(https://orcid.org/0000-0003-3288-4229)[2], Mamoona Khan(https://orcid.org/0000-0003-3301-9536)[1,3] Ulrich Güldener(https://orcid.org/0000-0001-5052-8610)[2], Armin Djamei(https://orcid.org/0000-0002-8087-9566)[1,3*]

[1] Gregor Mendel Institute (GMI), Austrian Academy of Sciences, Vienna BioCenter (VBC), Dr. Bohr-Gasse 3, 1030 Vienna, Austria

[2]TUM School of Life Sciences, Technical University of Munich, Department of Bioinformatics, Maximus-von-Imhof-Forum 3, 85354 Freising, Germany

[3]Leibniz Institute of Plant Genetics and Crop Plant Research (IPK), OT Gatersleben, Corrensstraße 3, D-06466 Stadt Seeland, Germany

*For correspondence: djamei@ipk-gatersleben.de

Abstract

Pathogenic fungi can have devastating effects on agriculture and health. One potential challenge in dealing with pathogens is the possibility of a host jump, i.e. when a pathogen infects a new host species. This can lead to the emergence of new diseases or complicate the management of existing threats. We studied host-specificity by using a hybrid fungus formed by mating two closely-related fungi; *Ustilago bromivora* which normally infects *Brachypodium spp.* and *Ustilago hordei* which normally infects barley. Although *U. hordei* was unable to infect *Brachypodium*, the hybrid could. These hybrids also displayed the same mating type bias that had been observed in *U. bromivora* and provide evidence of a dominant

spore-killer-like system on the sex chromosome of *U. bromivora*. By analysing the genomic composition of 109 hybrid strains, backcrossed with *U. hordei* over four generations, we identified three regions associated with infection on *Brachypodium spp* and 75 potential virulence candidates. The most strongly associated region was located on chromosome 8, where 7 genes encoding predicted secreted proteins were identified. The fact that we identified several regions relevant for pathogenicity on *Brachypodium spp.* but that none were essential, suggests that host specificity, in the case of *U. bromivora*, is a multifactorial trait which can be achieved through different subsets of virulence factors.

Introduction

Pathogenic fungi have a large impact on our ecosystem, infecting an array of hosts with effects on biodiversity, medicine and agriculture. The consequences of a pathogen outbreak can be disastrous. A recent estimate based on climate modelling and the 2016 outbreak of wheat blast, caused by *Magnaporthe oryzae*, found that 7 million hectares in South Asia are vulnerable to an outbreak with a potential crop loss of 1.77 million tons(Mottaleb et al. 2018).

Knowing the host range of a fungus is important for understanding, predicting and combatting fungal outbreaks, especially as a pathogen could take refuge in wild species, complicating disease management; for example, *Phakopsora pachyrhizi,* is suspected to winter in kudzu vine between soybean seasons(Jarvie 2010). While some fungi have narrow host ranges of only one or two plant species, others can infect more broadly; *Botrytis cinerea* is notable for being able to infect over 200 plant species(Dean et al. 2012).

It is important to bear in mind that differences in the number of hosts can reflect differences in the pathogen's life cycle. While *B. cinerea* is a necrotrophic fungal pathogen which kills its host to extract nutrients, other pathogens, such as *Ustilago maydis,* are highly specialised

biotrophic pathogens and require a living host in order to complete their life cycle. In order to accomplish this, *U. maydis* carefully controls gene expression and protein secretion, both temporally(Lanver et al. 2018) and spatially(Skibbe et al. 2010; Schilling et al. 2014; Matei et al. 2018). Due to the complex regulation of gene expression required by biotrophic pathogens, they are generally expected to have a limited host range(Freeman and Beattie 2008) and researchers have cautioned that broad host ranges may be indicative of species complexes(Kruse et al. 2018). Occasionally, a biotrophic fungus is able to achieve some growth in a non-host, but is unable to complete its life cycle(Bettgenhaeuser et al. 2018; Frantzeskakis et al. 2017).

Infection of a plant by a pathogen depends on three major factors, the genotype of the pathogen (which effectors, enzymes, detectable signatures, etc. it expresses), the genotype of the plant (the structure of its cell walls, which receptors are expressed and so on) and the environmental conditions (weather, nutrients, microbiome, etc.) that can have either a positive or negative impact on infection rates.

From the pathogen side, host-pathogen interactions are controlled by effectors; small, secreted molecules which manipulate the host's defences(De Jonge et al. 2011; Uhse and Djamei 2018). As a species, the fungal pathogen *Verticillium dahliae* has a wide host range but most isolates can only infect a small subset of those hosts(Bhat and Subbarao 1999). It has been shown that *V. dahliae* strains have lineage-specific genes that are both expressed *in planta* and are important for virulence(de Jonge et al. 2013). Furthermore, expression of one of these lineage specific genes, *Ave1*, can enhance the virulence of strains which naturally lack *Ave1* on tomato(de Jonge et al. 2012). This is a classic characteristic of an effector.

Plants have evolved the ability to recognise some effectors, or their activity, and elicit a strong, specific defence response, known as effector triggered immunity. In the case of *V. dahliae,* expression of the effector *Ave1* increases virulence on tomato only if the plant does

not express the *Ve1* receptor gene. *Ve1* recognises *Ave1* and triggers a hypersensitive response, preventing infection(de Jonge et al. 2012). This opens up the possibility for a strain of *V. dahliae* to experience a "host jump," i.e. the ability of a fungal strain to infect a previously-resistant host, that allows it to infect tomato lines expressing *Ve1* by losing the recognised *Ave1*. Loss of recognised effectors has been described as underlying a host jump of *M. oryzae* to common wheat(Inoue et al. 2017) and is a potential explanation for the gene loss observed in the smut fungus *Melanopsichium pennsylvanicum* after a host jump from a monocotyledonous host to the dicotyledonous *Persicaria*(Sharma et al. 2014). Alternatively, a host jump could be enabled by the loss of an effector recognition gene, like *Ve1*, on the plant side. In such a case, the plant would no longer recognise the pathogen, would not trigger the hypersensitive response and would therefore be susceptible to infection.

The ability of a pathogen to jump to a new, previously-resistant host can present a serious problem as it can not be anticipated and could result in a threat from an endemic, but previously non-pathogenic, microbe. This can be mediated by environmental effects such as a change in climate that creates conditions favourable for infections(Casadevall 2018). In Kentucky, an endemic strain of *M. oryzae,* which usually infects annual ryegrass, was observed to infect wheat under the right conditions(Farman et al. 2016). Infection of new hosts can also be facilitated by interactions with other species. While *Phytophthora infestans* can not usually infect *Arabidopsis thaliana,* infection is possible if the plant is already colonised by *Albugo laibachii*(Belhaj et al. 2017). These rare infections can be very important as, once host resistance is overcome, it opens up a new niche for the pathogen to adapt to.

Different species which come in contact with one another may also be able to facilitate a host jump through hybridisation(Brasier 2000; Olson and Stenlid 2002). The fungal pathogen *Blumeria graminis*, the causal agent of powdery mildew, occurs in host-specific varieties; *B. graminis* f. sp. *tritici* infects bread wheat while *B. graminis* f. sp. *secalis* infects rye. Triticale,

the hybrid of wheat and rye, appeared to be immune to powdery mildew since its formation approximately 50 years ago. However, in 2001, triticale was reported to show signs of powdery mildew infection and it was recently found that powdery mildew in triticale is caused by *B. graminis* f. sp. *triticale,* a hybrid of *B. graminis* f. sp. *tritici* and *B. graminis* f. sp. *secalis*(Menardo et al. 2015). This example is not merely an isolated event. Pathogenic hybrids have also been described for *Verticillium longisporum,* which has arisen multiple times and displays an expanded host range compared to its parental species(Inderbitzin et al. 2011), and *Melampsora xcolumbiana* which has an intermediate phenotype compared to its parental species and infects a greater range of poplar hosts(Newcombe et al. 2000). Many other examples exist(Depotter et al. 2016), all highlighting the need for more research on hybridisation and host jumps.

We recently described a new system for studying biotrophic plant-pathogen interactions using the fungus *Ustilago bromivora* and grasses from the genus *Brachypodium*(Rabe et al. 2016). We performed a genomic comparison between *U. bromivora* and several other smut fungi which showed that the *Brachypodium*-infecting *U. bromivora* is very closely related to the barley-infecting *Ustilago hordei. U. bromivora* and *U. hordei* share 6,180 orthologs with each other and have 1,053 and 933 species-specific genes respectively(Rabe et al. 2016). Both *U. bromivora* and *U. hordei* are biotrophs capable of being cultured as haploid saprophytes but which require a plant host to complete their sexual life cycle.

In order to successfully infect a plant host, it is necessary for haploid cells of opposite mating types to mate and form a dikaryon. Mating is accompanied by a morphological switch from yeast-like budding to filamentous growth upon formation of mating hyphae. We observed that the mating locus on chromosome 1 of *U. bromivora*(Rabe et al. 2016) is very similar to that of *U. hordei*(Bakkeren and Kronstad 1994). Both fungi have a bipolar mating system with an *a* mating locus, containing a pheromone/receptor pair necessary for mating, and a *b* mating

locus, containing a homeodomain transcription factor necessary for pathogenesis, on a single chromosome forming the MAT locus. Furthermore, many fungi in the genus *Ustilaginaceae* are known to be able to form interspecific crosses(Kellner et al. 2011; Huang and Nielsen 1984) or can be manipulated into forming interspecific crosses(Bakkeren and Kronstad 1996).

In this paper, we describe *U. bromivora* and *U. hordei* hybrids which were able to form spores after infecting various *Brachypodium* species. In order to understand the difference in host specificity between the two genetically-similar fungi, we backcrossed the *U. bromivora* X *U. hordei* hybrid with *U. hordei* over several generations. As spores can only be produced *in planta*, there was a constant selection for the ability to infect *Brachypodium spp.* while simultaneously diluting the *U. bromivora* genetic information which was not required for infection. This revealed three genomic loci which were linked with virulence on *U. bromivora* chromosomes 8, 13 and 22.

Results

U. bromivora and *U. hordei* form viable hybrids

We mated *U. bromivora* and *U. hordei,* showing that there is no incompatibility between the two fungi (Fig S2) and that the hybrid fungus is able to successfully infect *B. distachyon* ABR4 (Figs 1 + 2) as well as the allotetraploid *B. hybridum* Bd28 (Fig S3). While the overall infection timeline and symptoms of the hybrid were similar to that of wildtype *U. bromivora* (Attempted *U. hordei* infections produced no symptoms on *Brachypodium spp.*), there were a few subtle differences. We noticed that the hybrid infections tended to distort the plant spikelets more than wild-type *U. bronivora*. (Fig 1D-F) In addition, the hybrid sometimes produced spores in the nodes of the *B. distachyon* ABR4 stem. (Fig 1G-I) Microscopically, we neither saw obvious difference in how the fungi grow inside the plants (Fig 2 A-C, Fig S4)

nor between the morphology and size of the spores of the hybrid and *U. bromivora*. (Fig 2 D-F)

Using the Phenobox automated phenotyping system(Czedik-Eysenberg et al. 2018), it was possible to distinguish *U. bromivora*-infected and hybrid-infected plants from uninfected plants. (Fig 3A) Plants that were treated with either *U. bromivora* or the hybrid, but did not develop symptoms, were indistinguishable from uninfected control plants. The data shows that even a few days after vernalisation, the difference in plant height between control and infected plants is significant. (Fig 3B) This suggests that "failed infections" represent a complete failure to enter the plant and not merely a failure to develop spores, as one would expect colonisation, with or without spore formation, to result in the same growth phenotype of the plant. Fig 3B also shows an interesting phenomenon whereby *B. distachyon* ABR4 infected with the hybrid fungus fails to bolt, resulting in very little increase in height from 28 days after vernalisation when compared with *B. distachyon* ABR4 infected with *U. bromivora.*

As the hybrid fungus is a dikaryon, it contains the complete genomic information of both *U. bromivora* and *U. hordei.* Since the hybrid was capable of infecting *B. distachyon* ABR4, it suggested either that *B. distachyon* ABR4 can not recognise *U. hordei* or that some factor in *U. bromivora* is able to prevent the recognition. Altogether, this suggested that there are specific factors encoded by *U. bromivora* that allow it to infect *Brachypodium spp.* while the closely-related *U. hordei* can not.

Backcrossing hybrids with *U. hordei*

In order to save time, we continued working with *B. hybridum* Bd28 for the hybrid infections as this host does not require vernalisation for floral induction and is equally well infected by

the fungus. We designed an experimental approach to identify the important pathogenicity regions of *U. bromivora* by repeatedly backcrossing the hybrid lines with *U. hordei*. (Fig 4) Single spore cultures were obtained from plants infected by the original hybrid. The sporidia released after spore germination are haploid and consist of a mixture of genomic information from *U. bromivora* and *U. hordei.* Some sporidia can be expected to have maintained the relevant pathogenicity regions from *U. bromivora* while others will have randomly lost it. These F1, hybrid-derived strains are then backcrossed with *U. hordei*. As *U. bromivora* and *U. hordei* are extremely close genetically, we assume that the *U. hordei* orthologs will be able to complement the missing regions of *U. bromivora*, the exception being those *U. bromivora*-specific regions important for pathogenicity in *Brachypodium spp*. After mating, further spore production is obtained by infection of *B. hybridum* Bd28. This is what maintains the selection for those regions of *U. bromivora* that are necessary for infection. Following several rounds of backcrossing, we obtain a population of hybrid strains of various generations with a decreasing proportion of their genome coming from *U. bromivora;* some of which are still able to infect *B. hybridum* Bd28 and others which have lost this ability.

We observed a clear decrease in the percentage of strains that were able to cause infection symptoms in each subsequent generation. (Fig 5A) In addition, while the original hybrid of *U. bromivora* X *U. hordei* led to the development of infection symptoms on a median of 60% of infected plants, we saw a rapid drop in infection strength as we progressed through the generations. (Fig 5B) This showed that the loss of *U. bromivora* genomic regions had a negative, quantitative effect on the ability of the hybrids to infect *B. hybridum* Bd28.

We analysed the genomic sequences of 109 hybrid strains by NGS in order to identify which regions of the genome were contributed from *U. bromivora* and to correlate that information with which strains were able to cause symptom development on *B. hybridum* Bd28. (Table S2) By aligning the Illumina reads to perfectly match *U. hordei* genes, we could count those

reads which are either derived from *U. hordei* or are perfectly conserved. We could then take the remaining reads and map them onto the *U. bromivora* genes. This allowed us to see which genes are present (defined as at least 5 reads, covering 90% of the gene length) and express that as a percentage of the total number of *U. bromivora* genes or the number of genes which are either shared or *U. hordei*-specific. This provides a simple proxy for assessing how the genomic contribution changes through the generations and shows that the amount of the genome coming from *U. bromivora* decreases through the generations and the amount contributed from or shared with *U. hordei* increases. (Fig 5C) The percentage of *U. bromivora* gene content in the hybrid strains is correlated with their ability to cause infection symptoms on plants (r = 0.407988).

Finally, when crossing *U. bromivora* MAT1 with *U. hordei* MAT2 and we saw a mating type bias where 320 out of 342 sporidia (93.56%) from 99 spores were MAT1. Although there was variation in later generations whether MAT1 or MAT2 predominated, there was always a strong bias to a specific mating type. This indicates that the MAT1 bias that we previously reported for *U. bromivora* is based on a dominant in trans acting factor that is genetically linked to the region close to the mat1 locus on the fungal sex-chromosome(Rabe et al. 2016).

Genomic regions responsible for the host jump

The 109 Illumina-sequenced hybrids were divided into 31 strains which were observed to cause infection symptoms on *B. distachyon* Bd28 and 78 strains which were not. Combining the phenotypic and genotypic data allowed us to generate associations between them. We used two independent methods to identify regions and genes that were required for pathogenicity on *B. hybridum* Bd28.

In our first approach we looked exclusively at non-synonymous changes in the hybrids compared to both the *U. hordei* or *U. bromivora* reference genomes. This allowed us to find genes which may have been mutated since sequencing and identify if those mutations affected virulence. In total, 17,231 non-synonymous changes were identified, 5,214 of which were more common in the infecting hybrid strains with 51 reaching statistical significance ($p < 0.01$). (Fig 6A) This gives a list of 35 genes which are associated with pathogenicity (Table S3) but none of which are predicted to be secreted and thus would not likely fulfil the function of an effector. Non-synonymous mutations found between hybrid strains and the *U. hordei* genome are not expected to have an effect on the ability of the hybrid to infect. While it is possible that mutations in *U. hordei* genes may have some effect on infection, given the lack of predicted secreted proteins for both *U. hordei* and *U. bromivora,* it is more likely that these mutations lead to a general improvement in growth which then contributes to an improved outcome *in planta*.

An additional 11,978 non-synonymous changes were associated with those strains which could no longer infect, with 1,179 reaching statistical significance ($p < 0.01$). (Fig 6B) The 198 genes represented by these SNPs (Table S4) are primarily found in *U. bromivora* with fairly even representation across the genome. Only four are predicted to be secreted; two from chromosome 1 are predicted to have a membrane function, one from chromosome 3 is predicted to be involved in intracellular protein transport and the last, on chromosome 8, has no functional annotation but was identified as an orthologue of *U. maydis mig1*. Functional annotation suggests that the majority of these 198 genes which have GO terms are involved in DNA binding and endonuclease activity and located either in cell membranes or the mitochondria. It seems likely that most of the affected genes are important for the growth of the hybrids and mutations result in impaired infection even when the necessary effectors are present. Given the large difference in the occurrence of these SNPs between *U. bromivora* and *U. hordei*, it could also be suspected that these are genes which are not easily

compensated by the *U. hordei* genome. Any impaired function from the *U. hordei* SNPs would be compensated for during infection by the full genome of *U. hordei* during mating. For *U. bromivora*, there is no such opportunity to compensate for species-specific pathways or structural changes that have taken place over evolution. The few *U. hordei* SNPs that are associated with a reduction in pathogenicity are then likely either dose dependent or represent dominant, gain of function mutations which can have wide-ranging effects.

In our second approach, by using a combination of Multiplexed Shotgun Genotyping (MSG)(Andolfatto et al. 2011) to determine ancestry-specific SNPs (SNPs which identify the sequence as originating from either *U. bromivora* or *U. hordei*) and the R package r/qtl(R Core Team 2013; Broman et al. 2003) to analyse the resultant files, it was possible to generate associations with pathogenicity over the entire *U. bromivora* genome. The outputs of the analysis not only showed how SNPs were associated with pathogenicity (Fig 7) but also allowed us to predict the parental contribution of each chromosome. (Fig S5)

We assessed the association of 260,109 ancestry-specific SNPs with two different phenotypes; a binary trait considering whether a strain was capable of infecting *B. hybridum* Bd28 and a quantitative trait based on the percentage of infected plants which displayed symptoms. Three regions, occurring on *U. bromivora* chromosomes 8, 13 and 22, showed a significant association with the ability to infect at an alpha value of 0.01. Only the region on chromosome 8 was associated with both the binary and the quantitative measure of infection. An association with chromosome 13 was found for the quantitative trait and with chromosome 22 for the binary trait. If we lowered the threshold to an alpha value of 0.05 then those three regions are the only ones which reach significance for both traits. Despite its prominence in the association tests, the region on chromosome 8 is not essential for virulence as several strains maintain the ability to infect while lacking part or all of the *U. bromivora* sequence. This indicates that host specificity in *U. bromivora* is a multifactorial trait which is

influenced by at least three loci and that infection can be achieved through multiple, independent combinations of genes.

Altogether, we identified 75 genes in regions associated with virulence (Table S5). Out of these, six lack an ortholog in *U. hordei* and all occur on chromosome 8. As we are looking for factors unique to *U. bromivora* when compared to *U. hordei,* these may be of special significance. One of the genes, UBRO_04981, is identified as a probable GFA1- glucosamine fructose-6-phosphate transaminase and can be annotated with GO terms relating to chitin biosynthesis and carbohydrate binding. Although not identified as secreted, this does identify a function where a mutation could potentially improve pathogenesis as recognition of chitin can lead to PAMP (pathogen associated molecular pattern)-triggered-immunity. Four of the other five genes (UBRO_20681 – UBRO_20684) occur sequentially on chromosome 8. This is interesting because it might suggest that these genes have a similar origin or are clustered together for a shared function. Two have DNA-related functions while the other two have no functional annotation at all.

Out of the 75 potential virulence genes, nine are predicted to be secreted, although three (UBRO_04936, UBRO_06823 and UBRO_06828) are likely to have enzymatic functions unrelated to virulence. Furthermore, the *U. maydis* orthologs of UBRO_04936 and UBRO_06828 are downregulated during infection(Lanver et al. 2018). UBRO_06823 has two *U. maydis* orthologs, one of which is upregulated during late infection and one of which is upregulated at a low level during infection. UBRO_06823 has a function in glucan catabolism, which could serve to help weaken the plant cell wall but which may just be involved in harvesting sugar from the surrounding environment.

Two of the 75 virulence candidates (UBRO_04990 and UBRO_04923) are related to *mig1*, which is known to be upregulated by *U. maydis in planta* and is likely an effector(Basse et al. 2000). The *U. maydis* ortholog of UBRO_04923 is UMAG_12126, which has been observed

to have a virulence defect upon deletion(Uhse et al. 2018). All of the genes encoding predicted secreted proteins of unknown function or those related to *mig1* are located on chromosome 8. Of the final four effector candidates (UBRO_05003, UBRO_04986, UBRO_04984 and UBRO_04921), only UBRO_04921 does not have an ortholog in *U. maydis* and all the orthologs are significantly upregulated during infection(Lanver et al. 2018). Most of the orthologs are upregulated approximately 10-fold during infection with the exception of UBRO_05003, which has the GO annotation "defense response to other organism," which is only upregulated about 5-fold.

Discussion

Our study used hybridisation of two closely-related smut fungi to gain an understanding of host specificity. We demonstrated that *U. bromivora* and *U. hordei* are capable of forming a viable hybrid which can cause infection symptoms on *Brachypodium spp.* similar to, and perhaps even stronger than, the parental *U. bromivora*. We can not say whether this is due to the combined complement of effector proteins or some other effect of the combined genomes.

A particularly interesting observation was that there were several instances were there were large numbers of ancestry-specific SNPs from both *U. bromivora* and *U. hordei*. When MSG tried to predict ancestry of the chromosomes, these regions remained ambiguous and we interpreted this as evidence of partial or complete duplication of chromosomes. Genome sequencing was performed on the haploid sporidia, so it was unexpected to see multiple copies of a chromosome or region of a chromosome. Chromosomal duplications are one of the reasons that the fraction of *U. bromivora*-specific reads and shared or *U. hordei*-specific reads do not always add up to 1. The genome content in our analysis is also affected by sequencing depth in some cases, number and distribution of SNPs in a gene and other technical biases.

One region was particularly notable in terms of duplication; a 265 kb region of *U. bromivora*, containing the mating type locus, was present in nearly every hybrid. Even when there was evidence of a complete *U. hordei* version of chromosome 1, we also saw *U. bromivora*-specific SNPs at the centre of chromosome 1, creating ambiguity in predicting ancestry. We believe that this region encodes a spore-killer gene which results in a mating type bias. Dominant spore-killer traits which lead to a mating type bias have been described in several other fungi(Turner and Perkins 1979; Kathariou and Spieth 1982). Previously, we reported that *U. bromivora* has a mating type bias where all 225 sporidia (100%) from 21 spores tested found to be MAT1(Rabe et al. 2016) though the cause of the bias remained speculative. This mating type bias persisted in our hybrid crosses although *U. hordei* does not display a mating type bias. This provides evidence that the mating type bias is a dominant trait carried by *U. bromivora* MAT1, although the mechanism of action is still unknown. Interestingly, likely due to the genomic rearrangements accompanying hybridisation, the mating type which was favoured by the bias differed between generations. However, all the strains analysed here maintained this spore-killer region, presumably as those which did not were unable to survive saprophytically on plate without being rescued by a strain containing it. The sole exception to this rule was F4 strain 72784 which has a reduced number of *U. bromivora*-specific SNPs in that region and differs in mating type from the other F4 strains in the analysis.

Excluding the locus on *U. bromivora* chromosome 1 and the unassigned *U. bromivora* genome scaffold, which has few SNP markers, we observed ambiguous ancestry and potential duplications in 40 to 50% of all hybrid strains, e.g. chromosome 9 in the F3 and F4 generations. Genomic changes during hybridisation have been observed before in diverse lineages including yeasts(Pryszcz et al. 2015), plants(Gaeta et al. 2007) and marsupials(O'Neill et al. 2001). It is possible that chromosomal differences may arise to aid speciation and the rearrangements seen here could indicate partial incompatibility between *U. bromivora* and *U. hordei*. *Saccharomyces* can be divided into two groups; sensu stricto and

sensu lato. It has been shown that interspecific hybrids between two yeasts in the sensu stricto group maintain both sets of parental chromosomes(Marinoni et al. 1999) and chromosomal stability approximately equal to a diploid parental strain(Kumaran et al. 2013). However, interspecific matings involving a sensu lato species show much lower rates of viable hybrid formation and a failure to maintain both complete sets of parental chromosomes(Marinoni et al. 1999). It is unclear exactly what effect genomic rearrangements might have on pathogenicity beyond the specific genetic composition of the hybrids but changes in gene expression, which could potentially have virulence effects, have been observed in hybrid fungal genomes(Cox et al. 2014). It would be interesting if future research could identify any changes in gene expression among the hybrids due to these rearrangements.

By associating genetic differences between the hybrids with their ability to cause infection symptoms, we identified three regions in *U. bromivora* which are likely to be important for *U. bromivora* pathogenicity on *Brachypodium spp.* These regions occur on *U. bromivora* chromosomes 8, 13 and 22. The strongest association with hybrid virulence came from *U. bromivora* chromosome 8. We showed that this region has more putative effector proteins but it is not essential for virulence, which suggests that infection can be accomplished with different effector complements.

It could be possible that there was originally one major factor allowing *U. bromivora* to colonise *Brachypodium spp.* but over time, its significance has faded during adaptation. The evidence we provide does not exclude this possibility but it doesn't provide strong support for it either. It seems more likely that this host specificity might have arisen slowly rather than as a specific event. Perhaps the ancestral species of *U. bromivora* and *U. hordei* encountered *Brachypodium spp.* due to a migration on the plant or fungal side or a change in climate allowed infection, similar to *M. oryzae* infection of wheat(Farman et al. 2016). With no particular adaptation to the host, the infection would be very weak and only occasionally lead

to spore formation, not unlike *Puccinia striiformis f. sp. tritici* on *Brachypodium spp.* today(Gilbert et al. 2018). These weak infections would allow for natural selection to act on the ancestral fungus in order to adapt to better infect and reproduce on *Brachypodium spp.*

Although our work here was focused on host specificity of *U. bromivora* infecting *Brachypodium spp.*, the hybrid fungus approach is not limited to this system. If it were shown that *U. bromivora* alone is unable to infect barley and that the hybrid maintains the ability, then one could investigate host specificity of *U. hordei* on barley in much the same manner. Given the widespread possibilities for hybridisation among the *Ustilaginaceae*(Kellner et al. 2011; Huang and Nielsen 1984) and the possibility of enabling hybridisation through manipulating mating loci(Bakkeren and Kronstad 1996), one could imagine hybrid infections as a useful tool for examining host-specific pathogenicity in smuts generally and, perhaps, even more widely.

Materials and Methods

Strains, growth and infection

We used *U. bromivora* strains Mat 1 and Mat 2 which were previously described(Rabe et al. 2016) and *U. hordei* Mat 1 (strain 4875-4) and Mat 2 (strain 4875-5) which were provided by Jan Schirawski. Growth conditions for *U. bromivora*, *U. hordei*, *B. distachyon* ABR4 and *B. hybridum* Bd28 as well as the infection protocol were all previously described(Rabe et al. 2016). *U. bromivora* and the *U. bromivora* x *U. hordei* hybrids were originally used to infect *B. distachyon* ABR4. Images of whole plants and the phenotypic data for a comparison of growth effects were acquired using the PhenoBox automated plant phenotyping platform(Czedik-Eysenberg et al. 2018). Whole plants were stored in 100% ethanol before microscopy and images of fungal infections in plant tissue were acquired following the

protocol of Dawson et al.(Dawson et al. 2015) Spores from the hybrid-infected plants were isolated from infected spikelets and germinated as previously described(Bosch and Djamei 2017). The mating type of the haploid hybrid strains was determined, they were mated with *U. hordei* of the opposite mating type (Mat 1 hybrid with Mat 2 *U. hordei* and vice versa) and the dikaryotic fungi were used to infect *B. hybridum* Bd28. *B. hybridum* Bd28 was used because of the easier growth conditions and shorter time to flowering compared to *B. distachyon* ABR4(Rabe et al. 2016).

DNA extraction and PCR

Fungal cultures were grown in potato dextrose medium and genomic DNA was extracted using a phenol/chloroform extraction. Mating type was determined by a PCR approach based on Kellner et. al.(Kellner et al. 2011) Primers were designed to amplify the fungal mating loci; *U. bromivora* pra1 (GCTTTGTTGAGTGTCGATGC and ACCAATGTCGCCATGTACTC, 494bp product) and *U. hordei* pra2 (TCCCTCTCTTCTTCGTGGTT and GCTGGAGTAAGGCAGAAGTC, 418bp product). Mating could also be shown by inducing filamentation by growing a mixture of two compatible mating types on potato dextrose plates with the addition of activated charcoal (10 g/L).

Next Generation Sequencing

Extracted fungal gDNA was adjusted to 2.5 ng/µl after quantification using picogreen dye (Thermo Fisher Scientific) to exclusively measure double-stranded DNA. We followed a modification of the Illumina library preparation protocol prepared by Sergey Kryazhimskiy (V. 2.1 (2013-06-06)) which was later published, after further modifications, by Baym et. al. (Baym et al. 2015) Barcoding was done using an Illumina Nextera kit (Illumina) for labelling 24 samples. We performed library amplification using either Veraseq polymerase (Biozyme) or Phusion polymerase (Thermo Fisher Scientific) and size selection with AMPure XP beads

(Beckman Coulter). Fragment profiles of the libraries were determined with a Fragment Analyzer (Advanced Analytical) and libraries were pooled to equal concentrations, either based on the concentration determined by the Fragment Analyzer or a second round of quantification with picogreen fluorescent spectrometry. The libraries were sequenced using Illumina HiSeqV4 PE125 on a HiSeq2500 at the VBCF NGS Unit (www.vbcf.ac.at).

To get an idea of how well the sequencing covered the *U. bromivora* part of the hybrid genome and to identify the presence or absence of specific genes, we performed the following steps: The demultiplexed .bam files received from the NGS facility were converted to paired .fastq files with the use of BAM2FQ.jar. BAM2FQ.jar is a VBCF NGS modification of the Picard tools from the Broad Institute (http://broadinstitute.github.io/picard) to include a graphical user interface. These paired fastq files were imported into CLC Genomic Workbench 9 (Qiagen), aligned perfectly first to the *U. hordei* protein-coding genes and then to the *U. bromivora* protein-coding genes and summary tables for both alignments were produced. The *U. bromivora* reference genome (GCA_900080155.1) was sequenced from *U. bromivor*a UB1 (formerly strain UB2112)(Rabe et al. 2016). The *U. hordei* reference genome (GCA_000286035.1) was sequenced from *U. hordei* Mat 1 (strain Uh4857-4)(Laurie et al. 2012).

The workflow uses *U. bromivora* specific reads only to show which genes are present. Due to how closely related the two fungi are, it is not always possible to distinguish between them, but regions from *U. bromivora* that are identical to those from *U. hordei* are not expected to be relevant to pathogenicity.

In order to make comparisons between different hybrid strains, the gene-by-gene information was reduced to strain-specific summaries and these were joined together into a single table through custom bash and R(R Core Team 2013) scripts.

The install file for the CLC Genomic Workbench 9 workflow and the custom bash and R scripts are archived on Zenodo (DOI: 10.5281/zenodo.2563198).

Virulence associations with potentially damaging SNPs

Initial quality control, adapter removal and filtering of raw sequence reads was performed using Trim Galore! (v0.4.5) (https://www.bioinformatics.babraham.ac.uk/projects/trim_galore/) in the default mode. Processed paired-end reads were mapped against *U. hordei* and *U. bromivora* chromosomes using BWA mem (v0.7.17)(Li and Durbin 2009). Subsequently, we marked all potential PCR duplicates using Picard Tools (v2.18.3) (http://broadinstitute.github.io/picard) to reduce the amount of potential technical artefacts. SNPs and Indels were called using GATK HaplotypeCaller (v3.8-1)(McKenna et al. 2010) in gVCF mode. We applied hard-filtering on raw variant calls according to 'GATK Best Practices' to remove potential false-positive variants. Due to the absence of any gold standard variant set, we used the set of remaining high confidence variants to apply the GATK BaseRecalibrator on the PCR-marked BAM files. Afterwards, the final variant calling was performed. Variant filtering was done using the same parameters as before. The resulting SNPs were annotated using snpEff (v4.3q)(Cingolani et al. 2012). Subsequently, SNPs with putative damaging effects (non-synonymous and loss-of-function) were used as input for association tests using PLINK (v1.9)(Purcell et al. 2007). Association p-values were corrected for multiple testing according to Benjamini-Hochberg(Benjamini and Hochberg 1995).

Multiplex Shotgun Genotyping and r/qtl

In order to estimate the likely ancestry of chromosomal regions within the hybrids, we made use of the Multiplexed Shotgun Genotyping (MSG) technique(Andolfatto et al. 2011) on the first of the paired fastq files. The ancestry tables which are outputted by MSG were cleaned to remove SNPs where more than 10% of the strains lacked data and were then submitted to

pull_thin (https://github.com/dstern/pull_thin) to remove redundant SNPs. The cleaned ancestry files were then used as input to r/qtl(Broman et al. 2003) with the read_cross (https://github.com/dstern/read_cross_msg) function, along with information on which strains caused symptoms on plants in order to show linkage between SNPs and pathogenicity over the whole genome. We used 1,000 permutations of r/qtl's scanone function to determine that measuring association with a lod (logarithm of odds) threshold of 4.13 would be equivalent to an alpha of 0.01. Genes that fell within regions with a lod score equal to or greater than 4.13 were considered as potential virulence candidates. For chromosome 22, the relevant region is only ~500 bp in length but this falls entirely within the gene UBRO_08780 which was then added to the potential virulence candidates list.

In order to estimate the size of the region involved in the mating type bias, we modified the analysis above. Instead of performing the r/qtl analysis with the virulence data, we used the mating type of the hybrid strains. Due to presence of the mating type bias region in nearly every strain, there is a sudden, strong drop in association scores over that region. By identifying which SNPs where assigned a LOD score below 0,5, we were able to assign specific co-ordinates to this region. The region that was identified fell within a larger region that had previously been identified in unpublished data as important for the mating type bias.

Functional annotation of potential virulence candidates

Potential functions of the candidate genes were obtained through annotations of the genomes(Laurie et al. 2012; Rabe et al. 2016) and via analysis with Blast2GO(Gotz et al. 2008). We obtained functional annotations in Blast2GO by integrating the built-in Interpro scan with the BLAST search, mapping and annotation, all using the default settings.

Acknowledgements

We would like to thank the GMI/IMBA/IMP service facilities, especially the High Performance Computing service, as well as the Vienna BioCenter Core Facilities (VBCF), particularly Next Generation Sequencing and Plant Science, for technical support. Next-generation sequencing was performed at the VBCF NGS Unit (www.vbcf.ac.at). We would like to thank Franziska Rabe and Marina Perez for their involvement in starting this project, Julia Riefler and Daniel Pleyer for plant support, Patrick Reilly for assistance with MSG and Maria Gutin for advice about pull_thin and r/qtl. In addition, we would like to extend our thanks to the other members of the Djamei lab, particularly Simon Uhse, as well as J. Matthew Watson for their comments on the draft manuscript. Finally, we are grateful to the two anonymous reviewers for their constructive comments on our earlier manuscript.

Literature Cited

Andolfatto, P., Davison, D., Erezyilmaz, D., Hu, T. T., Mast, J., Sunayama-morita, T., and Stern, D. L. 2011. Multiplexed shotgun genotyping for rapid and efficient genetic mapping Multiplexed shotgun genotyping for rapid and efficient genetic mapping. Genome Res. 21:610–617

Bakkeren, G., and Kronstad, J. W. 1994. Linkage of mating-type loci distinguishes bipolar from tetrapolar mating in basidiomycetous smut fungi. Proc. Natl. Acad. Sci. 91:7085–7089

Bakkeren, G., and Kronstad, J. W. 1996. The pheromone cell signaling components of the Ustilago a mating-type loci determine intercompatibility between species. Genetics. 143:1601–13

Basse, C. W., Stumpferl, S., and Kahmann, R. 2000. Characterization of a Ustilago maydis Gene Specifically Induced during the Biotrophic Phase: Evidence for Negative as Well

as Positive Regulation. Mol. Cell. Biol. 20:329–339

Baym, M., Kryazhimskiy, S., Lieberman, T. D., Chung, H., Desai, M. M., and Kishony, R. 2015. Inexpensive Multiplexed Library Preparation for Megabase-Sized Genomes S.J. Green, ed. PLoS One. 10:e0128036

Belhaj, K., Cano, L. M., Prince, D. C., Kemen, A., Yoshida, K., Dagdas, Y. F., Etherington, G. J., Schoonbeek, H., van Esse, H. P., Jones, J. D. G., Kamoun, S., and Schornack, S. 2017. Arabidopsis late blight: infection of a nonhost plant by Albugo laibachii enables full colonization by Phytophthora infestans. Cell. Microbiol. 19:e12628

Benjamini, Y. ., and Hochberg, Y. 1995. Controlling the False Discovery Rate : A Practical and Powerful Approach to Multiple Testing. J. R. Stat. Soc. Ser. B. 57:289–300

Bettgenhaeuser, J., Gardiner, M., Spanner, R., Green, P., Hernández-Pinzón, I., Hubbard, A., Ayliffe, M., and Moscou, M. J. 2018. The genetic architecture of colonization resistance in Brachypodium distachyon to non-adapted stripe rust (Puccinia striiformis) isolates. PLOS Genet. 14:e1007637

Bhat, R. G., and Subbarao, K. V. 1999. Host Range Specificity in Verticillium dahliae. Phytopathology. 89:1218–1225

Bosch, J., and Djamei, A. 2017. Isolation of Ustilago bromivora Strains from Infected Spikelets through Spore Recovery and Germination. BIO-PROTOCOL. 7

Brasier, C. 2000. Plant pathology: The rise of the hybrid fungi. Nature. 405:134–135

Broman, K. W., Wu, H., Sen, S., and Churchill, G. a. 2003. R/qtl: QTL mapping in experimental crosses. Bioinformatics. 19:889–890

Casadevall, A. 2018. Fungal Diseases in the 21st Century: The Near and Far Horizons. Pathog. Immun. 3:183

Cingolani, P., Platts, A., Wang, L. L., Coon, M., Nguyen, T., Wang, L., Land, S. J., Lu, X., and Ruden, D. M. 2012. A program for annotating and predicting the effects of single nucleotide polymorphisms, SnpEff. Fly (Austin). 6:80–92

Cox, M. P., Dong, T., Shen, G., Dalvi, Y., Scott, D. B., and Ganley, A. R. D. 2014. An interspecific fungal hybrid reveals cross-kingdom rules for allopolyploid gene expression patterns. PLoS Genet. 10:e1004180

Czedik-Eysenberg, A., Seitner, S., Güldener, U., Koemeda, S., Jez, J., Colombini, M., and Djamei, A. 2018. The "PhenoBox", a flexible, automated, open-source plant phenotyping solution. New Phytol. 219:808–823

Dawson, A. M., Bettgenhaeuser, J., Gardiner, M., Green, P., Hernández-Pinzón, I., Hubbard, A., and Moscou, M. J. 2015. The development of quick, robust, quantitative phenotypic assays for describing the host–nonhost landscape to stripe rust. Front. Plant Sci. 6:1–9

Dean, R., Van Kan, J. a L., Pretorius, Z. a., Hammond-Kosack, K. E., Di Pietro, A., Spanu, P. D., Rudd, J. J., Dickman, M., Kahmann, R., Ellis, J., and Foster, G. D. 2012. The Top 10 fungal pathogens in molecular plant pathology. Mol. Plant Pathol. 13:414–430

Depotter, J. R. L., Seidl, M. F., Wood, T. a., and Thomma, B. P. H. J. 2016. Interspecific hybridization impacts host range and pathogenicity of filamentous microbes. Curr. Opin. Microbiol. 32:7–13

Farman, M., Peterson, G. L., Chen, L., Starnes, J. H., Valent, B., Bachi, P., Murdock, L., Hershman, D. E., Pedley, K. F., Fernandes, J. M. C., and Bavaresco, J. 2016. The Lolium Pathotype of *Magnaporthe oryzae* Recovered From a Single Blasted Wheat Plant in the United States. Plant Dis. 101:PDIS-05-16-0700-RE

Frantzeskakis, L., Courville, K. J., Plücker, L., Kellner, R., Kruse, J., Brachmann, A., Feldbrügge, M., and Göhre, V. 2017. The Plant-Dependent Life Cycle of Thecaphora

thlaspeos : A Smut Fungus Adapted to Brassicaceae. Mol. Plant-Microbe Interact. 30:271–282

Freeman, B. C., and Beattie, G. A. 2008. An Overview of Plant Defenses against Pathogens and Herbivores. Plant Heal. Instr. Available at: http://www.apsnet.org/edcenter/intropp/topics/Pages/OverviewOfPlantDiseases.aspx [Accessed March 21, 2019].

Gaeta, R. T., Pires, J. C., Iniguez-Luy, F., Leon, E., and Osborn, T. C. 2007. Genomic Changes in Resynthesized Brassica napus and Their Effect on Gene Expression and Phenotype. PLANT CELL ONLINE. 19:3403–3417

Gilbert, B., Bettgenhaeuser, J., Upadhyaya, N., Soliveres, M., Singh, D., Park, R. F., Moscou, M. J., and Ayliffe, M. 2018. Components of Brachypodium distachyon resistance to nonadapted wheat stripe rust pathogens are simply inherited. PLOS Genet. 14:e1007636

Gotz, S., Garcia-Gomez, J. M., Terol, J., Williams, T. D., Nagaraj, S. H., Nueda, M. J., Robles, M., Talon, M., Dopazo, J., and Conesa, A. 2008. High-throughput functional annotation and data mining with the Blast2GO suite. Nucleic Acids Res. 36:3420–3435

Huang, H.-Q., and Nielsen, J. 1984. Hybridization of the seedling-infecting Ustilago spp. pathogenic on barley and oats, and a study of the genotypes conditioning the morphology of their spore walls. Can. J. Bot. 62:603–608

Inderbitzin, P., Davis, R. M., Bostock, R. M., and Subbarao, K. V. 2011. The Ascomycete Verticillium longisporum Is a Hybrid and a Plant Pathogen with an Expanded Host Range A. Litvintseva, ed. PLoS One. 6:e18260

Inoue, Y., Vy, T. T. P., Yoshida, K., Asano, H., Mitsuoka, C., Asuke, S., Anh, V. L., Cumagun, C. J. R., Chuma, I., Terauchi, R., Kato, K., Mitchell, T., Valent, B., Farman, M., and Tosa, Y. 2017. Evolution of the wheat blast fungus through functional losses in a

host specificity determinant. Science (80-.). 357:80–83

Jarvie, J. A. 2010. A review of soybean rust from a South African perspective. S. Afr. J. Sci. 105:103

de Jonge, R., Bolton, M. D., Kombrink, A., van den Berg, G. C. M., Yadeta, K. A., and Thomma, B. P. H. J. 2013. Extensive chromosomal reshuffling drives evolution of virulence in an asexual pathogen. Genome Res. 23:1271–1282

De Jonge, R., Bolton, M. D., and Thomma, B. P. H. J. 2011. How filamentous pathogens co-opt plants: The ins and outs of fungal effectors. Curr. Opin. Plant Biol. 14:400–406

de Jonge, R., Peter van Esse, H., Maruthachalam, K., Bolton, M. D., Santhanam, P., Saber, M. K., Zhang, Z., Usami, T., Lievens, B., Subbarao, K. V., and Thomma, B. P. H. J. 2012. Tomato immune receptor Ve1 recognizes effector of multiple fungal pathogens uncovered by genome and RNA sequencing. Proc. Natl. Acad. Sci. 109:5110–5115

Kathariou, S., and Spieth, P. T. 1982. Spore Killer Polymorphism in FUSARIUM MONILIFORME. Genetics. 102:19–24

Kellner, R., Vollmeister, E., Feldbrügge, M., and Begerow, D. 2011. Interspecific sex in grass smuts and the genetic diversity of their pheromone-receptor system. PLoS Genet. 7

Kruse, J., Piątek, M., Lutz, M., and Thines, M. 2018. Broad host range species in specialised pathogen groups should be treated with suspicion – a case study on Entyloma infecting Ranunculus. Persoonia - Mol. Phylogeny Evol. Fungi. 41:175–201

Kumaran, R., Yang, S. Y., and Leu, J. Y. 2013. Characterization of Chromosome Stability in Diploid, Polyploid and Hybrid Yeast Cells. PLoS One. 8

Lanver, D., Müller, A. N., Happel, P., Schweizer, G., Haas, F. B., Franitza, M., Pellegrin, C., Reissmann, S., Altmüller, J., Rensing, S. A., and Kahmann, R. 2018. The Biotrophic

Development of Ustilago maydis Studied by RNA-Seq Analysis. Plant Cell. 30:300–323

Laurie, J. D., Ali, S., Linning, R., Mannhaupt, G., Wong, P., Guldener, U., Munsterkotter, M., Moore, R., Kahmann, R., Bakkeren, G., and Schirawski, J. 2012. Genome Comparison of Barley and Maize Smut Fungi Reveals Targeted Loss of RNA Silencing Components and Species-Specific Presence of Transposable Elements. Plant Cell. 24:1733–1745

Li, H., and Durbin, R. 2009. Fast and accurate short read alignment with Burrows-Wheeler transform. Bioinformatics. 25:1754–1760

Marinoni, G., Manuel, M., Petersen, R. F., Hvidtfeldt, J., Sulo, P., and Piškur, J. 1999. Horizontal transfer of genetic material among Saccharomyces yeasts. J. Bacteriol. 181:6488–6496

Matei, A., Ernst, C., Günl, M., Thiele, B., Altmüller, J., Walbot, V., Usadel, B., and Doehlemann, G. 2018. How to make a tumour: cell type specific dissection of Ustilago maydis-induced tumour development in maize leaves. New Phytol. 217:1681–1695

McKenna, A., Hanna, M., Banks, E., Sivachenko, A., Cibulskis, K., Kernytsky, A., Garimella, K., Altshuler, D., Gabriel, S., Daly, M., and DePristo, M. A. 2010. The Genome Analysis Toolkit: A MapReduce framework for analyzing next-generation DNA sequencing data. Genome Res. 20:1297–1303

Menardo, F., Praz, C., Wyder, S., Bourras, S. . A., McNally, K. E., Parlange, F., Riba, A., Roffler, S., Schaefer, L., Shimizu, K. K., Valenti, L., Zbinden, H., Wicker, T., and Keller, B. 2015. Hybridization of powdery mildew strains gives raise to pathogens on novel agricultural crop species. Nat. Genet. 48:1–24

Mottaleb, K. A., Singh, P. K., Sonder, K., Kruseman, G., Tiwari, T. P., Barma, N. C. D., Malaker, P. K., Braun, H.-J., and Erenstein, O. 2018. Threat of wheat blast to South Asia's food security: An ex-ante analysis W. Ma, ed. PLoS One. 13:e0197555

Newcombe, G., Stirling, B., McDonald, S., and Bradshaw, H. D. 2000. Melampsora × columbiana, a natural hybrid of M. medusae and M. occidentalis. Mycol. Res. 104:261–274

O'Neill, R. J. W., Eldridge, M. D. B., and Graves, J. A. M. 2001. Chromosome heterozygosity and de novo chromosome rearrangements in mammalian interspecies hybrids. Mamm. Genome. 12:256–259

Olson, Å., and Stenlid, J. 2002. Pathogenic fungal species hybrids infecting plants. Microbes Infect. 4:1353–1359

Pryszcz, L. P., Németh, T., Saus, E., Ksiezopolska, E., Hegedűsová, E., Nosek, J., Wolfe, K. H., Gacser, A., and Gabaldón, T. 2015. The Genomic Aftermath of Hybridization in the Opportunistic Pathogen Candida metapsilosis. PLOS Genet. 11:e1005626

Purcell, S., Neale, B., Todd-Brown, K., Thomas, L., Ferreira, M. A. R., Bender, D., Maller, J., Sklar, P., de Bakker, P. I. W., Daly, M. J., and Sham, P. C. 2007. PLINK: A Tool Set for Whole-Genome Association and Population-Based Linkage Analyses. Am. J. Hum. Genet. 81:559–575

Rabe, F., Bosch, J., Stirnberg, A., Guse, T., Bauer, L., Seitner, D., Rabanal, F. a, Czedik-Eysenberg, A., Uhse, S., Bindics, J., Genenncher, B., Navarrete, F., Kellner, R., Ekker, H., Kumlehn, J., Vogel, J. P., Gordon, S. P., Marcel, T. C., Münsterkötter, M., Walter, M. C., Sieber, C. M., Mannhaupt, G., Güldener, U., Kahmann, R., and Djamei, A. 2016. A complete toolset for the study of Ustilago bromivora and Brachypodium sp. as a fungal-temperate grass pathosystem. Elife. 5:1–35

R Core Team. 2013. R: A Language and Environment for Statistical Computing.

Schilling, L., Matei, A., Redkar, A., Walbot, V., and Doehlemann, G. 2014. Virulence of the maize smut Ustilago maydis is shaped by organ-specific effectors. Mol. Plant Pathol.

15:780–789

Sharma, R., Mishra, B., Runge, F., and Thines, M. 2014. Gene loss rather than gene gain is associated with a host jump from Monocots to Dicots in the Smut Fungus Melanopsichium pennsylvanicum. Genome Biol. Evol. 6:2034–49

Skibbe, D. S., Doehlemann, G., Fernandes, J., and Walbot, V. 2010. Maize tumors caused by Ustilago maydis require organ-specific genes in host and pathogen. Science. 328:89–92

Turner, B. C., and Perkins, D. D. 1979. Spore killer, a chromosomal factor in neurospora that kills meiotic products not containing it. Genetics. 93:587–606

Uhse, S., and Djamei, A. 2018. Effectors of plant-colonizing fungi and beyond C. Zipfel, ed. PLOS Pathog. 14:e1006992

Uhse, S., Pflug, F. G., Stirnberg, A., Ehrlinger, K., von Haeseler, A., and Djamei, A. 2018. In vivo insertion pool sequencing identifies virulence factors in a complex fungal–host interaction J. Heitman, ed. PLOS Biol. 16:e2005129

Author-Recommended Internet Resources

Raw sequencing data in the form of demultiplexed BAM files has been deposited in the National Center for Biotechnology Information's (NCBI) Sequence Read Archive (SRA) with BioProject ID: PRJNA508607.

Figure Captions

Fig 1. Macroscopic infection phenotype on *B. distachyon* ABR4

Macroscopic phenotype of ABR4 plants when uninfected or infected by either *U. bromivora* or the *U. bromivora* X *U. hordei* hybrid. (A, B, C) The overall appearance of the plant at 42 days after vernalization (DAV). Scale bar represents 2 cm. (D, E, F) A close-up of the spikelets. Scale bar represents 20 mm. (G, H, I) The stem nodes. On rare occasions, the hybrid produces spores in the nodes. Scale bar represent 1 mm.

Fig 2. Microscopic infection phenotype on *B. distachyon* ABR4

Microscopic phenotype of ABR4 plants when uninfected or infected by either *U. bromivora* or the *U. bromivora* X *U. hordei* hybrid. (A,B,C) Maximum intensity z-stack projection showing fungal and plant cells in the stem, 3 weeks after vernalization. The plant cell walls are stained with propidium iodide and fungal cells are stained with wheat germ agglutinin(WGA)-Alexafluor. Scale bar represents 50 µm. (D,E,F) Differential interference contrast (DIC) microscopy images of the spores released from grinding the spikelet. The uninfected spikelet shows no spores at all whereas both *U. bromivora* and hybrid infected spikelets stain the water black with the spores. Scale bar represents 10 µm.

Fig 3. Phenotypic differences between uninfected, U. *bromivora*-infected and hybrid-infected *B. distachyon* ABR4

While the end phenotypes of the *U. bromivora* X *U. hordei* hybrid and *U. bromivora* infection are quite similar, there are subtle differences in their effects on the plant. (A) A principle components analysis (PCA) of uninfected (pale yellow), *U. bromivora*-infected (red) and hybrid-infected (blue) *B. distachyon* ABR4 plants 42 days after vernalisation based on visual data collected by the Phenobox automated phenotyping system. The lighter coloured spots are plants which were infected with *U. bromivora* or the hybrid but did not develop symptoms.

These failed infections are indistinguishable from uninfected plants on the PCA. *U. bromivora* and hybrid infected plants are both distinct from the uninfected plants and from each other. The parameters describing the loading of the displayed principal components can be seen in Table S1. Further details on the parameters determined by the Phenobox are available in Czedik-Eysenberg et. al.(Czedik-Eysenberg et al. 2018) (B) A more detailed look at a single phenotypic trait (plant height) when measured over time. *U. bromivora* and the hybrid are both significantly smaller than uninfected plants. From 28 days after vernalisation, there is a clear difference between hybrid-infected and *U. bromivora* infected plants as the former fails to undergo bolting. Error bars indicate standard deviation. P-values were corrected for multiple testing using the Benjamini–Hochberg method. *, $P < 0.05$; **, $P < 0.01$; ***, $P < 0.001$; ****, $P < 0.0001$.

Fig 4. Schematic of the hybrid backcrossing

Schematic describing the hybrid backcrossing approach. Running down the left-hand side is the name of each hybrid generation. On the yellow background, haploid parental strains (Generation P) each contain 100% of their respective genome. These parental strains are mated to form an infectious dikaryon with 100% of each parent's genome (Generation dP, where the "d" indicates the dikaryon formed by mating with *U. hordei*).

From generation F1 onwards, only the haploid hybrid is shown in detail. Between each generation the hybrid is mated with *U. hordei* to form a dikaryon which is used to infect *B. hybridum* Bd28. This dikaryotic form is depicted by a black dot on the line between haploid generations and both produces the spores for the next generation and shows which strains are still pathogenic. Different F1 strains were used to create several sets of independent F2 progeny. The main hybrid line, marked in bold, shows the strains descended from the same parent in each generation. At the bottom right of each set of hybrids is a pair of numbers that

represents the number of strains which were able to cause infection symptoms on plants as well as the total number of strains tested.

Fig 5. Hybrid strain virulence and *U. bromivora* genome content decreases with each generation

(A) The percentage of hybrid strains capable of causing infection symptoms on *B. hybridum* Bd28 when mated with *U. hordei* decreases with each generation. (B) For hybrid strains capable of causing infection symptoms, the strength of the infections decreases with each generation. The strength of the infection is measured as the number of plants infected which go on to develop symptoms for a particular hybrid strain. For the dP generation (*U. bromivora* X *U. hordei*) the individual points show independent infections. For the backcrossed generations, the individual points show specific hybrid strains. No dF4 strains were observed to cause symptoms. (C) With each generation the percentage of *U. bromivora* genes (red), detected by *U. bromviora*-specific reads, in the hybrid strains decreased while the percentage of *U. hordei* or shared genes (blue), detected by *U. hordei*-specific or shared reads, increased.

Fig 6. Potentially damaging SNPs associated with the ability to infect *B. hybridum* Bd28

An analysis of potentially damaging (non-synonymous and loss-of-function) SNPs in hybrids which may be associated with the ability to infect *B. hybridum Bd28*. These SNPs were obtained by comparing the reads to the reference genomes and can be found in both parental species. They are divided into SNPs that are (A) found more often in strains which are capable of infecting and (B) more often in strains which are not capable of infecting. Points above the red line represent SNPs which are overrepresented in infectious samples with a p-

value < 0.01. P-values were corrected for multiple testing using the Benjamini–Hochberg method. Due to space constraints, not all scaffolds or chromosomes are labelled.

Fig 7. Linkage of ancestry markers with the ability to infect *B. hybridum* Bd28

Certain regions of the *U. bromivora* genome show an association with the ability to infect *B. hybridum* Bd28. The red line shows the lod (logarithm of odds) score cut-off of 4.13, representing $\alpha = 0.01$. The lod score is a measure of the association of a particular SNP with the phenotype under consideration. Regions on chromosome 8, 13 and 22 exceed the threshold. (A) Lod scores of chromosomal regions when the phenotype is defined as a binary trait of causing infection symptoms on *B. hybridum* Bd28 or not. (B) Lod scores of chromosomal regions when the phenotype is the percentage of total plants that show infection symptoms. Due to space constraints, the mitochondria and an unassigned scaffold are not labelled.

e-Xtras Captions

Figure S1: *U. bromivora* and *U. hordei* fungal cultures

Fungal cultures growing in liquid potato dextrose medium. Phenotypically, the haploid cells of *U. bromivora* and *U. hordei* are very similar. Scale bar represents 10 µm.

Figure S2: Charcoal mating

U. bromivora (UB) and *U. hordei* (UH) are able to mate and form filaments on charcoal plates. The number refers to the strain's mating type, e.g. UB1 is *U. bromivora* Mat1. When the same mating only one mating type is present, filamentation does not occur and the

colonies have a smooth border. When opposite mating types are present, e.g. UB1 and UB2, then the mated fungus filaments and the border of the colony appears fuzzy.

Figure S3: Infection phenotype on *B. hybridum* Bd28

Phenotypes of *B. hybridum* Bd28 infected with *U. bromivora*, *U. bromivora* X *U. hordei* hybrid or uninfected. Infection phenotypes are comparable with those observed in *B. distachyon* ABR4. (Fig 1) A, B and C show *B. hybridum* Bd28 plants 48 days after planting (DAP). Scale bar represents 2 cm. D, E and F show a close-up of the spikelets. Scale bar represents 20 mm. G, H and I show differential interference contrast (DIC) microscopy images of the spores released from grinding the spikelet. Scale bar represents 10 µm.

Figure S4: Microscopy of *U. bromivora* and hybrid infection on *B. hybridum* ABR4.

Microscopic phenotype of ABR4 plants infected by either *U. bromivora* or the *U. bromivora* X *U. hordei* hybrid. Maximum intensity z-stack projection showing fungal and plant cells in the stem, 3 weeks after vernalization. The plant cell walls are stained with propidium iodide and fungal cells are stained with wheat germ agglutinin(WGA)-Alexafluor. Scale bar represents 50 µm.

Figure S5: Chromosome ancestry of hybrid strains

Ancestry of each chromosome predicted by unique *U. bromivora* or *U. hordei* SNPs. The ancestry informative SNPs run along the top and bottom of each plot. Red shows *U. bromivora* specific SNPs and blue shows *U. hordei* specific SNPs. When there are sufficient SNPs from one progenitor and not the other, that chromosomal region is filled in with the

colour of the ancestral progenitor. In cases where the ancestry is ambiguous the region is left blank, e.g. chromosome 9 in F3. This likely represents a situation where chromosomes from both parents are present. Each generation is represented by a single hybrid; F1 is the parental strain for F2, which is the parental strain of F3 and F3 is the parental strain of F4. Each generation shows a reduction in the genomic regions contributed by the original *U. bromivora* strain. Due to space constraints, the mitochondria and an unassigned scaffold are not labelled.

e-Xtras

Figure S1: *U. bromivora* and *U. hordei* fungal cultures

Figure S2: Charcoal mating

Figure S3: Infection phenotype on *B. hybridum* Bd28

Figure S4: Microscopy of *U. bromivora* and hybrid infection on *B. hybridum* ABR4.

Figure S5: Chromosome ancestry of hybrid strains

Table S1: Phenobox PCA loadings

Table S2: Strains for NGS

Table S3: Genes containing potentially damaging SNPs which are more common in infecting strains.

Table S4: Genes containing potentially damaging SNPs which are more common in non-infecting strains.

Table S5: Potential pathogenicity genes

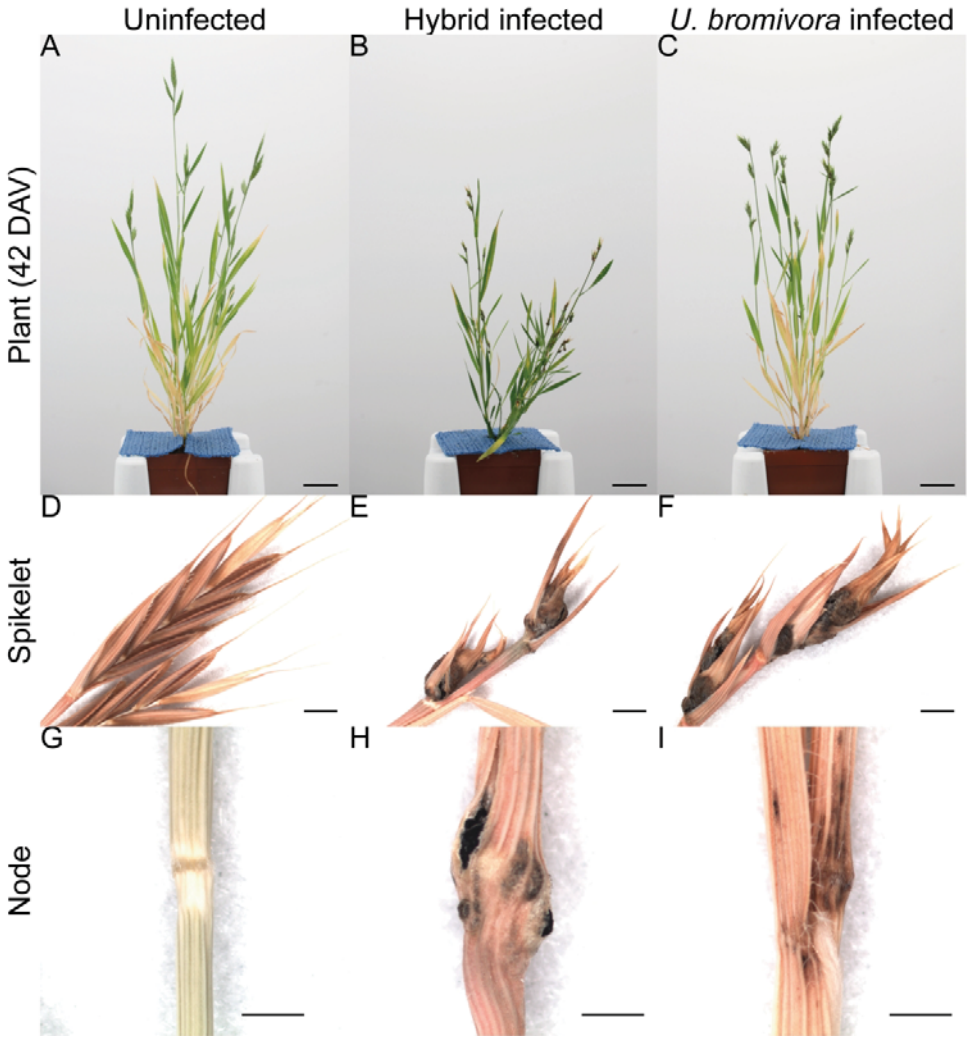

Fig 1. Macroscopic infection phenotype on B. distachyon ABR4
Macroscopic phenotype of ABR4 plants when uninfected or infected by either U. bromivora or the U. bromivora X U. hordei hybrid. (A, B, C) The overall appearance of the plant at 42 days after vernalization (DAV). Scale bar represents 2 cm. (D, E, F) A close-up of the spikelets. Scale bar represents 20 mm. (G, H, I) The stem nodes. On rare occasions, the hybrid produces spores in the nodes. Scale bar represent 1 mm.

160x169mm (300 x 300 DPI)

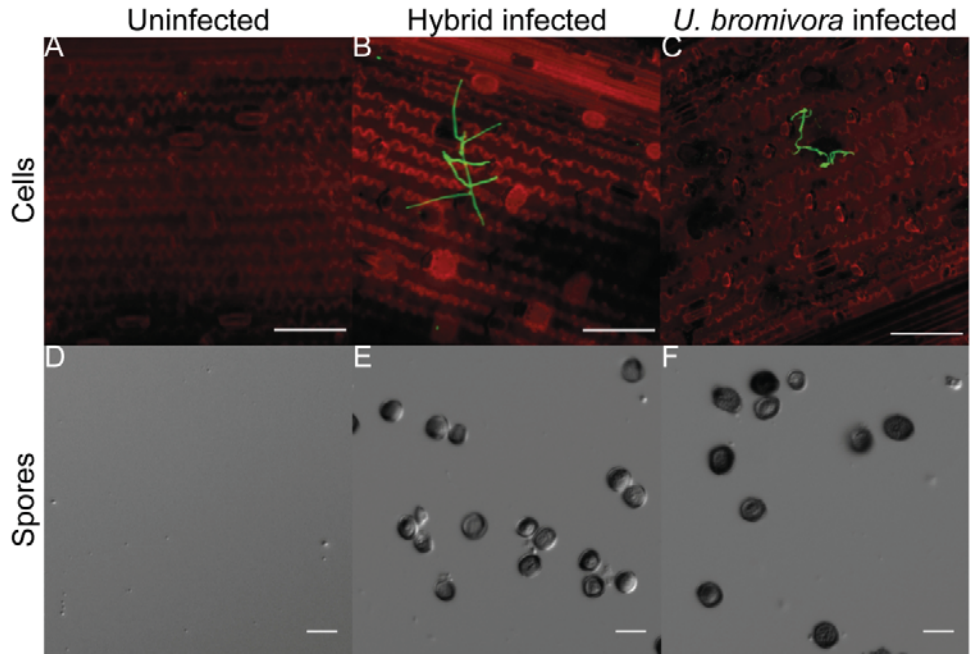

Microscopic phenotype of ABR4 plants when uninfected or infected by either U. bromivora or the U. bromivora X U. hordei hybrid. (A,B,C) Maximum intensity z-stack projection showing fungal and plant cells in the stem, 3 weeks after vernalization. The plant cell walls are stained with propidium iodide and fungal cells are stained with wheat germ agglutinin(WGA)-Alexafluor. Scale bar represents 50 µm. (D,E,F) Differential interference contrast (DIC) microscopy images of the spores released from grinding the spikelet. The uninfected spikelet shows no spores at all whereas both U. bromivora and hybrid infected spikelets stain the water black with the spores. Scale bar represents 10 µm.

159x106mm (300 x 300 DPI)

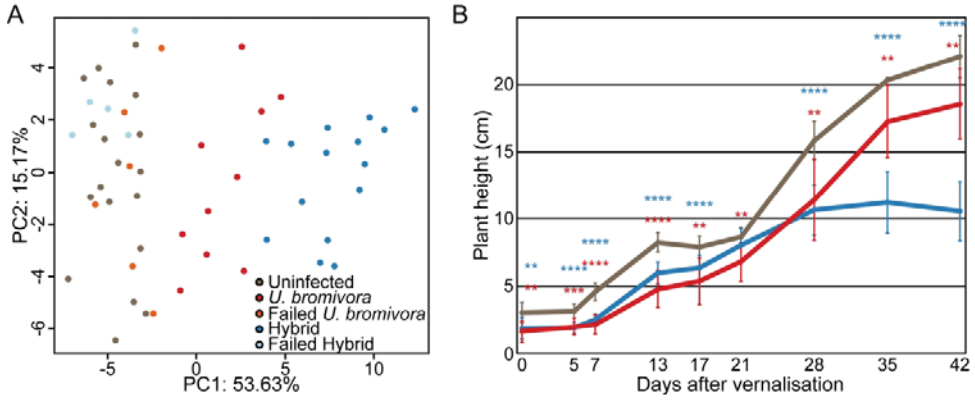

While the end phenotypes of the U. bromivora X U. hordei hybrid and U. bromivora infection are quite similar, there are subtle differences in their effects on the plant. (A) A principle components analysis (PCA) of uninfected (pale yellow), U. bromivora-infected (red) and hybrid-infected (blue) B. distachyon ABR4 plants 42 days after vernalisation based on visual data collected by the Phenobox automated phenotyping system. The lighter coloured spots are plants which were infected with U. bromivora or the hybrid but did not develop symptoms. These failed infections are indistinguishable from uninfected plants on the PCA. U. bromivora and hybrid infected plants are both distinct from the uninfected plants and from each other. The parameters describing the loading of the displayed principal components can be seen in Table S1. Further details on the parameters determined by the Phenobox are available in Czedik-Eysenberg et. al.(Czedik-Eysenberg et al. 2018) (B) A more detailed look at a single phenotypic trait (plant height) when measured over time. U. bromivora and the hybrid are both significantly smaller than uninfected plants. From 28 days after vernalisation, there is a clear difference between hybrid-infected and U. bromivora infected plants as the former fails to undergo bolting. Error bars indicate standard deviation. P-values were corrected for multiple testing using the Benjamini–Hochberg method. *, $P < 0.05$; **, $P < 0.01$; ***, $P < 0.001$; ****, $P < 0.0001$.

190x77mm (300 x 300 DPI)

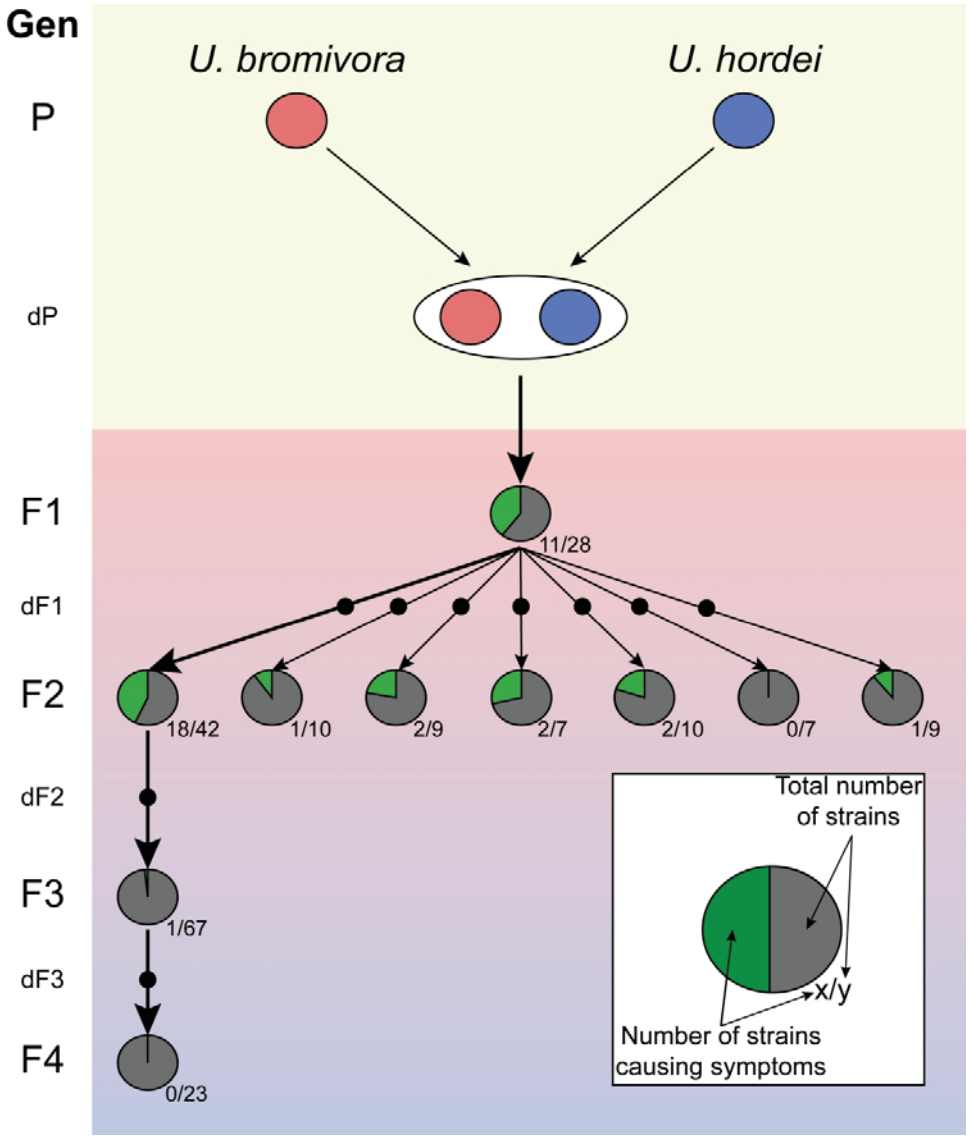

Fig 4. Schematic of the hybrid backcrossing

Schematic describing the hybrid backcrossing approach. Running down the left-hand side is the name of each hybrid generation. On the yellow background, haploid parental strains (Generation P) each contain 100% of their respective genome. These parental strains are mated to form an infectious dikaryon with 100% of each parent's genome (Generation dP, where the "d" indicates the dikaryon formed by mating with U. hordei).

From generation F1 onwards, only the haploid hybrid is shown in detail. Between each generation the hybrid is mated with U. hordei to form a dikaryon which is used to infect B. hybridum Bd28. This dikaryotic form is depicted by a black dot on the line between haploid generations and both produces the spores for the next generation and shows which strains are still pathogenic. Different F1 strains were used to create several sets of independent F2 progeny. The main hybrid line, marked in bold, shows the strains descended from the same parent in each generation. At the bottom right of each set of hybrids is a pair of numbers that represents the number of strains which were able to cause infection symptoms on plants as well as the total number of strains tested.

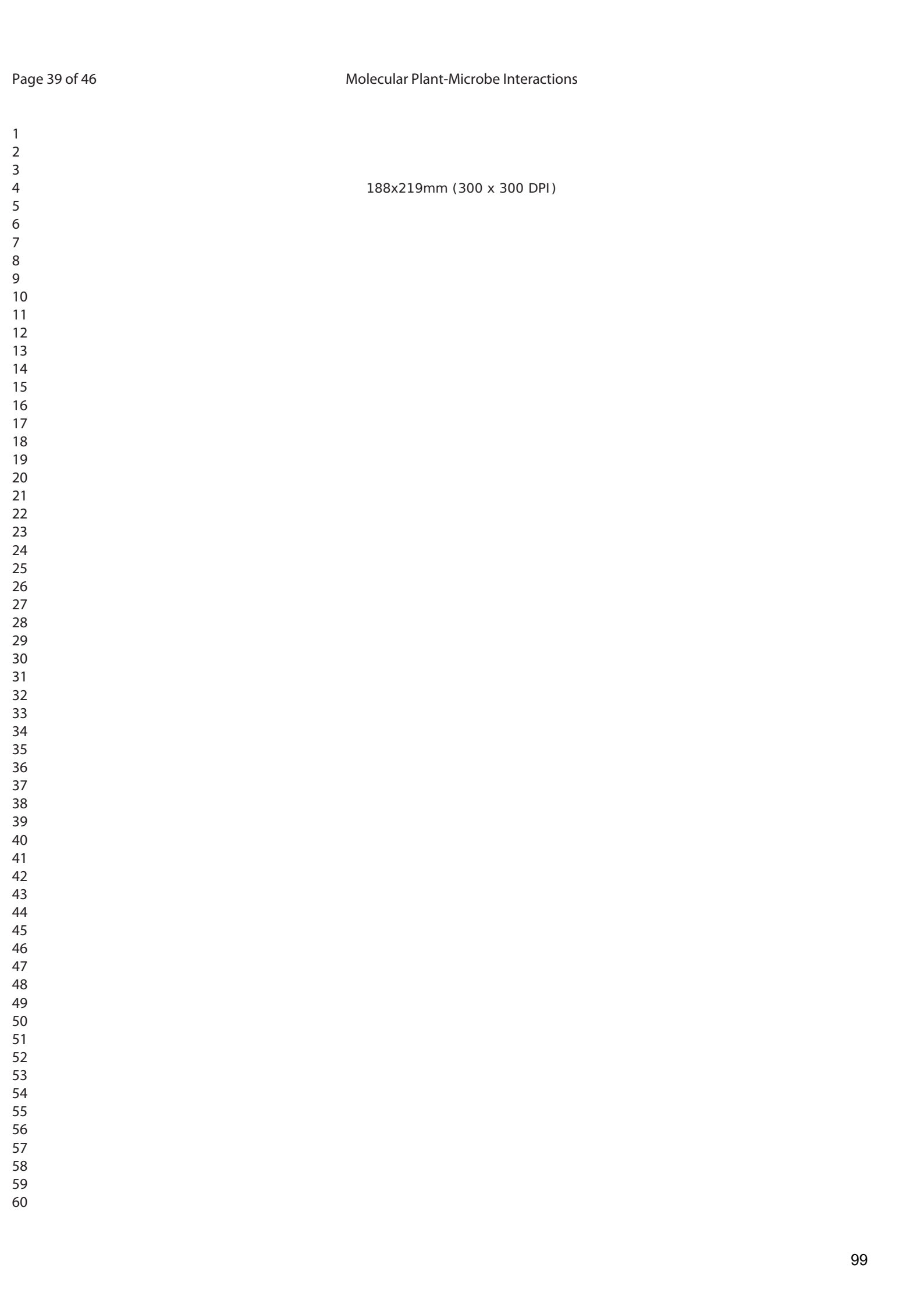
188x219mm (300 x 300 DPI)

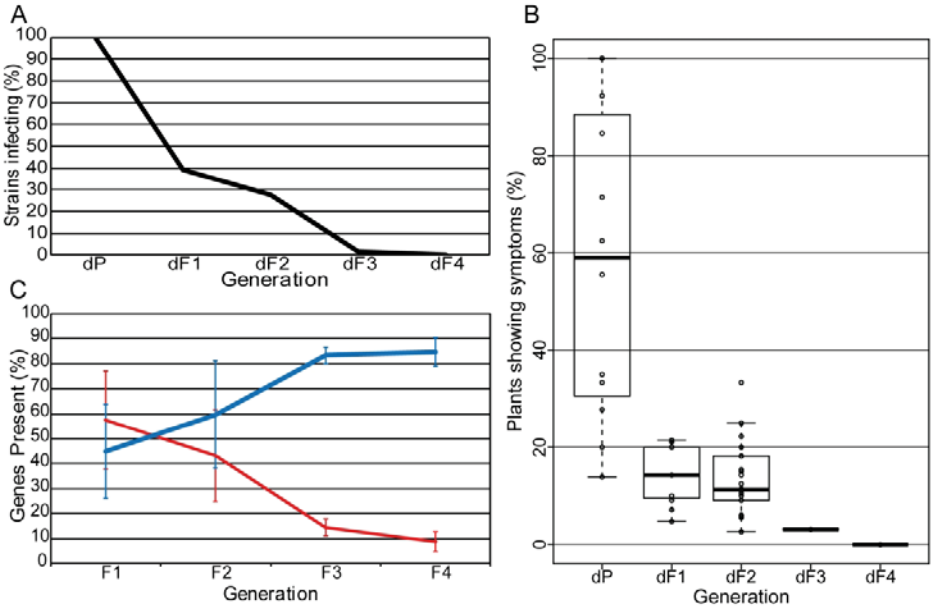

Fig 5. Hybrid strain virulence and U. bromivora genome content decreases with each generation (A) The percentage of hybrid strains capable of causing infection symptoms on B. hybridum Bd28 when mated with U. hordei decreases with each generation. (B) For hybrid strains capable of causing infection symptoms, the strength of the infections decreases with each generation. The strength of the infection is measured as the number of plants infected which go on to develop symptoms for a particular hybrid strain. For the dP generation (U. bromivora X U. hordei) the individual points show independent infections. For the backcrossed generations, the individual points show specific hybrid strains. No dF4 strains were observed to cause symptoms. (C) With each generation the percentage of U. bromivora genes (red), detected by U. bromviora-specific reads, in the hybrid strains decreased while the percentage of U. hordei or shared genes (blue), detected by U. hordei-specific or shared reads, increased.

193x123mm (300 x 300 DPI)

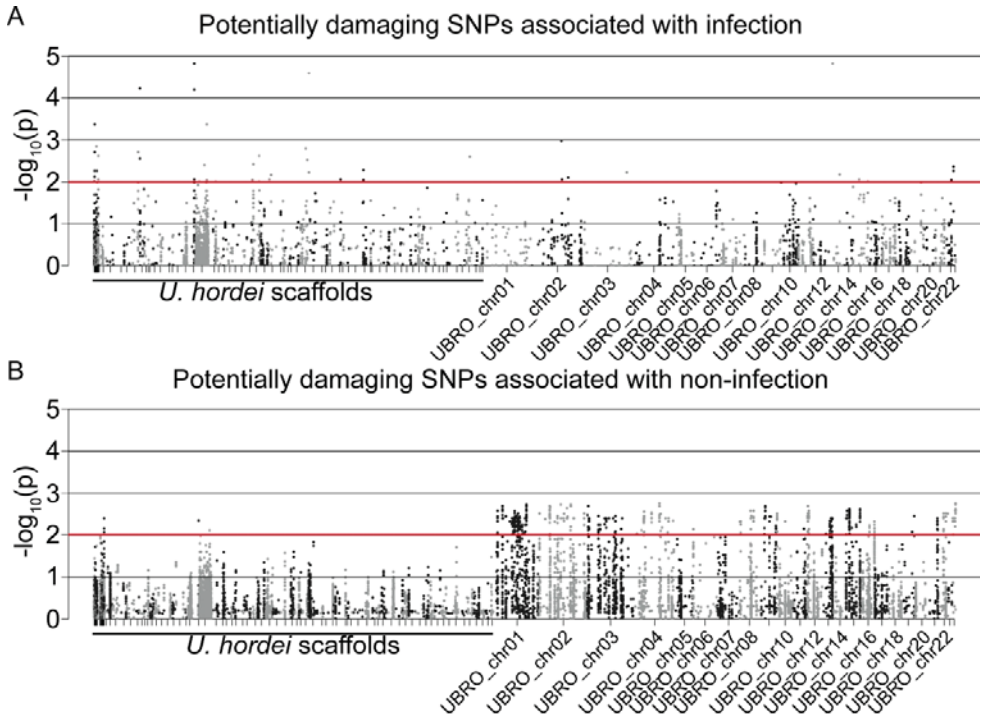

Fig 6. Potentially damaging SNPs associated with the ability to infect B. hybridum Bd28
An analysis of potentially damaging (non-synonymous and loss-of-function) SNPs in hybrids which may be associated with the ability to infect B. hybridum Bd28. These SNPs were obtained by comparing the reads to the reference genomes and can be found in both parental species. They are divided into SNPs that are (A) found more often in strains which are capable of infecting and (B) more often in strains which are not capable of infecting. Points above the red line represent SNPs which are overrepresented in infectious samples with a p-value < 0.01. P-values were corrected for multiple testing using the Benjamini–Hochberg method. Due to space constraints, not all scaffolds or chromosomes are labelled.

184x135mm (300 x 300 DPI)

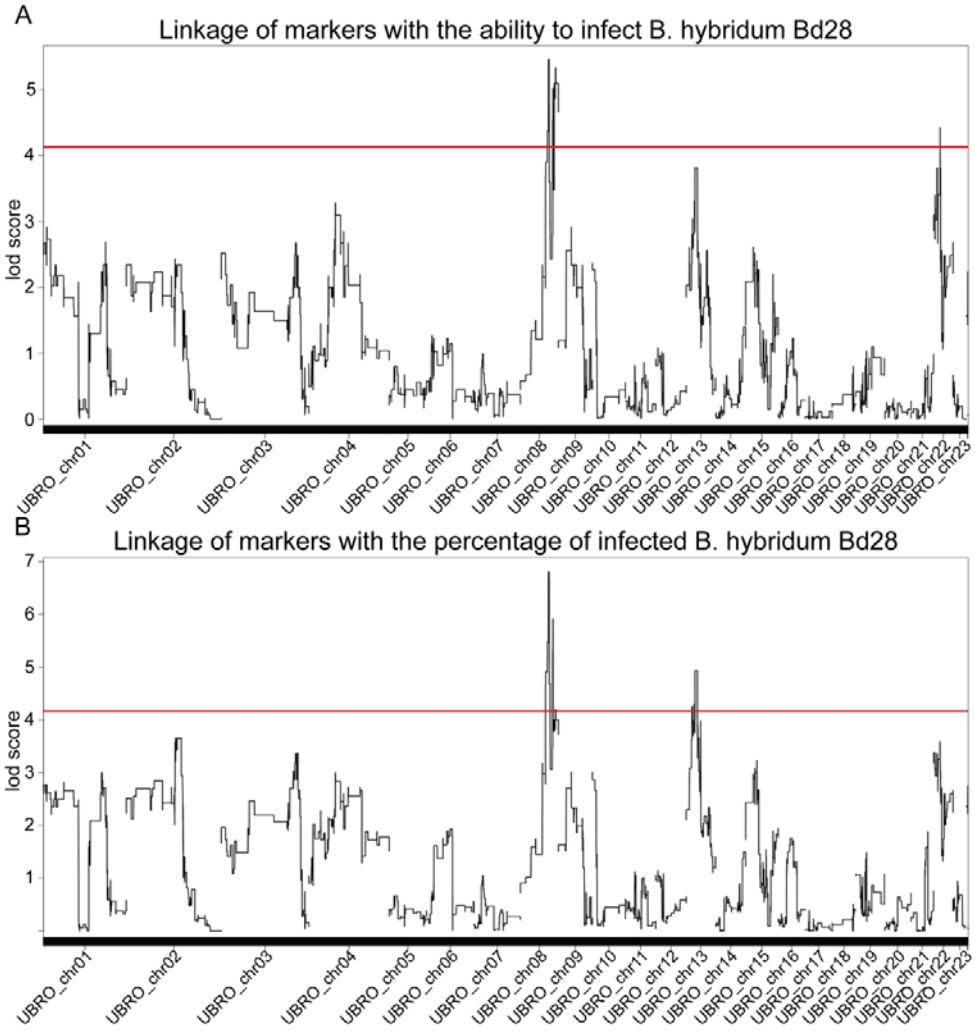

Fig 7. Linkage of ancestry markers with the ability to infect B. hybridum Bd28
Certain regions of the U. bromivora genome show an association with the ability to infect B. hybridum Bd28. The red line shows the lod (logarithm of odds) score cut-off of 4.13, representing α = 0.01. The lod score is a measure of the association of a particular SNP with the phenotype under consideration. Regions on chromosome 8, 13 and 22 exceed the threshold. (A) Lod scores of chromosomal regions when the phenotype is defined as a binary trait of causing infection symptoms on B. hybridum Bd28 or not. (B) Lod scores of chromosomal regions when the phenotype is the percentage of total plants that show infection symptoms. Due to space constraints, the mitochondria and an unassigned scaffold are not labelled.

187x198mm (300 x 300 DPI)

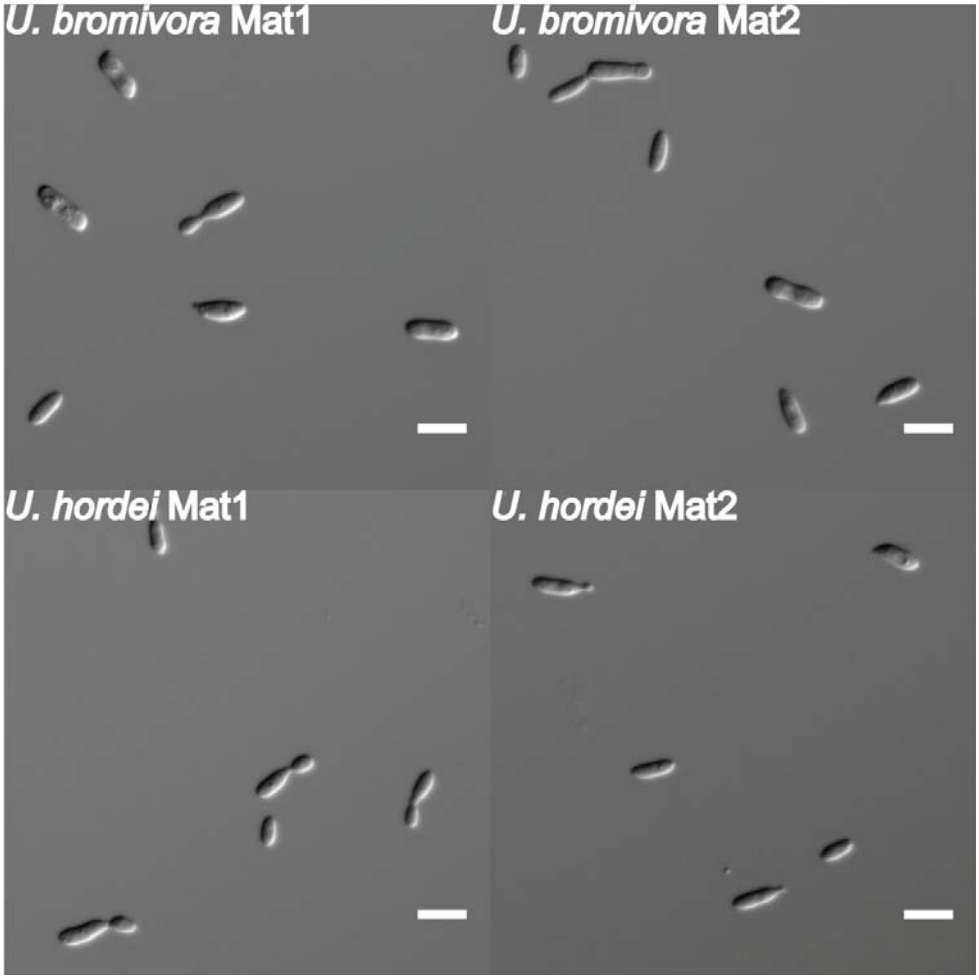

Figure S1: U. bromivora and U. hordei fungal cultures
Fungal cultures growing in liquid potato dextrose medium. Phenotypically, the haploid cells of U. bromivora and U. hordei are very similar. Scale bar represents 10 μm.

163x164mm (300 x 300 DPI)

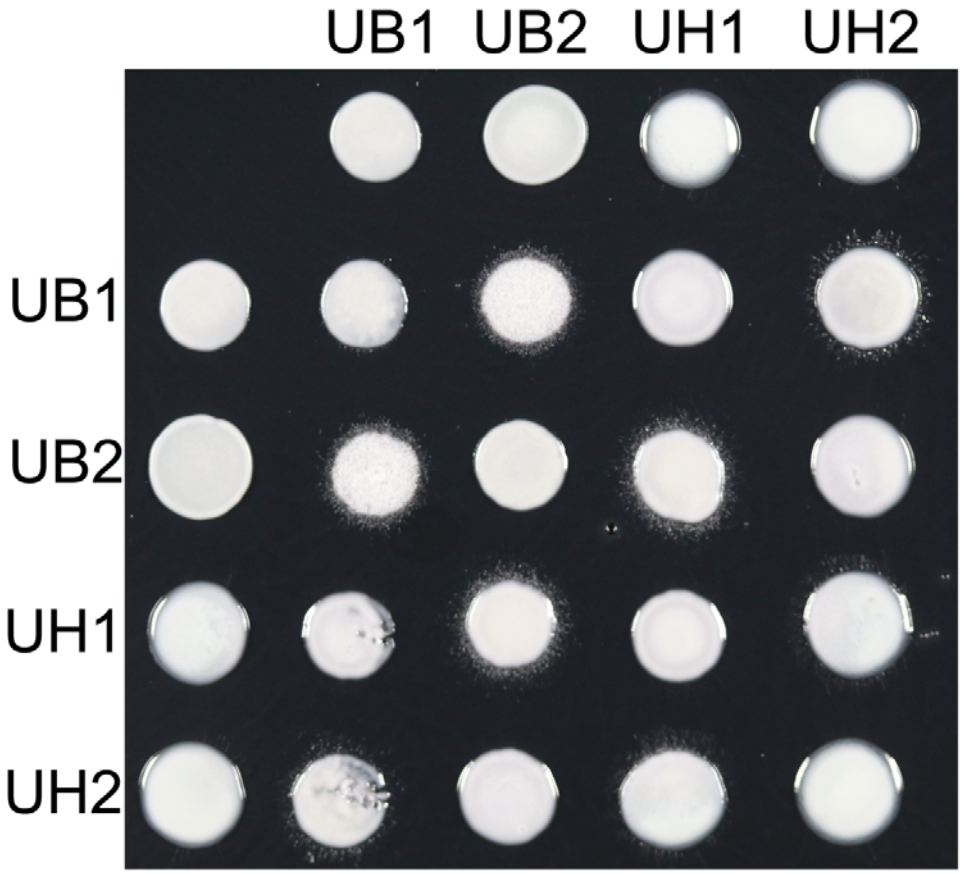

Figure S2: Charcoal mating
U. bromivora (UB) and U. hordei (UH) are able to mate and form filaments on charcoal plates. The number refers to the strain's mating type, e.g. UB1 is U. bromivora Mat1. When mated in a pair-wise manner we can see that the same mating types never filament (demonstrated by the smooth colony boundaries) whereas opposite mating types between all species are capable of filamentation.

171x155mm (300 x 300 DPI)

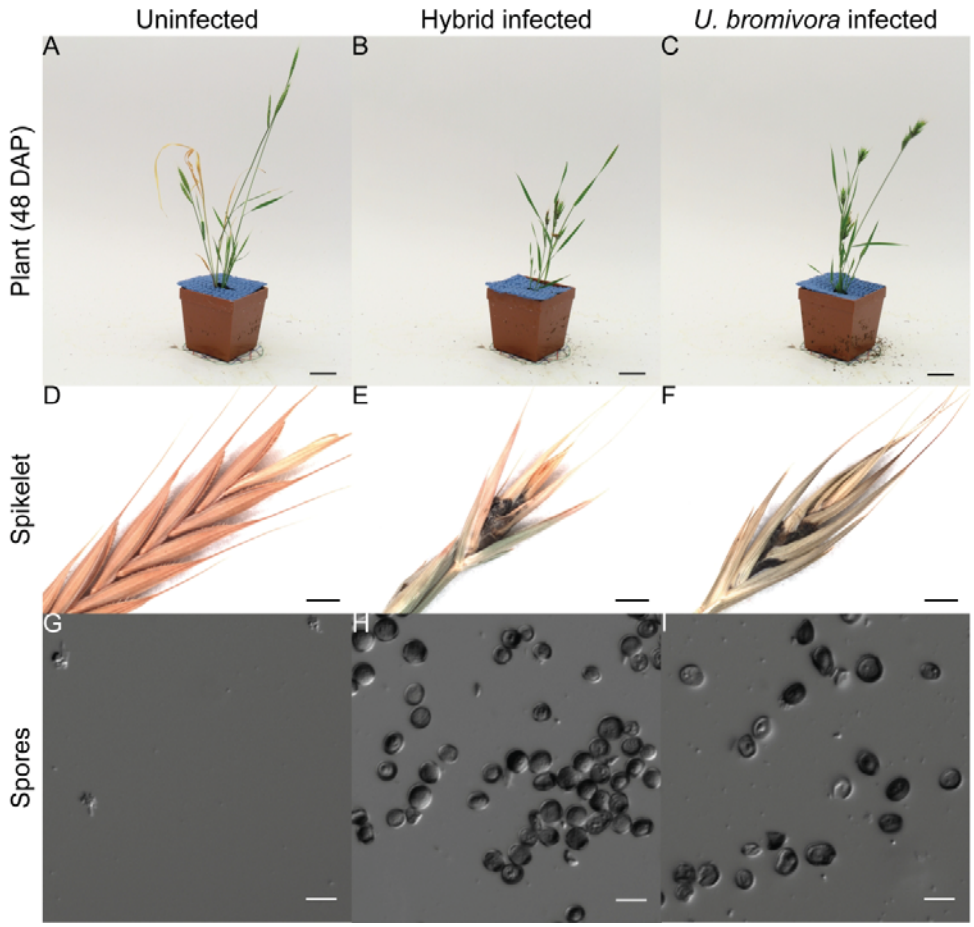

Figure S3: Infection phenotype on B. hybridum Bd28
Phenotypes of B. hybridum Bd28 infected with U. bromivora, U. bromivora X U. hordei hybrid or uninfected. Infection phenotypes are comparable with those observed in B. distachyon ABR4. (Fig 1) A, B and C show B. hybridum Bd28 plants 48 days after planting (DAP). Scale bar represents 2 cm. D, E and F show a close-up of the spikelets. Scale bar represents 20 mm. G, H and I show differential interference contrast (DIC) microscopy images of the spores released from grinding the spikelet. Scale bar represents 10 µm.

186x176mm (300 x 300 DPI)

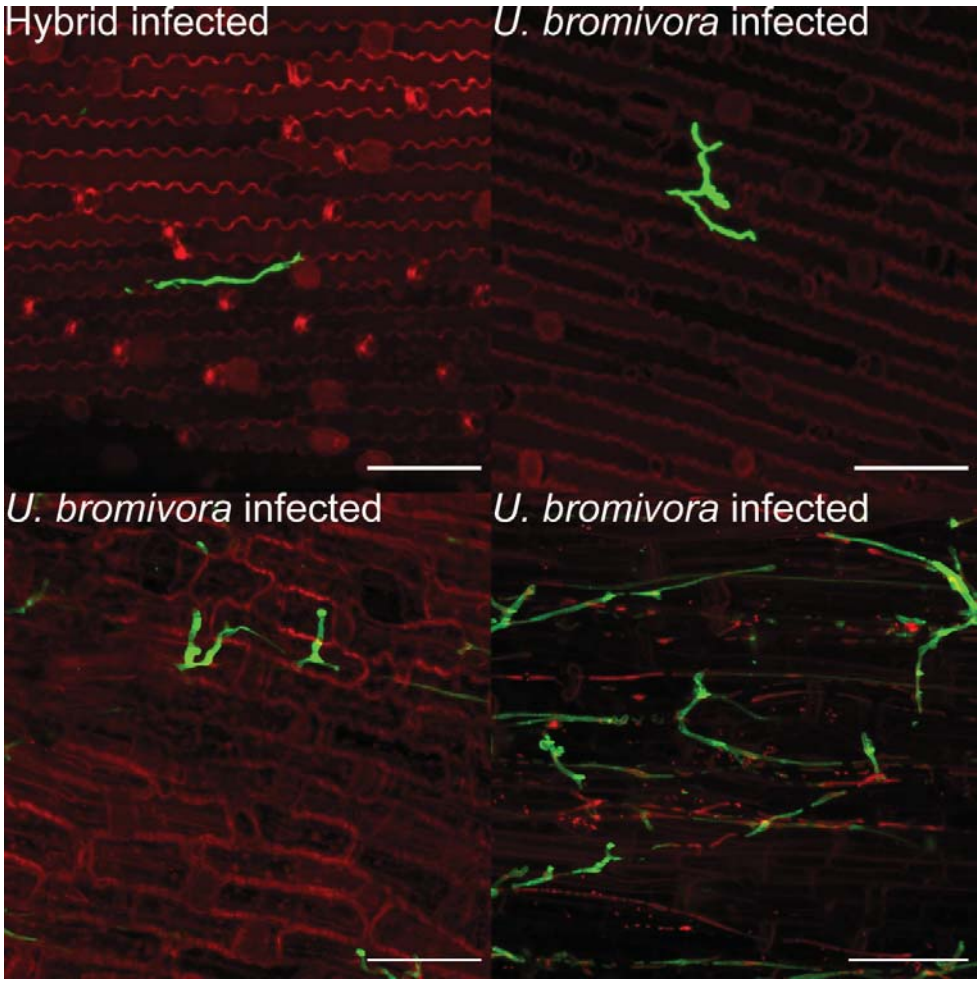

Microscopic phenotype of ABR4 plants infected by either U. bromivora or the U. bromivora X U. hordei hybrid. Maximum intensity z-stack projection showing fungal and plant cells in the stem, 3 weeks after vernalization. The plant cell walls are stained with propidium iodide and fungal cells are stained with wheat germ agglutinin(WGA)-Alexafluor. Scale bar represents 50 µm.

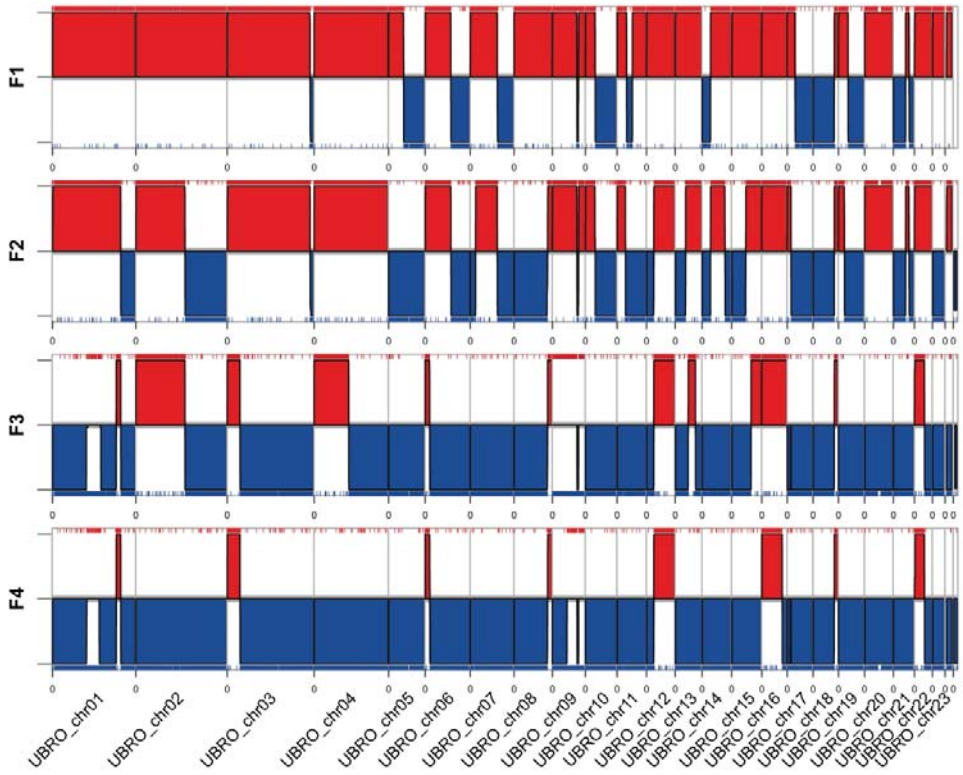

Ancestry of each chromosome predicted by unique U. bromivora or U. hordei SNPs. The ancestry informative SNPs run along the top and bottom of each plot. Red shows U. bromivora specific SNPs and blue shows U. hordei specific SNPs. When there are sufficient SNPs from one progenitor and not the other, that chromosomal region is filled in with the colour of the ancestral progenitor. In cases where the ancestry is ambiguous the region is left blank, e.g. chromosome 9 in F3. This likely represents a situation where chromosomes from both parents are present. Each generation is represented by a single hybrid; F1 is the parental strain for F2, which is the parental strain of F3 and F3 is the parental strain of F4. Each generation shows a reduction in the genomic regions contributed by the original U. bromivora strain. Due to space constraints, the mitochondria and an unassigned scaffold are not labelled.

185x149mm (300 x 300 DPI)

Discussion

Host specificity in the *U. bromivora – Brachypodium* pathosystem

This thesis shows the establishment of a new biotrophic model system described in Publication 1[49], with some of the methods expanded in more detail in Publication 2[65] and an accompanying paper by Czedik-Eysenberg et al.[85]. *U. bromivora* shares many of the characteristics that made *U. maydis* a good research subject and many current *U. maydis* techniques are likely to be easily adapted to *U. bromivora*. This new system addresses difficulties in the use of maize as a research subject which can impose limitations on the widespread model system of *U. maydis* – maize. *B. distachyon* is recognised as a model grass and is both amenable to genetic manipulation and already used to study non-host resistance. *U. bromivora* infection on *B. distachyon* is suitable for analysis through the Phenobox automated phenotyping platform[86] which removes potential biases and subjectivity which might arise in manual phenotyping of an *U. maydis* infection.

In publication 3(Bosch et al., 2019 (submitted to Mpmi)), this system is further expanded by creating hybrid fungal strains of *U. bromivora* and *U. hordei*. This provides a new way of investigating *U. bromivora* biology and an alternative to techniques such as mutation screens. When investigating the factors that enable *U. bromivora* host specificity on *Brachypodium spp.,* the hybrid approach shows distinct advantages to a mutation screen. While a mutation screen will identify factors that are required, it will be more difficult to tease out whether the genetic elements that were mutated are essential for *U. bromivora*'s growth, are important for virulence in a broad sense or are specific for virulence on *Brachypodium*. By using the hybrid approach, with a species that shares 6180 orthologous genes[49], we can focus our attention on the specific aspects of *U. bromivora* that promote virulence on *Brachypodium spp*.

A further advantage of the hybrid system when compared to mutational screening is that no individual genes are rendered inactive; everything in the hybrid system is, at least in theory, still functional. With the mutation screen, it would be possible to find genes involved in a process but more difficult to find what is causing a difference between two species. Using hybrids, we can investigate differences between different genomes or alleles that lead to a specific phenotype.

Although we focussed on host specificity in *U. bromivora*, there is no reason that the same approaches couldn't be used for any phenotypic differences[79]. For example, *U. bromivora* and *U. hordei* also differ in their growth rate and how readily the cultures form a pellet when centrifuged. By using a variety of hybrids, the genetic basis underlying these differences could be determined.

Knowing the genes responsible for these varying phenotypes may shed some light on the different evolutionary pressures acting on each species.

In the plant immune system, recent research has emphasised how defensive responses are networked together in detection[87] and response[68], creating redundancy and durability of the immune system[88]. One could speculate that pathogens may have a similar network of protein-protein interactions which strengthen their ability to infect and deal with different host genetic backgrounds. If this were true, the lack of a specific signal may indicate that the loss of any particular component of the infection network is compensated for by changes in other components of the network. If this doesn't compensate perfectly then it would explain the observed decrease in virulence in the hybrid strains and the lack of a specific signal. There is evidence that bacterial effectors, termed metaeffectors, are capable of directly regulating one another[40]. Furthermore, we have some evidence of effector-effector interactions in the related *U. maydis(*Alcantara & Bosch et al., 2019, submitted to Frontiers in Plant Science).

Future work

With the *U. bromivora – Brachypodium* pathosystem established for research, most new tools will no doubt be developed to answer the specific questions that the system will be used for. However, one development which should be prioritised is the development of a solopathogenic strain of *U. bromivora*. The current *U. bromivora* workflow involves the growth of both Mat 1 and Mat 2 strains, with mating necessary before infection. The removal of the mating step will bring a number of benefits to *U. bromivora* research including decreasing the time taken for experiments, allowing genetic manipulation of only a single, haploid organism and opening up the possibility of using pooled strain techniques such as iPool-Seq[58].

With our current hybrid data, we were not able to refine the genomic loci contributing to host specificity in *U. bromivora* down to the level of specific genes. There could be several reasons behind this which would need to be mitigated in different ways.

We have already shown that there does not appear to be any single locus which is essential for virulence on *Brachypodium spp.* This would suggest that the ideal approach would be to follow a single hybrid line through the generations to be sure that we are only following one method of achieving virulence. Although we tried this, we did not see an association with virulence before we could no longer see infections occurring. I would expect that we could improve our signal by increasing the number of plants that are infected, in order to better exclude false negative infections, and increasing the number of strains sequenced, to achieve better resolution.

We may still struggle to achieve a decent signal as there is possibility of many confounding variations. In our hybrid system, we are switching many different genes between the *U. bromivora* and *U. hordei* versions with the assumption that the orthologs will interact with one another correctly. It may be that certain combinations of *U. bromivora* and *U. hordei* genes are simply non-functional. This could introduce too much variation into our experiment to pull out a clear signal without greatly increased sample sizes.

Lastly, our end point is spore production. Different hybrids could fail at very different stages of the infection process. If this is the case, we may be measuring several separate phenomena which will make teasing out the actual factors related to host specificity very difficult. Those factors may be quantitative in nature which would further add complexity to our results. In human genetics, the omnigenic model suggests that the majority of heritability in complex genetic diseases is due to small effects from across the genome[89]. As a complex trait, virulence may be subject to a similar model.

Alternatively, there is the possibility that measuring the presence or absence of ancestry-specific SNPs does not provide the required information to come to a definite conclusion about which genes are necessary or important for infection. It may be that, despite their presence in a hybrid, certain genes exhibit abnormal levels or patterns of expression which could have an effect on virulence. One paper on fungal hybrids suggests that this is not the case for the majority of the genes[90]. However, this study used an ancient allopolyploid with very little gene loss which is unlikely to accurately represent our backcrossed strains. In an ideal situation, we would combine the genomic information with an RNAseq time course of the hybrid infection for a number of different strains. Such an experiment is currently infeasible due to the vast difference in the number of fungal versus plant cells, approximately 600X more plant than fungal reads[85]. Some form of enrichment will need to be developed if this is to be done. The simplest and most cost-effective solution might be isolation of fungal cells from infected plant material as DNA binding approaches may not retain the necessary quantitative information. Similar techniques have been developed for bacterial plant infections but would need to be tested for feasibility with fungi[91].

It would be ideal to acquire other, independent *U. bromivora* strains to compare the genome content and virulence on different hosts. Evolutionary Molecular Plant-Microbe Interactions (EvoMPMI) stresses the need to include more evolutionary concepts into the study of plant-pathogen interactions[92]. Evolution, unlike most laboratory analyses, works on populations of competing variants. There is a risk that our results on a particular strain of *U. bromivora* may not be representative of *U. bromivora* as a whole and this lack of variation has been identified as a cause for concern in plant pathology[93]. The question of host specificity is an evolutionary question and

many insights could be gained from a comparison of different strains of the same species. For example, in the plant-pathogenic oomycete *Phytophtora infestans*, it has been observed that different strains display variation in gene expression without variation in sequence, presumably due to an epigenetic mechanism[94]. This variation has implications for a pathogen's host range.

Conclusion

I have described a new model biotrophic pathosystem based on *U. bromivora* infection of *Brachypodium spp. U. bromivora* possesses many of the traits that make *U. maydis* a successful model organism and it should be simple to adapt the techniques of *U. maydis* to work in *U. bromivora*. The main advantage of this pathosystem over that of *U. maydis* and maize is the ease of genetically manipulating *Brachypodium spp. U. bromivora* is also related to several sequenced smut fungi which provides many opportunities for comparative analyses and it is even possible to form viable, infectious hybrids with the closely-related fungus *U. hordei*. This opens up new avenues of investigation and an alternative to mutational screening approaches. I used the hybrid fungus and backcrossing with *U. hordei* to demonstrate that there are three genomic loci which play the largest roles in *U. bromivora* virulence on *Brachypodium spp.* but that none of them are essential. This shows that virulence on *Brachypodium spp.* is a quantitative, multifactorial trait.

References

1. Stajich JE, Berbee ML, Blackwell M, Hibbett DS, James TY, Spatafora JW, et al. The fungi. Curr Biol. 2009;19: R840-5. doi:10.1016/j.cub.2009.07.004

2. Klein T, Siegwolf RTW, Korner C. Belowground carbon trade among tall trees in a temperate forest. Science (80-). 2016;352: 342–344. doi:10.1126/science.aad6188

3. Gehring CA, Sthultz CM, Flores-Rentería L, Whipple A V, Whitham TG. Tree genetics defines fungal partner communities that may confer drought tolerance. Proc Natl Acad Sci. 2017;114: 11169–11174. doi:10.1073/pnas.1704022114

4. Hacquard S, Kracher B, Hiruma K, Münch PC, Garrido-Oter R, Thon MR, et al. Survival trade-offs in plant roots during colonization by closely related beneficial and pathogenic fungi. Nat Commun. 2016;7: 11362. doi:10.1038/ncomms11362

5. Almario J, Jeena G, Wunder J, Langen G, Zuccaro A, Coupland G, et al. Root-associated fungal microbiota of nonmycorrhizal Arabis alpina and its contribution to plant phosphorus nutrition. Proc Natl Acad Sci. 2017; 201710455. doi:10.1073/pnas.1710455114

6. Glazebrook J. Contrasting mechanisms of defense against biotrophic and necrotrophic pathogens. Annu Rev Phytopathol. 2005;43: 205–227. doi:10.1146/annurev.phyto.43.040204.135923

7. Knogge W. Fungal Infection of Plants. PLANT CELL ONLINE. 1996;8: 1711–1722. doi:10.1105/tpc.8.10.1711

8. Carris LM, Little CR, Stiles CM. Introduction to Fungi. In: The Plant Health Instructor [Internet]. [cited 11 Feb 2019]. doi:10.1094/PHI-I-2012-0426-01

9. Stukenbrock EH, McDonald B a. The origins of plant pathogens in agro-ecosystems. Annu Rev Phytopathol. 2008;46: 75–100. doi:10.1146/annurev.phyto.010708.154114

10. Strange RN, Scott PR. Plant disease: a threat to global food security. Annu Rev Phytopathol. 2005;43: 83–116. doi:10.1146/annurev.phyto.43.113004.133839

11. Dean R, Van Kan J a L, Pretorius Z a., Hammond-Kosack KE, Di Pietro A, Spanu PD, et al. The Top 10 fungal pathogens in molecular plant pathology. Mol Plant Pathol. 2012;13: 414–430. doi:10.1111/j.1364-3703.2011.00783.x

12. Talbot NJ. On the Trail of a Cereal Killer: Exploring the Biology of Magnaporthe grisea. Annu Rev Microbiol. 2003;57: 177–202. doi:10.1146/annurev.micro.57.030502.090957

13. Islam MT, Croll D, Gladieux P, Soanes DM, Persoons A, Bhattacharjee P, et al. Emergence of wheat blast in Bangladesh was caused by a South American lineage of Magnaporthe oryzae. BMC Biol. BMC Biology; 2016;14: 84. doi:10.1186/s12915-016-0309-7

14. Mottaleb KA, Singh PK, Sonder K, Kruseman G, Tiwari TP, Barma NCD, et al. Threat of wheat blast to South Asia's food security: An ex-ante analysis. Ma W, editor. PLoS One. 2018;13: e0197555. doi:10.1371/journal.pone.0197555

15. Berch SM, Kroeger P, Finston T. The death cap mushroom (Amanita phalloides) moves to a native tree in Victoria, British Columbia. Botany. 2017;95: 435–440. doi:10.1139/cjb-2016-0183

16. Casadevall A. Fungal Diseases in the 21st Century: The Near and Far Horizons. Pathog Immun. 2018;3: 183. doi:10.20411/pai.v3i2.249

17. Revich BA, Podolnaya MA. Thawing of permafrost may disturb historic cattle burial grounds in East Siberia. Glob Health Action. 2011;4: 8482. doi:10.3402/gha.v4i0.8482

18. Jansson JK, Taş N. The microbial ecology of permafrost. Nat Rev Microbiol. 2014;12: 414–425. doi:10.1038/nrmicro3262

19. Stop neglecting fungi. Nat Microbiol. 2017;2: 17120. doi:10.1038/nmicrobiol.2017.120

20. Steinberg G, Perez-Martin J. Ustilago maydis, a new fungal model system for cell biology. Trends Cell Biol. 2008;18: 61–7. doi:10.1016/j.tcb.2007.11.008

21. Brefort T, Doehlemann G, Mendoza-Mendoza A, Reissmann S, Djamei A, Kahmann R. Ustilago maydis as a Pathogen. Annu Rev Phytopathol. 2009;47: 423–45. doi:10.1146/annurev-phyto-080508-081923

22. Valverde ME, Paredes-López O, Pataky JK, Guevara-Lara F, Pineda TS. Huitlacoche (ustilago maydis) as a food source — biology, composition, and production. Crit Rev Food Sci Nutr. 1995;35: 191–229. doi:10.1080/10408399509527699

23. Juárez-Montiel M, Romero-Maldonado A, Monreal-Escalante E, Becerra-Flora A, Korban SS, Rosales-Mendoza S, et al. The Corn Smut (‘Huitlacoche’) as a New Platform for Oral Vaccines. PLoS One. 2015;10: e0133535. doi:10.1371/journal.pone.0133535

24. Christensen JJ. Corn smut caused by Ustilago maydis. Am Phytophatological Soc. 1963;1119: 52.

25. Lawrence GJ, Dodds PN, Ellis JG. TECHNICAL ADVANCE: Transformation of the flax rust fungus, Melampsora lini: selection via silencing of an avirulence gene. Plant J. 2009;61: 364–369. doi:10.1111/j.1365-313X.2009.04052.x

26. Bölker M, Genin S, Lehmler C, Kahmann R. Genetic regulation of mating and dimorphism in Ustilago maydis. Can J Bot. 1995;73: 320–325. doi:10.1139/b95-262

27. Kämper J, Kahmann R, Bölker M, Ma L-J, Brefort T, Saville BJ, et al. Insights from the genome of the biotrophic fungal plant pathogen Ustilago maydis. Nature. 2006;444: 97–101. doi:10.1038/nature05248

28. Matei A, Ernst C, Günl M, Thiele B, Altmüller J, Walbot V, et al. How to make a tumour: cell type specific dissection of Ustilago maydis-induced tumour development in maize leaves. New Phytol. 2018;217: 1681–1695. doi:10.1111/nph.14960

29. Skibbe DS, Doehlemann G, Fernandes J, Walbot V. Maize tumors caused by Ustilago maydis require organ-specific genes in host and pathogen. Science. 2010;328: 89–92. doi:10.1126/science.1185775

30. Lanver D, Müller AN, Happel P, Schweizer G, Haas FB, Franitza M, et al. The Biotrophic Development of Ustilago maydis Studied by RNA-Seq Analysis. Plant Cell. 2018;30: 300–323. doi:10.1105/tpc.17.00764

31. Chang C, Bowman JL, Meyerowitz EM. Field Guide to Plant Model Systems. Cell. Elsevier; 2016;167: 325–339. doi:10.1016/j.cell.2016.08.031

32. McCaw ME, Wallace JG, Albert PS, Buckler ES, Birchler JA. Fast-Flowering Mini-Maize: Seed to Seed in 60 Days. Genetics. 2016;204: 35–42. doi:10.1534/genetics.116.191726

33. Pammel LH. New Fungous Diseases of Iowa. J Mycol. 1892;7: 95. doi:10.2307/3752255

34. Barbieri M, Marcel T, Niks R. Host status of false brome grass to the leaf rust fungus Puccinia brachypodii and the stripe rust fungus P. Striiformis. Plant Dis. 2011; 1339–1345. doi:10.1094/PDIS-11-10-0825

35. Draper J, Mur LAJ, Jenkins G, Ghosh-Biswas GC, Bablak P, Hasterok R, et al. Brachypodium distachyon. A New Model System for Functional Genomics in Grasses. PLANT Physiol. 2001;127: 1539–1555. doi:10.1104/pp.010196

36. Vogel JP, Garvin DF, Mockler TC, Schmutz J, Rokhsar D, Bevan MW, et al. Genome sequencing and analysis of the model grass Brachypodium distachyon. Nature. 2010;463: 763–768. doi:10.1038/nature08747

37. An T, Cai Y, Zhao S, Zhou J, Song B, Bux H, et al. Brachypodium distachyon T-DNA insertion lines: a model pathosystem to study nonhost resistance to wheat stripe rust. Sci Rep. Nature Publishing Group; 2016;6: 25510. doi:10.1038/srep25510

38. Dawson AM, Bettgenhaeuser J, Gardiner M, Green P, Hernández-Pinzón I, Hubbard A, et al. The development of quick, robust, quantitative phenotypic assays for describing the host–nonhost landscape to stripe rust. Front Plant Sci. 2015;6: 1–9. doi:10.3389/fpls.2015.00876

39. Popov G, Fraiture M, Brunner F, Sessa G. Multiple Xanthomonas euvesicatoria Type III Effectors Inhibit flg22-Triggered Immunity. 2016;X: 1–10.

40. Urbanus ML, Quaile AT, Stogios PJ, Morar M, Rao C, Di Leo R, et al. Diverse mechanisms of metaeffector activity in an intracellular bacterial pathogen, Legionella pneumophila. Mol Syst Biol. 2016;12: 893. doi:10.15252/msb.20167381

41. Tyler BM. Entering and breaking: virulence effector proteins of oomycete plant pathogens. Cell Microbiol. 2009;11: 13–20. doi:10.1111/j.1462-5822.2008.01240.x

42. Franceschetti M, Maqbool A, Jiménez-Dalmaroni MJ, Pennington HG, Kamoun S, Banfield MJ. Effectors of Filamentous Plant Pathogens: Commonalities amid Diversity. Microbiol Mol Biol Rev. 2017;81: e00066-16. doi:10.1128/MMBR.00066-16

43. De Wit PJGM, Mehrabi R, Van Den Burg H a., Stergiopoulos I. Fungal effector proteins: past, present and future. Mol Plant Pathol. 2009;10: 735–747. doi:10.1111/j.1364-3703.2009.00591.x

44. Stergiopoulos I, de Wit PJGM. Fungal Effector Proteins. Annu Rev Phytopathol. 2009;47: 233–263. doi:10.1146/annurev.phyto.112408.132637

45. De Jonge R, Bolton MD, Thomma BPHJ. How filamentous pathogens co-opt plants: The ins and outs of fungal effectors. Curr Opin Plant Biol. Elsevier Ltd; 2011;14: 400–406. doi:10.1016/j.pbi.2011.03.005

46. Mitchum MG, Hussey RS, Baum TJ, Wang X, Elling AA, Wubben M, et al. Nematode effector proteins: An emerging paradigm of parasitism. New Phytol. 2013;199: 879–894. doi:10.1111/nph.12323

47. Weiberg A, Wang M, Lin F-M, Zhao H, Zhang Z, Kaloshian I, et al. Fungal Small RNAs Suppress Plant Immunity by Hijacking Host RNA Interference Pathways. Science (80-). 2013;342: 118–123. doi:10.1126/science.1239705

48. Petersen TN, Brunak S, von Heijne G, Nielsen H. SignalP 4.0: discriminating signal peptides from transmembrane regions. Nat Methods. Nature Publishing Group; 2011;8: 785–786. doi:10.1038/nmeth.1701

49. Rabe F, Bosch J, Stirnberg A, Guse T, Bauer L, Seitner D, et al. A complete toolset for the study of Ustilago bromivora and Brachypodium sp. as a fungal-temperate grass pathosystem. Elife. 2016;5: 1–35. doi:10.7554/eLife.20522

50. Schuster M, Schweizer G, Kahmann R. Comparative analyses of secreted proteins in plant pathogenic smut fungi and related basidiomycetes. Fungal Genet Biol. 2017; doi:10.1016/j.fgb.2016.12.003

51. Sperschneider J, Gardiner DM, Dodds PN, Tini F, Covarelli L, Singh KB, et al. EFFECTORP : predicting fungal effector proteins from secretomes using machine learning. 2015; doi:10.1111/nph.13794

52. Sperschneider J, Dodds PN, Gardiner DM, Singh KB, Taylor JM. Improved prediction of fungal effector proteins from secretomes with EffectorP 2.0. bioRxiv. 2018; 250464. doi:10.1101/250464

53. Galán JE, Lara-Tejero M, Marlovits TC, Wagner S. Bacterial Type III Secretion Systems: Specialized Nanomachines for Protein Delivery into Target Cells. Annu Rev Microbiol. 2014;68: 415–438. doi:10.1146/annurev-micro-092412-155725

54. Wawra S, Trusch F, Matena A, Apostolakis K, Linne U, Zhukov I, et al. The RxLR Motif of the Host Targeting Effector AVR3a of Phytophthora infestans Is Cleaved Before Secretion. Plant Cell. 2017; tpc.00552.2016. doi:10.1105/tpc.16.00552

55. Zhang S, Xu J-R. Effectors and Effector Delivery in Magnaporthe oryzae. Heitman J, editor. PLoS Pathog. 2014;10: e1003826. doi:10.1371/journal.ppat.1003826

56. Petre B, Kamoun S. How Do Filamentous Pathogens Deliver Effector Proteins into Plant Cells? PLoS Biol. 2014;12. doi:10.1371/journal.pbio.1001801

57. Lo Presti L, Kahmann R. How filamentous plant pathogen effectors are translocated to host cells. Curr Opin Plant Biol. Elsevier Ltd; 2017;38: 19–24. doi:10.1016/j.pbi.2017.04.005

58. Uhse S, Pflug FG, Stirnberg A, Ehrlinger K, von Haeseler A, Djamei A. In vivo insertion pool sequencing identifies virulence factors in a complex fungal–host interaction. Heitman J, editor. PLOS Biol. 2018;16: e2005129. doi:10.1371/journal.pbio.2005129

59. Stirnberg A, Djamei A. Characterization of ApB73, a virulence factor important for colonization of Zea mays by the smut Ustilago maydis. Mol Plant Pathol. 2016;17: 1467–1479. doi:10.1111/mpp.12442

60. Białas A, Zess EK, De la Concepcion JC, Franceschetti M, Pennington HG, Yoshida K, et al. Lessons in Effector and NLR Biology of Plant-Microbe Systems. Mol Plant-Microbe Interact. 2018;31: 34–45. doi:10.1094/MPMI-08-17-0196-FI

61. Papkou A, Guzella T, Yang W, Koepper S, Pees B, Schalkowski R, et al. The genomic basis of Red Queen dynamics during rapid reciprocal host–pathogen coevolution. Proc Natl Acad Sci. 2019;116: 923–928. doi:10.1073/pnas.1810402116

62. Dong S, Raffaele S, Kamoun S. The two-speed genomes of filamentous pathogens: waltz with plants. Curr Opin Genet Dev. Elsevier Ltd; 2015;35: 57–65. doi:10.1016/j.gde.2015.09.001

63. Paulus JK, Kourelis J, van der Hoorn RAL. Bodyguards: Pathogen-Derived Decoys That Protect Virulence Factors. Trends Plant Sci. Elsevier Ltd; 2017;22: 355–357. doi:10.1016/j.tplants.2017.03.004

64. Jones JDG, Dangl JL. The plant immune system. Nature. 2006;444: 323–9. doi:10.1038/nature05286

65. Bosch J, Djamei A. Isolation of Ustilago bromivora Strains from Infected Spikelets through Spore Recovery and Germination. BIO-PROTOCOL. 2017;7. doi:10.21769/BioProtoc.2392

66. Whon TW, Kim M-S, Roh SW, Shin N-R, Lee H-W, Bae J-W. Metagenomic characterization of airborne viral DNA diversity in the near-surface atmosphere. J Virol. 2012;86: 8221–31. doi:10.1128/JVI.00293-12

67. Frohlich-Nowoisky J, Pickersgill DA, Despres VR, Poschl U. High diversity of fungi in air particulate matter. Proc Natl Acad Sci. 2009;106: 12814–12819. doi:10.1073/pnas.0811003106

68. Wu C-H, Abd-El-Haliem A, Bozkurt TO, Belhaj K, Terauchi R, Vossen JH, et al. NLR network mediates immunity to diverse plant pathogens. Proc Natl Acad Sci. 2017; 201702041. doi:10.1073/pnas.1702041114

69. Bolton MD, Thomma BPHJ, Nelson BD. Sclerotinia sclerotiorum (Lib.) de Bary: Biology and molecular traits of a cosmopolitan pathogen. Mol Plant Pathol. 2006;7: 1–16. doi:10.1111/j.1364-3703.2005.00316.x

70. Mbengue M, Navaud O, Peyraud R, Barascud M, Badet T, Vincent R, et al. Emerging Trends in Molecular Interactions between Plants and the Broad Host Range Fungal Pathogens Botrytis cinerea and Sclerotinia sclerotiorum. Front Plant Sci. 2016;7: 1–9. doi:10.3389/fpls.2016.00422

71. Liang X, Rollins JA. Mechanisms of Broad Host Range Necrotrophic Pathogenesis in Sclerotinia sclerotiorum. Phytopathology. 2018;108: 1128–1140. doi:10.1094/PHYTO-06-18-0197-RVW

72. Duplessis S. Obligate biotrophy features unraveled by the genomic analysis of rust fungi. Proc Natl Acad Sci U S A. 2011; 1–23. doi:10.1073/pnas.1019315108/-/DCSupplementalwww.pnas.org/cgi/doi/10.1073/pnas.1019315108

73. Schipper K. Charakterisierung eines Ustilago maydis Genclusters, das für drei neuartige sekretierte Effektoren kodiert. Philipps-Universität Marburg. 2009.

74. Bettgenhaeuser J, Gardiner M, Spanner R, Green P, Hernández-Pinzón I, Hubbard A, et al. The genetic architecture of colonization resistance in Brachypodium distachyon to non-adapted stripe rust (Puccinia striiformis) isolates. PLOS Genet. 2018;14: e1007637. doi:10.1371/journal.pgen.1007637

75. Olson Å, Stenlid J. Pathogenic fungal species hybrids infecting plants. Microbes Infect. 2002;4: 1353–1359. doi:10.1016/S1286-4579(02)00005-9

76. Vaz Pinto P, Beja P, Ferrand N, Godinho R. Hybridization following population collapse in a critically endangered antelope. Nat Publ Gr. Nature Publishing Group; 2016; 1–9. doi:10.1038/srep18788

77. Soltis PS, Soltis DE. The Role of Hybridization in Plant Speciation. Annu Rev Plant Biol. 2009;60: 561–588. doi:10.1146/annurev.arplant.043008.092039

78. Kellner R, Vollmeister E, Feldbrügge M, Begerow D. Interspecific sex in grass smuts and the genetic diversity of their pheromone-receptor system. PLoS Genet. 2011;7. doi:10.1371/journal.pgen.1002436

79. Huang H-Q, Nielsen J. Hybridization of the seedling-infecting Ustilago spp. pathogenic on barley and oats, and a study of the genotypes conditioning the morphology of their spore walls. Can J Bot. 1984;62: 603–608. doi:10.1139/b84-091

80. Olson A, Stenlid J. Plant pathogens. Mitochondrial control of fungal hybrid virulence. Nature. 2001;411: 438. doi:10.1038/35078147

81. Brasier C. Plant pathology: The rise of the hybrid fungi. Nature. 2000;405: 134–135. doi:10.1038/35012193

82. Depotter JRL, Seidl MF, Wood T a., Thomma BPHJ. Interspecific hybridization impacts host range and pathogenicity of filamentous microbes. Curr Opin Microbiol. Elsevier Ltd; 2016;32: 7–13. doi:10.1016/j.mib.2016.04.005

83. Oettler G. The fortune of a botanical curiosity - Triticale: Past, present and future. J Agric Sci. 2005;143: 329–346. doi:10.1017/S0021859605005290

84. Menardo F, Praz C, Wyder S, Bourras S. A, McNally KE, Parlange F, et al. Hybridization of powdery mildew strains gives raise to pathogens on novel agricultural crop species. Nat Genet. Nature Publishing Group; 2015;48: 1–24. doi:10.1038/ng.3485

85. Czedik-Eysenberg A, Rabe F, Ekker H, Czepe C, Djamei A. Overrepresentation Analyses of Differentially Expressed Genes in the Smut Fungus Ustilago bromivora during Saprophytic and in planta Growth. BIO-PROTOCOL. 2017;7. doi:10.21769/BioProtoc.2426

86. Czedik-Eysenberg A, Seitner S, Güldener U, Koemeda S, Jez J, Colombini M, et al. The 'PhenoBox', a flexible, automated, open-source plant phenotyping solution. New Phytol. 2018;219: 808–823. doi:10.1111/nph.15129

87. Smakowska-Luzan E, Mott GA, Parys K, Stegmann M, Howton TC, Layeghifard M, et al. An extracellular network of Arabidopsis leucine-rich repeat receptor kinases. Nature. Nature Publishing Group; 2018;553: 342–346. doi:10.1038/nature25184

88. Wu C-H, Derevnina L, Kamoun S. Receptor networks underpin plant immunity. Science (80-). 2018;360: 1300–1301. doi:10.1126/science.aat2623

89. Boyle EA, Li YI, Pritchard JK. An Expanded View of Complex Traits: From Polygenic to Omnigenic. Cell. Elsevier; 2017;169: 1177–1186. doi:10.1016/j.cell.2017.05.038

90. Cox MP, Dong T, Shen G, Dalvi Y, Scott DB, Ganley ARD. An interspecific fungal hybrid reveals cross-kingdom rules for allopolyploid gene expression patterns. PLoS Genet. 2014;10: e1004180. doi:10.1371/journal.pgen.1004180

91. Nobori T, Tsuda K. In planta Transcriptome Analysis of Pseudomonas syringae. BIO-PROTOCOL. 2018;8: 1–8. doi:10.21769/BioProtoc.2987

92. Upson JL, Zess EK, Białas A, Wu C, Kamoun S. The coming of age of EvoMPMI: evolutionary molecular plant–microbe interactions across multiple timescales. Curr Opin Plant Biol. 2018;44: 108–116. doi:10.1016/j.pbi.2018.03.003

93. Rowe HC, Kliebenstein DJ. All mold is not alike: The importance of intraspecific diversity in necrotrophic plant pathogens. PLoS Pathog. 2010;6: 1–3. doi:10.1371/journal.ppat.1000759

94. Pais M, Yoshida K, Giannakopoulou A, Pel MA, Cano LM, Oliva RF, et al. Gene expression polymorphism underpins evasion of host immunity in an asexual lineage of the Irish potato famine pathogen. BMC Evol Biol. BMC Evolutionary Biology; 2018;18: 93. doi:10.1186/s12862-018-1201-6

Appendices

Publication 1

Supplementary file 1: Primers, plasmids and strains used in this study

Primers used in this study

Primer	5' - 3' Sequence	Description
5_pra1	GCTTTGTTGAGTGTCGATGC	primer for diagnostic PCR to assess mating type (MAT-1)
3_pra1	ACCAATGTCGCCATGTACTC	primer for diagnostic PCR to assess mating type (MAT-1)
5_pra2	TTACCGGCGTAGATAGAGCA	primer for diagnostic PCR to assess mating type (MAT-2)
3_pra2	ACGGCATGTCTTTCCATCTC	primer for diagnostic PCR to assess mating type (MAT-2)
5_UmCBX_1	ACAATCACGAGAAATGCGCG	p123UB-GFP cloning; amplification of flanking region of gene conferring Carboxin resistance present in p123 (Aichinger et al., 2003)
3_UmCBX_1	TAGTGGTCTCCGACATGGTCGGTGTGGATGTATGAAC	p123UB-GFP cloning; amplification of flanking region of gene conferring Carboxin resistance present in p123 (Aichinger et al., 2003)
5_UBCBX_2	ACTAGGTCTCATGTCGCTATTCAACGTCAGC	p123UB-GFP cloning; amplification of UBRO_01267
3_UBCBX_mut1_2	TAGTGGTCTCTCGTAAAGACCATCTAGACGACGACG	p123UB-GFP cloning; amplification of UBRO_01267
5_UBCBX_mut1_3	ACTAGGTCTCCTACGAGTGCATCCTTTGCGC	p123UB-GFP cloning; amplification of UBRO_01267, removal of internal BsaI sites and introduction of His to Leu mutation conferring CBX resistance
3_UBCBX_mut2_3	TGATGGTCTCTGGTGAGGCAACGGTAGAGCGAGAAG	p123UB-GFP cloning; amplification of UBRO_01267, removal of internal BsaI sites and introduction of His to Leu mutation conferring Carboxin resistance
5_UBCBX_mut2_4	ATCAGGTCTCACACCATCATGAACTGCTCC	p123UB-GFP cloning; amplification of UBRO_01267, removal of internal BsaI sites and introduction of His to Leu mutation conferring Carboxin resistance
3_UBCBX_4	TGATGGTCTCAGATTACGACGAGGCCATGATAGGAC	p123UB-GFP cloning; amplification of UBRO_01267, removal of internal BsaI sites and introduction of His to Leu mutation conferring Carboxin resistance
5_UmCBX_5	ATCAGGTCTCTAATCTTGATATATCATATC	p123UB-GFP cloning; amplification of flanking region of gene conferring Carboxin resistance present in p123 (Aichinger et al., 2003)
3_UmCBX_5	CTCAGTACAATCTGCTCTGATG	p123UB-GFP cloning; amplification of flanking region of gene conferring Carboxin resistance present in p123 (Aichinger et al., 2003)
5_Um01987_RB	ATATGCTCTTCACGAACCGCTGCGACGTCGTTG	right border pep1 deletion construct
3_Um01987_RB	ATATGCTCTTCTCGCGGCGCGCCCCCCAGACTGGGTTGGTGGAC	right border pep1 deletion construct
5_Um01987_LB	ATATGCTCTTCACAGGGCGCGCCAATCGTGGCTGTCCACGAAAG	left border pep1 deletion construct
3_Um01987_LB	ATATGCTCTTCTGCCGTTGATGTCGAGAGTCCTC	left border pep1 deletion construct
5_Um02475_RB	ATATGCTCTTCACGAAGCTCTGCTGTAAAGAATC	right border stp1 deletion construct
3_Um02475_RB	ATATGCTCTTCTCGCGGCGCGCCCCCGACAACTATGTAATCGCC	right border stp1 deletion construct
5_Um02475_LB	ATATGCTCTTCACAGGGCGCGCCATGATCAACCAGGATCAAC	left border stp1 deletion construct
3_Um02475_LB	ATATGCTCTTCTGCCGTGTTCTCTGCTTTATTTTC	left border stp1 deletion construct
5_UbStp1_CD	ATATGGTCTCAggctCAATGCGAGCCGACTTTTTATC	UBRO_stp1 CDS for pUG_UBRO_Stp1 cloning
3_UbStp1_CD	ATATggtctcActgaTTGCTTCGGAGGGGGAGCAG	UBRO_stp1 CDS for pUG_UBRO_Stp1 cloning
5_UbPep1_CD	ATATGGTCTCAggcTCAATGAAGCTCACACTCAACAC	UBRO_pep1 CDS for pUG_UBRO_Pep1 cloning

3_UbPep1_CD	ATATggtctcACTGAGAGCCCAAA-CATCTTACCAAG	UBRO_pep1 CDS for pUG_UBRO_Pep1 cloning
5_CFP-SKL	ataACTAGTATGGTGAGCAAGGGC-GAGGAGC	p6U_eCFP-SKL cloning
3_CFP-SKL	ATAAAGCTTTTACAGCTTCG-ATCTCTTGTACAGC	p6U_eCFP-SKL cloning
5_UmPep1_AB	ATATGGTCTCAACCTACGACGGAT-GCGCTATCGTC	UMAG_pep1 promoter for pUG_UBRO_Pep1 cloning
3_UmPep1_AB	ATATGGTCTCATGTTCGTTGATGTC-GAGAGTCCTC	UMAG_pep1 promoter for pUG_UBRO_Pep1 cloning

References

Aichinger, C., Hansson, K., Eichhorn, H., Lessing, F., Mannhaupt, G., Mewes, W., and Kahmann, R. (2003) Identification of plant-regulated genes in Ustilago maydis by enhancer-trapping mutagenesis. Mol Genet Genomics **270**: 303-314.

DiCarlo, J.E., Norville, J.E., Mali, P., Rios, X., Aach, J., and Church, G.M. (2013) Genome engineering in Saccharomyces cerevisiae using CRISPR-Cas systems. Nucleic Acids Res **41**: 4336-4343.

Plasmids used in this study

plasmid	cloning strategy	resistance	application/comments	source
pNEBuC-GFP	Gateway cloning of pEntryGFP with gateway compatible pNEBuC (A. Djamei, unpublished)	Amp, CBX	U. bromvivora transformation test; autonomously replicating plasmid encoding GFP-HA under control of otef promoter	this study
pNEBuC-mCherry	Gateway cloning of pEntry-mCherry with gateway-compatible pNEBuC (A. Djamei, unpublished)	Amp, CBX	U. bromvivora transformation test; autonomously replicating plasmid encoding mCherry-HA under control of otef promoter	this study
pNEBuH		Amp, Hyg	U. bromvivora transformation test; autonomously replicating plasmid conferring Hygromycin resistance	Mueller et al., 1999
pNEBuG	pNEBuC (Brachmann, 2001) was linearized with NotI to remove CBX resistance cassette and to introduce Geneticin G418 resistance cassette that is flanked by NotI sites (Baumann et al., 2012)	Amp, G418	U. bromvivora transformation test; autonomously replicating plasmid conferring Geneticin G418 resistance	this study
p123UB-GFP	classical cloning via BsaI to combine flanking regions of UMAG_00844 (gene conferring CBX resistance + for homologous recombination in ip locus) present in p123 (Aichinger et al., 2003) with mutagenized UBRO_01267 and subsequent AccI-ZraI cloning into AccI-ZraI linearized p123 (Aichinger et al., 2003)	Amp, CBX	plasmid for integrations in U. bromivora ip locus, encoding GFP and mutagenzied version of UBRO_01267 conferring CBX resistance	this study
pUKO_stp1	SapI-based Golden Gate*	Spec, Hyg	deletion construct for UMAG_stp1 (UMAG_02475)	this study
pUKO_pep1	SapI-based Golden Gate*	Spec, Hyg	deletion construct for UMAG_pep1 (UMAG_01987)	this study
pUG_UBRO_stp1	BsaI-based Golden Gate*	Spec, CBX	complementation assay/ plasmid contains U. bromivora stp1 (UBRO_12209) under control of the U. maydis stp1 promoter (UMAG_02475)	this study
pUG_UBRO_pep1	BsaI-based Golden Gate*	Spec, CBX	complementation assay / plasmid contains U. bromivora pep1 (UBRO_02965) under control of the U. maydis pep1 promoter (UMAG_01987)	this study
p6U_eCFP-SKL	eCFP-SKL (Nelsen et al., 2007) was cloned via SpeI-HindIII into pUBI-ABM (Jochen Kumlehn, IPK Gatersleben) followed by SfiI cloning into p6Uint-Ubi (Jochen Kumlehn, IPK Gatersleben)	Spec, Hyg	plasmid harboring eCFP-SKL under the ubiquitin promoter for A. tumefaciens-mediated transformation of Brachypodium sp.	this study

*for Golden Gate-based pUKO and pUG cloning strategies see Stirnberg and Djamei (2016); GoldenGate reactions were based on the Green Gate system (Lampropoulos et al., 2013); promoter module of UMAG_stp1 is described in Stirnberg and Djamei (2016); CBX = Carboxin, Hyg = Hygromycin B, G418 = Geneticin G418, Amp = Ampicillin, Spec = Spectinomycin

References

Aichinger, C., Hansson, K., Eichhorn, H., Lessing, F., Mannhaupt, G., Mewes, W., and Kahmann, R. (2003) Identification of plant-regulated genes in Ustilago maydis by enhancer-trapping mutagenesis. Mol Genet Genomics **270**: 303-314.

Baumann, S., Pohlmann, T., Jungbluth, M., Brachmann, A., and Feldbrugge, M. (2012) Kinesin-3 and dynein mediate microtubule-dependent co-transport of mRNPs and endosomes. J Cell Sci **125**: 2740-2752

Brachmann, A. (2001) Die frühe Infektionsphase von U. maydis: Genregulation durch das bW/bEHeterodimer. Dissertation, LMU München, Faculty of Biology.

Lampropoulos, A., Sutikovic, Z., Wenzl, C., Maegele, I., Lohmann, J.U., and Forner, J. (2013) GreenGate---a novel, versatile, and efficient cloning system for plant transgenesis. PLoS One **8**: e83043.

Mueller, P., Aichinger, C., Feldbrugge, M., and Kahmann, R. (1999) The MAP kinase kpp2 regulates mating and pathogenic development in Ustilago maydis. Mol Microbiol **34**: 1007-1017.

Nelson,B. K., Cai, X., Nebenführ, A. (2007) A multi-color set of in vivo organelle markers for colocalization studies in Arabidopsis and other plants. Plant Journal **51**:1126-1136

Stirnberg, A., and Djamei, A. (2016) Characterization of ApB73, a virulence factor important for colonization of Zea mays by the smut Ustilago maydis. Mol Plant Pathol. doi: 10.1111/mpp.12442

Fungal strains used in this study

strain	genotype	resistance	source
UB1	a1 b1		this study
UB2	a2 b2		this study
UB1-GFP	a1 b1 Potef:GFP-HA	CBX	this study
FB1	a1 b1		Banuett and Herskowitz, 1989
Uh4875-4	a1 b1		Linning et al., 2004
SG200	a1 mfa2 b1 b2	Phleo	Kaemper et al., 2006
SG200Δstp1	a1 mfa2 b1 b2 ΔUMAG_02475	Phleo, Hyg	this study
SG200Δpep1	a1 mfa2 b1 b2 ΔUMAG_01987	Phleo, Hyg	this study
SG200Δstp1-UBRO_stp1	a1 mfa2 b1 b2 Δ ipr[PUMAG_02475:UBRO_12209]ips	Phleo, Hyg, CBX	this study
SG200Δpep1-UBRO_pep1	a1 mfa2 b1 b2 ΔUMAG_01987 ipr[PUMAG_01987:UBRO_02965]ips	Phleo, Hyg, CBX	this study

References

Banuett, F., and Herskowitz, I. (1989) Different a alleles of Ustilago maydis are necessary for maintenance of filamentous growth but not for meiosis. Proc Natl Acad Sci U S A 86: 5878-5882.

Kaemper, J., Kahmann, R., Bolker, M., Ma, L.J., Brefort, T., Saville, B.J., Banuett, F., Kronstad, J.W., et al. (2006) Insights from the genome of the biotrophic fungal plant pathogen Ustilago maydis. Nature 444: 97-101.

Linning, R., Lin, D., Lee, N., Abdennadher, M., Gaudet, D., Thomas, P., Mills, D., Kronstad, J.W., et al. (2004) Marker-based cloning of the region containing the UhAvr1 avirulence gene from the basidiomycete barley pathogen Ustilago hordei. Genetics 166: 99-111.

Supplementary file 2: Maps of plasmids used in this study

https://doi.org/10.7554/eLife.20522.028

Publication 3

Table S1: Phenobox PCA loadings

	PC1	PC2	PC3	PC4	PC5
side.geometry.vis.hull.-centroid.y..px.	0.174851400204901	-0.008477962267192	-0.058637227049273	0.028896280642577	-0.004489558708238
side.intensity.vis.lab.l.stddev	0.171792906609783	-0.009625691767697	0.026624505033303	-0.071460314473296	0.077451292788587
side.geometry.vis.cog.y..px.	0.170850861020123	0.001343279530392	-0.072606482325205	0.050446386949991	0.022047026904349
side.intensity.vis.hs-v.v.stddev	0.166030264376018	-0.065111880083153	-0.005944200896688	-0.074510661672205	0.072529664576452
side.geometry.vis.hull.-fillgrade....	0.159891045654063	0.023566654983170	0.059466415852944	0.173905566148663	-0.100107158520960
side.geometry.vis.hull.com-pactness.01	0.156085641541339	0.040794033496069	-0.131106486513530	0.165843615277125	-0.110457276513854
side.geometry.vis.compact-ness.01	0.153549548691035	0.006474860364002	-0.113751719661000	0.105113649878786	-0.086244699905122
side.intensity.vis.hs-v.dgci.mean	0.152547949781857	0.114238126520374	0.060316318816690	-0.204822546829680	0.050144161375299
side.intensity.vis.hs-v.h.stddev	0.151397783922661	-0.087359227333388	0.178414599720541	-0.012901428874198	0.128775787064743
side.intensity.vis.hs-v.s.stddev	0.150180143491848	0.071564621394807	0.163145536663006	0.109176813505400	0.112659358932531
side.intensity.vis.lab.b.skew-ness	0.147905874155279	-0.023902829124744	0.030924145270989	-0.219648158562266	0.094535576851500
side.intensity.vis.hsv.s.skew-ness	0.142789719516491	-0.025124722967918	0.176290024813360	-0.213961894079171	0.115891379571051
side.intensity.vis.hsv.h.mean	0.123309111097507	0.180097464213979	0.162623016607177	-0.171396209073505	0.057352846017375
side.geometry.vis.hull.circu-larity	0.098312842341865	0.086832989701847	-0.345612882417604	-0.047765322114257	-0.005113191990822
side.intensity.vis.lab.a.mean	0.074835201899741	-0.274044110382808	-0.135642842886445	-0.019592687921786	0.028792444643952
side.intensity.vis.hsv.v.skew-ness	0.074282355250615	0.274616717872587	0.036182699670089	-0.060498111299567	0.032050339013364
side.intensity.vis.lab.l.skew-ness	0.064875284713096	0.283535848968085	0.070798755588734	-0.028983377876185	0.039462314996707
side.geo-metry.vis.leaf.width.mean..px.	0.064708919421316	-0.030648351018815	0.273195324907382	0.290175430892303	0.047889538651565
side.geometry.vis.leaf.-curvature.avg	0.051861382240549	-0.053754926686184	-0.073986316891162	0.112584313920067	0.382129695760106
side.intensity.vis.lab.a.stddev	0.048970227921468	-0.255111624841089	0.035498935805731	0.186314965804650	0.033548216033192
side.intensity.vis.hsv.h.red2-green	0.014693417822454	-0.275891964552819	-0.146696029464540	0.107968516548213	-0.026925699529430
side.geometry.vis.cog.avg_distance_to_vertical_image_center_line..px.	0.002255703542709	0.167932971384247	-0.052112449597390	0.164807675059505	0.395799550991497
side.geometry.vis.cog.x..px.	-0.018295637390195	0.198440945976574	-0.024718249740881	0.212081933102325	0.264126955215246
side.geometry.vis.hull.-centroid.x..px.	-0.020827610760453	0.195434865791632	-0.026739709385493	0.212548724608280	0.249230605356547
side.intensity.vis.r-gb.blue.mean	-0.032655316027948	-0.235928457583183	0.257081851741510	-0.202185058157414	0.087800569017500
side.intens-ity.vis.lab.b.stddev	-0.035349028982318	-0.089909295252184	0.306218296316481	0.218254981551409	0.112037697427877
side.intensity.vis.hs-v.h.brown2green	-0.041800190581421	-0.273179458566736	-0.195341189849896	0.101350854334737	-0.024172253914965
side.geometry.vis.leaf.count	-0.064963553544493	0.160129518539592	0.117775501473364	0.050366658280877	-0.356816320045949
side.geometry.vis.area..px.2.	-0.066877875741975	0.170735057785491	0.136235464037443	0.246829416821700	-0.005541758655288
side.geometry.vis.hull.points	-0.091308879526549	-0.012672563451571	0.194762371185883	-0.014600944272732	0.070966044957166

side.geometry.vis.leaf.-curvature.sum	-0.092460456412351	-0.003042306120814	-0.139059886035139	-0.014722812810516	0.366681033077098
side.intensity.vis.hsv.s.mean	-0.108030799671473	0.126184582682743	-0.135596785506085	0.336812071937113	-0.090488643203065
side.intensity.vis.hsv.h.yel-low2green	-0.117256776444562	-0.180857808722725	-0.135148114550108	0.135248645311008	0.014081252758827
side.geometry.vis.branch-point.count	-0.120328287461685	0.133590061548925	-0.056662709124865	-0.143385499962733	-0.168982620087520
side.geo-metry.vis.leaf.length.mean..px.	-0.121343123000004	-0.048958096493151	-0.123930791073007	-0.120365045191502	0.255546054697589
side.intensity.vis.lab.a.skew-ness	-0.121405513313953	0.205074193174650	-0.016226107021715	0.038349726445645	-0.090718734602208
side.geometry.vis.hull.pc2..px.	-0.124104330854089	0.055332371110506	-0.252621310610907	-0.095756347024549	0.059454230723798
side.geometry.vis.width..px.	-0.128842726706772	0.043327597486806	-0.234824397857917	-0.068904923692054	0.123356414829150
side.geometry.vis.minrect-angle.length.b..px.	-0.130309123290017	-0.051255317765804	0.004062137250452	0.024888136329926	0.068867024967779
side.geometry.vis.minrect-angle.length.a..px.	-0.135324851522936	0.073176477700099	0.005904231623926	-0.090611435018349	0.002724149880669
side.intensity.vis.r-gb.red.mean	-0.143614236179736	-0.189705382156517	0.045375213517962	0.065067161667001	-0.015464871389324
side.geometry.vis.hull.com-pactness.16	-0.149542506707520	-0.089269098225041	0.026428050607789	-0.166898636192005	0.107426505011512
side.intensity.vis.hsv.h.skew-ness	-0.152706621666149	0.147125336333725	-0.054630230565439	0.050828720224211	-0.043262672598728
side.geometry.vis.border-.length..px.	-0.158233255684736	0.097055920538714	0.099252613494437	0.010727173389704	0.002853953891878
side.intensity.vis.hsv.v.mean	-0.158886928388560	-0.126672554755516	0.094057227018227	0.062847416093806	-0.024925797236746
side.intensity.vis.lab.l.mean	-0.159966459220401	-0.116012743202473	0.110225776477561	0.051917493166072	-0.016172601276589
side.intensity.vis.rgb.-green.mean	-0.162698872378977	-0.089949643353554	0.125231304248854	0.050325962001261	-0.018071724482718
side.geo-metry.vis.leaf.length.sum..px.	-0.164811209939714	0.093085645139938	-0.042155849221137	-0.075051808631144	-0.024358310148643
side.geometry.vis.compact-ness.16	-0.165964872649882	0.046318011769573	0.029337577327476	-0.101290543905613	-0.005382411344010
side.geometry.vis.hull.area..px.	-0.166991274771262	0.044581346356191	-0.089451796867690	-0.070957874862694	0.040478552860072
side.geometry.vis.minrect-angle.area..px.	-0.167075002169144	0.035930250160517	-0.089156185410542	-0.073461026148713	0.033279509706772
side.intensity.vis.lab.b.mean	-0.167502739555012	0.001702822372275	-0.019276704506100	0.179830361915050	-0.065371864620083
side.geometry.vis.hull.length	-0.168879339349225	0.018752855275062	0.107283700486389	-0.044627183264777	0.086935756848037
side.geometry.vis.height..px.	-0.169845687308079	0.006300567299638	0.114536693496418	-0.009289879919499	0.027212402155781
side.geometry.vis.hull.pc1..px.	-0.170478261337160	0.003416456718609	0.112309235554262	-0.015237442337841	0.046438706598115
side.geometry.vis.circum-circle.d..px.	-0.170602188191303	0.003531805134576	0.111345064358562	-0.014833335807075	0.046677477746130
height.to.width.ratio	-0.171918495538601	0.007009203201882	0.025472377151153	-0.084965386582854	0.002757843804938
side.geometry.vis.cog.avg_distance_to_center..px.	-0.171968002998622	-0.016758557768877	0.038440934103580	-0.077076356822147	0.046582920579426

Table S2: Strains for NGS

NGS_Number	Plants_showing_infection	Total_plants	Percentage_Infection	Mating_Type	Notes	Ambiguous_genome_regions_(excluding_Chr_1_sporekiller_and_scaffold)	Ubromi_genes_(specific_reads)	Uhordei_genes_(specific_and_shared_reads)	Hybrid_Generation	Parent
33767	0	15	0.00	1		Yes	0.5102183	0.4545071	F1	U. bromivora Mat 1
33768	0	25	0.00	1		Yes	0.6057278	0.3569118	F1	U. bromivora Mat 1
33769	0	19	0.00	1		Yes	0.6082302	0.3570525	F1	U. bromivora Mat 1
33770	0	17	0.00	1		Yes	0.8940637	0.5232738	F1	U. bromivora Mat 1
33771	0	15	0.00	1		No	0.5070207	0.4438194	F1	U. bromivora Mat 1
33772	0	19	0.00	1		No	0.5060475	0.4436788	F1	U. bromivora Mat 1
33773	0	20	0.00	1		No	0.4261087	0.5076642	F1	U. bromivora Mat 1
33774	1	14	0.07	1	Source of F2	No	0.4338941	0.5093517	F1	U. bromivora Mat 1
33775	0	16	0.00	1		No	0.4336160	0.5110392	F1	U. bromivora Mat 1
33776	1	10	0.10	1	Source of F2	No	0.6723203	0.2566446	F1	U. bromivora Mat 1
33777	3	14	0.21	1	Source of F2	No	0.5957181	0.3265364	F1	U. bromivora Mat 1
33778	5	25	0.20	1	Source of F2	Yes	0.8858613	0.5186331	F1	U. bromivora Mat 1
33779	1	21	0.05	1	Source of F2	No	0.4010844	0.3974125	F1	U. bromivora Mat 1
33780	0	8	0.00	1		Yes	0.4908939	0.3940374	F1	U. bromivora Mat 1
33781	0	7	0.00	1		Yes	0.5658279	0.4014906	F1	U. bromivora Mat 1
33782	0	4	0.00	1		Yes	0.2078410	0.1693151	F1	U. bromivora Mat 1
33783	1	10	0.10	1		Yes	0.5820937	0.3445366	F1	U. bromivora Mat 1
33784	0	7	0.00	1		No	0.4907549	0.4199128	F1	U. bromivora Mat 1
33785	0	6	0.00	1		Yes	0.8063395	0.8496695	F1	U. bromivora Mat 1
33786	1	7	0.14	1		No	0.7358543	0.1856279	F1	U. bromivora Mat 1
33787	6	30	0.20	1	Source of F2	No	0.7352982	0.1853466	F1	U. bromivora Mat 1
33788	0	3	0.00	1		No	0.2409287	0.7077767	F1	U. bromivora Mat 1
33790	0	10	0.00	1		Yes	0.1741971	0.2286598	F1	U. bromivora Mat 1
34649	4	19	0.21	1	Source of F2	Yes	0.8106492	0.7651526	F1	U. bromivora Mat 1
34650	2	10	0.20	1		Yes	0.8233004	0.7685276	F1	U. bromivora Mat 1
34651	0	10	0.00	1		No	0.5820937	0.3552243	F1	U. bromivora Mat 1
34652	0	11	0.00	2		No	0.2400945	0.7077767	F2	Pool of 33780, non-sequenced strain, 33782, 33783 and 33784
34654	0	11	0.00	2		Yes	0.4183234	0.8804669	F2	Pool of 33780, non-sequenced strain, 33782, 33783 and 33784

34655	0	10	0.00	2		Yes	0.4255526	0.8832794	F2	Pool of 33780, non-sequenced strain, 33782, 33783 and 33784
34656	0	11	0.00	1		No	0.4452940	0.4966953	F2	Pool of 33785, 33786, 33787, 33788, non-sequenced strain
34657	0	8	0.00	1		Yes	0.5282914	0.4332724	F2	Pool of 33785, 33786, 33787, 33788, non-sequenced strain
34659	0	8	0.00	1		Yes	0.5300987	0.4335536	F2	Pool of 33785, 33786, 33787, 33788, non-sequenced strain
34660	0	8	0.00	1		No	0.5310719	0.4045844	F2	Pool of 33789, 33790, 34649, 34650, 34651
34661	0	8	0.00	1		No	0.5200890	0.4031782	F2	Pool of 33789, 33790, 34649, 34650, 34651
39081	0	11	0.00	1		No	0.4515501	0.5103361	F2	33787
39082	1	11	0.09	1		No	0.4826915	0.3965687	F2	33787
39083	0	9	0.00	1		No	0.4434867	0.5033047	F2	33787
39084	0	11	0.00	1		No	0.4313916	0.5078048	F2	33787
39086	0	10	0.00	1		Yes	0.5688864	0.5512586	F2	33787
39087	1	7	0.14	1		No	0.5184207	0.4061313	F2	33787
39088	0	10	0.00	1		No	0.4915890	0.4398819	F2	33787
39089	0	12	0.00	1		No	0.4514111	0.4829138	F2	33787
39090	0	10	0.00	1		No	0.4473794	0.4813669	F2	33787
39091	0	9	0.00	1		No	0.4511330	0.4822107	F2	33787
39092	1	9	0.11	1		No	0.5719449	0.3543805	F2	33787
39093	0	9	0.00	1		No	0.4490477	0.4822107	F2	33787
39094	0	11	0.00	1		Yes	0.5015988	0.4384756	F2	33787
39095	3	9	0.33	1		Yes	0.5046573	0.4387569	F2	33787
39096	1	10	0.10	1		Yes	0.5061866	0.4396006	F2	33787
39097	0	9	0.00	1		Yes	0.4661476	0.4629447	F2	33787
39098	1	11	0.09	1		Yes	0.4981232	0.4374912	F2	33787
39099	2	10	0.20	1	Source of F3	No	0.5298207	0.3889748	F2	33787
39100	2	8	0.25	1		No	0.4658696	0.4428350	F2	33787
39101	0	9	0.00	1		Yes	0.4461282	0.5117424	F2	33787
39102	2	11	0.18	1		No	0.4915890	0.4500070	F2	33787
39105	1	9	0.11	1		No	0.4920061	0.4501477	F2	33787
39106	0	9	0.00	1		No	0.4409843	0.5011953	F2	33787
39107	0	11	0.00	1		No	0.4095649	0.5369146	F2	33787
39108	1	10	0.10	1		No	0.6147644	0.3179581	F2	33787
39109	0	8	0.00	1		No	0.6162936	0.3186612	F2	33787
39110	0	10	0.00	1		No	0.5460865	0.3917874	F2	33787
39111	2	11	0.18	1		Yes	0.4566940	0.5042891	F2	33787
39112	0	9	0.00	1		Yes	0.5879327	0.5083673	F2	33787
39113	0	9	0.00	1		No	0.5451133	0.3919280	F2	33787
39114	0	9	0.00	1		No	0.5239816	0.4211785	F2	33787
39115	2	13	0.15	1		Yes	0.4904769	0.4699761	F2	33787
39116	0	10	0.00	1		Yes	0.5079939	0.4405850	F2	33787
72766	0	11	0.00	2		No	0.1076046	0.8472789	F3	39099
72767	0	10	0.00	2		No	0.1073266	0.8469976	F3	39099
72768	0	11	0.00	2		No	0.1070485	0.8484039	F3	39099
72769	0	10	0.00	2		No	0.1598777	0.8055126	F3	39099

72770	0	13	0.00	2		No	0.1643264	0.7877936	F3	39099
72771	0	12	0.00	2		Yes	0.1709996	0.8637322	F3	39099
72772	0	10	0.00	2		Yes	0.1697484	0.8610603	F3	39099
72773	0	11	0.00	2		Yes	0.1548728	0.8514977	F3	39099
72774	0	11	0.00	2		Yes	0.1515362	0.8453101	F3	39099
72775	0	11	0.00	2		Yes	0.1527874	0.8474195	F3	39099
72776	1	32	0.03	2	Source of F4	Yes	0.2203531	0.7494023	F3	39099
72778	0	4	0.00	2		No	0.1092729	0.8239347	F3	39099
72782	0	6	0.00	2		Yes	0.1063534	0.8564196	F4	72776
72783	0	13	0.00	2		Yes	0.1048241	0.8488258	F4	72776
72784	0	13	0.00	1	Missing spore killer?	No	0.1208119	0.8522008	F4	72776
72785	0	13	0.00	2		Yes	0.0859169	0.6893545	F4	72776
72786	0	14	0.00	2		No	0.0792437	0.8737168	F4	72776
72787	0	12	0.00	2		No	0.0980120	0.8454507	F4	72776
72788	0	9	0.00	2		No	0.0155707	0.9319364	F4	72776
72790	0	20	0.00	2		No	0.1340192	0.8187315	F2	33774
72791	1	38	0.03	2		No	0.0688169	0.8853888	F2	33774
72792	0	22	0.00	2		No	0.1409704	0.8118408	F2	33774
72794	0	17	0.00	2		No	0.2013068	0.7471523	F2	33776
72795	0	20	0.00	2		Yes	0.1741971	0.7799184	F2	33776
72796	2	33	0.06	2		No	0.1195607	0.8087470	F2	33776
72797	0	20	0.00	2		Yes	0.1445850	0.8021375	F2	33776
72798	0	20	0.00	2		Yes	0.2051995	0.7451835	F2	33777
72799	0	19	0.00	2		Yes	0.1644655	0.8173253	F2	33777
72800	3	20	0.15	2		Yes	0.4742110	0.9161862	F2	33777
72801	1	18	0.06	2		Yes	0.4244404	0.9319364	F2	33777
72802	4	35	0.11	1		Yes	0.8068956	0.8450288	F2	33778
72803	0	20	0.00	1		Yes	0.7960517	0.8976234	F2	33778
72804	1	17	0.06	1		Yes	0.7802030	0.8679511	F2	33778
72805	0	20	0.00	1		Yes	0.8609759	0.9413585	F2	33778
72806	0	36	0.00	2		Yes	0.1452801	0.8897483	F2	33779
72807	0	19	0.00	2		Yes	0.1351314	0.8678104	F2	33779
72808	0	20	0.00	2		Yes	0.3336577	0.9139362	F2	33779
72809	0	20	0.00	2		Yes	0.3723064	0.9184362	F2	33779
72810	0	35	0.00	2		No	0.0000000	0.9631557	F2	34649
72811	0	32	0.00	2		Yes	0.5249548	0.9513430	F2	34649
72812	2	19	0.11	2		Yes	0.3846795	0.9555618	F2	34649
72813	0	20	0.00	2		No	0.0000000	0.9635776	F2	34649

Table S3: Genes containing potentially damaging SNPs which are more common in infecting strains

Gene	Predicted Secreted	Chromosome/ Contig	Source	Feature	Start	End	Score	Strand	Frame	Attribute	Orthologs (including self)	Functional Annotation
UBRO_20472	FALSE	UBRO_chr02	MIPS	mRNA	1227023	1228661	.	+	.	ID=mRNA:UBRO_20472;Note=+uncharacterized+protein	SPSC_02149 SPSC_06524 UBRO_06511 UBRO_20174 UBRO_20469 UBRO_20472 UBRO_20630 UBRO_20759 UBRO_20057 UBRO_20400 UBRO_20401 BN887_03037 sr15411 SPSC_05615 UHOR_06511 UMAG_04525	
UBRO_21045	*	UBRO_chr02	MIPS	mRNA	1250468	1252014	.	+	.	ID=mRNA:UBRO_21045;Note=+uncharacterized+protein		GO:0016021 integral component of membrane,GO:0003677 DNA binding
UBRO_20479	FALSE	UBRO_chr02	MIPS	mRNA	1500822	1501909	.	+	.	ID=mRNA:UBRO_20479;Note=+uncharacterized+protein		GO:0016021 integral component of membrane
UBRO_01988	FALSE	UBRO_chr03	MIPS	mRNA	1737859	1739775	.	+	.	ID=mRNA:UBRO_01988;Note=+uncharacterized+protein	SPSC_00011 SPSC_00012 UBRO_01988 UBRO_20775 UBRO_08867 UBRO_20326 UHOR_01988 UHOR_14700 UHOR_08867 UHOR_09014 BN887_02167 BN887_06186 SPSC_02318	
UBRO_20814	FALSE	UBRO_chr13	MIPS	mRNA	161112	162608	.	+	.	ID=mRNA:UBRO_20814;Note=+uncharacterized+protein	sr07366 sr11325 sr15209 SPSC_01813 SPSC_04725 UBRO_20361 UBRO_20409 UBRO_20420 UBRO_20465 UBRO_20481 UBRO_20591 UBRO_20814 UBRO_20827 UBRO_20916 UBRO_20413 UBRO_20416 UBRO_20499 UBRO_20568 UBRO_20763 UBRO_20793 UBRO_20994 UBRO_21002	GO:0003677 DNA binding
UBRO_20825	FALSE	UBRO_chr13	MIPS	mRNA	436916	437809	.	-	.	ID=mRNA:UBRO_20825;Note=+probable+transposase	UBRO_20297 UBRO_20462 UBRO_20825 UBRO_20876 UHOR_03913 UHOR_10023 UHOR_10025 sr11477 SPSC_03451	GO:0003677 DNA binding,GO:0006313 transposition, DNA-mediated,GO:0015074 DNA integration
UBRO_20846	FALSE	UBRO_chr15	MIPS	mRNA	249359	250537	.	-	.	ID=mRNA:UBRO_20846;Note=+uncharacterized+protein	UBRO_20402 UBRO_20555 UBRO_20435 UBRO_20473 UBRO_20476 UBRO_20544 UBRO_20606 UBRO_20846 UBRO_21007 UBRO_20772 UHOR_14039 UHOR_14142 UHOR_14176 SPSC_01964	
UBRO_20860	FALSE	UBRO_chr15	MIPS	mRNA	593548	594902	.	+	.	ID=mRNA:UBRO_20860;Note=+uncharacterized+protein	UBRO_20110 UBRO_20406 UBRO_20860 UBRO_20886 UBRO_20914 UHOR_14108 UHOR_14114 UHOR_14168	
UBRO_20278	FALSE	UBRO_chr22	MIPS	mRNA	265779	266447	.	-	.	ID=mRNA:UBRO_20278;Note=+uncharacterized+protein	UBRO_21062 UBRO_20218 UBRO_20278 UBRO_20483 UBRO_20529 UBRO_20533 UBRO_20546 UBRO_20590 UBRO_20873 UBRO_20998 UBRO_21009 UBRO_21033 UBRO_21041 UBRO_21053 UBRO_21054 UBRO_21069 UBRO_21084 UBRO_20454 UBRO_20861 UBRO_21034 UBRO_21076 UBRO_20691 UBRO_20887 UBRO_21085 sr16557 UMAG_02745 SPSC_01947 UHOR_03466	
UBRO_08867	FALSE	UBRO_chr22	MIPS	mRNA	349012	352350	.	-	.	ID=mRNA:UBRO_08867;Note=+uncharacterized+protein	SPSC_00011 SPSC_00012 UBRO_01988 UBRO_20775 UBRO_08867 UBRO_20326 UHOR_01988 UHOR_14700 UHOR_08867 UHOR_09014 BN887_02167 BN887_06186 SPSC_02318	
UHOR_12027	FALSE	UHOR_scaffold_4.00047	orf	mRNA	493	1106	.	+	.	ID=mRNA_UHOR_12027;Parent=UHOR_12027;Name=UHOR_12027;Note=related+to+retrotransposon+nucleocapsid+protein;pedant_db=p3_t120017_Ust_hordе_v2;		
UHOR_12032	FALSE	UHOR_scaffold_4.00047	orf	mRNA	11125	12563	.	-	.	ID=mRNA_UHOR_12032;Parent=UHOR_12032;Name=UHOR_12032;Note=related+to+retrotransposon+protein;pedant_db=p3_t120017		

										_Ust_horde_v2;		
UHOR_12077	FALSE	UHOR_scaffold_4.00107	orf	mRNA	3674	4252	.	-	.	ID=mRNA_UHOR_12077;Parent=UHOR_12077;Name=UHOR_12077;Note=uncharacterized+protein;pedant_db=p3_t120017_Ust_horde_v2;	BN887_02600 BN887_02713 UHOR_00833 UHOR_12077 UHOR_14059 UHOR_01674 UHOR_13996 UHOR_04106 UHOR_06224 UHOR_10015 UHOR_10031 UHOR_12673 UHOR_13044 UHOR_13272 UHOR_13991 UHOR_14014 UHOR_14086 UHOR_14161 UHOR_14170 UHOR_14669 UHOR_04108 UHOR_15109 UHOR_10014 UHOR_12378 UHOR_13752 UHOR_14060 UHOR_14564 UHOR_15610 UHOR_16664 UHOR_10028 UHOR_13992 UHOR_12602 UHOR_16322 UHOR_13400 UHOR_14013 UHOR_15903 UHOR_14895 UHOR_16372 SPSC_04529 UBRO_20328 UBRO_12371 UBRO_20143 UBRO_20214 UMAG_02565	
UHOR_12478	FALSE	UHOR_scaffold_4.00674	orf	mRNA	618	1211	.	-	.	ID=mRNA_UHOR_12478;Parent=UHOR_12478;Name=UHOR_12478;Note=uncharacterized+protein;pedant_db=p3_t120017_Ust_horde_v2;		
UHOR_12662	FALSE	UHOR_scaffold_4.00883	orf	mRNA	207	680	.	-	.	ID=mRNA_UHOR_12662;Parent=UHOR_12662;Name=UHOR_12662;Note=uncharacterized+protein;pedant_db=p3_t120017_Ust_horde_v2;		GO:0003676 nucleic acid binding
UHOR_13030	FALSE	UHOR_scaffold_4.01246	orf	mRNA	123	563	.	+	.	ID=mRNA_UHOR_13030;Parent=UHOR_13030;Name=UHOR_13030;Note=uncharacterized+protein;pedant_db=p3_t120017_Ust_horde_v2;	UHOR_13030 UHOR_15088 UHOR_16659 UHOR_13563 BN887_02654	GO:0005488 binding
UHOR_13044	FALSE	UHOR_scaffold_4.01260	orf	mRNA	1388	2431	.	+	.	ID=mRNA_UHOR_13044;Parent=UHOR_13044;Name=UHOR_13044;Note=uncharacterized+protein;pedant_db=p3_t120017_Ust_horde_v2;	BN887_02600 BN887_02713 UHOR_00833 UHOR_12077 UHOR_14059 UHOR_01674 UHOR_13996 UHOR_04106 UHOR_06224 UHOR_10015 UHOR_10031 UHOR_12673 UHOR_13044 UHOR_13272 UHOR_13991 UHOR_14014 UHOR_14086 UHOR_14161 UHOR_14170 UHOR_14669 UHOR_04108 UHOR_15109 UHOR_10014 UHOR_12378 UHOR_13752 UHOR_14060 UHOR_14564 UHOR_15610 UHOR_16664 UHOR_10028 UHOR_13992 UHOR_12602 UHOR_16322 UHOR_13400 UHOR_14013 UHOR_15903 UHOR_14895 UHOR_16372 SPSC_04529 UBRO_20328 UBRO_12371 UBRO_20143 UBRO_20214 UMAG_02565	GO:0000943 retrotransposon nucleocapsid,GO:0003676 nucleic acid binding,GO:0015074 DNA integration
UHOR_13400	FALSE	UHOR_scaffold_5.00006	orf	mRNA	346832	347704	.	+	.	ID=mRNA_UHOR_13400;Parent=UHOR_13400;Name=UHOR_13400;Note=related+to+retrotransposon+protein;pedant_db=p3_t120017_Ust_horde_v2;	BN887_02600 BN887_02713 UHOR_00833 UHOR_12077 UHOR_14059 UHOR_01674 UHOR_13996 UHOR_04106 UHOR_06224 UHOR_10015 UHOR_10031 UHOR_12673 UHOR_13044 UHOR_13272 UHOR_13991 UHOR_14014 UHOR_14086 UHOR_14161 UHOR_14170 UHOR_14669 UHOR_04108 UHOR_15109 UHOR_10014 UHOR_12378 UHOR_13752 UHOR_14060 UHOR_14564 UHOR_15610 UHOR_16664 UHOR_10028 UHOR_13992 UHOR_12602 UHOR_16322 UHOR_13400 UHOR_14013 UHOR_15903 UHOR_14895 UHOR_16372 SPSC_04529 UBRO_20328 UBRO_12371 UBRO_20143 UBRO_20214 UMAG_02565	GO:0003676 nucleic acid binding,GO:0008270 zinc ion binding
UHOR_13437	FALSE	UHOR_scaffold_5.00007	orf	mRNA	64651	65639	.	+	.	ID=mRNA_UHOR_13437;Parent=UHOR_13437;Name=UHOR_13437;Note=uncharacterized+protein;pedant_db=p3_t120017_Ust_horde_v2;		

UHOR_08264	FALSE	UHOR_scaffold_5.00018	orf	mRNA	267785	268183	.	-	.	ID=mRNA_UHOR_08264;Parent=UHOR_08264;Name=UHOR_08264;Note=uncharacterized+protein;pedant_db=p3_t120017_Ust_horde_v2;		
UHOR_14038	FALSE	UHOR_scaffold_5.00019	orf	mRNA	174942	176285	.	-	.	ID=mRNA_UHOR_14038;Parent=UHOR_14038;Name=UHOR_14038;Note=uncharacterized+protein;pedant_db=p3_t120017_Ust_horde_v2;	UBRO_20403 UBRO_20494 UBRO_20581 UBRO_20600 UBRO_20693 UBRO_20773 UBRO_20905 UBRO_21046 UBRO_21083 UBRO_20434 UBRO_20451 UBRO_20527 UBRO_20538 UBRO_20707 UBRO_20586 UBRO_20665 UBRO_20701 UHOR_14038 UHOR_14159 UHOR_14178 SPSC_01963 UHOR_14003 UBRO_20842	GO:0003677 DNA binding
UHOR_00833	FALSE	UHOR_scaffold_5.00019	orf	mRNA	379787	380902	.	-	.	ID=mRNA_UHOR_00833;Parent=UHOR_00833;Name=UHOR_00833;Note=uncharacterized+protein;pedant_db=p3_t120017_Ust_horde_v2;	BN887_02600 BN887_02713 UHOR_00833 UHOR_12077 UHOR_14059 UHOR_01674 UHOR_13996 UHOR_04106 UHOR_06224 UHOR_10015 UHOR_10031 UHOR_12673 UHOR_13044 UHOR_13272 UHOR_13991 UHOR_14014 UHOR_14086 UHOR_14161 UHOR_14170 UHOR_14669 UHOR_04108 UHOR_15109 UHOR_10014 UHOR_12378 UHOR_13752 UHOR_14060 UHOR_14564 UHOR_15610 UHOR_16664 UHOR_10028 UHOR_13992 UHOR_12602 UHOR_16322 UHOR_13400 UHOR_14013 UHOR_15903 UHOR_14895 UHOR_16372 SPSC_04529 UBRO_20328 UBRO_12371 UBRO_20143 UBRO_20214 UMAG_02565	
UHOR_14168	FALSE	UHOR_scaffold_5.00019	orf	mRNA	473789	475059	.	-	.	ID=mRNA_UHOR_14168;Parent=UHOR_14168;Name=UHOR_14168;Note=uncharacterized+protein;pedant_db=p3_t120017_Ust_horde_v2;	UBRO_20110 UBRO_20406 UBRO_20860 UBRO_20886 UBRO_20914 UHOR_14108 UHOR_14114 UHOR_14168	GO:0016021 integral component of membrane
UHOR_14319	FALSE	UHOR_scaffold_5.00022	orf	mRNA	15660	17797	.	+	.	ID=mRNA_UHOR_14319;Parent=UHOR_14319;Name=UHOR_14319;Note=related+to+TNA1+-+high+affinity+nicotinic+acid+plasma+membrane+permease;pedant_db=p3_t120017_Ust_horde_v2;		
UHOR_06744	FALSE	UHOR_scaffold_5.00028	orf	mRNA	199	561	.	-	.	ID=mRNA_UHOR_06744;Parent=UHOR_06744;Name=UHOR_06744;Note=uncharacterized+protein;pedant_db=p3_t120017_Ust_horde_v2;		
UHOR_06758	FALSE	UHOR_scaffold_5.00028	orf	mRNA	38136	38939	.	-	.	ID=mRNA_UHOR_06758;Parent=UHOR_06758;Name=UHOR_06758;Note=uncharacterized+protein+(N-terminal+fragment);pedant_db=p3_t120017_Ust_horde_v2;	UBRO_20208 UHOR_06758	GO:0016021 integral component of membrane,GO:0005488 binding
UHOR_14699	FALSE	UHOR_scaffold_5.00028	orf	mRNA	265676	266554	.	-	.	ID=mRNA_UHOR_14699;Parent=UHOR_14699;Name=UHOR_14699;Note=uncharacterized+protein;pedant_db=p3_t120017_Ust_horde_v2;		GO:0003676 nucleic acid binding,GO:0015074 DNA integration
UHOR_00956	FALSE	UHOR_scaffold_5.00030	orf	mRNA	45079	46290	.	-	.	ID=mRNA_UHOR_00956;Parent=UHOR_00956;Name=UHOR_00956;Note=uncharacterized+protein;pedant_db=p3_t120017_Ust_horde_v2;	sr11895 SPSC_01870 UBRO_00956 UHOR_00956 UMAG_00616	GO:0016021 integral component of membrane
UHOR_14792	FALSE	UHOR_scaffold_5.00030	orf	mRNA	113463	114929	.	-	.	ID=mRNA_UHOR_14792;Parent=UHOR_14792;Name=UHOR_14792;Note=un-		GO:0000943 retrotransposon nucleocapsid

										characterized+protein;pedant_db=p3_t120017_Ust_horde_v2;			
UHOR_15109	FALSE	UHOR_scaffold_5.00036	orf	mRNA	203226	204892	.	+	.	ID=mRNA_UHOR_15109;Parent=UHOR_15109;Name=UHOR_15109;Note=uncharacterized+protein;pedant_db=p3_t120017_Ust_horde_v2;	BN887_02600 BN887_02713 UHOR_00833 UHOR_12077 UHOR_14059 UHOR_01674 UHOR_13996 UHOR_04106 UHOR_06224 UHOR_10015 UHOR_10031 UHOR_12673 UHOR_13044 UHOR_13272 UHOR_13991 UHOR_14014 UHOR_14086 UHOR_14161 UHOR_14170 UHOR_14669 UHOR_04108 UHOR_15109 UHOR_10014 UHOR_12378 UHOR_13752 UHOR_14060 UHOR_14564 UHOR_15610 UHOR_16664 UHOR_10028 UHOR_13992 UHOR_12602 UHOR_16322 UHOR_13400 UHOR_14013 UHOR_15903 UHOR_14895 UHOR_16372 SPSC_04529 UBRO_20328 UBRO_12371 UBRO_20143 UBRO_20214 UMAG_02565	GO:0003676 nucleic acid binding,GO:0008270 zinc ion binding
UHOR_15131	FALSE	UHOR_scaffold_5.00036	orf	mRNA	262671	263774	.	+	.	ID=mRNA_UHOR_15131;Parent=UHOR_15131;Name=UHOR_15131;Note=uncharacterized+protein;pedant_db=p3_t120017_Ust_horde_v2;		GO:0003676 nucleic acid binding,GO:0008270 zinc ion binding
UHOR_03849	FALSE	UHOR_scaffold_5.00036	orf	mRNA	330856	332265	.	+	.	ID=mRNA_UHOR_03849;Parent=UHOR_03849;Name=UHOR_03849;Note=probable+translation+initiation+factor+eIF2+gamma+chain;pedant_db=p3_t120017_Ust_horde_v2;	BN887_05401 sr13562 SPSC_01777 UBRO_03849 UHOR_03849 UMAG_10129	GO:0005829 cytosol,GO:0005850 eukaryotic translation initiation factor 2 complex,GO:0003743 translation initiation factor activity,GO:0003746 translation elongation factor activity,GO:0003924 GTPase activity,GO:0005525 GTP binding,GO:0001731 formation of translation preinitiation complex,GO:0006414 translational elongation
UHOR_15354	FALSE	UHOR_scaffold_5.00041	orf	mRNA	253328	254368	.	+	.	ID=mRNA_UHOR_15354;Parent=UHOR_15354;Name=UHOR_15354;Note=uncharacterized+protein+(N-terminal+fragment);pedant_db=p3_t120017_Ust_horde_v2;	UHOR_01827 UHOR_15092 UHOR_16068 UHOR_14844 UHOR_15354 UHOR_16801 UBRO_20258	GO:0000943 retrotransposon nucleocapsid
UHOR_04813	FALSE	UHOR_scaffold_5.00045	orf	mRNA	147799	150252	.	+	.	ID=mRNA_UHOR_04813;Parent=UHOR_04813;Name=UHOR_04813;Note=uncharacterized+protein;pedant_db=p3_t120017_Ust_horde_v2;	SPSC_01802 SPSC_02044 SPSC_03529 UBRO_02119 UBRO_04813 UBRO_20573 UBRO_20574 UBRO_20867 UBRO_20967 UMAG_11874 UMAG_01443 UMAG_03635 UMAG_04689 UMAG_04693 UMAG_04887 UMAG_05066 UMAG_05621 UMAG_06351 UMAG_06356 UMAG_06479 UMAG_06505 UMAG_10981 UMAG_11979 UMAG_11109 UMAG_05436 UMAG_06514 UMAG_10169 BN887_04509 sr14681 UHOR_13031 UHOR_02119 UHOR_04813	
UHOR_07800	FALSE	UHOR_scaffold_5.00063	orf	mRNA	212409	213065	.	+	.	ID=mRNA_UHOR_07800;Parent=UHOR_07800;Name=UHOR_07800;Note=uncharacterized+protein;pedant_db=p3_t120017_Ust_horde_v2;	UHOR_07800 UHOR_12031 UHOR_12112	GO:0000943 retrotransposon nucleocapsid

Table S4: Genes containing potentially damaging SNPs which are more common in non-infecting strains

Gene	Predicted Secreted	Chromosome/Contig	Source	Feature	Start	End	Score	Strand	Frame	Attribute	Orthologs (including self)	Functional Annotation
UBRO_20402	FALSE	UBRO_chr01	orf	mRNA	177838	179013	.	+	.	ID=mRNA_UBRO_20402;Parent=UBRO_20402;Name=UBRO_20402;Note=uncharacterized+protein;pedant_db=p3_i2_t307758_Ust_bromi_v3;	UBRO_20402 UBRO_20555 UBRO_20435 UBRO_20473 UBRO_20476 UBRO_20544 UBRO_20606 UBRO_20846 UBRO_21007 UBRO_20772 UHOR_14039 UHOR_14142 UHOR_14176 SPSC_01964	
UBRO_20403	FALSE	UBRO_chr01	orf	mRNA	179986	181224	.	+	.	ID=mRNA_UBRO_20403;Parent=UBRO_20403;Name=UBRO_20403;Note=uncharacterized+protein;pedant_db=p3_i2_t307758_Ust_bromi_v3;	UBRO_20403 UBRO_20494 UBRO_20581 UBRO_20600 UBRO_20693 UBRO_20773 UBRO_20905 UBRO_21046 UBRO_21083 UBRO_20434 UBRO_20451 UBRO_20527 UBRO_20538 UBRO_20707 UBRO_20586 UBRO_20665 UBRO_20701 UHOR_14038 UHOR_14159 UHOR_14178 SPSC_01963 UHOR_14003 UBRO_20842	GO:0003677 DNA binding
UBRO_20406	TRUE	UBRO_chr01	orf	mRNA	387097	388419	.	+	.	ID=mRNA_UBRO_20406;Parent=UBRO_20406;Name=UBRO_20406;Note=uncharacterized+protein;pedant_db=p3_i2_t307758_Ust_bromi_v3;	UBRO_20110 UBRO_20406 UBRO_20860 UBRO_20886 UBRO_20914 UHOR_14108 UHOR_14114 UHOR_14168	GO:0016020 membrane
UBRO_01081	FALSE	UBRO_chr01	orf	mRNA	408093	410111	.	+	.	ID=mRNA_UBRO_01081;Parent=UBRO_01081;Name=UBRO_01081;Note=uncharacterized+protein;pedant_db=p3_i2_t307758_Ust_bromi_v3;	BN887_03556 sr11989 SPSC_01965 UBRO_01081 UHOR_01081 UMAG_00701	GO:0003676 nucleic acid binding,GO:0006355 regulation of transcription, DNA-templated
UBRO_20218	FALSE	UBRO_chr01	orf	mRNA	529301	530659	.	-	.	ID=mRNA_UBRO_20218;Parent=UBRO_20218;Name=UBRO_20218;Note=uncharacterized+protein;pedant_db=p3_i2_t307758_Ust_bromi_v3;	UBRO_21062 UBRO_20218 UBRO_20278 UBRO_20483 UBRO_20529 UBRO_20533 UBRO_20546 UBRO_20590 UBRO_20873 UBRO_20998 UBRO_21009 UBRO_21033 UBRO_21041 UBRO_21053 UBRO_21054 UBRO_21069 UBRO_21084 UBRO_20454 UBRO_20861 UBRO_21034 UBRO_21076 UBRO_20691 UBRO_20887 UBRO_21085 sr16557 UMAG_02745 SPSC_01947 UHOR_03466	
UBRO_00952	FALSE	UBRO_chr01	orf	mRNA	687157	693033	.	+	.	ID=mRNA_UBRO_00952;Parent=UBRO_00952;Name=UBRO_00952;Note=related+to+RKR1+-+RING+domain+E3+ubiquitin+ligase;pedant_db=p3_i2_t307758_Ust_bromi_v3;	BN887_03874 sr11891 SPSC_01866 UBRO_00952 UHOR_00952 UMAG_00612	GO:0005829 cytosol,GO:1990112 RQC complex,GO:0008270 zinc ion binding,GO:0016874 ligase activity,GO:0043023 ribosomal large subunit binding,GO:0061630 ubiquitin protein ligase activity,GO:0016567 protein ubiquitination,GO:0072344 rescue of stalled ribosome,GO:1990116 ribosome-associated ubiquitin-dependent protein catabolic process
UBRO_00877	FALSE	UBRO_chr01	orf	mRNA	783110	788053	.	-	.	ID=mRNA_UBRO_00877;Parent=UBRO_00877;Name=UBRO_00877;Note=related+to+RAD16+-+nucleotide+excision+repair+protein;pedant_db=p3_i2_t307758_Ust_bromi_v3;	BN887_02691 sr11849 SPSC_01833 UBRO_00877 UHOR_00877 UMAG_10467	GO:0003676 nucleic acid binding,GO:0005524 ATP binding,GO:0016818 hydrolase activity, acting on acid anhydrides, in phosphorus-containing anhydrides,GO:0046872 metal ion binding
UBRO_	FALSE	UBRO_chr01	orf	mRNA	795531	798260	.	-	.	ID=mRNA_UBRO_	BN887_02673 sr11829	GO:0003676 nuc-

00851										00851;Parent=UBRO_00851;Name=UBRO_00851;Note=related+to+putative+C2H2+zinc+finger+protein+flbC;pedant_db=p3_i2_t307758_Ust_bromi_v3;	SPSC_02800 UBRO_00851 UHOR_00851 UMAG_00551	leic acid binding
UBRO_00905	FALSE	UBRO_chr01	orf	mRNA	808986	811133	.	+	.	ID=mRNA_UBRO_00905;Parent=UBRO_00905;Name=UBRO_00905;Note=uncharacterized+protein;pedant_db=p3_i2_t307758_Ust_bromi_v3;	BN887_02697 sr11864 SPSC_01817 UBRO_00905 UHOR_00905 UMAG_00586	GO:0006270 DNA replication initiation
UBRO_21028	*	UBRO_chr01	orf	mRNA	816201	816758	.	-	.	ID=mRNA_UBRO_21028;Parent=UBRO_21028;Name=UBRO_21028;Note=uncharacterized+protein;pedant_db=p3_i2_t307758_Ust_bromi_v3;		GO:0003677 DNA binding
UBRO_00870	FALSE	UBRO_chr01	orf	mRNA	819845	820360	.	-	.	ID=mRNA_UBRO_00870;Parent=UBRO_00870;Name=UBRO_00870;Note=related+to+MRPL33+-+mitochondrial+ribosomal+protein,+large+subunit;pedant_db=p3_i2_t307758_Ust_bromi_v3;	BN887_02679 sr11841 SPSC_02810 UBRO_00870 UHOR_00870 UMAG_00563	GO:0015934 large ribosomal subunit,GO:0003735 structural constituent of ribosome,GO:0006412 translation
UBRO_00869	FALSE	UBRO_chr01	orf	mRNA	823171	824448	.	+	.	ID=mRNA_UBRO_00869;Parent=UBRO_00869;Name=UBRO_00869;Note=uncharacterized+protein;pedant_db=p3_i2_t307758_Ust_bromi_v3;	BN887_02698 sr11840 SPSC_02809 UBRO_00869 UHOR_00869 UMAG_00562	
UBRO_00866	FALSE	UBRO_chr01	orf	mRNA	826756	828093	.	+	.	ID=mRNA_UBRO_00866;Parent=UBRO_00866;Name=UBRO_00866;Note=related+to+cell+cycle+arrest+protein+BUB2;pedant_db=p3_i2_t307758_Ust_bromi_v3;	BN887_02699 sr11839 SPSC_02808 UBRO_00866 UHOR_00866 UMAG_00561	GO:0044732 mitotic spindle pole body,GO:1990334 Bfa1-Bub2 complex,GO:0005096 GTPase activator activity,GO:0017137 Rab GTPase binding,GO:0006886 intracellular protein transport,GO:0031030 negative regulation of septation initiation signaling,GO:0045737 positive regulation of cyclin-dependent protein serine/threonine kinase activity,GO:0090630 activation of GTPase activity
UBRO_00864	FALSE	UBRO_chr01	orf	mRNA	828871	830389	.	-	.	ID=mRNA_UBRO_00864;Parent=UBRO_00864;Name=UBRO_00864;Note=probable+glycogen+synthase+kinase+3+alpha;pedant_db=p3_i2_t307758_Ust_bromi_v3;	BN887_02678 sr11838 SPSC_02807 UBRO_00864 UHOR_00864 UMAG_00560	GO:0004674 protein serine/threonine kinase activity,GO:0005524 ATP binding,GO:0006468 protein phosphorylation
UBRO_00862	FALSE	UBRO_chr01	orf	mRNA	833387	835840	.	+	.	ID=mRNA_UBRO_00862;Parent=UBRO_00862;Name=UBRO_00862;Note=uncharacterized+protein;pedant_db=p3_i2_t307758_Ust_bromi_v3;	BN887_02700 UBRO_00862 UHOR_00862	GO:0016787 hydrolase activity
UBRO_20210	FALSE	UBRO_chr01	orf	mRNA	846764	848005	.	-	.	ID=mRNA_UBRO_20210;Parent=UBRO_20210;Name=UBRO_20210;Note=uncharacterized+protein;pedant_db=p3_i2_t307758_Ust_bromi_v	UBRO_20342 UBRO_21048 UHOR_10026 UHOR_10032 UHOR_12026 UHOR_13117 UHOR_13979 UHOR_13994 UHOR_14022 UHOR_14049 UHOR_14093 UHOR_14103 UHOR_14152 UHOR_14181 UHOR_14949 UHOR_15002	GO:0005634 nucleus,GO:0003676 nucleic acid binding,GO:0015074 DNA integration

										3;	UHOR_12028 UHOR_12910 UHOR_13005 UHOR_13006 UHOR_14132 UHOR_14739 BN887_02598 UBRO_20153 UBRO_20210 UBRO_20516 UBRO_20889	
UBRO_00859	FALSE	UBRO_chr01	orf	mRNA	850166	852153	.	+	.	ID=mRNA_UBRO_00859;Parent=UBRO_00859;Name=UBRO_00859;Note=related+to+GDP/GTP+exchange+factor+for+Gsp1p/Gsp2p;pedant_db=p3_i2_t307758_Ust_bromi_v3;	BN887_02701 sr11835 SPSC_02805 UBRO_00859 UHOR_00859 UMAG_10463	
UBRO_00858	FALSE	UBRO_chr01	orf	mRNA	856800	857885	.	+	.	ID=mRNA_UBRO_00858;Parent=UBRO_00858;Name=UBRO_00858;Note=probable+glycerol-3-phosphate+dehydrogenase+(NAD);pedant_db=p3_i2_t307758_Ust_bromi_v3;	BN887_02702 sr11834 SPSC_02804 UBRO_00858 UHOR_00858 UMAG_00555	GO:0009331 glycerol-3-phosphate dehydrogenase complex,GO:0004367 glycerol-3-phosphate dehydrogenase [NAD+] activity,GO:0042803 protein homodimerization activity,GO:0051287 NAD binding,GO:0005975 carbohydrate metabolic process,GO:0046168 glycerol-3-phosphate catabolic process,GO:0055114 oxidation-reduction process
UBRO_12050	FALSE	UBRO_chr01	orf	mRNA	858157	859897	.	-	.	ID=mRNA_UBRO_12050;Parent=UBRO_12050;Name=UBRO_12050;Note=uncharacterized+protein;pedant_db=p3_i2_t307758_Ust_bromi_v3;	BN887_02675 sr11833 SPSC_02803 UBRO_12050 UHOR_12050 UMAG_10462	
UBRO_00854	FALSE	UBRO_chr01	orf	mRNA	861298	864351	.	+	.	ID=mRNA_UBRO_00854;Parent=UBRO_00854;Name=UBRO_00854;Note=related+to+GTPase+activating+protein+sec2;pedant_db=p3_i2_t307758_Ust_bromi_v3;	BN887_02703 sr11832 SPSC_02802 UBRO_00854 UHOR_00854 UMAG_00553	
UBRO_00853	FALSE	UBRO_chr01	orf	mRNA	865267	870312	.	-	.	ID=mRNA_UBRO_00853;Parent=UBRO_00853;Name=UBRO_00853;Note=uncharacterized+protein;pedant_db=p3_i2_t307758_Ust_bromi_v3;	BN887_02674 sr11831 SPSC_02801 UBRO_00853 UHOR_00853 UMAG_10461	GO:0005086 ARF guanyl-nucleotide exchange factor activity,GO:0032012 regulation of ARF protein signal transduction
UBRO_00879	FALSE	UBRO_chr01	orf	mRNA	891928	894405	.	-	.	ID=mRNA_UBRO_00879;Parent=UBRO_00879;Name=UBRO_00879;Note=uncharacterized+protein;pedant_db=p3_i2_t307758_Ust_bromi_v3;	BN887_02690 sr11850 SPSC_01832 UBRO_00879 UHOR_00879 UMAG_00572	
UBRO_00880	FALSE	UBRO_chr01	orf	mRNA	894825	895678	.	-	.	ID=mRNA_UBRO_00880;Parent=UBRO_00880;Name=UBRO_00880;Note=uncharacterized+protein;pedant_db=p3_i2_t307758_Ust_bromi_v3;	BN887_02689 sr11851 SPSC_01831 UBRO_00880 UHOR_00880 UMAG_00573	
UBRO_12088	FALSE	UBRO_chr01	orf	mRNA	898327	903384	.	-	.	ID=mRNA_UBRO_12088;Parent=UBRO_12088;Name=UBRO_12088;Note=probable+DNA/RNA+helicase+(DEAD/H+box+family+II);pedant_db=p3_i2_t307758_Ust_bromi_v3;	BN887_02688 sr11852 SPSC_01830 UBRO_12088 UHOR_12088 UMAG_00574	
UBRO_00883	FALSE	UBRO_chr01	orf	mRNA	903800	906433	.	+	.	ID=mRNA_UBRO_00883;Parent=UB	BN887_02693 sr11853 SPSC_01829 UBRO_00883	GO:0031011 Ino80 complex,GO:0042

											RO_00883;Name=UBRO_00883;Note=related+to+IES1+-+Subunit+1+of+the+INO80+chromatin+remodeling+complex;pedant_db=p3_i2_t307758_Ust_bromi_v3;	UHOR_00883 UMAG_00575	766 nucleosome mobilization
UBRO_00884	FALSE	UBRO_chr01	orf	mRNA	906591	907328	.	-	.	ID=mRNA_UBRO_00884;Parent=UBRO_00884;Name=UBRO_00884;Note=related+to+LRP1+-+nuclear+exosome-associated+nucleic+acid+binding+protein;pedant_db=p3_i2_t307758_Ust_bromi_v3;	BN887_02687 sr11854 SPSC_01828 UBRO_00884 UHOR_00884 UMAG_00576	
UBRO_00885	FALSE	UBRO_chr01	orf	mRNA	908242	909732	.	-	.	ID=mRNA_UBRO_00885;Parent=UBRO_00885;Name=UBRO_00885;Note=probable+b+mating+type+locus,+bE1+allele;pedant_db=p3_i2_t307758_Ust_bromi_v3;	BN887_02686 sr11855 SPSC_01827 UBRO_00885 UHOR_00885 UMAG_12052	GO:0005634 nucleus,GO:0003677 DNA binding,GO:0006355 regulation of transcription, DNA-templated
UBRO_00887	FALSE	UBRO_chr01	orf	mRNA	909933	912155	.	+	.	ID=mRNA_UBRO_00887;Parent=UBRO_00887;Name=UBRO_00887;Note=probable+b+mating+type+locus,+bW1+allele;pedant_db=p3_i2_t307758_Ust_bromi_v3;	BN887_02694 sr11856 SPSC_01826 UBRO_00887 UHOR_00887 UMAG_00578	GO:0005634 nucleus,GO:0003677 DNA binding
UBRO_00894	FALSE	UBRO_chr01	orf	mRNA	916072	916884	.	+	.	ID=mRNA_UBRO_00894;Parent=UBRO_00894;Name=UBRO_00894;Note=uncharacterized+protein;pedant_db=p3_i2_t307758_Ust_bromi_v3;	BN887_02695 sr11858 SPSC_01811 UBRO_00894 UHOR_00894 UMAG_10468	GO:0016021 integral component of membrane
UBRO_03911	FALSE	UBRO_chr01	orf	mRNA	928922	929822	.	+	.	ID=mRNA_UBRO_03911;Parent=UBRO_03911;Name=UBRO_03911;Note=related+to+subunit+of+the+Arp2/3+complex;pedant_db=p3_i2_t307758_Ust_bromi_v3;	BN887_03007 sr13589 SPSC_01808 UBRO_03911 UHOR_03911 UMAG_02388	GO:0005826 actomyosin contractile ring,GO:0005885 Arp2/3 protein complex,GO:0030479 actin cortical patch,GO:0031097 medial cortex,GO:0031315 extrinsic component of mitochondrial outer membrane,GO:0043332 mating projection tip,GO:0003729 mRNA binding,GO:0005198 structural molecule activity,GO:0051015 actin filament binding,GO:0000001 mitochondrion inheritance,GO:0000147 actin cortical patch assembly,GO:0034314 Arp2/3 complex-mediated actin nucleation
UBRO_00849	FALSE	UBRO_chr01	orf	mRNA	970417	973560	.	-	.	ID=mRNA_UBRO_00849;Parent=UBRO_00849;Name=UBRO_00849;Note=related+to+UTR1+(associated+with+ferric+reductase+activity);pedant_db=p3_i2_t307758_Ust_bromi_v3;	BN887_02672 sr11828 SPSC_02799 UBRO_00849 UHOR_00849 UMAG_00549	GO:0003951 NAD+ kinase activity,GO:0006741 NADP biosynthetic process,GO:0016310 phosphorylation,GO:0019674 NAD metabolic process
UBRO_00845	FALSE	UBRO_chr01	orf	mRNA	974504	976447	.	+	.	ID=mRNA_UBRO_00845;Parent=UBRO_00845;Name=UBRO_00845;Note=related+to+GDA	BN887_02704 sr11827 SPSC_02798 UBRO_00845 UHOR_00845 UMAG_00548	GO:0016021 integral component of membrane,GO:0016787 hydrolase activity

											1+-+guanosine+diphosphatase;pedant_db=p3_i2_t307758_Ust_bromi_v3;		
UBRO_00844	FALSE	UBRO_chr01	orf	mRNA	976672	977598	.	-	.	ID=mRNA_UBRO_00844;Parent=UBRO_00844;Name=UBRO_00844;Note=probable+PRO3+-+delta+1-pyrroline-5-carboxylate+reductase;pedant_db=p3_i2_t307758_Ust_bromi_v3;	BN887_02671 sr11826 SPSC_02797 UBRO_00844 UHOR_00844 UMAG_00547	GO:0016021 integral component of membrane,GO:0004735 pyrroline-5-carboxylate reductase activity,GO:0055114 oxidation-reduction process,GO:0055129 L-proline biosynthetic process
UBRO_20414	FALSE	UBRO_chr01	orf	mRNA	978276	978556	.	-	.	ID=mRNA_UBRO_20414;Parent=UBRO_20414;Name=UBRO_20414;Note=uncharacterized+protein;pedant_db=p3_i2_t307758_Ust_bromi_v3;		
UBRO_00840	FALSE	UBRO_chr01	orf	mRNA	980743	981309	.	+	.	ID=mRNA_UBRO_00840;Parent=UBRO_00840;Name=UBRO_00840;Note=related+to+MIC17+-+mitochondrial+intermembrane+space+protein,+required+for+normal+oxygen+consumption;pedant_db=p3_i2_t307758_Ust_bromi_v3;	BN887_02705 sr11824 SPSC_02795 UBRO_00840 UHOR_00840 UMAG_15006	
UBRO_00839	FALSE	UBRO_chr01	orf	mRNA	981650	982804	.	-	.	ID=mRNA_UBRO_00839;Parent=UBRO_00839;Name=UBRO_00839;Note=uncharacterized+protein;pedant_db=p3_i2_t307758_Ust_bromi_v3;	BN887_02669 sr11823 SPSC_02794 UBRO_00839 UHOR_00839 UMAG_00545	
UBRO_00832	FALSE	UBRO_chr01	orf	mRNA	986582	990754	.	+	.	ID=mRNA_UBRO_00832;Parent=UBRO_00832;Name=UBRO_00832;Note=uncharacterized+protein;pedant_db=p3_i2_t307758_Ust_bromi_v3;	BN887_02706 sr11822 SPSC_02793 UBRO_00832 UHOR_00832 UMAG_00543	GO:0016740 transferase activity
UBRO_00829	FALSE	UBRO_chr01	orf	mRNA	990960	993182	.	-	.	ID=mRNA_UBRO_00829;Parent=UBRO_00829;Name=UBRO_00829;Note=related+to+HRD1+-+ubiquitin-protein+ligase;pedant_db=p3_i2_t307758_Ust_bromi_v3;	BN887_02668 sr11821 SPSC_02792 UBRO_00829 UHOR_00829 UMAG_00542	GO:0000836 Hrd1p ubiquitin ligase complex,GO:0016021 integral component of membrane,GO:0008270 zinc ion binding,GO:0016874 ligase activity,GO:0061630 ubiquitin protein ligase activity,GO:0016567 protein ubiquitination,GO:0030433 ubiquitin-dependent ERAD pathway
UBRO_12331	FALSE	UBRO_chr01	orf	mRNA	993989	996133	.	+	.	ID=mRNA_UBRO_12331;Parent=UBRO_12331;Name=UBRO_12331;Note=uncharacterized+protein;pedant_db=p3_i2_t307758_Ust_bromi_v3;	BN887_02667 sr11819 SPSC_02791 UBRO_12331 UHOR_12331 UMAG_00540	GO:0016021 integral component of membrane
UBRO_20130	FALSE	UBRO_chr01	orf	mRNA	996554	997219	.	-	.	ID=mRNA_UBRO_20130;Parent=UBRO_20130;Name=UBRO_20130;Note=uncharacterized+protein;pedant_db=p3_i2_t307758_Ust_bromi_v3;	sr11820 UBRO_20130 UHOR_12333 UMAG_11445	
UBRO_03919	FALSE	UBRO_chr01	orf	mRNA	1004037	1005104	.	+	.	ID=mRNA_UBRO_03919;Parent=UBRO_03919;Name=	BN887_03008 sr13592 SPSC_02812 UBRO_03919 UHOR_03919 UMAG_10141	GO:0016021 integral component of membrane

										UBRO_03919;Note=uncharacterized+protein;pedant_db=p3_i2_t307758_Ust_bromi_v3;		
UBRO_03920	FALSE	UBRO_chr01	orf	mRNA	1005603	1006895	.	-	.	ID=mRNA_UBRO_03920;Parent=UBRO_03920;Name=UBRO_03920;Note=uncharacterized+protein;pedant_db=p3_i2_t307758_Ust_bromi_v3;	BN887_02940 sr13593 SPSC_02813 UBRO_03920 UHOR_03920 UMAG_02392	GO:0016021 integral component of membrane
UBRO_03923	FALSE	UBRO_chr01	orf	mRNA	1009367	1010256	.	-	.	ID=mRNA_UBRO_03923;Parent=UBRO_03923;Name=UBRO_03923;Note=probable+TATA-box-binding+factor+TBP;pedant_db=p3_i2_t307758_Ust_bromi_v3;	BN887_02939 sr13595 SPSC_02815 UBRO_03923 UHOR_03923 UMAG_10143	GO:0000120 RNA polymerase I transcription factor complex,GO:0000126 transcription factor TFIIIB complex,GO:0005669 transcription factor TFIID complex,GO:0005672 transcription factor TFIIA complex,GO:0000978 RNA polymerase II proximal promoter sequence-specific DNA binding,GO:0000979 RNA polymerase II core promoter sequence-specific DNA binding,GO:0001006 RNA polymerase III type 3 promoter sequence-specific DNA binding,GO:0001092 TFIIA-class transcription factor complex binding,GO:0001102 RNA polymerase II activating transcription factor binding,GO:0001186 RNA polymerase I transcription regulator recruiting activity,GO:0003682 chromatin binding,GO:0003700 DNA-binding transcription factor activity,GO:0003743 translation initiation factor activity,GO:0008301 DNA binding, bending,GO:0097718 disordered domain specific binding,GO:0001188 RNA polymerase I preinitiation complex assembly,GO:0006355 regulation of transcription, DNA-templated,GO:0006413 translational initiation,GO:0042790 nucleolar large rRNA transcription by RNA polymerase I,GO:0051123 RNA polymerase II preinitiation complex assembly,GO:0070893 transposon integration,GO:0070898 RNA polymerase III preinitiation complex assembly
UBRO_20131	FALSE	UBRO_chr01	orf	mRNA	1011977	1013046	.	-	.	ID=mRNA_UBRO_20131;Parent=UBRO_20131;Name=UBRO_20131;Note=uncharacterized+protein;pedant_db=p3_i2_t307758_Ust_bromi_v	UBRO_14159 UBRO_20131 UBRO_20501 UBRO_20782 UBRO_20801 UBRO_21051 UBRO_21086	

										3;		
UBRO_20133	FALSE	UBRO_chr01	orf	mRNA	1015078	1015476	.	-	.	ID=mRNA_UBRO_20133;Parent=UBRO_20133;Name=UBRO_20133;Note=uncharacterized+protein;pedant_db=p3_i2_t307758_Ust_bromi_v3;	UBRO_20105 UBRO_20133 UBRO_20161 UBRO_20173 UBRO_20204 UBRO_20233 UBRO_20316 UBRO_20371 UBRO_20388 UBRO_20502 UBRO_20524 UBRO_20639 UBRO_20695 UBRO_20696 UBRO_20800 UBRO_20854 UBRO_20869	
UBRO_20415	FALSE	UBRO_chr01	orf	mRNA	1017047	1018881	.	-	.	ID=mRNA_UBRO_20415;Parent=UBRO_20415;Name=UBRO_20415;Note=related+to+ferric+reductase;pedant_db=p3_i2_t307758_Ust_bromi_v3;	BN887_02938 sr13596 SPSC_02816 UBRO_20415 UHOR_03924 UMAG_02395	GO:0016021 integral component of membrane,GO:0016491 oxidoreductase activity
UBRO_20136	TRUE	UBRO_chr01	orf	mRNA	1028727	1029576	.	-	.	ID=mRNA_UBRO_20136;Parent=UBRO_20136;Name=UBRO_20136;Note=uncharacterized+protein;pedant_db=p3_i2_t307758_Ust_bromi_v3;		GO:0016020 membrane
UBRO_00824	FALSE	UBRO_chr01	orf	mRNA	1031777	1037218	.	+	.	ID=mRNA_UBRO_00824;Parent=UBRO_00824;Name=UBRO_00824;Note=related+to+MON2+-+peripheral+membrane+protein+with+a+role+in+endocytosis+and+vacuole+integrity;pedant_db=p3_i2_t307758_Ust_bromi_v3;	BN887_02707 sr11818 SPSC_02790 UBRO_00824 UHOR_00824 UMAG_00539	GO:0015031 protein transport
UBRO_20137	FALSE	UBRO_chr01	orf	mRNA	1042252	1043136	.	+	.	ID=mRNA_UBRO_20137;Parent=UBRO_20137;Name=UBRO_20137;Note=uncharacterized+protein;pedant_db=p3_i2_t307758_Ust_bromi_v3;		
UBRO_20138	FALSE	UBRO_chr01	orf	mRNA	1043324	1043605	.	-	.	ID=mRNA_UBRO_20138;Parent=UBRO_20138;Name=UBRO_20138;Note=uncharacterized+protein;pedant_db=p3_i2_t307758_Ust_bromi_v3;	BN887_02664 sr11814 SPSC_02786 UBRO_20138 UMAG_11441	
UBRO_00820	FALSE	UBRO_chr01	orf	mRNA	1045538	1046368	.	+	.	ID=mRNA_UBRO_00820;Parent=UBRO_00820;Name=UBRO_00820;Note=uncharacterized+protein;pedant_db=p3_i2_t307758_Ust_bromi_v3;	BN887_02708 sr11813 SPSC_02785 UBRO_00820 UHOR_00820 UMAG_00536	GO:0016021 integral component of membrane
UBRO_00818	FALSE	UBRO_chr01	orf	mRNA	1046542	1047231	.	-	.	ID=mRNA_UBRO_00818;Parent=UBRO_00818;Name=UBRO_00818;Note=uncharacterized+protein;pedant_db=p3_i2_t307758_Ust_bromi_v3;	BN887_02663 sr11812 SPSC_02784 UBRO_00818 UHOR_00818	
UBRO_00816	FALSE	UBRO_chr01	orf	mRNA	1048133	1050622	.	+	.	ID=mRNA_UBRO_00816;Parent=UBRO_00816;Name=UBRO_00816;Note=uncharacterized+protein;pedant_db=p3_i2_t307758_Ust_bromi_v3;	BN887_02709 sr11811 SPSC_02783 UBRO_00816 UHOR_00816 UMAG_00535	GO:0005777 peroxisome,GO:0010468 regulation of gene expression
UBRO_00899	FALSE	UBRO_chr01	orf	mRNA	1066441	1068378	.	+	.	ID=mRNA_UBRO_00899;Parent=UBRO_00899;Name=UBRO_00899;Note=uncharacterized+protein;pedant_db=p3_i2_t307758_Ust_bromi_v3;	BN887_02684 sr11859 SPSC_01812 UBRO_00899 UHOR_00899 UMAG_00581	GO:0005886 plasma membrane,GO:0016021 integral component of membrane,GO:0032153 cell division site,GO:0035838 growing cell

												tip,GO:0007127 meiosis I
UBRO_03908	FALSE	UBRO_chr01	orf	mRNA	1082103	1085245	.	+	.	ID=mRNA_UBRO_03908;Parent=UBRO_03908;Name=UBRO_03908;Note=related+to+oligopeptide+transporter;pedant_db=p3_i2_t307758_Ust_bromi_v3;	BN887_02943 BN887_04986 sr13585 sr15234 sr16251 SPSC_00222 SPSC_01072 SPSC_00881 SPSC_01798 UBRO_03908 UBRO_06799 UBRO_07979 UHOR_03908 UHOR_06799 UHOR_07979 UMAG_02387 UMAG_04347 UMAG_10896 BN887_03178	
UBRO_03903	FALSE	UBRO_chr01	orf	mRNA	1090621	1091934	.	+	.	ID=mRNA_UBRO_03903;Parent=UBRO_03903;Name=UBRO_03903;Note=probable+pantoate--beta-alanine+ligase;pedant_db=p3_i2_t307758_Ust_bromi_v3;	BN887_02945 sr13581 SPSC_01803 UBRO_03903 UHOR_03903 UMAG_10139	
UBRO_03902	FALSE	UBRO_chr01	orf	mRNA	1092265	1092963	.	+	.	ID=mRNA_UBRO_03902;Parent=UBRO_03902;Name=UBRO_03902;Note=probable+a1-mating+type+protein+Rba1;pedant_db=p3_i2_t307758_Ust_bromi_v3;	BN887_02946 sr13580 UBRO_03902 UHOR_03902 UMAG_02384	GO:0016021 integral component of membrane
UBRO_03865	FALSE	UBRO_chr01	orf	mRNA	1107091	1110600	.	+	.	ID=mRNA_UBRO_03865;Parent=UBRO_03865;Name=UBRO_03865;Note=related+to+vacuolar+protein-sorting+protein+VPS35;pedant_db=p3_i2_t307758_Ust_bromi_v3;	BN887_05395 sr13574 SPSC_01766 UBRO_03865 UHOR_03865 UMAG_10136	GO:0005770 late endosome,GO:0005829 cytosol,GO:0030906 retromer, cargo-selective complex,GO:0008565 protein transporter activity,GO:0006886 intracellular protein transport,GO:0042147 retrograde transport, endosome to Golgi
UBRO_03861	FALSE	UBRO_chr01	orf	mRNA	1110999	1114061	.	-	.	ID=mRNA_UBRO_03861;Parent=UBRO_03861;Name=UBRO_03861;Note=related+to+MCM10+-+essential+chromatin-associated+protein+involved+in+the+initiation+of+DNA+replication;pedant_db=p3_i2_t307758_Ust_bromi_v3;	BN887_05417 sr13573 SPSC_01767 UBRO_03861 UHOR_03861 UMAG_10135	GO:0005634 nucleus,GO:0003690 double-stranded DNA binding,GO:0003697 single-stranded DNA binding,GO:0006270 DNA replication initiation
UBRO_20143	FALSE	UBRO_chr01	orf	mRNA	1116554	1119109	.	-	.	ID=mRNA_UBRO_20143;Parent=UBRO_20143;Name=UBRO_20143;Note=uncharacterized+protein;pedant_db=p3_i2_t307758_Ust_bromi_v3;	BN887_02600 BN887_02713 UHOR_00833 UHOR_12077 UHOR_14059 UHOR_01674 UHOR_13996 UHOR_04106 UHOR_06224 UHOR_10015 UHOR_10031 UHOR_12673 UHOR_13044 UHOR_13272 UHOR_13991 UHOR_14014 UHOR_14086 UHOR_14161 UHOR_14170 UHOR_14669 UHOR_04108 UHOR_15109 UHOR_10014 UHOR_12378 UHOR_13752 UHOR_14060 UHOR_14564 UHOR_15610 UHOR_16664 UHOR_10028 UHOR_13992 UHOR_12602 UHOR_16322 UHOR_13400 UHOR_14013 UHOR_15903 UHOR_14895 UHOR_16372 SPSC_04529 UBRO_20328 UBRO_12371 UBRO_20143 UBRO_20214 UMAG_02565	
UBRO_03832	FALSE	UBRO_chr01	orf	mRNA	1119818	1122811	.	+	.	ID=mRNA_UBRO_03832;Parent=UBRO_03832;Name=UBRO_03832;Note=related+to+translation+initiation+factor+IF-2,+mitochondrial;pedant_db=p3_i2_t307758_Ust_bromi_v3;	BN887_05007 sr13548 SPSC_01791 UBRO_03832 UHOR_03832 UMAG_02344	GO:0005739 mitochondrion,GO:0003743 translation initiation factor activity,GO:0003924 GTPase activity,GO:0005525 GTP binding,GO:0070124 mitochondrial translational initiation
UBRO_20146	FALSE	UBRO_chr01	orf	mRNA	1214859	1216285	.	+	.	ID=mRNA_UBRO_20146;Parent=UBRO_20146;Name=UBRO_20146;Not	UBRO_20146 UMAG_10485	GO:0003676 nucleic acid binding,GO:0008270 zinc ion binding

										e=uncharacter-ized+protein;ped-ant_db=p3_i2_t307758_Ust_bromi_v3;		
UBRO_20153	FALSE	UBRO_chr01	orf	mRNA	1273054	1275578	.	-	.	ID=mRNA_UBRO_20153;Parent=UBRO_20153;Name=UBRO_20153;Note=related+to+Gag-pol+polyprotein;pedant_db=p3_i2_t307758_Ust_bromi_v3;	UBRO_20342 UBRO_21048 UHOR_10026 UHOR_10032 UHOR_12026 UHOR_13117 UHOR_13979 UHOR_13994 UHOR_14022 UHOR_14049 UHOR_14093 UHOR_14103 UHOR_14152 UHOR_14181 UHOR_14949 UHOR_15002 UHOR_12028 UHOR_12910 UHOR_13005 UHOR_13006 UHOR_14132 UHOR_14739 BN887_02598 UBRO_20153 UBRO_20210 UBRO_20516 UBRO_20889	GO:0003676 nuc-leic acid binding,GO:0015074 DNA integration
UBRO_15112	FALSE	UBRO_chr01	orf	mRNA	1311016	1314363	.	+	.	ID=mRNA_UBRO_15112;Parent=UBRO_15112;Name=UBRO_15112;Note=uncharacterized+protein;pedant_db=p3_i2_t307758_Ust_bromi_v3;	BN887_03270 sr13507 SPSC_01723 UBRO_15112 UHOR_15112 UMAG_02311	GO:0046872 metal ion binding
UBRO_20156	FALSE	UBRO_chr01	orf	mRNA	1343559	1344458	.	+	.	ID=mRNA_UBRO_20156;Parent=UBRO_20156;Name=UBRO_20156;Note=uncharacter-ized+protein;ped-ant_db=p3_i2_t307758_Ust_bromi_v3;		GO:0005488 bind-ing,GO:0008152 metabolic process
UBRO_20157	FALSE	UBRO_chr01	orf	mRNA	1350600	1351609	.	+	.	ID=mRNA_UBRO_20157;Parent=UBRO_20157;Name=UBRO_20157;Note=uncharacter-ized+protein;ped-ant_db=p3_i2_t307758_Ust_bromi_v3;	UBRO_20157 UBRO_20217 UBRO_20242 UBRO_20277 UBRO_20314 UBRO_20389 UBRO_20449 UBRO_20455 UBRO_20458 UBRO_20482 UBRO_20504 UBRO_20528 UBRO_20534 UBRO_20548 UBRO_20589 UBRO_20670 UBRO_20671 UBRO_20690 UBRO_20790 UBRO_20848 UBRO_20874 UBRO_20859 SPSC_04004 UMAG_02747	
UBRO_21038	*	UBRO_chr01	orf	mRNA	1399654	1401071	.	+	.	ID=mRNA_UBRO_21038;Parent=UBRO_21038;Name=UBRO_21038;Note=uncharacter-ized+protein;ped-ant_db=p3_i2_t307758_Ust_bromi_v3;	UBRO_20340 UBRO_20995 UHOR_01754 UHOR_02803 UHOR_06991 UHOR_14945 UHOR_15241 UHOR_13171 UBRO_21038	GO:0003676 nuc-leic acid binding,GO:0008270 zinc ion binding
UBRO_20160	FALSE	UBRO_chr01	orf	mRNA	1401312	1402496	.	+	.	ID=mRNA_UBRO_20160;Parent=UBRO_20160;Name=UBRO_20160;Note=uncharacter-ized+protein;ped-ant_db=p3_i2_t307758_Ust_bromi_v3;	UBRO_20160 UHOR_07815	GO:0000943 retro-transposon nucleo-capsid
UBRO_21039	*	UBRO_chr01	orf	mRNA	1403257	1403649	.	+	.	ID=mRNA_UBRO_21039;Parent=UBRO_21039;Name=UBRO_21039;Note=uncharacter-ized+protein;ped-ant_db=p3_i2_t307758_Ust_bromi_v3;		
UBRO_20444	FALSE	UBRO_chr02	orf	mRNA	66845	67288	.	-	.	ID=mRNA_UBRO_20444;Parent=UBRO_20444;Name=UBRO_20444;Note=uncharacter-ized+protein;ped-ant_db=p3_i2_t307758_Ust_bromi_v3;	UBRO_20444 UBRO_20498	GO:0003677 DNA binding,GO:0006313 transposition, DNA-mediated,GO:0015074 DNA integra-tion
UBRO_20242	FALSE	UBRO_chr02	orf	mRNA	308977	309986	.	-	.	ID=mRNA_UBRO_20242;Parent=UBRO_20242;Name=UBRO_20242;Note=uncharacter-ized+protein;ped-ant_db=p3_i2_t307758_Ust_bromi_v3;	UBRO_20157 UBRO_20217 UBRO_20242 UBRO_20277 UBRO_20314 UBRO_20389 UBRO_20449 UBRO_20455 UBRO_20458 UBRO_20482 UBRO_20504 UBRO_20528 UBRO_20534 UBRO_20548 UBRO_20589 UBRO_20670 UBRO_20671 UBRO_20690 UBRO_20790 UBRO_20848 UBRO_20874 UBRO_20859 SPSC_04004 UMAG_02747	

UBRO_20244	FALSE	UBRO_chr02	orf	mRNA	496373	496963	.	+	.	ID=mRNA_UBRO_20244;Parent=UBRO_20244;Name=UBRO_20244;Note=uncharacterized+protein;pedant_db=p3_i2_t307758_Ust_bromi_v3;		GO:0016021 integral component of membrane,GO:0003676 nucleic acid binding,GO:0015074 DNA integration
UBRO_20450	FALSE	UBRO_chr02	orf	mRNA	506979	507443	.	-	.	ID=mRNA_UBRO_20450;Parent=UBRO_20450;Name=UBRO_20450;Note=uncharacterized+protein;pedant_db=p3_i2_t307758_Ust_bromi_v3;	UBRO_20450 UHOR_03156	GO:0003676 nucleic acid binding,GO:0008270 zinc ion binding
UBRO_20453	FALSE	UBRO_chr02	orf	mRNA	520928	521509	.	-	.	ID=mRNA_UBRO_20453;Parent=UBRO_20453;Name=UBRO_20453;Note=uncharacterized+protein;pedant_db=p3_i2_t307758_Ust_bromi_v3;		
UBRO_20454	FALSE	UBRO_chr02	orf	mRNA	712080	712895	.	-	.	ID=mRNA_UBRO_20454;Parent=UBRO_20454;Name=UBRO_20454;Note=uncharacterized+protein;pedant_db=p3_i2_t307758_Ust_bromi_v3;	UBRO_21062 UBRO_20218 UBRO_20278 UBRO_20483 UBRO_20529 UBRO_20533 UBRO_20546 UBRO_20590 UBRO_20873 UBRO_20998 UBRO_21009 UBRO_21033 UBRO_21041 UBRO_21053 UBRO_21054 UBRO_21069 UBRO_21084 UBRO_20454 UBRO_20861 UBRO_21034 UBRO_21076 UBRO_20691 UBRO_20887 UBRO_21085 sr16557 UMAG_02745 SPSC_01947 UHOR_03466	
UBRO_21041	*	UBRO_chr02	orf	mRNA	828635	829894	.	-	.	ID=mRNA_UBRO_21041;Parent=UBRO_21041;Name=UBRO_21041;Note=uncharacterized+protein;pedant_db=p3_i2_t307758_Ust_bromi_v3;	UBRO_21062 UBRO_20218 UBRO_20278 UBRO_20483 UBRO_20529 UBRO_20533 UBRO_20546 UBRO_20590 UBRO_20873 UBRO_20998 UBRO_21009 UBRO_21033 UBRO_21041 UBRO_21053 UBRO_21054 UBRO_21069 UBRO_21084 UBRO_20454 UBRO_20861 UBRO_21034 UBRO_21076 UBRO_20691 UBRO_20887 UBRO_21085 sr16557 UMAG_02745 SPSC_01947 UHOR_03466	
UBRO_20465	FALSE	UBRO_chr02	orf	mRNA	963745	964965	.	+	.	ID=mRNA_UBRO_20465;Parent=UBRO_20465;Name=UBRO_20465;Note=uncharacterized+protein;pedant_db=p3_i2_t307758_Ust_bromi_v3;	sr07366 sr11325 sr15209 SPSC_01813 SPSC_04725 UBRO_20361 UBRO_20409 UBRO_20420 UBRO_20465 UBRO_20481 UBRO_20591 UBRO_20814 UBRO_20827 UBRO_20916 UBRO_20413 UBRO_20416 UBRO_20499 UBRO_20568 UBRO_20763 UBRO_20793 UBRO_20994 UBRO_21002	GO:0003677 DNA binding
UBRO_20371	FALSE	UBRO_chr02	orf	mRNA	1073359	1073754	.	-	.	ID=mRNA_UBRO_20371;Parent=UBRO_20371;Name=UBRO_20371;Note=uncharacterized+protein;pedant_db=p3_i2_t307758_Ust_bromi_v3;	UBRO_20105 UBRO_20133 UBRO_20161 UBRO_20173 UBRO_20204 UBRO_20233 UBRO_20316 UBRO_20371 UBRO_20388 UBRO_20502 UBRO_20524 UBRO_20639 UBRO_20695 UBRO_20696 UBRO_20800 UBRO_20854 UBRO_20869	
UBRO_21042	*	UBRO_chr02	orf	mRNA	1101208	1101870	.	-	.	ID=mRNA_UBRO_21042;Parent=UBRO_21042;Name=UBRO_21042;Note=uncharacterized+protein;pedant_db=p3_i2_t307758_Ust_bromi_v3;	UBRO_21042 UHOR_12938	
UBRO_21043	*	UBRO_chr02	orf	mRNA	1102380	1103294	.	-	.	ID=mRNA_UBRO_21043;Parent=UBRO_21043;Name=UBRO_21043;Note=related+to+retrotransposon+protein;pedant_db=p3_i2_t307758_Ust_bromi_v3;		GO:0000943 retrotransposon nucleocapsid,GO:0003676 nucleic acid binding,GO:0015074 DNA integration
UBRO_20471	FALSE	UBRO_chr02	orf	mRNA	1213273	1213761	.	-	.	ID=mRNA_UBRO_20471;Parent=UBRO_20471;Name=UBRO_20471;Not		

										e=uncharacter-ized+protein;ped-ant_db=p3_i2_t307758_Ust_bromi_v3;		
UBRO_20472	FALSE	UBRO_chr02	orf	mRNA	1227023	1228661	.	+	.	ID=mRNA_UBRO_20472;Parent=UBRO_20472;Name=UBRO_20472;Note=uncharacter-ized+protein;ped-ant_db=p3_i2_t307758_Ust_bromi_v3;	SPSC_02149 SPSC_06524 UBRO_06511 UBRO_20174 UBRO_20469 UBRO_20472 UBRO_20630 UBRO_20759 UBRO_20057 UBRO_20400 UBRO_20401 BN887_03037 sr15411 SPSC_05615 UHOR_06511 UMAG_04525	
UBRO_20473	FALSE	UBRO_chr02	orf	mRNA	1248479	1249927	.	+	.	ID=mRNA_UBRO_20473;Parent=UBRO_20473;Name=UBRO_20473;Note=uncharacter-ized+protein;ped-ant_db=p3_i2_t307758_Ust_bromi_v3;	UBRO_20402 UBRO_20555 UBRO_20435 UBRO_20473 UBRO_20476 UBRO_20544 UBRO_20606 UBRO_20846 UBRO_21007 UBRO_20772 UHOR_14039 UHOR_14142 UHOR_14176 SPSC_01964	
UBRO_20476	FALSE	UBRO_chr02	orf	mRNA	1376860	1378374	.	-	.	ID=mRNA_UBRO_20476;Parent=UBRO_20476;Name=UBRO_20476;Note=uncharacter-ized+protein;ped-ant_db=p3_i2_t307758_Ust_bromi_v3;	UBRO_20402 UBRO_20555 UBRO_20435 UBRO_20473 UBRO_20476 UBRO_20544 UBRO_20606 UBRO_20846 UBRO_21007 UBRO_20772 UHOR_14039 UHOR_14142 UHOR_14176 SPSC_01964	
UBRO_21048	*	UBRO_chr02	orf	mRNA	1388292	1389989	.	-	.	ID=mRNA_UBRO_21048;Parent=UBRO_21048;Name=UBRO_21048;Note=related+to+retrotransposon+nucleo-capsid+protein;pedant_db=p3_i2_t307758_Ust_bromi_v3;	UBRO_20342 UBRO_21048 UHOR_10026 UHOR_10032 UHOR_12026 UHOR_13117 UHOR_13979 UHOR_13994 UHOR_14022 UHOR_14049 UHOR_14093 UHOR_14103 UHOR_14152 UHOR_14181 UHOR_14949 UHOR_15002 UHOR_12028 UHOR_12910 UHOR_13005 UHOR_13006 UHOR_14132 UHOR_14739 BN887_02598 UBRO_20153 UBRO_20210 UBRO_20516 UBRO_20889	
UBRO_21049	*	UBRO_chr02	orf	mRNA	1390262	1391428	.	-	.	ID=mRNA_UBRO_21049;Parent=UBRO_21049;Name=UBRO_21049;Note=uncharacter-ized+protein;ped-ant_db=p3_i2_t307758_Ust_bromi_v3;	UBRO_21049 UHOR_14179	GO:0003676 nucleic acid binding,GO:0008270 zinc ion binding
UBRO_20479	FALSE	UBRO_chr02	orf	mRNA	1500822	1501909	.	+	.	ID=mRNA_UBRO_20479;Parent=UBRO_20479;Name=UBRO_20479;Note=uncharacter-ized+protein;ped-ant_db=p3_i2_t307758_Ust_bromi_v3;		GO:0016021 integral component of membrane
UBRO_20481	FALSE	UBRO_chr02	orf	mRNA	1524795	1526405	.	+	.	ID=mRNA_UBRO_20481;Parent=UBRO_20481;Name=UBRO_20481;Note=uncharacter-ized+protein;ped-ant_db=p3_i2_t307758_Ust_bromi_v3;	sr07366 sr11325 sr15209 SPSC_01813 SPSC_04725 UBRO_20361 UBRO_20409 UBRO_20420 UBRO_20465 UBRO_20481 UBRO_20591 UBRO_20814 UBRO_20827 UBRO_20916 UBRO_20413 UBRO_20416 UBRO_20499 UBRO_20568 UBRO_20763 UBRO_20793 UBRO_20994 UBRO_21002	GO:0003677 DNA binding
UBRO_21052	*	UBRO_chr02	orf	mRNA	1957162	1957791	.	+	.	ID=mRNA_UBRO_21052;Parent=UBRO_21052;Name=UBRO_21052;Note=uncharacter-ized+protein;ped-ant_db=p3_i2_t307758_Ust_bromi_v3;	UBRO_04256 UBRO_20275 UBRO_20382 UBRO_20537 UBRO_20714 UBRO_20865 UBRO_20722 UBRO_20724 UBRO_20768 UBRO_20796 UBRO_20837 UBRO_21052 UBRO_20792 UBRO_20212 UBRO_20495 UHOR_04256	GO:0003677 DNA binding,GO:0006313 transposition, DNA-mediated,GO:0015074 DNA integration
UBRO_20499	FALSE	UBRO_chr03	orf	mRNA	14723	16096	.	+	.	ID=mRNA_UBRO_20499;Parent=UBRO_20499;Name=UBRO_20499;Note=uncharacter-ized+protein;ped-ant_db=p3_i2_t307758_Ust_bromi_v3;	sr07366 sr11325 sr15209 SPSC_01813 SPSC_04725 UBRO_20361 UBRO_20409 UBRO_20420 UBRO_20465 UBRO_20481 UBRO_20591 UBRO_20814 UBRO_20827 UBRO_20916 UBRO_20413 UBRO_20416 UBRO_20499 UBRO_20568 UBRO_20763 UBRO_20793 UBRO_20994 UBRO_21002	GO:0003677 DNA binding
UBRO_	FALSE	UBRO_chr03	orf	mRNA	46175	47233	.	-	.	ID=mRNA_UBRO_	UBRO_20105 UBRO_20133	

20502										20502;Parent=UBRO_20502;Name=UBRO_20502;Note=uncharacterized+protein;pedant_db=p3_i2_t307758_Ust_bromi_v3;	UBRO_20161 UBRO_20173 UBRO_20204 UBRO_20233 UBRO_20316 UBRO_20371 UBRO_20388 UBRO_20502 UBRO_20524 UBRO_20639 UBRO_20695 UBRO_20696 UBRO_20800 UBRO_20854 UBRO_20869	
UBRO_20248	FALSE	UBRO_chr03	orf	mRNA	77772	78497	.	+	.	ID=mRNA_UBRO_20248;Parent=UBRO_20248;Name=UBRO_20248;Note=related+to+GYP1+-+GTPase+activating+protein;pedant_db=p3_i2_t307758_Ust_bromi_v3;	UBRO_20248 UHOR_15967	GO:0016491 oxidoreductase activity,GO:0055114 oxidation-reduction process
UBRO_21055	*	UBRO_chr03	orf	mRNA	476808	477551	.	-	.	ID=mRNA_UBRO_21055;Parent=UBRO_21055;Name=UBRO_21055;Note=uncharacterized+protein;pedant_db=p3_i2_t307758_Ust_bromi_v3;		GO:0003677 DNA binding
UBRO_21056	*	UBRO_chr03	orf	mRNA	479182	479889	.	-	.	ID=mRNA_UBRO_21056;Parent=UBRO_21056;Name=UBRO_21056;Note=uncharacterized+protein;pedant_db=p3_i2_t307758_Ust_bromi_v3;		
UBRO_20515	FALSE	UBRO_chr03	orf	mRNA	553307	554303	.	+	.	ID=mRNA_UBRO_20515;Parent=UBRO_20515;Name=UBRO_20515;Note=uncharacterized+protein;pedant_db=p3_i2_t307758_Ust_bromi_v3;		
UBRO_20516	FALSE	UBRO_chr03	orf	mRNA	554926	556098	.	-	.	ID=mRNA_UBRO_20516;Parent=UBRO_20516;Name=UBRO_20516;Note=related+to+Gag-pol+polyprotein;pedant_db=p3_i2_t307758_Ust_bromi_v3;	UBRO_20342 UBRO_21048 UHOR_10026 UHOR_10032 UHOR_12026 UHOR_13117 UHOR_13979 UHOR_13994 UHOR_14022 UHOR_14049 UHOR_14093 UHOR_14103 UHOR_14152 UHOR_14181 UHOR_14949 UHOR_15002 UHOR_12028 UHOR_12910 UHOR_13005 UHOR_13006 UHOR_14132 UHOR_14739 BN887_02598 UBRO_20153 UBRO_20210 UBRO_20516 UBRO_20889	GO:0005634 nucleus,GO:0003676 nucleic acid binding,GO:0015074 DNA integration
UBRO_20524	FALSE	UBRO_chr03	orf	mRNA	739609	740649	.	-	.	ID=mRNA_UBRO_20524;Parent=UBRO_20524;Name=UBRO_20524;Note=uncharacterized+protein;pedant_db=p3_i2_t307758_Ust_bromi_v3;	UBRO_20105 UBRO_20133 UBRO_20161 UBRO_20173 UBRO_20204 UBRO_20233 UBRO_20316 UBRO_20371 UBRO_20388 UBRO_20502 UBRO_20524 UBRO_20639 UBRO_20695 UBRO_20696 UBRO_20800 UBRO_20854 UBRO_20869	
UBRO_20525	FALSE	UBRO_chr03	orf	mRNA	806001	806600	.	+	.	ID=mRNA_UBRO_20525;Parent=UBRO_20525;Name=UBRO_20525;Note=uncharacterized+protein;pedant_db=p3_i2_t307758_Ust_bromi_v3;		
UBRO_20527	FALSE	UBRO_chr03	orf	mRNA	923859	925121	.	+	.	ID=mRNA_UBRO_20527;Parent=UBRO_20527;Name=UBRO_20527;Note=uncharacterized+protein;pedant_db=p3_i2_t307758_Ust_bromi_v3;	UBRO_20403 UBRO_20494 UBRO_20581 UBRO_20600 UBRO_20693 UBRO_20773 UBRO_20905 UBRO_21046 UBRO_21083 UBRO_20434 UBRO_20451 UBRO_20527 UBRO_20538 UBRO_20707 UBRO_20586 UBRO_20665 UBRO_20701 UHOR_14038 UHOR_14159 UHOR_14178 SPSC_01963 UHOR_14003 UBRO_20842	GO:0016021 integral component of membrane,GO:0003677 DNA binding
UBRO_20361	FALSE	UBRO_chr03	orf	mRNA	1101535	1102350	.	+	.	ID=mRNA_UBRO_20361;Parent=UBRO_20361;Name=UBRO_20361;Note=uncharacterized+protein;pedant_db=p3_i2_t307758_Ust_bromi_v	sr07366 sr11325 sr15209 SPSC_01813 SPSC_04725 UBRO_20361 UBRO_20409 UBRO_20420 UBRO_20465 UBRO_20481 UBRO_20591 UBRO_20814 UBRO_20827 UBRO_20916 UBRO_20413 UBRO_20416 UBRO_20499	GO:0003677 DNA binding

										3;	UBRO_20568 UBRO_20763 UBRO_20793 UBRO_20994 UBRO_21002	
UBRO_20528	FALSE	UBRO_chr03	orf	mRNA	1103560	1104896	.	+	.	ID=mRNA_UBRO_20528;Parent=UBRO_20528;Name=UBRO_20528;Note=uncharacterized+protein;pedant_db=p3_i2_t307758_Ust_bromi_v3;	UBRO_20157 UBRO_20217 UBRO_20242 UBRO_20277 UBRO_20314 UBRO_20389 UBRO_20449 UBRO_20455 UBRO_20458 UBRO_20482 UBRO_20504 UBRO_20528 UBRO_20534 UBRO_20548 UBRO_20589 UBRO_20670 UBRO_20671 UBRO_20690 UBRO_20790 UBRO_20848 UBRO_20874 UBRO_20859 SPSC_04004 UMAG_02747	
UBRO_20533	FALSE	UBRO_chr03	orf	mRNA	1180215	1181369	.	-	.	ID=mRNA_UBRO_20533;Parent=UBRO_20533;Name=UBRO_20533;Note=uncharacterized+protein;pedant_db=p3_i2_t307758_Ust_bromi_v3;	UBRO_21062 UBRO_20218 UBRO_20278 UBRO_20483 UBRO_20529 UBRO_20533 UBRO_20546 UBRO_20590 UBRO_20873 UBRO_20998 UBRO_21009 UBRO_21033 UBRO_21041 UBRO_21053 UBRO_21054 UBRO_21069 UBRO_21084 UBRO_20454 UBRO_20861 UBRO_21034 UBRO_21076 UBRO_20691 UBRO_20887 UBRO_21085 sr16557 UMAG_02745 SPSC_01947 UHOR_03466	
UBRO_20537	FALSE	UBRO_chr03	orf	mRNA	1198178	1199245	.	-	.	ID=mRNA_UBRO_20537;Parent=UBRO_20537;Name=UBRO_20537;Note=uncharacterized+protein;pedant_db=p3_i2_t307758_Ust_bromi_v3;	UBRO_04256 UBRO_20275 UBRO_20382 UBRO_20537 UBRO_20714 UBRO_20865 UBRO_20722 UBRO_20724 UBRO_20768 UBRO_20796 UBRO_20837 UBRO_21052 UBRO_20792 UBRO_20212 UBRO_20495 UHOR_04256	GO:0003677 DNA binding,GO:0006313 transposition, DNA-mediated,GO:0015074 DNA integration
UBRO_20547	FALSE	UBRO_chr03	orf	mRNA	1438217	1438654	.	+	.	ID=mRNA_UBRO_20547;Parent=UBRO_20547;Name=UBRO_20547;Note=uncharacterized+protein;pedant_db=p3_i2_t307758_Ust_bromi_v3;	UBRO_20052 UBRO_20333 UBRO_20547 UBRO_20746	
UBRO_20553	TRUE	UBRO_chr03	orf	mRNA	1485475	1485981	.	-	.	ID=mRNA_UBRO_20553;Parent=UBRO_20553;Name=UBRO_20553;Note=uncharacterized+protein;pedant_db=p3_i2_t307758_Ust_bromi_v3;	BN887_05068 sr10318 SPSC_03544 UBRO_20553 UMAG_01241	GO:0005488 binding,GO:0006886 intracellular protein transport
UBRO_20567	FALSE	UBRO_chr04	orf	mRNA	144908	145419	.	-	.	ID=mRNA_UBRO_20567;Parent=UBRO_20567;Name=UBRO_20567;Note=uncharacterized+protein;pedant_db=p3_i2_t307758_Ust_bromi_v3;		GO:0005634 nucleus,GO:0005829 cytosol,GO:0003714 transcription corepressor activity,GO:0070370 cellular heat acclimation,GO:1903507 negative regulation of nucleic acid-templated transcription
UBRO_20572	FALSE	UBRO_chr04	orf	mRNA	338925	341589	.	-	.	ID=mRNA_UBRO_20572;Parent=UBRO_20572;Name=UBRO_20572;Note=related+to+retrotransposon+protein;pedant_db=p3_i2_t307758_Ust_bromi_v3;	BN887_02599 UBRO_20572 BN887_06274 UHOR_13182 UMAG_12288 UBRO_20518 UHOR_08447	GO:0000943 retrotransposon nucleocapsid,GO:0003676 nucleic acid binding,GO:0015074 DNA integration
UBRO_20573	FALSE	UBRO_chr04	orf	mRNA	437715	440294	.	+	.	ID=mRNA_UBRO_20573;Parent=UBRO_20573;Name=UBRO_20573;Note=uncharacterized+protein;pedant_db=p3_i2_t307758_Ust_bromi_v3;	SPSC_01802 SPSC_02044 SPSC_03529 UBRO_02119 UBRO_04813 UBRO_20573 UBRO_20574 UBRO_20867 UBRO_20967 UMAG_11874 UMAG_01443 UMAG_03635 UMAG_04689 UMAG_04693 UMAG_04887 UMAG_05066 UMAG_05621 UMAG_06351 UMAG_06356 UMAG_06479 UMAG_06505 UMAG_10981 UMAG_11979 UMAG_11109 UMAG_05436 UMAG_06514 UMAG_10169 BN887_04509 sr14681 UHOR_13031 UHOR_02119 UHOR_04813	
UBRO_20329	FALSE	UBRO_chr04	orf	mRNA	448532	449554	.	-	.	ID=mRNA_UBRO_20329;Parent=UBRO_20329;Name=UBRO_20329;Not		GO:0000943 retrotransposon nucleocapsid,GO:0003676 nucleic acid bind-

										e=uncharacter-ized+protein;ped-ant_db=p3_i2_t307758_Ust_bromi_v3;		ing,GO:0015074 DNA integration
UBRO_21062	*	UBRO_chr04	orf	mRNA	765814	766518	.	-	.	ID=mRNA_UBRO_21062;Parent=UBRO_21062;Name=UBRO_21062;Note=uncharacter-ized+protein;ped-ant_db=p3_i2_t307758_Ust_bromi_v3;	UBRO_21062 UBRO_20218 UBRO_20278 UBRO_20483 UBRO_20529 UBRO_20533 UBRO_20546 UBRO_20590 UBRO_20873 UBRO_20998 UBRO_21009 UBRO_21033 UBRO_21041 UBRO_21053 UBRO_21054 UBRO_21069 UBRO_21084 UBRO_20454 UBRO_20861 UBRO_21034 UBRO_21076 UBRO_20691 UBRO_20887 UBRO_21085 sr16557 UMAG_02745 SPSC_01947 UHOR_03466	
UBRO_20586	FALSE	UBRO_chr04	orf	mRNA	1100096	1101281	.	-	.	ID=mRNA_UBRO_20586;Parent=UBRO_20586;Name=UBRO_20586;Note=uncharacter-ized+protein;ped-ant_db=p3_i2_t307758_Ust_bromi_v3;	UBRO_20403 UBRO_20494 UBRO_20581 UBRO_20600 UBRO_20693 UBRO_20773 UBRO_20905 UBRO_21046 UBRO_21083 UBRO_20434 UBRO_20451 UBRO_20527 UBRO_20538 UBRO_20707 UBRO_20586 UBRO_20665 UBRO_20701 UHOR_14038 UHOR_14159 UHOR_14178 SPSC_01963 UHOR_14003 UBRO_20842	GO:0016021 integ-ral component of membrane,GO:0003677 DNA binding
UBRO_20587	FALSE	UBRO_chr04	orf	mRNA	1102143	1102604	.	-	.	ID=mRNA_UBRO_20587;Parent=UBRO_20587;Name=UBRO_20587;Note=uncharacter-ized+protein;ped-ant_db=p3_i2_t307758_Ust_bromi_v3;	UBRO_20452 UBRO_20539 UBRO_20580 UBRO_20587 UBRO_20610 UBRO_20999	
UBRO_20591	FALSE	UBRO_chr04	orf	mRNA	1150159	1151457	.	-	.	ID=mRNA_UBRO_20591;Parent=UBRO_20591;Name=UBRO_20591;Note=uncharacter-ized+protein;ped-ant_db=p3_i2_t307758_Ust_bromi_v3;	sr07366 sr11325 sr15209 SPSC_01813 SPSC_04725 UBRO_20361 UBRO_20409 UBRO_20420 UBRO_20465 UBRO_20481 UBRO_20591 UBRO_20814 UBRO_20827 UBRO_20916 UBRO_20413 UBRO_20416 UBRO_20499 UBRO_20568 UBRO_20763 UBRO_20793 UBRO_20994 UBRO_21002	GO:0003677 DNA binding
UBRO_20279	FALSE	UBRO_chr04	orf	mRNA	1206899	1211104	.	+	.	ID=mRNA_UBRO_20279;Parent=UBRO_20279;Name=UBRO_20279;Note=uncharacter-ized+protein;ped-ant_db=p3_i2_t307758_Ust_bromi_v3;	SPSC_00206 SPSC_01500 SPSC_01215 SPSC_05764 UBRO_20081 UBRO_20349 UBRO_20089 UBRO_20219 UBRO_20355 UBRO_20594 UBRO_20727 UBRO_20164 UBRO_20203 UBRO_20637 UBRO_20669 UBRO_20815 UBRO_20220 UBRO_20284 UBRO_20335 UBRO_20728 UBRO_20754 UBRO_20968 UBRO_20279 UBRO_20307 UBRO_20844 UBRO_20280 UBRO_20360 UBRO_20596 UBRO_20964 UBRO_20353 UBRO_20752 UHOR_01239 UHOR_07208 UHOR_12887 UHOR_16074 UHOR_12189 UHOR_14247 sr05445 UBRO_20884 UBRO_20085 UHOR_02454 SPSC_05299 SPSC_06576	
UBRO_20285	FALSE	UBRO_chr04	orf	mRNA	1358421	1359074	.	-	.	ID=mRNA_UBRO_20285;Parent=UBRO_20285;Name=UBRO_20285;Note=uncharacter-ized+protein;ped-ant_db=p3_i2_t307758_Ust_bromi_v3;		
UBRO_20596	FALSE	UBRO_chr04	orf	mRNA	1447104	1450846	.	+	.	ID=mRNA_UBRO_20596;Parent=UBRO_20596;Name=UBRO_20596;Note=uncharacter-ized+protein;ped-ant_db=p3_i2_t307758_Ust_bromi_v3;	SPSC_00206 SPSC_01500 SPSC_01215 SPSC_05764 UBRO_20081 UBRO_20349 UBRO_20089 UBRO_20219 UBRO_20355 UBRO_20594 UBRO_20727 UBRO_20164 UBRO_20203 UBRO_20637 UBRO_20669 UBRO_20815 UBRO_20220 UBRO_20284 UBRO_20335 UBRO_20728 UBRO_20754 UBRO_20968 UBRO_20279 UBRO_20307 UBRO_20844 UBRO_20280 UBRO_20360 UBRO_20596 UBRO_20964 UBRO_20353 UBRO_20752 UHOR_01239 UHOR_07208 UHOR_12887	GO:0005488 bind-ing

											UHOR_16074 UHOR_12189 UHOR_14247 sr05445 UBRO_20884 UBRO_20085 UHOR_02454 SPSC_05299 SPSC_06576	
UBRO_20598	FALSE	UBRO_chr04	orf	mRNA	1483093	1483674	.	+	.	ID=mRNA_UBRO_20598;Parent=UBRO_20598;Name=UBRO_20598;Note=uncharacterized+protein;pedant_db=p3_i2_t307758_Ust_bromi_v3;		
UBRO_20606	FALSE	UBRO_chr04	orf	mRNA	1679420	1680709	.	-	.	ID=mRNA_UBRO_20606;Parent=UBRO_20606;Name=UBRO_20606;Note=uncharacterized+protein;pedant_db=p3_i2_t307758_Ust_bromi_v3;	UBRO_20402 UBRO_20555 UBRO_20435 UBRO_20473 UBRO_20476 UBRO_20544 UBRO_20606 UBRO_20846 UBRO_21007 UBRO_20772 UHOR_14039 UHOR_14142 UHOR_14176 SPSC_01964	
UBRO_20622	FALSE	UBRO_chr06	orf	mRNA	24689	25850	.	+	.	ID=mRNA_UBRO_20622;Parent=UBRO_20622;Name=UBRO_20622;Note=uncharacterized+protein;pedant_db=p3_i2_t307758_Ust_bromi_v3;		
UBRO_21002	*	UBRO_chr08	orf	mRNA	11848	13221	.	-	.	ID=mRNA_UBRO_21002;Parent=UBRO_21002;Name=UBRO_21002;Note=uncharacterized+protein;pedant_db=p3_i2_t307758_Ust_bromi_v3;	sr07366 sr11325 sr15209 SPSC_01813 SPSC_04725 UBRO_20361 UBRO_20409 UBRO_20420 UBRO_20465 UBRO_20481 UBRO_20591 UBRO_20814 UBRO_20827 UBRO_20916 UBRO_20413 UBRO_20416 UBRO_20499 UBRO_20568 UBRO_20763 UBRO_20793 UBRO_20994 UBRO_21002	GO:0003677 DNA binding
UBRO_20714	FALSE	UBRO_chr08	orf	mRNA	43345	44412	.	+	.	ID=mRNA_UBRO_20714;Parent=UBRO_20714;Name=UBRO_20714;Note=uncharacterized+protein;pedant_db=p3_i2_t307758_Ust_bromi_v3;	UBRO_04256 UBRO_20275 UBRO_20382 UBRO_20537 UBRO_20714 UBRO_20865 UBRO_20722 UBRO_20724 UBRO_20768 UBRO_20796 UBRO_20837 UBRO_21052 UBRO_20792 UBRO_20212 UBRO_20495 UHOR_04256	GO:0003677 DNA binding,GO:0006313 transposition, DNA-mediated,GO:0015074 DNA integration
UBRO_20696	FALSE	UBRO_chr08	orf	mRNA	460266	460859	.	-	.	ID=mRNA_UBRO_20696;Parent=UBRO_20696;Name=UBRO_20696;Note=uncharacterized+protein;pedant_db=p3_i2_t307758_Ust_bromi_v3;	UBRO_20105 UBRO_20133 UBRO_20161 UBRO_20173 UBRO_20204 UBRO_20233 UBRO_20316 UBRO_20371 UBRO_20388 UBRO_20502 UBRO_20524 UBRO_20639 UBRO_20695 UBRO_20696 UBRO_20800 UBRO_20854 UBRO_20869	
UBRO_05068	FALSE	UBRO_chr08	orf	mRNA	471734	475339	.	-	.	ID=mRNA_UBRO_05068;Parent=UBRO_05068;Name=UBRO_05068;Note=related+to+STE23+-+Metalloprotease+involved+in+a-factor+processing;pedant_db=p3_i2_t307758_Ust_bromi_v3;	BN887_05458 sr14254 SPSC_04302 UBRO_05068 UHOR_05068 UMAG_11953	
UBRO_20690	FALSE	UBRO_chr08	orf	mRNA	493332	494633	.	-	.	ID=mRNA_UBRO_20690;Parent=UBRO_20690;Name=UBRO_20690;Note=uncharacterized+protein;pedant_db=p3_i2_t307758_Ust_bromi_v3;	UBRO_20157 UBRO_20217 UBRO_20242 UBRO_20277 UBRO_20314 UBRO_20389 UBRO_20449 UBRO_20455 UBRO_20458 UBRO_20482 UBRO_20504 UBRO_20528 UBRO_20534 UBRO_20548 UBRO_20589 UBRO_20670 UBRO_20671 UBRO_20690 UBRO_20790 UBRO_20848 UBRO_20874 UBRO_20859 SPSC_04004 UMAG_02747	
UBRO_20685	TRUE	UBRO_chr08	orf	mRNA	589807	590452	.	+	.	ID=mRNA_UBRO_20685;Parent=UBRO_20685;Name=UBRO_20685;Note=related+to+Mig1+protein;pedant_db=p3_i2_t307758_Ust_bromi_v3;	UBRO_04675 UBRO_20685 UBRO_20847 sr14220 SPSC_04271 UHOR_04675 UMAG_03223	
UBRO_20722	FALSE	UBRO_chr09	orf	mRNA	220244	220990	.	-	.	ID=mRNA_UBRO_20722;Parent=UBRO_20722;Name=UBRO_20722;Not	UBRO_04256 UBRO_20275 UBRO_20382 UBRO_20537 UBRO_20714 UBRO_20865 UBRO_20722 UBRO_20724	GO:0003677 DNA binding,GO:0006313 transposition, DNA-

											e=uncharacter-ized+protein;ped-ant_db=p3_i2_t307758_Ust_bromi_v3;	UBRO_20768 UBRO_20796 UBRO_20837 UBRO_21052 UBRO_20792 UBRO_20212 UBRO_20495 UHOR_04256	mediated,GO:0015074 DNA integra-tion
UBRO_20724	FALSE	UBRO_chr09	orf	mRNA	254663	255729	.	-	.	ID=mRNA_UBRO_20724;Parent=UBRO_20724;Name=UBRO_20724;Note=uncharacter-ized+protein;ped-ant_db=p3_i2_t307758_Ust_bromi_v3;	UBRO_04256 UBRO_20275 UBRO_20382 UBRO_20537 UBRO_20714 UBRO_20865 UBRO_20722 UBRO_20724 UBRO_20768 UBRO_20796 UBRO_20837 UBRO_21052 UBRO_20792 UBRO_20212 UBRO_20495 UHOR_04256	GO:0003677 DNA binding,GO:0006313 transposition, DNA-mediated,GO:0015074 DNA integra-tion
UBRO_20074	FALSE	UBRO_chr09	orf	mRNA	433150	434200	.	-	.	ID=mRNA_UBRO_20074;Parent=UBRO_20074;Name=UBRO_20074;Note=related+to+transposase;pedant_db=p3_i2_t307758_Ust_bromi_v3;		GO:0006259 DNA metabolic process
UBRO_20733	FALSE	UBRO_chr09	orf	mRNA	489983	490453	.	-	.	ID=mRNA_UBRO_20733;Parent=UBRO_20733;Name=UBRO_20733;Note=related+to+Transposase;pedant_db=p3_i2_t307758_Ust_bromi_v3;		GO:0003677 DNA binding,GO:0006313 transposition, DNA-mediated,GO:0015074 DNA integra-tion
UBRO_20738	FALSE	UBRO_chr09	orf	mRNA	708836	709777	.	-	.	ID=mRNA_UBRO_20738;Parent=UBRO_20738;Name=UBRO_20738;Note=uncharacter-ized+protein;ped-ant_db=p3_i2_t307758_Ust_bromi_v3;	UBRO_20738 UHOR_12238	
UBRO_20741	FALSE	UBRO_chr09	orf	mRNA	713395	713700	.	-	.	ID=mRNA_UBRO_20741;Parent=UBRO_20741;Name=UBRO_20741;Note=uncharacter-ized+protein;ped-ant_db=p3_i2_t307758_Ust_bromi_v3;		GO:0003676 nuc-leic acid binding,GO:0008270 zinc ion binding
UBRO_20752	FALSE	UBRO_chr10	orf	mRNA	26565	27932	.	-	.	ID=mRNA_UBRO_20752;Parent=UBRO_20752;Name=UBRO_20752;Note=uncharacter-ized+protein;ped-ant_db=p3_i2_t307758_Ust_bromi_v3;	SPSC_00206 SPSC_01500 SPSC_01215 SPSC_05764 UBRO_20081 UBRO_20349 UBRO_20089 UBRO_20219 UBRO_20355 UBRO_20594 UBRO_20727 UBRO_20164 UBRO_20203 UBRO_20637 UBRO_20669 UBRO_20815 UBRO_20220 UBRO_20284 UBRO_20335 UBRO_20728 UBRO_20754 UBRO_20968 UBRO_20279 UBRO_20307 UBRO_20844 UBRO_20280 UBRO_20360 UBRO_20596 UBRO_20964 UBRO_20353 UBRO_20752 UHOR_01239 UHOR_07208 UHOR_12887 UHOR_16074 UHOR_12189 UHOR_14247 sr05445 UBRO_20884 UBRO_20085 UHOR_02454 SPSC_05299 SPSC_06576	GO:0003676 nuc-leic acid binding,GO:0006259 DNA metabolic process
UBRO_20297	FALSE	UBRO_chr10	orf	mRNA	365393	366247	.	+	.	ID=mRNA_UBRO_20297;Parent=UBRO_20297;Name=UBRO_20297;Note=probable+trans-posase;pedant_db=p3_i2_t307758_Ust_bromi_v3;	UBRO_20297 UBRO_20462 UBRO_20825 UBRO_20876 UHOR_03913 UHOR_10023 UHOR_10025 sr11477 SPSC_03451	
UBRO_20204	FALSE	UBRO_chr11	orf	mRNA	455142	456176	.	-	.	ID=mRNA_UBRO_20204;Parent=UBRO_20204;Name=UBRO_20204;Note=uncharacter-ized+protein;ped-ant_db=p3_i2_t307758_Ust_bromi_v3;	UBRO_20105 UBRO_20133 UBRO_20161 UBRO_20173 UBRO_20204 UBRO_20233 UBRO_20316 UBRO_20371 UBRO_20388 UBRO_20502 UBRO_20524 UBRO_20639 UBRO_20695 UBRO_20696 UBRO_20800 UBRO_20854 UBRO_20869	
UBRO_20235	FALSE	UBRO_chr12	orf	mRNA	37072	38856	.	+	.	ID=mRNA_UBRO_20235;Parent=UBRO_20235;Name=UBRO_20235;Note=uncharacter-ized+protein;ped-ant_db=p3_i2_t307758_Ust_bromi_v3;	UBRO_20235 UHOR_15968	GO:0005739 mito-chondrion,GO:0016021 integral com-ponent of mem-brane,GO:0004222 metalloendopepti-dase activity,GO:0046872 metal ion bind-ing,GO:0051603

												proteolysis involved in cellular protein catabolic process
UBRO_20233	FALSE	UBRO_chr12	orf	mRNA	47584	48629	.	-	.	ID=mRNA_UBRO_20233;Parent=UBRO_20233;Name=UBRO_20233;Note=uncharacterized+protein;pedant_db=p3_i2_t307758_Ust_bromi_v3;	UBRO_20105 UBRO_20133 UBRO_20161 UBRO_20173 UBRO_20204 UBRO_20233 UBRO_20316 UBRO_20371 UBRO_20388 UBRO_20502 UBRO_20524 UBRO_20639 UBRO_20695 UBRO_20696 UBRO_20800 UBRO_20854 UBRO_20869	
UBRO_20232	FALSE	UBRO_chr12	orf	mRNA	49054	49934	.	+	.	ID=mRNA_UBRO_20232;Parent=UBRO_20232;Name=UBRO_20232;Note=uncharacterized+protein;pedant_db=p3_i2_t307758_Ust_bromi_v3;	sr02163 UBRO_20232	
UBRO_06175	FALSE	UBRO_chr12	orf	mRNA	51491	52084	.	-	.	ID=mRNA_UBRO_06175;Parent=UBRO_06175;Name=UBRO_06175;Note=uncharacterized+protein;pedant_db=p3_i2_t307758_Ust_bromi_v3;	UBRO_06175 UHOR_06175	
UBRO_21076	*	UBRO_chr12	orf	mRNA	90061	90762	.	-	.	ID=mRNA_UBRO_21076;Parent=UBRO_21076;Name=UBRO_21076;Note=uncharacterized+protein;pedant_db=p3_i2_t307758_Ust_bromi_v3;	UBRO_21062 UBRO_20218 UBRO_20278 UBRO_20483 UBRO_20529 UBRO_20533 UBRO_20546 UBRO_20590 UBRO_20873 UBRO_20998 UBRO_21009 UBRO_21033 UBRO_21041 UBRO_21053 UBRO_21054 UBRO_21069 UBRO_21084 UBRO_20454 UBRO_20861 UBRO_21034 UBRO_21076 UBRO_20691 UBRO_20887 UBRO_21085 sr16557 UMAG_02745 SPSC_01947 UHOR_03466	
UBRO_21077	*	UBRO_chr12	orf	mRNA	91149	91532	.	-	.	ID=mRNA_UBRO_21077;Parent=UBRO_21077;Name=UBRO_21077;Note=uncharacterized+protein;pedant_db=p3_i2_t307758_Ust_bromi_v3;		
UBRO_21078	*	UBRO_chr12	orf	mRNA	92110	92445	.	+	.	ID=mRNA_UBRO_21078;Parent=UBRO_21078;Name=UBRO_21078;Note=uncharacterized+protein;pedant_db=p3_i2_t307758_Ust_bromi_v3;		
UBRO_20814	FALSE	UBRO_chr13	orf	mRNA	161112	162608	.	+	.	ID=mRNA_UBRO_20814;Parent=UBRO_20814;Name=UBRO_20814;Note=uncharacterized+protein;pedant_db=p3_i2_t307758_Ust_bromi_v3;	sr07366 sr11325 sr15209 SPSC_01813 SPSC_04725 UBRO_20361 UBRO_20409 UBRO_20420 UBRO_20465 UBRO_20481 UBRO_20591 UBRO_20814 UBRO_20827 UBRO_20916 UBRO_20413 UBRO_20416 UBRO_20499 UBRO_20568 UBRO_20763 UBRO_20793 UBRO_20994 UBRO_21002	
UBRO_20817	FALSE	UBRO_chr13	orf	mRNA	320434	321228	.	-	.	ID=mRNA_UBRO_20817;Parent=UBRO_20817;Name=UBRO_20817;Note=uncharacterized+protein;pedant_db=p3_i2_t307758_Ust_bromi_v3;	sr02164 UBRO_20817	
UBRO_20324	FALSE	UBRO_chr13	orf	mRNA	321890	323270	.	-	.	ID=mRNA_UBRO_20324;Parent=UBRO_20324;Name=UBRO_20324;Note=uncharacterized+protein;pedant_db=p3_i2_t307758_Ust_bromi_v3;	UBRO_20324 UHOR_14711	
UBRO_20822	FALSE	UBRO_chr13	orf	mRNA	371419	372054	.	-	.	ID=mRNA_UBRO_20822;Parent=UBRO_20822;Name=UBRO_20822;Not		GO:0000943 retrotransposon nucleocapsid

											e=uncharacter-ized+protein;ped-ant_db=p3_i2_t307758_Ust_bromi_v3;		
UBRO_06907	FALSE	UBRO_chr13	orf	mRNA	415295	416167	.	-	.	ID=mRNA_UBRO_06907;Parent=UBRO_06907;Name=UBRO_06907;Note=uncharacter-ized+protein;ped-ant_db=p3_i2_t307758_Ust_bromi_v3;	BN887_06194 sr15307 SPSC_00956 UBRO_06907 UHOR_06907 UMAG_04421	GO:0005634 nuc-leus,GO:0003677 DNA binding,GO:0008270 zinc ion binding,GO:0000981 DNA-binding transcription factor activity, RNA poly-merase II-specific,GO:0006357 regulation of transcription by RNA polymerase II
UBRO_20824	FALSE	UBRO_chr13	orf	mRNA	420392	421333	.	-	.	ID=mRNA_UBRO_20824;Parent=UBRO_20824;Name=UBRO_20824;Note=uncharacter-ized+protein;ped-ant_db=p3_i2_t307758_Ust_bromi_v3;		
UBRO_20825	FALSE	UBRO_chr13	orf	mRNA	436916	437809	.	-	.	ID=mRNA_UBRO_20825;Parent=UBRO_20825;Name=UBRO_20825;Note=probable+trans-posase;pedant_db=p3_i2_t307758_Ust_bromi_v3;	UBRO_20297 UBRO_20462 UBRO_20825 UBRO_20876 UHOR_03913 UHOR_10023 UHOR_10025 sr11477 SPSC_03451	GO:0003677 DNA binding,GO:0006313 transposition, DNA-mediated,GO:0015074 DNA integra-tion
UBRO_20837	FALSE	UBRO_chr15	orf	mRNA	7511	8290	.	+	.	ID=mRNA_UBRO_20837;Parent=UBRO_20837;Name=UBRO_20837;Note=uncharacter-ized+protein;ped-ant_db=p3_i2_t307758_Ust_bromi_v3;	UBRO_04256 UBRO_20275 UBRO_20382 UBRO_20537 UBRO_20714 UBRO_20865 UBRO_20722 UBRO_20724 UBRO_20768 UBRO_20796 UBRO_20837 UBRO_21052 UBRO_20792 UBRO_20212 UBRO_20495 UHOR_04256	GO:0003677 DNA binding,GO:0006313 transposition, DNA-mediated,GO:0015074 DNA integra-tion
UBRO_06154	FALSE	UBRO_chr15	orf	mRNA	37772	40963	.	+	.	ID=mRNA_UBRO_06154;Parent=UBRO_06154;Name=UBRO_06154;Note=related+to+va-cuolar+protein+sor-ting+16;pedant_db=p3_i2_t307758_Ust_bromi_v3;	BN887_02451 sr14985 SPSC_05285 UBRO_06154 UHOR_06154 UMAG_11636	GO:0005737 cyto-plasm,GO:0008237 metallopeptidase activity,GO:0006508 proteolysis,GO:0006886 intracellular protein transport,GO:0007033 vacuole organ-ization
UBRO_20841	FALSE	UBRO_chr15	orf	mRNA	136888	138379	.	+	.	ID=mRNA_UBRO_20841;Parent=UBRO_20841;Name=UBRO_20841;Note=uncharacter-ized+protein;ped-ant_db=p3_i2_t307758_Ust_bromi_v3;	UBRO_20764 UBRO_20841	
UBRO_20843	FALSE	UBRO_chr15	orf	mRNA	145270	145971	.	-	.	ID=mRNA_UBRO_20843;Parent=UBRO_20843;Name=UBRO_20843;Note=uncharacter-ized+protein;ped-ant_db=p3_i2_t307758_Ust_bromi_v3;		
UBRO_20844	FALSE	UBRO_chr15	orf	mRNA	146494	148224	.	-	.	ID=mRNA_UBRO_20844;Parent=UBRO_20844;Name=UBRO_20844;Note=uncharacter-ized+protein;ped-ant_db=p3_i2_t307758_Ust_bromi_v3;	SPSC_00206 SPSC_01500 SPSC_01215 SPSC_05764 UBRO_20081 UBRO_20349 UBRO_20089 UBRO_20219 UBRO_20355 UBRO_20594 UBRO_20727 UBRO_20164 UBRO_20203 UBRO_20637 UBRO_20669 UBRO_20815 UBRO_20220 UBRO_20284 UBRO_20335 UBRO_20728 UBRO_20754 UBRO_20968 UBRO_20279 UBRO_20307 UBRO_20844 UBRO_20280 UBRO_20360 UBRO_20596 UBRO_20964 UBRO_20353 UBRO_20752 UHOR_01239 UHOR_07208 UHOR_12887 UHOR_16074 UHOR_12189 UHOR_14247 sr05445 UBRO_20884 UBRO_20085 UHOR_02454 SPSC_05299 SPSC_06576	GO:0003676 nuc-leic acid binding,GO:0006259 DNA metabolic process
UBRO_	FALSE	UBRO_chr15	orf	mRNA	149934	150311	.	-	.	ID=mRNA_UBRO_		

20845										20845;Parent=UBRO_20845;Name=UBRO_20845;Note=uncharacterized+protein;pedant_db=p3_i2_t307758_Ust_bromi_v3;		
UBRO_20846	FALSE	UBRO_chr15	orf	mRNA	249359	250537	.	-	.	ID=mRNA_UBRO_20846;Parent=UBRO_20846;Name=UBRO_20846;Note=uncharacterized+protein;pedant_db=p3_i2_t307758_Ust_bromi_v3;	UBRO_20402 UBRO_20555 UBRO_20435 UBRO_20473 UBRO_20476 UBRO_20544 UBRO_20606 UBRO_20846 UBRO_21007 UBRO_20772 UHOR_14039 UHOR_14142 UHOR_14176 SPSC_01964	
UBRO_21012	*	UBRO_chr15	orf	mRNA	432534	433183	.	-	.	ID=mRNA_UBRO_21012;Parent=UBRO_21012;Name=UBRO_21012;Note=uncharacterized+protein;pedant_db=p3_i2_t307758_Ust_bromi_v3;		
UBRO_20854	FALSE	UBRO_chr15	orf	mRNA	436204	437139	.	-	.	ID=mRNA_UBRO_20854;Parent=UBRO_20854;Name=UBRO_20854;Note=uncharacterized+protein;pedant_db=p3_i2_t307758_Ust_bromi_v3;	UBRO_20105 UBRO_20133 UBRO_20161 UBRO_20173 UBRO_20204 UBRO_20233 UBRO_20316 UBRO_20371 UBRO_20388 UBRO_20502 UBRO_20524 UBRO_20639 UBRO_20695 UBRO_20696 UBRO_20800 UBRO_20854 UBRO_20869	
UBRO_20860	FALSE	UBRO_chr15	orf	mRNA	593548	594902	.	+	.	ID=mRNA_UBRO_20860;Parent=UBRO_20860;Name=UBRO_20860;Note=uncharacterized+protein;pedant_db=p3_i2_t307758_Ust_bromi_v3;	UBRO_20110 UBRO_20406 UBRO_20860 UBRO_20886 UBRO_20914 UHOR_14108 UHOR_14114 UHOR_14168	GO:0016021 integral component of membrane
UBRO_20861	FALSE	UBRO_chr15	orf	mRNA	595268	596807	.	+	.	ID=mRNA_UBRO_20861;Parent=UBRO_20861;Name=UBRO_20861;Note=uncharacterized+protein;pedant_db=p3_i2_t307758_Ust_bromi_v3;	UBRO_21062 UBRO_20218 UBRO_20278 UBRO_20483 UBRO_20529 UBRO_20533 UBRO_20546 UBRO_20590 UBRO_20873 UBRO_20998 UBRO_21009 UBRO_21033 UBRO_21041 UBRO_21053 UBRO_21054 UBRO_21069 UBRO_21084 UBRO_20454 UBRO_20861 UBRO_21034 UBRO_21076 UBRO_20691 UBRO_20887 UBRO_21085 sr16557 UMAG_02745 SPSC_01947 UHOR_03466	
UBRO_20876	FALSE	UBRO_chr16	orf	mRNA	350134	351153	.	+	.	ID=mRNA_UBRO_20876;Parent=UBRO_20876;Name=UBRO_20876;Note=probable+transposase;pedant_db=p3_i2_t307758_Ust_bromi_v3;	UBRO_20297 UBRO_20462 UBRO_20825 UBRO_20876 UHOR_03913 UHOR_10023 UHOR_10025 sr11477 SPSC_03451	GO:0003677 DNA binding,GO:0006313 transposition, DNA-mediated,GO:0015074 DNA integration
UBRO_20085	FALSE	UBRO_chr16	orf	mRNA	558801	561262	.	-	.	ID=mRNA_UBRO_20085;Parent=UBRO_20085;Name=UBRO_20085;Note=uncharacterized+protein;pedant_db=p3_i2_t307758_Ust_bromi_v3;	SPSC_00206 SPSC_01500 SPSC_01215 SPSC_05764 UBRO_20081 UBRO_20349 UBRO_20089 UBRO_20219 UBRO_20355 UBRO_20594 UBRO_20727 UBRO_20164 UBRO_20203 UBRO_20637 UBRO_20669 UBRO_20815 UBRO_20220 UBRO_20284 UBRO_20335 UBRO_20728 UBRO_20754 UBRO_20968 UBRO_20279 UBRO_20307 UBRO_20844 UBRO_20280 UBRO_20360 UBRO_20596 UBRO_20964 UBRO_20353 UBRO_20752 UHOR_01239 UHOR_07208 UHOR_12887 UHOR_16074 UHOR_12189 UHOR_14247 sr05445 UBRO_20884 UBRO_20085 UHOR_02454 SPSC_05299 SPSC_06576	GO:0005488 binding
UBRO_20084	FALSE	UBRO_chr16	orf	mRNA	562971	564301	.	-	.	ID=mRNA_UBRO_20084;Parent=UBRO_20084;Name=UBRO_20084;Note=uncharacterized+protein;pedant_db=p3_i2_t307758_Ust_bromi_v3;	UBRO_20084 UBRO_20912 UMAG_05313	

UBRO_20173	FALSE	UBRO_chr19	orf	mRNA	454099	455139	.	-	.	ID=mRNA_UBRO_20173;Parent=UBRO_20173;Name=UBRO_20173;Note=uncharacterized+protein;pedant_db=p3_i2_t307758_Ust_bromi_v3;	UBRO_20105 UBRO_20133 UBRO_20161 UBRO_20173 UBRO_20204 UBRO_20233 UBRO_20316 UBRO_20371 UBRO_20388 UBRO_20502 UBRO_20524 UBRO_20639 UBRO_20695 UBRO_20696 UBRO_20800 UBRO_20854 UBRO_20869	
UBRO_20169	FALSE	UBRO_chr19	orf	mRNA	543704	544633	.	-	.	ID=mRNA_UBRO_20169;Parent=UBRO_20169;Name=UBRO_20169;Note=uncharacterized+protein;pedant_db=p3_i2_t307758_Ust_bromi_v3;	UBRO_20035 UBRO_20394 UBRO_20169 UBRO_20647 UBRO_20955 UBRO_20959 UBRO_20985 sr11443 SPSC_05561 UHOR_15672	
UBRO_21021	*	UBRO_chr21	orf	mRNA	328492	329342	.	+	.	ID=mRNA_UBRO_21021;Parent=UBRO_21021;Name=UBRO_21021;Note=uncharacterized+protein;pedant_db=p3_i2_t307758_Ust_bromi_v3;		
UBRO_20966	FALSE	UBRO_chr21	orf	mRNA	335842	339416	.	-	.	ID=mRNA_UBRO_20966;Parent=UBRO_20966;Name=UBRO_20966;Note=uncharacterized+protein;pedant_db=p3_i2_t307758_Ust_bromi_v3;		GO:0008622 epsilon DNA polymerase complex,GO:0003677 DNA binding,GO:0003887 DNA-directed DNA polymerase activity,GO:0016491 oxidoreductase activity,GO:0006261 DNA-dependent DNA replication,GO:0055114 oxidation-reduction process,GO:0071897 DNA biosynthetic process
UBRO_20342	FALSE	UBRO_chr22	orf	mRNA	167444	169115	.	+	.	ID=mRNA_UBRO_20342;Parent=UBRO_20342;Name=UBRO_20342;Note=related+to+retrotransposon+nucleocapsid+protein;pedant_db=p3_i2_t307758_Ust_bromi_v3;	UBRO_20342 UBRO_21048 UHOR_10026 UHOR_10032 UHOR_12026 UHOR_13117 UHOR_13979 UHOR_13994 UHOR_14022 UHOR_14049 UHOR_14093 UHOR_14103 UHOR_14152 UHOR_14181 UHOR_14949 UHOR_15002 UHOR_12028 UHOR_12910 UHOR_13005 UHOR_13006 UHOR_14132 UHOR_14739 BN887_02598 UBRO_20153 UBRO_20210 UBRO_20516 UBRO_20889	GO:0003676 nucleic acid binding,GO:0008270 zinc ion binding
UBRO_21023	*	UBRO_chr22	orf	mRNA	171486	171836	.	+	.	ID=mRNA_UBRO_21023;Parent=UBRO_21023;Name=UBRO_21023;Note=uncharacterized+protein;pedant_db=p3_i2_t307758_Ust_bromi_v3;	UBRO_20199 UBRO_20439 UBRO_20997 UBRO_21023	GO:0003677 DNA binding,GO:0006313 transposition, DNA-mediated,GO:0015074 DNA integration
UBRO_20277	FALSE	UBRO_chr22	orf	mRNA	267461	268389	.	-	.	ID=mRNA_UBRO_20277;Parent=UBRO_20277;Name=UBRO_20277;Note=uncharacterized+protein;pedant_db=p3_i2_t307758_Ust_bromi_v3;	UBRO_20157 UBRO_20217 UBRO_20242 UBRO_20277 UBRO_20314 UBRO_20389 UBRO_20449 UBRO_20455 UBRO_20458 UBRO_20482 UBRO_20504 UBRO_20528 UBRO_20534 UBRO_20548 UBRO_20589 UBRO_20670 UBRO_20671 UBRO_20690 UBRO_20790 UBRO_20848 UBRO_20874 UBRO_20859 SPSC_04004 UMAG_02747	
UBRO_08867	FALSE	UBRO_chr22	orf	mRNA	349012	352350	.	-	.	ID=mRNA_UBRO_08867;Parent=UBRO_08867;Name=UBRO_08867;Note=uncharacterized+protein;pedant_db=p3_i2_t307758_Ust_bromi_v3;	SPSC_00011 SPSC_00012 UBRO_01988 UBRO_20775 UBRO_08867 UBRO_20326 UHOR_01988 UHOR_14700 UHOR_08867 UHOR_09014 BN887_02167 BN887_06186 SPSC_02318	
UBRO_21201	*	UBRO_mito	orf	mRNA	34362	39765	.	+	.	ID=mRNA_UBRO_21201;Parent=UBRO_21201;Name=UBRO_21201;Note=intron-encoded+LAGLIDADG+endonuclease;pedant_db=p	*	GO:0005751 mitochondrial respiratory chain complex IV,GO:0005886 plasma membrane,GO:0016021 integral component of mem-

										3_i2_t307758_Ust_bromi_v3;		brane,GO:0004129 cytochrome-c oxidase activity,GO:0004519 endonuclease activity,GO:0020037 heme binding,GO:0046872 metal ion binding,GO:0006123 mitochondrial electron transport, cytochrome c to oxygen,GO:0006314 intron homing,GO:0015990 electron transport coupled proton transport,GO:0090305 nucleic acid phosphodiester bond hydrolysis
UBRO_21202	*	UBRO_mito	orf	mRNA	34362	44491	.	+	.	ID=mRNA_UBRO_21202;Parent=UBRO_21202;Name=UBRO_21202;Note=intron-encoded+GIY-YIG+endonuclease;pedant_db=p3_i2_t307758_Ust_bromi_v3;	*	GO:0005751 mitochondrial respiratory chain complex IV,GO:0005886 plasma membrane,GO:0016021 integral component of membrane,GO:0004129 cytochrome-c oxidase activity,GO:0004519 endonuclease activity,GO:0020037 heme binding,GO:0046872 metal ion binding,GO:0006123 mitochondrial electron transport, cytochrome c to oxygen,GO:0006314 intron homing,GO:0015990 electron transport coupled proton transport,GO:0090305 nucleic acid phosphodiester bond hydrolysis
UBRO_21203	*	UBRO_mito	orf	mRNA	34362	47004	.	+	.	ID=mRNA_UBRO_21203;Parent=UBRO_21203;Name=UBRO_21203;Note=intron-encoded+LAGLIDADG+endonuclease;pedant_db=p3_i2_t307758_Ust_bromi_v3;	*	GO:0005751 mitochondrial respiratory chain complex IV,GO:0005886 plasma membrane,GO:0016021 integral component of membrane,GO:0004129 cytochrome-c oxidase activity,GO:0004519 endonuclease activity,GO:0020037 heme binding,GO:0046872 metal ion binding,GO:0006123 mitochondrial electron transport, cytochrome c to oxygen,GO:0006314 intron homing,GO:0015990 electron transport coupled proton transport,GO:0090305 nucleic acid phosphodiester bond hydrolysis
UBRO_21204	*	UBRO_mito	orf	mRNA	34362	49774	.	+	.	ID=mRNA_UBRO_21204;Parent=UBRO_21204;Name=UBRO_21204;Note=intron-encoded+LAGLIDADG+endonuclease;pedant_db=p3_i2_t307758_Ust_bromi_v3;	*	GO:0005751 mitochondrial respiratory chain complex IV,GO:0005886 plasma membrane,GO:0016021 integral component of membrane,GO:0004129 cytochrome-c oxidase activity,GO:0004519 endonuclease activity,GO:0020037 heme binding,GO:0046872 metal ion bind-

												ing,GO:0006123 mitochondrial electron transport, cytochrome c to oxygen,GO:0006314 intron homing,GO:0015990 electron transport coupled proton transport,GO:0090305 nucleic acid phosphodiester bond hydrolysis
UBRO_21206	*	UBRO_mito	orf	mRNA	34362	55414	.	+	.	ID=mRNA_UBRO_21206;Parent=UBRO_21206;Name=UBRO_21206;Note=intron-encoded+LAGLIDADG+endonuclease;pedant_db=p3_i2_t307758_Ust_bromi_v3;	*	GO:0005751 mitochondrial respiratory chain complex IV,GO:0005886 plasma membrane,GO:0016021 integral component of membrane,GO:0004129 cytochrome-c oxidase activity,GO:0004519 endonuclease activity,GO:0020037 heme binding,GO:0046872 metal ion binding,GO:0006123 mitochondrial electron transport, cytochrome c to oxygen,GO:0006314 intron homing,GO:0015990 electron transport coupled proton transport,GO:0090305 nucleic acid phosphodiester bond hydrolysis
UBRO_21207	*	UBRO_mito	orf	mRNA	35113	36825	.	+	.	ID=mRNA_UBRO_21207;Parent=UBRO_21207;Name=UBRO_21207;Note=probable+group+II+intron+reverse+transcriptase/maturase;pedant_db=p3_i2_t307758_Ust_bromi_v3;	*	GO:0003964 RNA-directed DNA polymerase activity,GO:0006278 RNA-dependent DNA biosynthetic process,GO:0006397 mRNA processing
UBRO_21208	*	UBRO_mito	orf	mRNA	42751	43146	.	+	.	ID=mRNA_UBRO_21208;Parent=UBRO_21208;Name=UBRO_21208;Note=intron-encoded+LAGLIDADG+endonuclease;pedant_db=p3_i2_t307758_Ust_bromi_v3;	*	GO:0005751 mitochondrial respiratory chain complex IV,GO:0016021 integral component of membrane,GO:0004129 cytochrome-c oxidase activity,GO:0004519 endonuclease activity,GO:0020037 heme binding,GO:0006123 mitochondrial electron transport, cytochrome c to oxygen,GO:0006314 intron homing,GO:0015990 electron transport coupled proton transport,GO:0090305 nucleic acid phosphodiester bond hydrolysis
UBRO_21209	*	UBRO_mito	orf	mRNA	43955	44491	.	+	.	ID=mRNA_UBRO_21209;Parent=UBRO_21209;Name=UBRO_21209;Note=intron-encoded+GIYYIG+endonuclease;pedant_db=p3_i2_t307758_Ust_bromi_v3;	*	GO:0005743 mitochondrial inner membrane,GO:0016021 integral component of membrane,GO:0070469 respirasome,GO:0004129 cytochrome-c oxidase activity,GO:0004519 endonuclease activity,GO:0020037 heme binding,GO:0046872 metal ion binding,GO:0006119 oxidative phosphorylation,GO:0006314 intron hom-

												ing,GO:0009060 aerobic respiration,GO:0022900 electron transport chain,GO:0090305 nucleic acid phosphodiester bond hydrolysis,GO:1902600 proton transmembrane transport
UBRO_21210	*	UBRO_mito	orf	mRNA	45029	45850	.	+	.	ID=mRNA_UBRO_21210;Parent=UBRO_21210;Name=UBRO_21210;Note=intron-encoded+LAGLIDADG+endonuclease;pedant_db=p3_i2_t307758_Ust_bromi_v3;	*	GO:0005751 mitochondrial respiratory chain complex IV,GO:0016021 integral component of membrane,GO:0004129 cytochrome-c oxidase activity,GO:0004519 endonuclease activity,GO:0020037 heme binding,GO:0006123 mitochondrial electron transport, cytochrome c to oxygen,GO:0006314 intron homing,GO:0015990 electron transport coupled proton transport,GO:0090305 nucleic acid phosphodiester bond hydrolysis
UBRO_21212	*	UBRO_mito	orf	mRNA	55841	56569	.	+	.	ID=mRNA_UBRO_21212;Parent=UBRO_21212;Name=UBRO_21212;Note=intron-encoded+GIY+endonuclease;pedant_db=p3_i2_t307758_Ust_bromi_v3;	*	GO:0004519 endonuclease activity,GO:0090305 nucleic acid phosphodiester bond hydrolysis
UBRO_21214	*	UBRO_mito	orf	mRNA	60291	61055	.	+	.	ID=mRNA_UBRO_21214;Parent=UBRO_21214;Name=UBRO_21214;Note=ATP+synthase+subunit+6;pedant_db=p3_i2_t307758_Ust_bromi_v3;	*	GO:0005743 mitochondrial inner membrane,GO:0016021 integral component of membrane,GO:0045263 proton-transporting ATP synthase complex, coupling factor F(o),GO:0015078 proton transmembrane transporter activity,GO:0015986 ATP synthesis coupled proton transport
UBRO_21216	*	UBRO_mito	orf	mRNA	65593	66822	.	+	.	ID=mRNA_UBRO_21216;Parent=UBRO_21216;Name=UBRO_21216;Note=Cytochrome+c+oxidase+subunit+2+++/+GIY-YIG+domain+of+intron+endonuclease+I;pedant_db=p3_i2_t307758_Ust_bromi_v3;	*	GO:0005751 mitochondrial respiratory chain complex IV,GO:0016021 integral component of membrane,GO:0004129 cytochrome-c oxidase activity,GO:0004519 endonuclease activity,GO:0005507 copper ion binding,GO:0020037 heme binding,GO:0009060 aerobic respiration,GO:0042773 ATP synthesis coupled electron transport,GO:0090305 nucleic acid phosphodiester bond hydrolysis,GO:1902600 proton transmembrane transport
UBRO_21218	*	UBRO_mito	orf	mRNA	69538	71966	.	+	.	ID=mRNA_UBRO_21218;Parent=UBRO_21218;Name=UBRO_21218;Note=NADH-ubiquinone+oxidore-	*	GO:0005743 mitochondrial inner membrane,GO:0005886 plasma membrane,GO:0016021 integral component

										ductase+chain+1;pedant_db=p3_i2_t307758_Ust_bromi_v3;		of membrane,GO:0070469 respirasome,GO:0008137 NADH dehydrogenase (ubiquinone) activity,GO:0048038 quinone binding,GO:0009060 aerobic respiration
UBRO_21225	*	UBRO_mito	orf	mRNA	91600	97075	.	+	.	ID=mRNA_UBRO_21225;Parent=UBRO_21225;Name=UBRO_21225;Note=intron-encoded+LAGLIDADG+endonuclease;pedant_db=p3_i2_t307758_Ust_bromi_v3;	*	GO:0005743 mitochondrial inner membrane,GO:0016021 integral component of membrane,GO:0045275 respiratory chain complex III,GO:0003677 DNA binding,GO:0004129 cytochrome-c oxidase activity,GO:0004519 endonuclease activity,GO:0008121 ubiquinol-cytochrome-c reductase activity,GO:0020037 heme binding,GO:0046872 metal ion binding,GO:0006122 mitochondrial electron transport, ubiquinol to cytochrome c,GO:0006314 intron homing,GO:0009060 aerobic respiration,GO:0090305 nucleic acid phosphodiester bond hydrolysis,GO:1902600 proton transmembrane transport
UBRO_21224	*	UBRO_mito	orf	mRNA	91600	99986	.	+	.	ID=mRNA_UBRO_21224;Parent=UBRO_21224;Name=UBRO_21224;Note=apocytochrome+b;pedant_db=p3_i2_t307758_Ust_bromi_v3;	*	GO:0005743 mitochondrial inner membrane,GO:0016021 integral component of membrane,GO:0045275 respiratory chain complex III,GO:0004129 cytochrome-c oxidase activity,GO:0008121 ubiquinol-cytochrome-c reductase activity,GO:0020037 heme binding,GO:0046872 metal ion binding,GO:0006122 mitochondrial electron transport, ubiquinol to cytochrome c,GO:0009060 aerobic respiration,GO:1902600 proton transmembrane transport
UBRO_21227	*	UBRO_mito	orf	mRNA	106770	112713	.	+	.	ID=mRNA_UBRO_21227;Parent=UBRO_21227;Name=UBRO_21227;Note=NADH-ubiquinone+oxidoreductase+chain+5;pedant_db=p3_i2_t307758_Ust_bromi_v3;	*	GO:0005743 mitochondrial inner membrane,GO:0016021 integral component of membrane,GO:0045263 proton-transporting ATP synthase complex, coupling factor F(o),GO:0070469 respirasome,GO:0008137 NADH dehydrogenase (ubiquinone) activity,GO:0015078 proton transmembrane transporter activity,GO:0015986 ATP synthesis

												coupled proton transport,GO:0042773 ATP synthesis coupled electron transport
UBRO_21229	*	UBRO_mito	orf	mRNA	110238	110969	.	+	.	ID=mRNA_UBRO_21229;Parent=UBRO_21229;Name=UBRO_21229;Note=intron-encoded+LAGLIDADG+endonuclease;pedant_db=p3_i2_t307758_Ust_bromi_v3;	*	GO:0043231 intracellular membrane-bounded organelle,GO:0044444 cytoplasmic part,GO:0004519 endonuclease activity,GO:0090305 nucleic acid phosphodiester bond hydrolysis
UBRO_21231	*	UBRO_mito	orf	mRNA	129712	130587	.	-	.	ID=mRNA_UBRO_21231;Parent=UBRO_21231;Name=UBRO_21231;Note=NADH-ubiquinone+oxidoreductase+chain+6;pedant_db=p3_i2_t307758_Ust_bromi_v3;	*	GO:0005747 mitochondrial respiratory chain complex I,GO:0016021 integral component of membrane,GO:0008137 NADH dehydrogenase (ubiquinone) activity,GO:0055114 oxidation-reduction process
UBRO_21234	*	UBRO_mito	orf	mRNA	134976	135932	.	+	.	ID=mRNA_UBRO_21234;Parent=UBRO_21234;Name=UBRO_21234;Note=probable+LAGLIDADG+endonuclease;pedant_db=p3_i2_t307758_Ust_bromi_v3;	*	GO:0004519 endonuclease activity,GO:0090305 nucleic acid phosphodiester bond hydrolysis
UBRO_21235	*	UBRO_mito	orf	mRNA	137218	137715	.	+	.	ID=mRNA_UBRO_21235;Parent=UBRO_21235;Name=UBRO_21235;Note=probable+LAGLIDADG+endonuclease;pedant_db=p3_i2_t307758_Ust_bromi_v3;	*	GO:0005739 mitochondrion,GO:0004519 endonuclease activity,GO:0090305 nucleic acid phosphodiester bond hydrolysis
UBRO_21236	*	UBRO_mito	orf	mRNA	140632	141384	.	+	.	ID=mRNA_UBRO_21236;Parent=UBRO_21236;Name=UBRO_21236;Note=probable+LAGLIDADG+endonuclease;pedant_db=p3_i2_t307758_Ust_bromi_v3;	*	GO:0005739 mitochondrion,GO:0004519 endonuclease activity,GO:0006314 intron homing,GO:0090305 nucleic acid phosphodiester bond hydrolysis
UBRO_21237	*	UBRO_mito	orf	mRNA	149959	150774	.	+	.	ID=mRNA_UBRO_21237;Parent=UBRO_21237;Name=UBRO_21237;Note=ribosomal+protein+S3;pedant_db=p3_i2_t307758_Ust_bromi_v3;	*	GO:0005761 mitochondrial ribosome,GO:0003735 structural constituent of ribosome,GO:0006412 translation
UBRO_21238	*	UBRO_mito	orf	mRNA	152264	153958	.	+	.	ID=mRNA_UBRO_21238;Parent=UBRO_21238;Name=UBRO_21238;Note=NADH-ubiquinone+oxidoreductase+chain+2;pedant_db=p3_i2_t307758_Ust_bromi_v3;	*	GO:0005743 mitochondrial inner membrane,GO:0016021 integral component of membrane,GO:0070469 respirasome,GO:0008137 NADH dehydrogenase (ubiquinone) activity,GO:0042773 ATP synthesis coupled electron transport
UBRO_21239	*	UBRO_mito	orf	mRNA	153958	154365	.	+	.	ID=mRNA_UBRO_21239;Parent=UBRO_21239;Name=UBRO_21239;Note=NADH-ubiquinone+oxidoreductase+subunit+3;pedant_db=p3_i2_t307758_Ust_bromi_v3;	*	GO:0005747 mitochondrial respiratory chain complex I,GO:0005886 plasma membrane,GO:0016021 integral component of membrane,GO:0004519 endonuclease activity,GO:0008137 NADH dehydrogenase (ubiquinone) activity,GO:0048038 quinone binding,GO:0055114 oxidation-reduction

													process,GO:0090305 nucleic acid phosphodiester bond hydrolysis
UBRO_21240	*	UBRO_mito	orf	mRNA	156798	158249	.	+	.	ID=mRNA_UBRO_21240;Parent=UBRO_21240;Name=UBRO_21240;Note=NADH-ubiquinone+oxidoreductase+chain+4;pedant_db=p3_i2_t307758_Ust_bromi_v3;	*		GO:0005747 mitochondrial respiratory chain complex I,GO:0016021 integral component of membrane,GO:0004519 endonuclease activity,GO:0008137 NADH dehydrogenase (ubiquinone) activity,GO:0048039 ubiquinone binding,GO:0009060 aerobic respiration,GO:0015990 electron transport coupled proton transport,GO:0042773 ATP synthesis coupled electron transport,GO:0090305 nucleic acid phosphodiester bond hydrolysis
UHOR_13044	FALSE	UHOR_scaffold_4.01260	orf	mRNA	1388	2431	.	+	.	ID=mRNA_UHOR_13044;Parent=UHOR_13044;Name=UHOR_13044;Note=uncharacterized+protein;pedant_db=p3_t120017_Ust_horde_v2;	BN887_02600 BN887_02713 UHOR_00833 UHOR_12077 UHOR_14059 UHOR_01674 UHOR_13996 UHOR_04106 UHOR_06224 UHOR_10015 UHOR_10031 UHOR_12673 UHOR_13044 UHOR_13272 UHOR_13991 UHOR_14014 UHOR_14086 UHOR_14161 UHOR_14170 UHOR_14669 UHOR_04108 UHOR_15109 UHOR_10014 UHOR_12378 UHOR_13752 UHOR_14060 UHOR_14564 UHOR_15610 UHOR_16664 UHOR_10028 UHOR_13992 UHOR_12602 UHOR_16322 UHOR_13400 UHOR_14013 UHOR_15903 UHOR_14895 UHOR_16372 SPSC_04529 UBRO_20328 UBRO_12371 UBRO_20143 UBRO_20214 UMAG_02565	
UHOR_08264	FALSE	UHOR_scaffold_5.00018	orf	mRNA	267785	268183	.	-	.	ID=mRNA_UHOR_08264;Parent=UHOR_08264;Name=UHOR_08264;Note=uncharacterized+protein;pedant_db=p3_t120017_Ust_horde_v2;		
UHOR_14161	FALSE	UHOR_scaffold_5.00019	orf	mRNA	460682	464908	.	-	.	ID=mRNA_UHOR_14161;Parent=UHOR_14161;Name=UHOR_14161;Note=uncharacterized+protein;pedant_db=p3_t120017_Ust_horde_v2;	BN887_02600 BN887_02713 UHOR_00833 UHOR_12077 UHOR_14059 UHOR_01674 UHOR_13996 UHOR_04106 UHOR_06224 UHOR_10015 UHOR_10031 UHOR_12673 UHOR_13044 UHOR_13272 UHOR_13991 UHOR_14014 UHOR_14086 UHOR_14161 UHOR_14170 UHOR_14669 UHOR_04108 UHOR_15109 UHOR_10014 UHOR_12378 UHOR_13752 UHOR_14060 UHOR_14564 UHOR_15610 UHOR_16664 UHOR_10028 UHOR_13992 UHOR_12602 UHOR_16322 UHOR_13400 UHOR_14013 UHOR_15903 UHOR_14895 UHOR_16372 SPSC_04529 UBRO_20328 UBRO_12371 UBRO_20143 UBRO_20214 UMAG_02565	GO:0003676 nucleic acid binding,GO:0008270 zinc ion binding

Table S5: Potential pathogenicity genes

Gene	Predicted Secreted	Chromosome/ Contig	Source	Feature	Start	End	Score	Strand	Frame	Attribute	Orthologs (including self)	Functional Annotation
UBRO_05009	FALSE	UBRO_chr08	MIPS	mRNA	612228	614219	.	-	.	ID=mRNA:UBRO_05009;Note=+related+to+dihydroorotate+dehydrogenase,+mitochondrial+precursor	BN887_01069 sr11120 SPSC_04251 UBRO_05009 UHOR_05009 UMAG_10643	GO:0006207 'de novo' pyrimidine nucleobase biosynthetic process,GO:0016021 integral component of membrane,GO:0004152 dihydroorotate dehydrogenase activity,GO:0055114 oxidation-reduction process,GO:0044205 'de novo' UMP biosynthetic process,GO:0005886 plasma membrane,GO:0005743 mitochondrial inner membrane
UBRO_05007	FALSE	UBRO_chr08	MIPS	mRNA	614875	615165	.	+	.	ID=mRNA:UBRO_05007;Note=+related+to+LSM8+-+Component+of+small+nuclear+ribonucleoprotein+complexes+involved+in+RNA+processing+and+splicing	sr11118 UBRO_05007 UHOR_05007 UMAG_10642	GO:0005681 spliceosomal complex,GO:0005688 U6 snRNP,GO:0046540 U4/U6 x U5 tri-snRNP complex,GO:0003723 RNA binding,GO:0000398 mRNA splicing, via spliceosome
UBRO_05006	FALSE	UBRO_chr08	MIPS	mRNA	615651	618932	.	-	.	ID=mRNA:UBRO_05006;Note=+related+to+SKT5+-+protoplast+regeneration+and+killer+toxin+resistance+protein	BN887_01068 sr11117 SPSC_04250 UBRO_05006 UHOR_05006 UMAG_10641	GO:0005515 protein binding,GO:0008047 enzyme activator activity,GO:0043085 positive regulation of catalytic activity
UBRO_05003	TRUE	UBRO_chr08	MIPS	mRNA	622143	622659	.	+	.	ID=mRNA:UBRO_05003;Note=+uncharacterized+protein	BN887_01067 sr11116 SPSC_04249 UBRO_05003 UHOR_05003 UMAG_10640	GO:0098542 defense response to other organism
UBRO_05002	FALSE	UBRO_chr08	MIPS	mRNA	624169	626397	.	+	.	ID=mRNA:UBRO_05002;Note=+related+to+peroxiredoxin+q	BN887_01071 sr11115 SPSC_04247 UBRO_05002 UHOR_05002 UMAG_03211	GO:0005623 cell,GO:0016209 antioxidant activity,GO:0016491 oxidoreductase activity,GO:0045454 cell redox homeostasis,GO:0055114 oxidation-reduction process,GO:0098869 cellular oxidant detoxification
UBRO_04999	FALSE	UBRO_chr08	MIPS	mRNA	626644	627578	.	-	.	ID=mRNA:UBRO_04999;Note=+related+to+CKS1+-+cyclin-dependent+kinases+regulatory+subunit	BN887_01064 sr11114 SPSC_04246 UBRO_04999 UHOR_04999 UMAG_03210	GO:0051301 cell division,GO:0019901 protein kinase binding,GO:0061575 cyclin-dependent protein serine/threonine kinase activator activity,GO:0045737 positive regulation of cyclin-dependent protein serine/threonine kinase activity,GO:0043130 ubiquitin binding,GO:0042393 histone binding,GO:0000307 cyclin-dependent protein kinase holoenzyme complex,GO:0019005 SCF ubiquitin ligase complex,GO:0016301 kinase activity,GO:0007346 regulation of mitotic cell cycle
UBRO_20684	FALSE	UBRO_chr08	MIPS	mRNA	629429	630529	.	+	.	ID=mRNA:UBRO_20684;Note=+uncharacterized+protein	UBRO_20096 UBRO_20255 UBRO_20367 UBRO_20532 UBRO_20595 UBRO_20684 UBRO_20805 UBRO_20809 UBRO_20890 UBRO_20933 UBRO_20980 UBRO_21035 SPSC_03839	
UBRO_20683	FALSE	UBRO_chr08	MIPS	mRNA	631390	632859	.	+	.	ID=mRNA:UBRO_20683;Note=+un-	UBRO_20098 UBRO_20167 UBRO_20213 UBRO_20366	

											characterized+protein	UBRO_20531 UBRO_20683 UBRO_20804 UBRO_20808 UBRO_20256 UBRO_20938 UBRO_20979 UBRO_20362 UBRO_20682 UBRO_20803 UBRO_20097 SPSC_03840	
UBRO_20682	FALSE	UBRO_chr08	MIPS	mRNA	633283	633843	.	+	.	ID=mRNA:UBRO_20682;Note=+uncharacterized+protein	UBRO_20098 UBRO_20167 UBRO_20213 UBRO_20366 UBRO_20531 UBRO_20683 UBRO_20804 UBRO_20808 UBRO_20256 UBRO_20938 UBRO_20979 UBRO_20362 UBRO_20682 UBRO_20803 UBRO_20097 SPSC_03840	GO:0003824 catalytic activity,GO:0006259 DNA metabolic process
UBRO_20681	FALSE	UBRO_chr08	MIPS	mRNA	635514	636269	.	-	.	ID=mRNA:UBRO_20681;Note=+uncharacterized+protein		GO:0000943 retrotransposon nucleocapsid,GO:0003676 nucleic acid binding,GO:0015074 DNA integration
UBRO_04997	FALSE	UBRO_chr08	MIPS	mRNA	637190	640180	.	-	.	ID=mRNA:UBRO_04997;Note=+probable+SEC24+-+COPII+coated+vesicle+component	BN887_01063 sr11112 SPSC_04245 UBRO_04997 UHOR_04997 UMAG_03209	GO:0000139 Golgi membrane,GO:0005789 endoplasmic reticulum membrane,GO:0030127 COPII vesicle coat,GO:0070971 endoplasmic reticulum exit site,GO:0005515 protein binding,GO:0008270 zinc ion binding,GO:0006886 intracellular protein transport,GO:0006888 endoplasmic reticulum to Golgi vesicle-mediated transport
UBRO_04996	FALSE	UBRO_chr08	MIPS	mRNA	640773	642854	.	+	.	ID=mRNA:UBRO_04996;Note=+related+to+SNU71+-+component+of+U1+snRNP+required+for+mRNA+splicing+via+spliceosome	BN887_01072 sr11111 SPSC_04244 UBRO_04996 UHOR_04996 UMAG_10639	GO:0003723 RNA binding,GO:0006397 mRNA processing
UBRO_04994	FALSE	UBRO_chr08	MIPS	mRNA	643289	643885	.	-	.	ID=mRNA:UBRO_04994;Note=+related+to+glomerulosclerosis+protein+Mpv17	BN887_02489 sr11109 SPSC_04243 UBRO_04994 UHOR_04994 UMAG_03207	GO:0005743 mitochondrial inner membrane,GO:0016021 integral component of membrane
UBRO_04991	FALSE	UBRO_chr08	MIPS	mRNA	644342	648028	.	-	.	ID=mRNA:UBRO_04991;Note=+related+to+thymidylate+kinase	BN887_02488 sr11108 SPSC_04242 UBRO_04991 UHOR_04991 UMAG_03206	GO:0004798 thymidylate kinase activity,GO:0005524 ATP binding,GO:0006233 dTDP biosynthetic process,GO:0016310 phosphorylation,GO:0046940 nucleoside monophosphate phosphorylation
UBRO_04990	TRUE	UBRO_chr08	MIPS	mRNA	649098	649613	.	+	.	ID=mRNA:UBRO_04990;Note=+related+to+Mig1+-+Mig1+protein,+induced+during+biotrophic+phase	SPSC_04259 SPSC_04264 UBRO_04990 UHOR_04990	
UBRO_04989	FALSE	UBRO_chr08	MIPS	mRNA	650591	652951	.	+	.	ID=mRNA:UBRO_04989;Note=+related+to+TFG1+-+TFIIF+subunit+(transcription+initiation+factor)	BN887_02490 sr11107 SPSC_04241 UBRO_04989 UHOR_04989 UMAG_15003	GO:0005634 nucleus,GO:0003677 DNA binding,GO:0006367 transcription initiation from RNA polymerase II promoter,GO:0032968 positive regulation of transcription elongation from RNA polymerase II promoter
UBRO_04988	FALSE	UBRO_chr08	MIPS	mRNA	654272	660401	.	+	.	ID=mRNA:UBRO_04988;Note=+probable+chitin+synthase+8	BN887_02491 BN887_03783 sr11106 sr14109 SPSC_04240 SPSC_06424 UBRO_04780 UBRO_04988 UHOR_04780 UHOR_04988 UMAG_03204 UMAG_10367	GO:0031505 fungal-type cell wall organization,GO:0005524 ATP binding,GO:0016459 myosin complex,GO:0030428 cell septum,GO:0030659 cytoplasmic vesicle membrane,GO:0003779 actin binding,GO:0016021 integral component of membrane,GO:0004

												100 chitin synthase activity,GO:0005886 plasma membrane,GO:0003774 motor activity
UBRO_04987	FALSE	UBRO_chr08	MIPS	mRNA	661536	663098	.	-	.	ID=mRNA:UBRO_04987;Note=+uncharacterized+protein	sr11104 SPSC_04239 UBRO_04987 UHOR_04987	
UBRO_04986	TRUE	UBRO_chr08	MIPS	mRNA	663968	664357	.	-	.	ID=mRNA:UBRO_04986;Note=+related+to+conserved+hypothetical+Ustilaginaceae-specific+protein	UMAG_03202 UMAG_10403 sr11101 SPSC_04237 UBRO_04986 UHOR_04986 sr11102 SPSC_04238	
UBRO_20680	FALSE	UBRO_chr08	MIPS	mRNA	668255	668608	.	-	.	ID=mRNA:UBRO_20680;Note=+uncharacterized+protein		GO:0016021 integral component of membrane
UBRO_04984	TRUE	UBRO_chr08	MIPS	mRNA	670014	670869	.	+	.	ID=mRNA:UBRO_04984;Note=+uncharacterized+protein	sr11100 SPSC_04236 UBRO_04984 UHOR_04984 UMAG_03201	
UBRO_04983	FALSE	UBRO_chr08	MIPS	mRNA	671110	674172	.	-	.	ID=mRNA:UBRO_04983;Note=+probable+Rad51-associated+protein+Brh2	BN887_02487 sr11099 SPSC_04235 UBRO_04983 UHOR_04983 UMAG_03200	GO:0000724 double-strand break repair via homologous recombination
UBRO_20679	FALSE	UBRO_chr08	MIPS	mRNA	675164	678280	.	-	.	ID=mRNA:UBRO_20679;Note=+uncharacterized+protein	UBRO_20170 UBRO_20191 UBRO_20222 UBRO_20396 UBRO_20491 UBRO_20649 UBRO_20679 UBRO_20791 UBRO_20813 UBRO_20943 UBRO_20947 UBRO_20906 UBRO_20954 UBRO_20958 UBRO_20485 UHOR_15671	
UBRO_04981	FALSE	UBRO_chr08	MIPS	mRNA	681469	683709	.	+	.	ID=mRNA:UBRO_04981;Note=+probable+GFA1+-+glucosamine--fructose-6-phosphate+transaminase		GO:0097367 carbohydrate derivative binding,GO:0034221 fungal-type cell wall chitin biosynthetic process,GO:0004360 glutamine-fructose-6-phosphate transaminase (isomerizing) activity,GO:0006002 fructose 6-phosphate metabolic process,GO:0016021 integral component of membrane,GO:0006047 UDP-N-acetylglucosamine metabolic process,GO:0006487 protein N-linked glycosylation
UBRO_04980	FALSE	UBRO_chr08	MIPS	mRNA	684162	685763	.	-	.	ID=mRNA:UBRO_04980;Note=+related+to+lipoamide+acyltransferase+component+of+branched-chain+alpha-keto+acid+dehydrogenase+complex,+mitochondrial+precursor	BN887_02486 sr11096 SPSC_04233 UBRO_04980 UHOR_04980 UMAG_10402	GO:0005634 nucleus,GO:0005524 ATP binding,GO:0003677 DNA binding,GO:0031405 lipoic acid binding,GO:0016407 acetyltransferase activity,GO:0032508 DNA duplex unwinding,GO:0005739 mitochondrion,GO:0004003 ATP-dependent DNA helicase activity,GO:0006139 nucleobase-containing compound metabolic process
UBRO_04978	FALSE	UBRO_chr08	MIPS	mRNA	686294	689151	.	-	.	ID=mRNA:UBRO_04978;Note=+related+to+CHL1+-+protein+of+the+DEAH+box+family	BN887_02485 sr11094.2 SPSC_04232 UBRO_04978 UHOR_04978 UMAG_10401	GO:0005634 nucleus,GO:0005524 ATP binding,GO:0034085 establishment of sister chromatid cohesion,GO:0003677 DNA binding,GO:0016746 transferase activity, transferring acyl groups,GO:0032508 DNA duplex unwinding,GO:0016021 integral component of membrane,GO:0004003 ATP-dependent DNA helicase activity,GO:0006139 nuc-

												leobase-containing compound metabolic process
UBRO_04977	FALSE	UBRO_chr08	MIPS	mRNA	689839	691005	.	-	.	ID=mRNA:UBRO_04977;Note=+related+to+triose+phosphate/3-phosphoglycerate/ phosphate+translocator	BN887_02484 sr11093 SPSC_04231 UBRO_04977 UHOR_04977 UMAG_10400	GO:0016021 integral component of membrane
UBRO_04976	FALSE	UBRO_chr08	MIPS	mRNA	692293	693370	.	-	.	ID=mRNA:UBRO_04976;Note=+related+to+C-type+cyclin	BN887_02482 sr11091.2 SPSC_04230 UBRO_04976 UHOR_04976 UMAG_10399	GO:0000307 cyclin-dependent protein kinase holoenzyme complex,GO:0005634 nucleus,GO:0016538 cyclin-dependent protein serine/ threonine kinase regulator activity,GO:0000079 regulation of cyclin-dependent protein serine/threonine kinase activity,GO:0070816 phosphorylation of RNA polymerase II C-terminal domain
UBRO_04975	FALSE	UBRO_chr08	MIPS	mRNA	694312	695613	.	-	.	ID=mRNA:UBRO_04975;Note=+uncharacterized+protein	BN887_02481 sr11090 SPSC_04229 UBRO_04975 UHOR_04975 UMAG_03194	
UBRO_04974	FALSE	UBRO_chr08	MIPS	mRNA	696716	697825	.	+	.	ID=mRNA:UBRO_04974;Note=+uncharacterized+protein	BN887_02493 sr11089.2 SPSC_04228 UBRO_04974 UHOR_04974 UMAG_10398	GO:0000307 cyclin-dependent protein kinase holoenzyme complex,GO:0005634 nucleus,GO:0016538 cyclin-dependent protein serine/ threonine kinase regulator activity,GO:0070816 phosphorylation of RNA polymerase II C-terminal domain
UBRO_04973	FALSE	UBRO_chr08	MIPS	mRNA	698132	698752	.	-	.	ID=mRNA:UBRO_04973;Note=+uncharacterized+protein	BN887_02480 sr11087 SPSC_04227 UBRO_04973 UHOR_04973 UMAG_03192	
UBRO_04921	TRUE	UBRO_chr08	MIPS	mRNA	762046	762451	.	+	.	ID=mRNA:UBRO_04921;Note=+uncharacterized+protein	UBRO_04921 UHOR_04921	
UBRO_04923	TRUE	UBRO_chr08	MIPS	mRNA	765755	766447	.	+	.	ID=mRNA:UBRO_04923;Note=+related+to+Mig1+protein	sr14222 SPSC_04273 UBRO_04923 UHOR_04923 UMAG_12216	
UBRO_04924	FALSE	UBRO_chr08	MIPS	mRNA	766867	767352	.	-	.	ID=mRNA:UBRO_04924;Note=+related+to+MRPL51++mitochondrial+ribosomal+protein, +large+subunit	sr14198 SPSC_04201 UBRO_04924 UHOR_04924 UMAG_10382	GO:0005762 mitochondrial large ribosomal subunit,GO:0003735 structural constituent of ribosome,GO:0032543 mitochondrial translation
UBRO_04938	FALSE	UBRO_chr08	MIPS	mRNA	797738	799105	.	+	.	ID=mRNA:UBRO_04938;Note=+probable+platelet-activating+factor+acetylhydrolase+ib+alpha+subunit	BN887_02505 sr14206 SPSC_04193 UBRO_04938 UHOR_04938 UMAG_03164	GO:0005515 protein binding
UBRO_04936	TRUE	UBRO_chr08	MIPS	mRNA	799345	800071	.	-	.	ID=mRNA:UBRO_04936;Note=+probable+1,4-Benzoquinone+reductase	BN887_02460 sr14207 SPSC_04192 UBRO_04936 UHOR_04936 UMAG_10387	GO:0010181 FMN binding,GO:0003955 NAD(P)H dehydrogenase (quinone) activity,GO:0055114 oxidation-reduction process
UBRO_04935	FALSE	UBRO_chr08	MIPS	mRNA	800884	802929	.	-	.	ID=mRNA:UBRO_04935;Note=+probable+glycine--tRNA+ligase+GRS1	BN887_02459 sr14208 SPSC_04191 UBRO_04935 UHOR_04935 UMAG_03162	GO:0004820 glycine-tRNA ligase activity,GO:0005524 ATP binding,GO:0070150 mitochondrial glycyl-tRNA aminoacylation,GO:0005739 mitochondrion
UBRO_04940	FALSE	UBRO_chr08	MIPS	mRNA	804475	805224	.	+	.	ID=mRNA:UBRO_04940;Note=+uncharacterized+protein	BN887_02506 sr14209 SPSC_04190 UBRO_04940 UHOR_04940 UMAG_03166	

UBRO_04942	FALSE	UBRO_chr08	MIPS	mRNA	805923	808511	.	+	.	ID=mRNA:UBRO_04942;Note=+related+to+endothelial+zinc+finger+protein+induced+by+tumor+necrosis+factor+alpha	BN887_02507 sr14210 SPSC_04189 UBRO_04942 UHOR_04942 UMAG_03167	GO:0003676 nucleic acid binding
UBRO_04943	FALSE	UBRO_chr08	MIPS	mRNA	809077	809544	.	+	.	ID=mRNA:UBRO_04943;Note=+uncharacterized+protein	BN887_06142 sr14211 SPSC_04188 UBRO_04943 UHOR_04943 UMAG_03168-A	
UBRO_04944	FALSE	UBRO_chr08	MIPS	mRNA	811083	812462	.	-	.	ID=mRNA:UBRO_04944;Note=+probable+CAR2+-+ornithine+aminotransferase	BN887_02458 sr14212 SPSC_04187 UBRO_04944 UHOR_04944 UMAG_03169	GO:0030170 pyridoxal phosphate binding,GO:0010121 arginine catabolic process to proline via ornithine,GO:0005737 cytoplasm,GO:0019544 arginine catabolic process to glutamate,GO:0055129 L-proline biosynthetic process,GO:0004587 ornithine-oxo-acid transaminase activity
UBRO_04945	FALSE	UBRO_chr08	MIPS	mRNA	813059	815863	.	+	.	ID=mRNA:UBRO_04945;Note=+related+to+DRS1+-+RNA+helicase+of+the+DEAD+box+family	BN887_02508 sr14213 SPSC_04186 UBRO_04945 UHOR_04945 UMAG_03170	GO:0005524 ATP binding,GO:0003723 RNA binding,GO:0042254 ribosome biogenesis,GO:0004386 helicase activity,GO:0005730 nucleolus
UBRO_04946	FALSE	UBRO_chr08	MIPS	mRNA	816102	817285	.	-	.	ID=mRNA:UBRO_04946;Note=+related+to+GCN3+-+translation+initiation+factor+eIF2B,+34+KD,+alpha+subunit	BN887_02457 sr14214 SPSC_04185 UBRO_04946 UHOR_04946 UMAG_03171	GO:0003743 translation initiation factor activity,GO:0050790 regulation of catalytic activity,GO:0005085 guanyl-nucleotide exchange factor activity,GO:0002183 cytoplasmic translational initiation,GO:1903833 positive regulation of cellular response to amino acid starvation,GO:0032045 guanyl-nucleotide exchange factor complex,GO:0006446 regulation of translational initiation,GO:0005851 eukaryotic translation initiation factor 2B complex,GO:0016740 transferase activity,GO:0030234 enzyme regulator activity
UBRO_04948	FALSE	UBRO_chr08	MIPS	mRNA	818090	819487	.	-	.	ID=mRNA:UBRO_04948;Note=+related+to+Zinc+finger+protein	BN887_02456 sr14215 SPSC_04184 UBRO_04948 UHOR_04948 UMAG_03172	GO:0003676 nucleic acid binding
UBRO_04949	FALSE	UBRO_chr08	MIPS	mRNA	821978	822906	.	-	.	ID=mRNA:UBRO_04949;Note=+uncharacterized+protein	UBRO_04949 UHOR_04949	
UBRO_04951	FALSE	UBRO_chr08	MIPS	mRNA	825282	826247	.	-	.	ID=mRNA:UBRO_04951;Note=+uncharacterized+protein	BN887_02455 sr14216 SPSC_04183 UBRO_04951 UHOR_04951 UMAG_10390	GO:0005829 cytosol,GO:0035539 8-oxo-7,8-dihydrodeoxyguanosine triphosphate pyrophosphatase activity,GO:0006203 dGTP catabolic process
UBRO_04953	FALSE	UBRO_chr08	MIPS	mRNA	827349	829910	.	+	.	ID=mRNA:UBRO_04953;Note=+related+to+SKT5+-+protoplast+regeneration+and+killer+toxin+resistance+protein	BN887_02509 sr14217 SPSC_04182 UBRO_04953 UHOR_04953 UMAG_10391	GO:0005515 protein binding
UBRO_04954	FALSE	UBRO_chr08	MIPS	mRNA	830734	831591	.	+	.	ID=mRNA:UBRO_04954;Note=+uncharacterized+protein	sr14193 SPSC_04178 UBRO_04954 UHOR_04954 UMAG_03178	GO:0044424 intracellular part,GO:0003676 nucleic acid binding,GO:0008380

													RNA splicing
UBRO_04955	FALSE	UBRO_chr08	MIPS	mRNA	831776	834148	.	-	.	ID=mRNA:UBRO_04955;Note=+uncharacterized+protein	UBRO_04955 UHOR_04955	GO:0005847 mRNA cleavage and polyadenylation specificity factor complex,GO:0003723 RNA binding,GO:0006378 mRNA polyadenylation,GO:0098789 pre-mRNA cleavage required for polyadenylation
UBRO_04956	FALSE	UBRO_chr08	MIPS	mRNA	836091	839372	.	+	.	ID=mRNA:UBRO_04956;Note=+related+to+white+collar+1+protein	BN887_05734 sr14191 SPSC_04176 UBRO_04956 UHOR_04956 UMAG_03180	GO:0005634 nucleus,GO:0006355 regulation of transcription, DNA-templated
UBRO_04897	FALSE	UBRO_chr08	MIPS	mRNA	842005	843078	.	+	.	ID=mRNA:UBRO_04897;Note=+uncharacterized+protein	sr14190 SPSC_04175 UBRO_04897 UHOR_04897 UMAG_03135	
UBRO_04896	FALSE	UBRO_chr08	MIPS	mRNA	843304	843990	.	-	.	ID=mRNA:UBRO_04896;Note=+uncharacterized+protein	sr14189 SPSC_04174 UBRO_04896 UHOR_04896 UMAG_03134	
UBRO_04895	FALSE	UBRO_chr08	MIPS	mRNA	844352	849331	.	+	.	ID=mRNA:UBRO_04895;Note=+related+to+SMC4++Stable+Maintenance+of+Chromosomes	BN887_05736 sr14188 SPSC_04173 UBRO_04895 UHOR_04895 UMAG_12209	GO:0005694 chromosome,GO:0005515 protein binding,GO:0005524 ATP binding,GO:0051276 chromosome organization
UBRO_04894	FALSE	UBRO_chr08	MIPS	mRNA	849509	851143	.	-	.	ID=mRNA:UBRO_04894;Note=+uncharacterized+protein	BN887_06137 sr14187 SPSC_04172 UBRO_04894 UHOR_04894 UMAG_03132	GO:0016021 integral component of membrane
UBRO_04893	FALSE	UBRO_chr08	MIPS	mRNA	851635	853836	.	+	.	ID=mRNA:UBRO_04893;Note=+related+to+SSN3++cyclin-dependent+CTD+kinase	BN887_05737 sr14186 SPSC_04171 UBRO_04893 UHOR_04893 UMAG_12208	GO:0005524 ATP binding,GO:0008353 RNA polymerase II CTD heptapeptide repeat kinase activity,GO:0046872 metal ion binding,GO:0016592 mediator complex,GO:0005719 nuclear euchromatin,GO:0051726 regulation of cell cycle,GO:0004693 cyclin-dependent protein serine/threonine kinase activity,GO:0045944 positive regulation of transcription by RNA polymerase II,GO:0006468 protein phosphorylation
UBRO_04892	FALSE	UBRO_chr08	MIPS	mRNA	854159	856516	.	-	.	ID=mRNA:UBRO_04892;Note=+related+to+CCR4++transcriptional+regulator+involved+in+carbon+catabolite+repression	BN887_05732 sr14185 SPSC_04170 UBRO_04892 UHOR_04892 UMAG_10379	GO:0000932 P-body,GO:0005634 nucleus,GO:0030015 CCR4-NOT core complex,GO:0003723 RNA binding,GO:0004535 poly(A)-specific ribonuclease activity,GO:0005515 protein binding,GO:0046872 metal ion binding,GO:0000289 nuclear-transcribed mRNA poly(A) tail shortening,GO:0090503 RNA phosphodiester bond hydrolysis, exonucleolytic
UBRO_04891	FALSE	UBRO_chr08	MIPS	mRNA	857932	860172	.	+	.	ID=mRNA:UBRO_04891;Note=+probable+heat+shock+protein+80	BN887_05738 sr14184 SPSC_04169 UBRO_04891 UHOR_04891 UMAG_11952	GO:0016887 ATPase activity,GO:0005524 ATP binding,GO:0070924 heterochromatin assembly involved in chromatin silencing by small RNA,GO:0061077 chaperone-mediated protein folding,GO:0051082 unfolded protein binding
UBRO_	FALSE	UBRO_chr08	MIPS	mRNA	861186	864446	.	+	.	ID=mRNA:UBRO_	SPSC_04168 UBRO_04890	GO:0015267 chan-

04890											04890;Note=+related+to+channel+protein	UHOR_04890	nel activity,GO:0055085 transmembrane transport,GO:0016021 integral component of membrane
UBRO_04889	FALSE	UBRO_chr08	MIPS	mRNA	864915	865934	.	-	.	ID=mRNA:UBRO_04889;Note=+related+to+lipase/esterase	UBRO_04889 UHOR_04889 sr15703 SPSC_04167 UMAG_03128	GO:0016787 hydrolase activity
UBRO_04888	FALSE	UBRO_chr08	MIPS	mRNA	867360	871409	.	+	.	ID=mRNA:UBRO_04888;Note=+uncharacterized+protein	BN887_05731 sr14183 SPSC_04166 UBRO_04888 UHOR_04888 UMAG_03127	GO:0005737 cytoplasm,GO:0005515 protein binding,GO:0042594 response to starvation
UBRO_04886	FALSE	UBRO_chr08	MIPS	mRNA	871790	873025	.	-	.	ID=mRNA:UBRO_04886;Note=+related+to+retinal+short-chain+dehydrogenase/reductase	UMAG_03126 UMAG_05069 BN887_05730 sr14182 SPSC_04165 UBRO_04886 UHOR_04886	GO:0005789 endoplasmic reticulum membrane,GO:0016021 integral component of membrane,GO:0047560 3-dehydrosphinganine reductase activity,GO:0006666 3-keto-sphinganine metabolic process,GO:0030148 sphingolipid biosynthetic process,GO:0055114 oxidation-reduction process
UBRO_04885	FALSE	UBRO_chr08	MIPS	mRNA	874750	875916	.	+	.	ID=mRNA:UBRO_04885;Note=+related+to+Ribonuclease+P+protein+subunit+p30	BN887_02715 sr14181 SPSC_04164 UBRO_04885 UHOR_04885 UMAG_03124	GO:0004526 ribonuclease P activity,GO:0003723 RNA binding,GO:0090501 RNA phosphodiester bond hydrolysis,GO:0008033 tRNA processing,GO:0005655 nucleolar ribonuclease P complex
UBRO_06814	FALSE	UBRO_chr13	MIPS	mRNA	195588	196303	.	-	.	ID=mRNA:UBRO_06814;Note=+uncharacterized+protein	UBRO_06814 UHOR_06814	
UBRO_06816	FALSE	UBRO_chr13	MIPS	mRNA	198307	201522	.	+	.	ID=mRNA:UBRO_06816;Note=+related+to+conserved+hypothetical+Ustilaginaceae-specific+protein	BN887_04930 sr15246 SPSC_00894 UBRO_06816 UHOR_06816 UMAG_11147	GO:0031072 heat shock protein binding,GO:0051082 unfolded protein binding
UBRO_20815	FALSE	UBRO_chr13	MIPS	mRNA	202510	206918	.	+	.	ID=mRNA:UBRO_20815;Note=+uncharacterized+protein	SPSC_00206 SPSC_01500 SPSC_01215 SPSC_05764 UBRO_20081 UBRO_20349 UBRO_20089 UBRO_20219 UBRO_20355 UBRO_20594 UBRO_20727 UBRO_20164 UBRO_20203 UBRO_20637 UBRO_20669 UBRO_20815 UBRO_20220 UBRO_20284 UBRO_20335 UBRO_20728 UBRO_20754 UBRO_20968 UBRO_20279 UBRO_20307 UBRO_20844 UBRO_20280 UBRO_20360 UBRO_20596 UBRO_20964 UBRO_20353 UBRO_20752 UHOR_01239 UHOR_07208 UHOR_12887 UHOR_16074 UHOR_12189 UHOR_14247 sr05445 UBRO_20884 UBRO_20085 UHOR_02454 SPSC_05299 SPSC_06576	
UBRO_06818	FALSE	UBRO_chr13	MIPS	mRNA	208660	210921	.	+	.	ID=mRNA:UBRO_06818;Note=+related+to+KRI1+-+KRRI-Interacting+protein+1	UBRO_06818 UBRO_06818c BN887_04979 sr15247 SPSC_00895 UHOR_06818 UMAG_04361	GO:0005730 nucleolus,GO:0030686 90S preribosome,GO:0005515 protein binding,GO:0000447 endonucleolytic cleavage in ITS1 to separate SSU-rRNA from 5.8S rRNA and LSU-rRNA from tricistronic rRNA transcript (SSU-rRNA, 5.8S rRNA, LSU-rRNA)
UBRO_06819	FALSE	UBRO_chr13	MIPS	mRNA	211032	212555	.	-	.	ID=mRNA:UBRO_06819;Note=+related+to+Cytochrome+P450+8B1	sr15248 UBRO_06819 UHOR_06819 UMAG_04362	GO:0016705 oxidoreductase activity, acting on paired donors, with incor-

												poration or reduction of molecular oxygen,GO:0005506 iron ion binding,GO:0055114 oxidation-reduction process,GO:0044425 membrane part,GO:0004497 monooxygenase activity,GO:0020037 heme binding
UBRO_06822	FALSE	UBRO_chr13	MIPS	mRNA	213847	216783	.	+	.	ID=mRNA:UBRO_06822;Note=+related+to+MTG2+-+Mitochondrial+GTP+binding+protein	BN887_04931 sr15249 SPSC_00896 UBRO_06822 UHOR_06822 UMAG_11148	GO:0003676 nucleic acid binding,GO:0005525 GTP binding
UBRO_06823	TRUE	UBRO_chr13	MIPS	mRNA	217004	218452	.	-	.	ID=mRNA:UBRO_06823;Note=+related+to+EXG1+-+exo-beta-1,3-glucanase	UMAG_04364 UMAG_05550 BN887_04978 sr15250 SPSC_00897 UBRO_06823 UHOR_06823	GO:0009251 glucan catabolic process,GO:0006073 cellular glucan metabolic process,GO:0005576 extracellular region,GO:0004553 hydrolase activity, hydrolyzing O-glycosyl compounds,GO:0009986 cell surface
UBRO_06825	FALSE	UBRO_chr13	MIPS	mRNA	219864	221504	.	+	.	ID=mRNA:UBRO_06825;Note=+related+to+SRM1+-+nucleotide+exchange+factor	BN887_04932 sr15251 SPSC_00898 UBRO_06825 UHOR_06825 UMAG_04365	GO:0046872 metal ion binding
UBRO_06826	FALSE	UBRO_chr13	MIPS	mRNA	222764	227508	.	+	.	ID=mRNA:UBRO_06826;Note=+uncharacterized+protein	BN887_04933 sr15252 SPSC_00901 UBRO_06826 UHOR_06826 UMAG_11149	GO:0016021 integral component of membrane
UBRO_06828	TRUE	UBRO_chr13	MIPS	mRNA	229085	231421	.	+	.	ID=mRNA:UBRO_06828;Note=+related+to+endo-1,3(4)-beta-glucanase	UBRO_06828 UHOR_06828 UMAG_04368	GO:0009251 glucan catabolic process,GO:0052861 glucan endo-1,3-beta-glucanase activity, C-3 substituted reducing group
UBRO_06829	FALSE	UBRO_chr13	MIPS	mRNA	232460	233740	.	+	.	ID=mRNA:UBRO_06829;Note=+uncharacterized+protein	BN887_04935 sr15255 SPSC_00904 UBRO_06829 UHOR_06829 UMAG_04370	GO:0016702 oxidoreductase activity, acting on single donors with incorporation of molecular oxygen, incorporation of two atoms of oxygen,GO:0055114 oxidation-reduction process
UBRO_06830	FALSE	UBRO_chr13	MIPS	mRNA	233877	235784	.	-	.	ID=mRNA:UBRO_06830;Note=+related+to+eukaryotic+translation+initiation+factor	BN887_04977 sr15256 SPSC_00905 UBRO_06830 UHOR_06830 UMAG_04371	GO:0022627 cytosolic small ribosomal subunit,GO:0000049 tRNA binding,GO:0003743 translation initiation factor activity,GO:0005515 protein binding,GO:0043022 ribosome binding,GO:0006413 translational initiation,GO:0006417 regulation of translation
UBRO_08780	FALSE	UBRO_chr22	MIPS	mRNA	141525	143752	.	+	.	ID=mRNA:UBRO_08780;Note=+related+to+MBP1+-+transcription+factor,+subunit+of+the+MBF+factor	BN887_02824 sr11315 SPSC_04490 UBRO_08780 UHOR_08780 UMAG_11222	GO:0033309 SBF transcription complex,GO:0005515 protein binding,GO:0000790 nuclear chromatin,GO:0005737 cytoplasm,GO:0000978 RNA polymerase II proximal promoter sequence-specific DNA binding,GO:0030907 MBF transcription complex,GO:0016021 integral component of membrane,GO:0071931 positive regulation of transcription involved in G1/S transition of mitotic cell cycle,GO:0001228 DNA-binding tran-

scription activator activity, RNA polymerase II-specific,GO:0045944 positive regulation of transcription by RNA polymerase II